der Bundeswehr
Universität München

Fakultät der Luft- und Raumfahrttechnik
Institut für Raumfahrttechnik und Weltraumnutzung

Innovative Approach for Effective and Safe Space Debris Removal

Dipl. Ing. Susanne Peters

Vollständiger Abdruck der von der Fakultät für Luft- und Raumfahrttechnik der Universität der Bundeswehr München zur Erlangung des akademischen Grades eines

Doktor-Ingenieur (Dr.-Ing.)

genehmigten Dissertation.

Vorsitzender:	Prof. Dr. rer. nat. Matthias Gerdts
1. Gutachter:	Prof. Dr.-Ing. Roger Förstner
2. Gutachter:	Prof. Dr.-Ing. Enrico Stoll

Die Dissertation wurde am 26. März 2019 bei der Universität der Bundeswehr München eingereicht und durch die Fakultät für Luft- und Raumfahrttechnik am 10. August 2019 angenommen. Die mündliche Prüfung fand am 6. Dezember 2019 statt.

An ounce of prevention is worth a pound of cure.

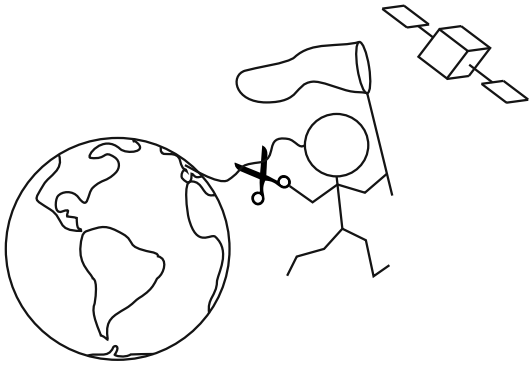

Kurzfassung

In dieser Arbeit wird ein innovativer Ansatz zur effektiven und sicheren Entfernung von Weltraumrückständen untersucht. Die Gefahr von Weltraumrückständen für den sicheren Betrieb von Satelliten in der Erdumlaufbahn hat in den letzten Jahren stark zugenommen. Weltraumrückstände sind ein wachsendes Problem der Menschen. Immer mehr Satelliten werden ins All gebracht. Bereits dort Befindliche erreichen ihr Lebensende, ohne, dass sich jemand darum kümmert wie es danach mit ihnen weiter geht. Einige der Satelliten treten unkontrolliert wieder in die Erdatmosphäre ein. Dabei haben sie das Potential Leben auf der Erde zu gefährden. Andere explodieren im Weltall und tragen damit zu einer steigenden Anzahl bei. Bereits angewandte Mittel wie Ausweichmanöver einleiten, die Richtlinien zur Verlangsamung des Anstiegs der die Erde umkreisenden unkontrollierten Körper einfordern und Methoden zur besseren Beobachtung und Vorhersage von Flugbahnen einführen, müssen durch die tatsächliche Entfernung von Objekten unterstützt werden.

Das Ziel der vorliegenden Studie ist es, einen wirksamen und sicheren Ansatz für die aktive Entfernung von Weltraumrückständen bereitzustellen, um die Anzahl der Objekte in der niedrigen Erdumlaufbahn tatsächlich zu begrenzen. *Wirksam*, da mindestens fünf große Objekte pro Jahr entfernt werden müssen, um einen Unterschied in den Vorhersagen zu machen und die Eskalation des bereits eingeleiteten Kaskadeneffekts zu vermeiden. *Sicher*, da das Szenario aufgrund eines unkooperativen Zielobjektes mit unbekannter Drehrate, ohne Signalreflektoren und fehlender vorgefertigter Kontaktstelle für den Andockvorgang äußerst kritisch ist. Da das Annäherungsszenario zudem zeitkritisch ist, wird die Umsetzung von Entscheidungsprozessen an Bord unterstützt.

Die Arbeit beginnt mit einer Einführung in das Thema Weltraumrückstände und dessen Bedrohung für Menschen auf der Erde sowie für Objekte im Weltraum. Es werden bereits getroffene und anvisierte Maßnahmen vorgestellt. Darüber hinaus werden die Herausforderungen der aktiven Entfernung von Weltraumrückständen dargestellt.

Als nächster Schritt wird eine Mission zur Entfernung mehrerer Ziele entwickelt. Angestrebt werden fünf SL-8-Raketenoberstufen, die sich in unmittelbarer Nähe zueinander mit einer Inklination von 83 Grad und einer Höhe von etwa 980 km befinden

- ein Gebiet, das stark durch andere Weltraumrückstände okkupiert ist. Die Mission selbst besteht aus einem Hauptsatelliten (ADReS-A) und mehreren De-Orbit-Kits. Der Missionsaufbau ist so gestaltet, dass ADReS-A jeweils ein De-Orbit-Kit tragen und an einem Zielobjekt anbringen kann. Dort dient das Kit als Schubersatz und ermöglicht eine aktive Entfernung der großen Raketenoberstufen. Während der Hauptsatellit ein einzelnes Kit zum Zielobjekt befördert, an der Raketenoberstufe anlegt und das Verbundsystem stabilisiert, warten die anderen Kits in einer entfernteren Umlaufbahn auf ihren Einsatz. Berechnungen für ein treibstoffsparendes Shuttleszenario werden präsentiert.

Im Weiteren bietet die Systemarchitektur einen detaillierteren Aufbau der zwei Raumfahrzeuge, einschließlich eines CAD-Modells und eines Massen- und Leistungsbudgets. Die Kombination aus ADReS-A und einem Kit ergibt annähernd das gleiche Gewicht und eine ähnliche Größe wie der angestrebte Raketenkörper.

Die Sicherheit der Mission und die Entscheidungsfindungskonzepte an Bord werden durch das Self- & Failure-Management adressiert. Es werden verschiedene Anforderungen für das präsentierte Konzept vorgestellt, eine Fehlerbaumanalyse bezüglich möglicher Fehler durch ADReS-A wird entwickelt. Das Entscheidungskonzept der Fuzzy-Logik wird in dieser Phase der Missionsentwicklung als am besten geeignet ausgewählt. Basierend auf der Fehlerbaumanalyse werden Fuzzy-Regeln entwickelt. Die resultierenden Vorschläge beinhalten Maßnahmen, wie in unterschiedlichen Fällen zu reagieren ist.

Basierend auf den Ergebnissen der oben beschriebenen Untersuchungen wird eine Simulation entwickelt, um denkbare Szenarien zu testen. Eine Analyse verschiedener Setups legt die Möglichkeiten und Grenzen des vorgestellten Konzeptes offen.

Zusammenfassend ist eine aktive Entfernung von Weltraumrückständen notwendig, um zukünftige Weltraumoperationen zu ermöglichen. Die vorgestellte Mission mit ihrer Möglichkeit eines Abbruchs während des Endanfluges ist ein geeigneter Ansatz.

Abstract

This work investigates an innovative approach for effective and safe space debris removal. The threat of space debris for the safe operation of satellites in Earth's orbit increased rapidly over the last few years. Space debris is a growing human-made issue. More and more satellites are launched into space, older ones reach their end-of-life without being taken care of. Some re-enter the Earth's atmosphere uncontrolled and may harm life on Earth. Others explode in space and add to the already large number of objects. Avoidance maneuver, confirmed guidelines to slow down the rising amount of uncontrolled bodies orbiting Earth, and developed mechanisms for better observation and prediction of trajectories will have to be supported by the actual removal of objects.

The objective of this study is to provide an effective and safe approach for active debris removal as a tool to actually limit the number of objects in low Earth orbit. *Effective* as at least five large objects per year will have to be removed to make a difference within the predictions and avoid the escalation of the cascade effect already initiated. *Safe* as the scenario is highly critical due to an uncooperative target with unknown rotation rate, no signal reflectors, and an absent pre-designed point of contact for the berthing process. As the approach scenario is also time-critical, the implementation of on-board decision-making processes is promoted.

The thesis starts with an introduction into the subject of space debris and its threat for humans on Earth and objects in space. Presented are measures already considered and taken. Additionally, the challenges of active debris removal are presented.

As a next step, a mission for a multiple target removal is developed. Targeted are five SL-8 rocket bodies orbiting in close proximity at an inclination of 83 deg and an altitude of about 980 km - an area crowded with space debris. The mission itself consists of a main satellite (ADReS-A) and multiple De-orbit Kits. The mission set-up enables ADReS-A to carry and attach one De-orbit Kit at a time to a target. There, the Kit serves as thrust extension and allows for an active removal of the large debris. While the main satellite carries one single Kit to the target, berths with it, and stabilizes the compound system, the other Kits wait in a different orbit for their transportation. Calculations for a fuel-efficient shuttling scenario are given.

The system architecture then provides a more detailed set-up of the two different kind of spacecraft including a CAD-model and a mass- and power budget. The combination of ADReS-A and one Kit results in approximately the same weight and similar size as the targeted rocket body.

The safety of the mission and on-board decision-making concepts are addressed by the self- & failure-management. Different requirements for such mission are presented, a fault tree analysis of possible failures for ADReS-A is developed. The decision-making concept of fuzzy-logic is chosen as most suitable at this stage of the mission development. Based on the fault tree analysis, fuzzy rules are developed with actions on how to react in various cases assigned.

On the basis of the results of the investigations described above, a simulation is developed to test for different scenarios. An analysis on different set-ups frames the capability of the introduced approach.

In conclusion, active debris removal is necessary to enable future space operations. The presented mission with its possibility for an abort during the final approach is one suitable approach for such removal mission.

Table of Contents

List of Figures

List of Tables

List of Symbols

a	Semi-Major Axis	km
$\Delta\alpha$	Angle Range	deg
α_{App}	Angle for Approach Phase	deg
α_{Ecl}	Angle for Eclipse Phase	deg
α_{Ill}	Angle for Illumination Phase	deg
$\alpha_{Sun/Ref}$	Angle for Glare Phase	deg
AU	Astronomical Unit ($1\,\mathrm{AU} = 149.6 \times 10^6\,\mathrm{km}$)	
C_{Err}	Parameter between 0...1	-
d_{Deb}	Diameter of Debris Bullet	cm
$\Delta\delta$	Declination Range	deg
δ_k	Declination	deg
D	Spacial Density	$1/m^3$
d_i^C	Docking Point Chaser	m
d_i^T	Docking Point Target	m
E	Eccentric Anomaly	deg
e	Eccentricity	-
E_{kin}	Kinetic Energy	MJ
$E_{kin,Deb}$	Kinetic Energy of the Debris	MJ
η	Vector within LVLH-system	m
η_0	Initial Position within LVLH-system	m
η_{CW}	Initial Position within LVLH-system for CW-Approach	m
η_{Eid}	Initial Position within LVLH-system for Eidel-Approach	m
η_{num}	Initial Position within LVLH-system for Numerical Approach	m
$\dot{\eta}$	Vector Velocity within LVLH-system	m/s
$\dot{\eta}_0$	Initial Vector Velocity within LVLH-system	m/s
F	Impact Flux	$1/m^2 s$
F	Thrust	N
g_0	Gravitational Acceleration	m/s^2
i	Inclination	deg
Δi	Inclination Range	deg

I_{sp}	Specific Impulse	s
J_2	Earth's Second Dynamic Form Factor ($1.08262668 \times 10^{-3}$)	
J_{ii}^C	Chaser's Moment of Inertia	kg/m^2
J_{ii}^T	Target's Moment of Inertia	kg/m^2
l_i^C	Chaser's Length CoM-front/back	m
l_i^T	Target's Length CoM-front/back	m
M	Mean Anomaly	deg
m^C	Mass of Chaser	kg
m_{end}	Dry Mass	kg
M_{max}	Maximum Torque	Nm
m_T	Mass of Propellant	kg
m^T	Mass of Target	kg
μ	Earth's Gravitational Parameter (Earth: $3.986 \times 10^{14}\, m^3/s^2$)	
q_i^C	Quaternion Chaser	-
q_i^T	Quaternion Target	-
Ω	Right Ascension of the Ascending Node	deg
$\Delta\Omega$	Right Ascension of the Ascending Node Range	deg
$\dot{\Omega}$	Precession Rate	deg/s
r_f	Targeted (final) Orbit Radius	m
r_i	Initial Orbit Radius	m
r_r	Radial Direction	km
Δr	Radial Direction Range	km
r^C	Sphere Radius around Chaser	m
r_{Cyl}^C	Radius Cylinder Chaser	m
r_e	Earth's Radius ($6.378 \times 10^6\, km$)	
$\vec{r}_{Err}$	Position Vector at the Time a Failure was realized	m
r^T	Sphere Radius around Target	m
r_{Cyl}^T	Radius Cylinder Target	m
$s_{t,Err}$	Safety Radius after Error	m
t	Time	s
t_0	Time at Passage of the Perigee	s
$t_{\alpha_{App}}$	Time of Approach Phase	s
$t_{\alpha_{Ecl}}$	Time of Eclipse Phase	s
Θ	True Anomaly	deg
$t_{\alpha_{Ill}}$	Time of Illumination Phase	s
u_{max}	Maximum Thrust	N
v	Velocity	km/s
Δv	Change in Velocity	m/s

Δv_{ch}	Impulsive Change in Velocity	m/s
V	Control Volume	m^3
x_C	Vector within BFC-system of Chaser	m
x_T	Vector within BFC-system of Target	m
ξ	Vector within LVLH-system	m
ξ_0	Initial Position within LVLH-system	m
ξ_{CW}	Initial Position within LVLH-system for CW-Approach	m
ξ_{Eid}	Initial Position within LVLH-system for Eidel-Approach	m
ξ_{num}	Initial Position within LVLH-system for Numerical Approach	m
$\dot{\xi}$	Vector Velocity within LVLH-system	m/s
$\dot{\xi}_0$	Initial Vector Velocity within LVLH-system	m/s
y_C	Vector within BFC-system of Chaser	m
y_T	Vector within BFC-system of Target	m
z_C	Vector within BFC-system of Chaser	m
z_T	Vector within BFC-system of Target	m
ζ	Vector within LVLH-system	m
ζ_0	Initial Position within LVLH-system	m
ζ_{CW}	Initial Position within LVLH-system for CW-Approach	m
ζ_{Eid}	Initial Position within LVLH-system for Eidel-Approach	m
ζ_{num}	Initial Position within LVLH-system for Numerical Approach	m
$\dot{\zeta}$	Vector Velocity within LVLH-system	m/s
$\dot{\zeta}_0$	Initial Vector Velocity within LVLH-system	m/s

Acronyms

A-FDIR	Advanced FDIR
ADR	Active Debris Removal
ADReS-A	Active Debris Removal Satellite - #A
AI	Artificial Intelligence
AOCS	Attitude and Orbital Control System
AP	Abort Path
ASAT	Anti-Satellite
ASI	Agenzia Spaziale Italiana
ATS	Approach Trajectory Section
ATV	Automated Transfer Vehicle
BFC	Body Fixed Coordinate
BNSC	British National Space Centre
CAD	Computer-Aided Design
CAM	Collision Avoidance Maneuver
CGT	Cold Gas Thruster
CIS	Commonwealth of Independent States
CNES	Centre National d'Etudes Spatiales
CNSA	China National Space Administration
CO	Catch Orbit
CoM	Center of Mass
CONOPS	Concept of Operations
COSA	Cognitive System Architecture
CPT	Conditional Probability Table
CSA	Canadian Space Agency
CSS	Coarse Sun Sensor
CW	Clohessy-Wiltshire
D-CoNe	Debris Collecting Net
D-S	Dempster-Shafer
DAE	Differential Equation
DAG	Directed Acyclic Graph

DAM	Debris Avoidance Maneuver
DAMAGE	Debris Analysis and Monitoring Architecture for the Geosynchronous Environment
DART	Demonstration of Autonomous Rendezvous Technology
DELTA	Debris Environment Long-Term Analysis Model
DEOS	Deutsche Orbitale Servicing Mission
df	Degrees of Freedom
DISCOS	Database and Information System Characterising Objects in Space
DLR	Deutsches Zentrum für Luft- und Raumfahrt
DP	Docking Point
DRAMA	Debris Risk Assessment and Mitigation Analysis
ECI	Earth-Centered Inertial
ECSS	European Cooperation for Space Standardization
EDDE	Electrodynamic Debris Eliminator
Envisat	Environmental Satellite
EOL	End of Life
ES	Earth Sensor
ESA	European Space Agency
ESTRACK	ESA Tracking Station
FDI	Fault Detection and Isolation
FDIR	Fault Detection, Isolation, and Recovery
FIR	Fuzzy Inductive Reasoning
FMECA	Failure Mode, Effects, and Criticality Analysis
FoV	Field of View
FREND	Front-end Robotics Enabling Near-term Demonstration
FSS	Fine Sun Sensor
FTA	Fault Tree Analysis
GEO	Geostationary Orbit
GMAT	General Mission Analysis Tool
GNC	Guidance, Navigation, and Control
GOCE	Gravity field and Ocean Circulation Explorer
GOLD	Gossamer Orbit Lowering Device
GPS	Global Positioning System
GTO	Geostationary Transfer Orbit
HST	Hubble Space Telescope
IADC	Inter-Agency Space Debris Coordination Committee
IBS	Ion Beam Shepard
IMU	Inertial Measurement Unit

IRL	Integration Readiness Level
ISRO	Indian Space Research Organisation
ISS	International Space Station
JAXA	Japan Aerospace Exploration Agency
KSCPROP	Kustaanheimo and Stiefel Canonical Propagation Model
LCH4	Liquid Methane
LEGEND	LEO-to-GEO Environment Debris Model
LEO	Low Earth Orbit
LEODEEM	LEO Debris Evolutionary Model
LIDAR	Light and Radar
LOX	Liquid Oxygen
LVLH	Local Vertical, Local Horizontal
MASTER	Meteoroid and Space Debris Terrestrial Environment Reference Model
MC	Monte Carlo
MF	Membership Function
MIPS	Million Instructions Per Second
MLI	Multi Layer Insulation
MoI	Moments of Inertia
MPPT	Maximum Power Point Tracking
MSS	Medium Sun Sensor
N2	Nitrogen
NASA	National Aeronautics and Space Administration
NSAU	National Space Agency of Ukraine
OA	Omnidirectional Antenna
OBC	On-board Computer
OBCP	On-Board Control Procedures
ODQN	Orbital Debris Quarterly News
OST	Outer Space Treaty
PCDU	Power Conditioning and Distribution Unite
PMD	Post-Mission Disposal
PO	Parking Orbit
PoO	Point of Origin
R/B	Rocket Body
R & C	Rendezvous & Capture
R & D	Rendezvous & Docking
RA	Robotic Arm
RAAN	Right Ascension of the Ascending Node

RCS	Radar Cross Section
REDCROC	Research and Development for the Capture and Removal of Orbital Clutter
ROGER	Robotic Geostationary Orbit Restorer
ROSCOSMOS	Russian Federal Space Agency
RW	Reaction Wheel
S/C	Spacecraft
SA	Solar Array
SDM	Space Debris Mitigation long-term Analysis Program
SDMR	Space Debris Micro Remover
SL-8 R/B	Sea Launch 8 Rocket Body
SMA	Semi-Major Axis
SMAD	Space Mission Analysis and Design
SQP	Sequential Quadratic Programming
SRL	System Readiness Level
SRM	Solid Rocket Motor
SSO	Sun Synchronous Orbit
SSR	Satellite Situation Report
ST	Star Tracker
TIRA	Tracking & Imaging Radar
TLE	Two-line Element
TO	Target Orbit
ToFC	Time of Flight Camera
TRL	Technology Readiness Level
TTC	Telemetry, Tracking and Command
UCS	Union of Concerned Scientists
UKSA	United Kingdom Space Agency
UNCOPUOS	United Nations Committee on the Peaceful Uses of Outer Space
US-DoD	United States Department of Defense
UV	Ultraviolet
VLC	Visual Light Camera

1 Introduction

Since Sputnik I reached Low Earth Orbit (LEO) on October 4th, 1957, the number of human-made objects around Earth has increased continuously. By now, about 2 200 operational satellites face nearly 17 600 cataloged space debris with sizes of 10 cm^2 and above. Due to their enormous kinetic energy, even the smallest particles can have hazardous effects when impacting on other objects. A great threat derives from collisions among the debris itself. With each collision, the number of particles in space increases many times over. The recorded number of particles is continuously growing - despite any further launches. The mitigation and removal of space debris and their various sources has, therefore, become one of the major concerns of space agencies. Political, legal, and financial aspects must be considered to realize such projects and need to be addressed by the designated experts. Meanwhile, this thesis concentrates on the technical part of a mission for active debris removal.

The presented research investigates a removal mission for objects never designed to be removed. Safety is one of the main requirements to fulfill when targeting such uncooperative objects, followed by efficiency. The work, thus, focuses on three main parts: (1) The mission design, based on investigations concerning the potential threat of space debris; (2) the satellite design, providing an example of a spacecraft concept able to remove objects from their operational orbit; and (3) the safety improvement of such mission through decision making processes and on-board failure management. By approaching the problem though those multiple perspectives, a realistic mission is created with the potential to support the active removal of space debris.

Chapter 2 introduces space debris in general. The motivation to actively intervene in the current development is provided. Additionally, an overview of the past and current approaches, challenges, and concept studies, aiming to limit the threat of space debris, is given. Deficits pinpointed by the overview are then approached in the following chapters. Chapter 3 focuses on the mission design. Potential targets are identified through a filter tool. A deeper understanding of past, current, and envisioned missions and technologies is provided. Based on this investigation an efficient mission design for the removal mission is derived. Chapter 4 addresses the system architecture and

spacecraft design following the conclusions of Chapter 3. This second main part of the research provides an example of a spacecraft concept for the removal of large uncooperative objects down to subsystem level. Specifications are explained and mass and power distributions are derived. Chapter 5 concentrates on the self-management capability of the spacecraft along with on-board failure-management during the close vicinity of target and spacecraft. It is explained how failures can be recognized and handled for specific applications. Chapter 6 ties together Chapter 3 - 5, and with such the three main parts of this thesis. The presented simulation is able to calculate approach and abort trajectories for the designed scenario. The failure-management is included through the different trajectories. Analyzed are the simplifications assumed and time and propellant requirements for different approach strategies. Those strategies include variable initial distances as well as adapting safety parameters. Chapter 7 summarizes the conclusions drawn from this work, recommendations for further development and future work are given. The Appendices provide additional information on mathematical backgrounds (Appendix A), list supporting tables (Appendix B), and show additional analyses of the relative dynamics (Appendix C).

2 Space Debris

2.1 Definition and Classification

2.1.1 Origin and Distribution

Space Debris technically refers to all human-made objects orbiting Earth unable to perform their intended tasks or still being in orbit without any use. Figure 2.1 plots their diverse origins, starting from rocket bodies and dead satellites not decayed, over test objects and mission related debris to abrasion particles and pieces from colliding or exploding objects. The resulting objects shatter into all possible forms with dimensions from several micrometers up to a few meters. Their number increases indirect proportional to their size. Orbital decay and removal - measures that limit their amount - are affecting the population slower than the sources feed their growth.

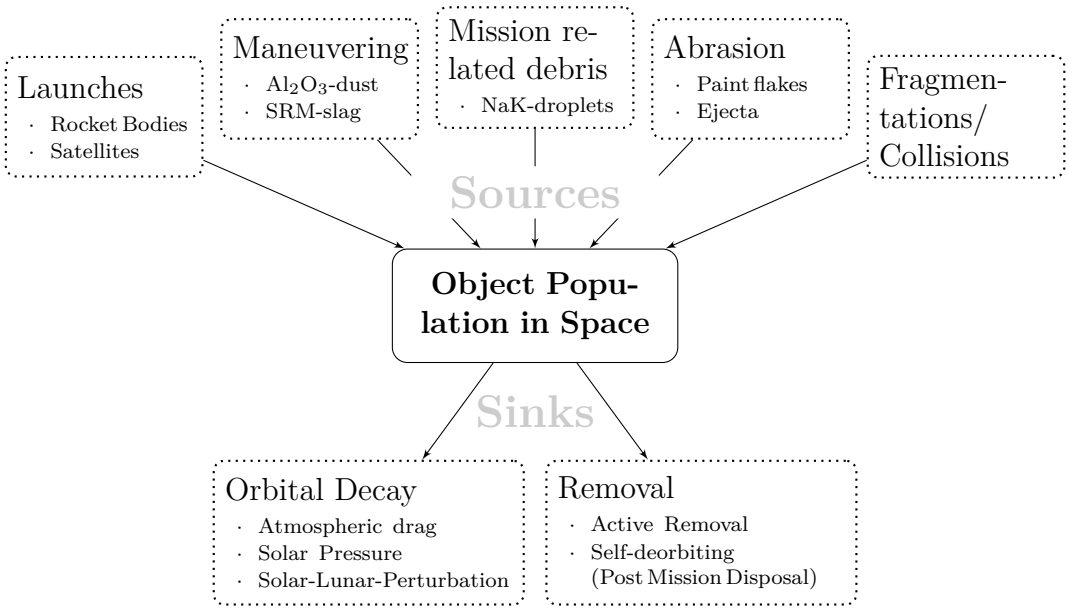

Figure 2.1: Sources and sinks for human-made objects orbiting Earth.

An overview of the traceable objects is provided by a network of 17 radar units and 8 telescopes, accessible through `www.space-track.org`. The given orbital data are extended by additional observations of different space agencies. Their calculations concerning unlisted objects vary. The National Aeronautics and Space Administration (NASA), for example, uses the LEO-to-GEO Environment Debris Model (LEGEND) and with such data about all known launches, two propagators, a satellite breakup model, and studies on returned objects such as parts of the Hubble Space Telescope (HST). The European Space Agency (ESA) uses the Meteoroid and Space Debris Terrestrial Environment Reference Model (MASTER) and/or the Debris Environment Long-Term Analysis Model (DELTA) and includes objects as small as 1 µm and 1 mm, respectively. In consequence of the different calculations, NASA mentions about 500 000 objects in the range of 1 to 10 cm [25]. Estimations performed by Wright [136], based on the Debris Risk Assessment and Mitigation Analysis (DRAMA) tool, expect about 750 000 particles in the same range. Table 2.1 shows suspected (1 - 10 cm) and measured (> 10 cm) data according to different references.

Table 2.1: Estimated amount of orbital debris according to different references. In 2012, pieces smaller than 1 cm were estimated to about 300 million.

	1 - 10 cm	**> 10 cm**	**Reference**
Number of objects orbiting Earth	750 000	22 000	Wright.2009 [136]
	700 000	24 000	Chen.2011 [15]
	500 000	22 000	NASA.2011 [25]
Objects in LEO	370 000	14 000	Wright.2009 [136]
	400 000	16 000	Chen.2011 [15]

The two following graphics display publicly available data of the Two-line Elements (TLEs) [110], retrieved June 2012. The index lists objects whose origin is known and whose launching state granted permission for the TLE's publication. As of today, more than 19 700 tracked objects are accessible. About 4 000 additional objects do not fulfill the requirements [42]. Following the TLE-catalog, the different kind of objects orbiting Earth are typed as fragments (about 66%), payloads (about 22%), and Rocket Bodies (R/Bs) (about 12%). The United States of America, the Commonwealth of Independent States (CIS), and China lead the box score in numbers of objects in space [73].

The distribution in the two figures is performed according to the objects' altitude, orbit inclination, and count within a designated area. Figure 2.2 displays all available objects of the TLE-catalog and reveals significant accumulation in lower altitudes. Figure 2.3 concentrates on orbits up to 2 000 km altitude. An accumulation of object accumulation is found in regions from 800 to 1 000 km altitude and 70 to 100 deg inclination. These

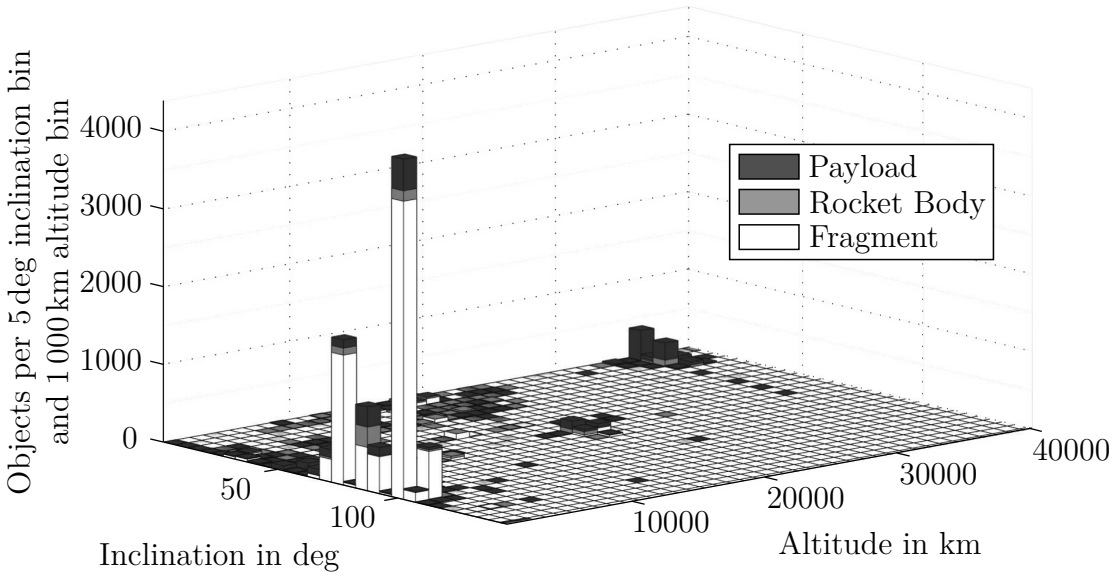

Figure 2.2: Distribution of different object types up to 35 800 km (GEO) as of June 2012. The inclination bin is set to 5 deg, the altitude bin to 1 000 km. [102]

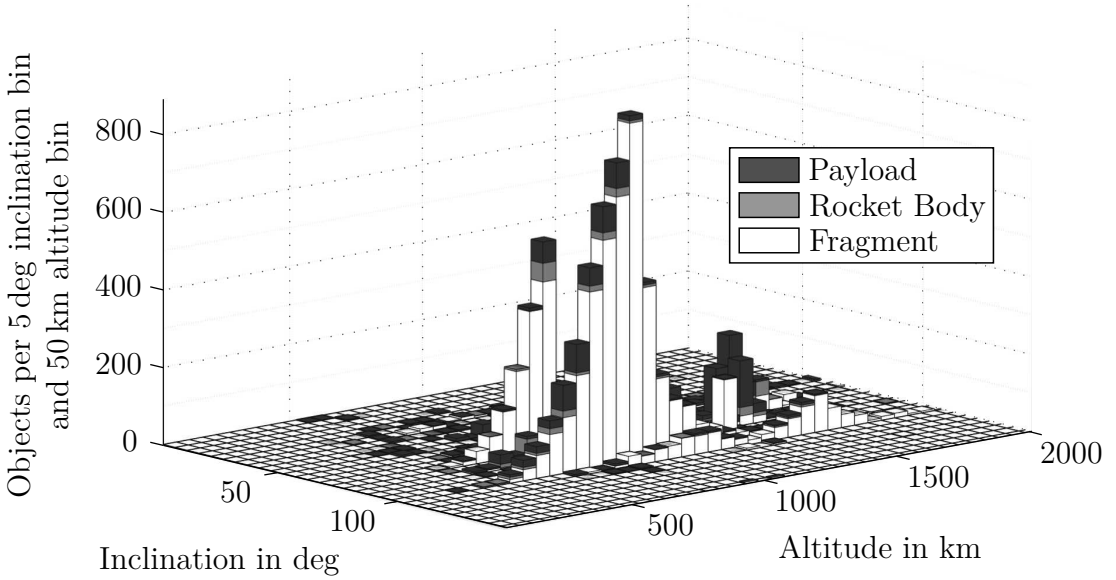

Figure 2.3: Distribution of different object types up to 2 000 km (LEO) as of June 2012. The inclination bin is set to 5 deg, the altitude bin to 50 km. [99]

orbits are highly endangered to generate a cascade-effect. The effect results in more debris generated by collisions among each other than by new launches or explosions. Once a cascade is initiated, it becomes even more difficult to mitigate the amount of debris for this region.

2.1.2 Size

Space junk, orbital debris, or space waste are terms used to describe space debris. The unofficial, though widely accepted classification of debris in space is arranged upon their diameter size into three categories with different challenges for mission operation:

(1)	Small sized objects:	$< 1\,\text{cm}$	Shielding in most cases sufficient
(2)	Medium sized objects:	1 cm - 10 cm	Shielding not sufficient
(3)	Large sized objects:	$> 10\,\text{cm}$	Visible by radar and telescopes

Category (1) Modern shielding, such as multiple walls or Kevlar, provide an adequate protection from small sized objects under most circumstances. Their impact will not lead to a hazardous fragmentation but can disable a satellite. Critical areas of the International Space Station (ISS), for example, are shielded for particles up to 1 cm in diameter, impacting with a collision velocity of 10 km/s [56].
Small sized particles have their origin in on-orbit fragmentation (e.g., explosions or collisions), NaK-droplets[1], copper needles[2], Al_2O_3-dust and Solid Rocket Motor (SRM)-slag[3], paint flakes due to surface degradation, and ejecta from impacts [38].

Category (2) Particularly dangerous for active satellites are medium sized objects. Neither an effective protection nor reliable monitoring exists or rather is affordable for this type of debris. Their origin is predominantly of fragmentation debris, but also of NaK-droplets as well as SRM-slag [38]. Their impact can lead to hazardous fragmentation and, thus, be a source for more particles amplifying the cascade effect.

Category (3) Larger objects are tracked with existing radar and telescope techniques. In case of a close approach, Collision- or Debris Avoidance Maneuvers (DAMs) can be performed - given that at least one object involved is maneuverable. Optical telescopes detect objects in distances above LEO and are able to identify particles as small as 15 cm at 36 000 km. For LEO-observation radar telescopes are in use. They are able to track particles as small as 2 to 5 cm at 1 000 km with the objects size estimated from the Radar Cross Section (RCS)[4]. As a global and intensive observation is required to detect all objects for the respective distances at such small sizes, the reliable tracking is limited to objects of 10 cm in diameter for LEO and to objects of about 1 m for the Geostationary Orbit (GEO) [42].

[1] from coolant release of nuclear reactors in space
[2] from the West Ford Projects in 1961 and 1963
[3] from solid rocket motor firings
[4] A target's RCS is a measure of its ability to reflect radar signals. It depends on the object's size, reflectivity of its surface, and the directivity of the radar reflection caused by the target's geometric shape.

2.2 Collision Probability

2.2.1 Theory

Prediction of Debris Development

Predictions concerning the future development of orbital debris date back as early as 1978. Warnings were given out by Kessler [60], predicting the mentioned cascade-effect. Multiple space agencies have adapted the warning and perform regular updates on their data. Figure 2.4, for example, represents NASA's investigations. For the graphic, future launch traffic is assumed to repeat the cycle of 1999-to-2006; with no explosion or deliberate breakups for future rocket bodies and payloads, except for collisions among each other. 100 Monte Carlo (MC) simulations were carried out and averaged. The results show a need for Post-Mission Disposal (PMD) and a removal (Active Debris Removal (ADR)) of at least 5 large objects per year, given that missions start in 2020 [71]. Considering, that the simulations ignored objects smaller than 10 cm in diameter and knowing about the impossibility to exactly predict years ahead the one object that is involved in the next upcoming collision, a removal of up to 15 large objects per year is implied [62].

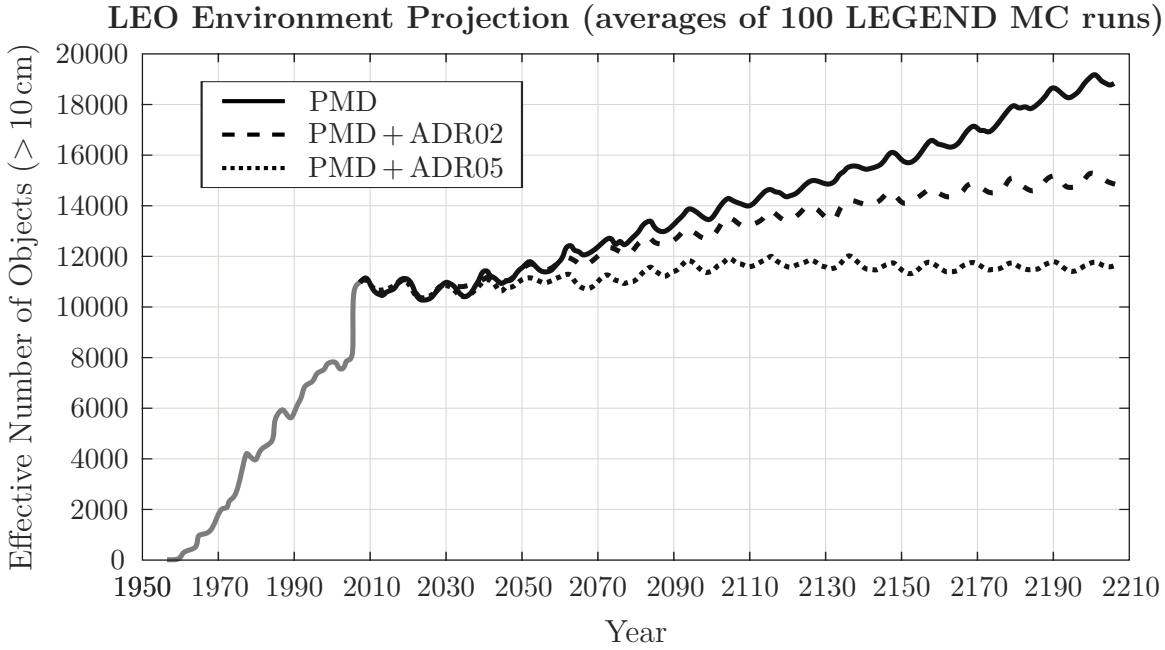

Figure 2.4: Three different remediation scenarios for space debris removal, issued in 2009. From top to bottom: Remediation within 25 years after end-of-mission (PMD) with 90% success rate and PMD + ADR with 2 and 5 large objects per year, respectively. [71]

Like the weather on Earth, space weather is difficult to predict, resulting in given probabilities rather than exact predictions. Recommendations for ADR are, thus, complicated and experts still argue about an official 'high-collision-probability'-ranking [11]. An attempt to find a common argumentation thread has been performed by the Inter-Agency Space Debris Coordination Committee (IADC) [52]. They compared studies that follow the sources and sinks plotted in Figure 2.1. As smaller particles are not tracked due to visibility challenges, simulation models are used to calculate existing population. The six involved parties and their respected models follow their own observations, data, and internally developed algorithms. Additionally, each model calculates predictions on the population development for the next 200 years. To generate comparable plots, any future launches were excluded. Table 2.2 lists the involved agencies, their model applied for the simulation and a short description of the model with the minimum object size for the predictions. All models are based on the NASA Standard Breakup Model, multiple MC simulations were run and averaged.

Table 2.2: Different simulation models of the IADC members, following Ref. [52] and [84].

Agency	Model	Description	Size
ASI[a]	SDM[b] 4.1	three-dimensional LEO to GEO simulation code	≥ 1 mm
ESA	DELTA v3.1	three-dimensional, semi-deterministic model, risk analysis	> 1 mm
ISRO[c]	KSCPROP[d]	valid for orbits with eccentricities less than 0.2	-
JAXA[e]	LEODEEM[f]	model for the low Earth orbit region	> 10 cm
NASA	LEGEND	modeling of the effectiveness of active debris removal, LEO-to-GEO	≥ 1 mm
UKSA[g]	DAMAGE[h]	three-dimensional, semi-deterministic LEO to GEO computational model implemented in C++	> 10 cm

[a] Agenzia Spaziale Italiana (ASI)
[b] Space Debris Mitigation long-term Analysis Program (SDM)
[c] Indian Space Research Organisation (ISRO)
[d] Kustaanheimo and Stiefel Canonical Propagation Model (KSCPROP)
[e] Japan Aerospace Exploration Agency (JAXA)
[f] LEO Debris Evolutionary Model (LEODEEM)
[g] United Kingdom Space Agency (UKSA)
[h] Debris Analysis and Monitoring Architecture for the Geosynchronous Environment (DAMAGE)

The study's conclusions confirm the instability predictions of the current LEO object population as displayed in Figure 2.4. All six IADC member models yield very similar qualitative results and in all cases the models predict a population growth. The average increase of debris is 30% in 200 years, driven by collision fragments from catastrophic

impacts[5]. The affected altitude is between 700 and 1000 km, a hazardous encounter is likely to occur every 5 to 9 years. The study also concludes that the compliance with existing national and international space debris mitigation measures will not be sufficient to constrain the future LEO object population. To stabilize the LEO environment, more aggressive measures need to be considered and implemented in a cost-effective manner. Especially the removal of the more massive non-functional spacecraft and launch vehicle stages must be realized [52].

Impact Energy

Regarding the impact colliding objects have on each other, the visualization displayed in Figure 2.5 gives an idea of the strength small particles can unfold: A bullet of about 4.5 cm in diameter and a velocity of 15 km/s, or with a diameter of about 7.2 cm and a velocity of 7 km/s, respectively, has the same energy as a kinetic energy penetrator used today. The penetrator's muzzle energy of 13 MJ results in a penetrating power of 81 cm armor steel at a distance of 2 km [63]. Knowing objects in LEO have relative velocities up to 15.8 km/s, no doubt can be left about the threat space debris has on active satellites in case of a collision.

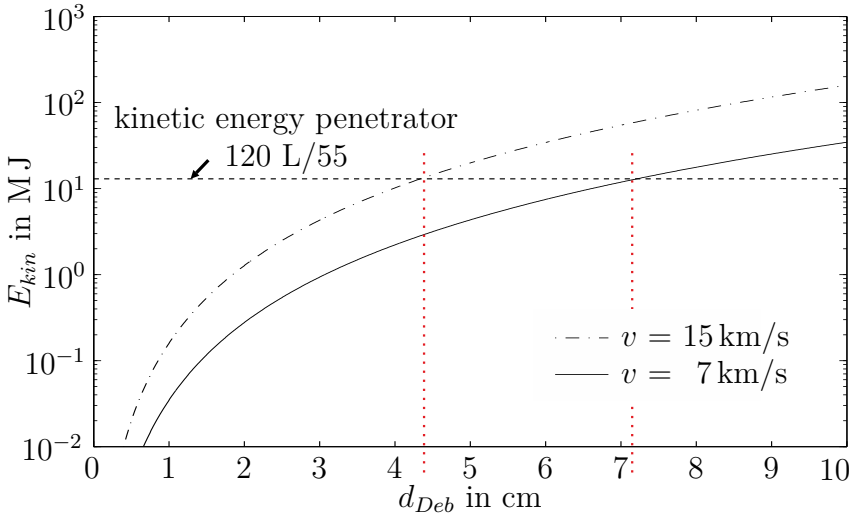

Figure 2.5: Development of the kinetic energy (E_{kin}) over the increasing diameter of the debris (d_{Deb}) at a velocity (v) of 7 km/s and 15 km/s, respectively. The dotted line represents a kinetic energy penetrator ("Wuchtgeschoss") with a caliber of 120 (120 mm diameter of the projectile) and a muzzle velocity of 1750 m/s, fired by an L/55 gun barrel (length of 6 600 mm).

[5]with the ratio of impact energy to target mass exceeding 40 J/g

2.2.2 Experience

Impact History

The presented predictions include, but are not limited to, the known impact history. As soon as an object is expected to converge as close as a few kilometers to an operational satellite, measures to observe its trajectory in more detail are pursued. The actions include updated tracking data and a shorter propagation period. Often, a smaller collision probability is concluded with no need for a DAM. If the involved objects, however, are predicted to converge closer, a maneuver is suggested to the operators[6] [72]. They decide to either take the risk of an impact or to move the satellite.
Table 2.3 lists the 4 known and 14 suspected collisions. The Anti-Satellite (ASAT)-test of Fengyun-1 marks the one intentional collision resulting in a long-term contamination of LEO. The suspected events are very likely to result from space debris. In addition to this data, tens of anomalous fragmentation with unknown source have occurred [70].

Table 2.3: Known and suspected collisions in Earth orbit, collected from Ref. [70].

Date	Objects involved	Altitude	Fragments	Collision
23.12.1991	Cosmos 1934 / Cosmos 926 Debris	980 km	2	known
24.07.1996	CERISE spacecraft / Ariane fragment	685 km	1	known
28.08.1997	NOAA 7 / uncataloged debris	830 km	3	suspected
16.03.2002	JASON-1 / uncataloged debris	1336 km	2	suspected
21.04.2002	Cosmos 539 / uncataloged debris	1370 km	1	suspected
15.12.2004	DMSP / uncataloged debris	840 km	56	suspected
17.01.2005	Thor-Burner 2A / CZ-4 fragment	885 km	3	known
22.06.2005	Cosmos 3M / uncataloged debris	950×1015 km	1	suspected
14.02.2006	Vanguard 3 / uncataloged debris	500×3300 km	-	suspected
03.12.2006	Delta II / uncataloged debris	685×790 km	-	suspected
11.01.2007	Fengyun-1 / ASAT-test	850 km	>3000	intentional
10.11.2007	UARS / uncataloged debris	500 km	4	suspected
10.02.2009	Iridium 33 / Cosmos 2251	790 km	>2000	known
30.08.2009	Cosmos 192 / uncataloged debris	745×760 km	20	suspected
22.01.2013	BLITS / uncataloged debris	832 km	1	suspected
22.05.2013	NOAA GEO3 / uncataloged debris	GEO	-	suspected
23.05.2013	NEE-01 Pegaso / uncataloged debris	627×654 km	-	suspected
07.06.2014	Iridium 47 / uncataloged debris	775 km	10	suspected
30.11.2014	Iridium 91 / uncataloged debris	775 km	4	suspected

[6] DAMs can be performed with about 80% of the operating satellites in LEO [68], assuming at least one of the objects involved in the forthcoming collision is maneuverable.

Debris Avoidance Maneuver of the International Space Station

In human space flight, measures to perform DAMs are taken as soon as the risk of collision exceeds 1/10 000. This includes evasive actions or evacuation of the crew, the latter in case of insufficient time for a DAM. Depending on the mission and its progress, spacecraft accept higher levels of risk on the order of 1/1000 in general.

Figure 2.6 displays the increasing number of DAMs of the ISS over the years. The orbit in about 400 km altitude is less burdened with debris then others. It is, however, crossed by descending pieces and, thus, endangered - delayed in time to the actual fragmentation event as the plot of cataloged objects shows.

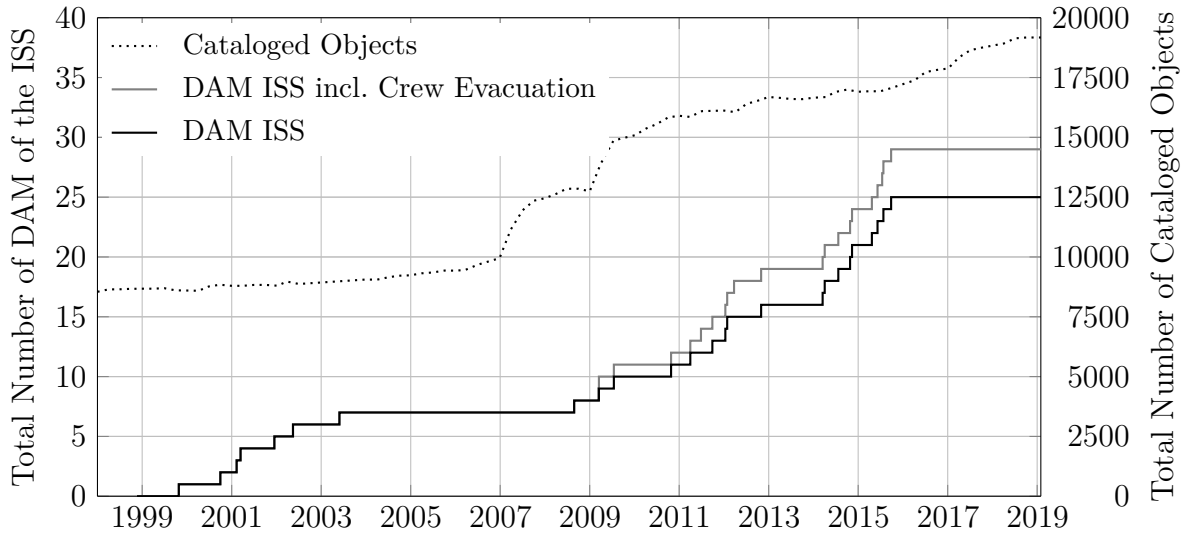

Figure 2.6: Totalized number of Debris Avoidance Maneuvers (DAMs) of the International Space Station (ISS), 1998 - 2019. Additionally, displayed are the crew evacuations and cataloged objects for the same period. The data is collected from Ref. [70] and [57].

Since November 20th, 1998 - the launch of the first module of the ISS, Zarya - the Space Station was endangered 29 times in total, 4 times of which the threat was detected too late, so the crew had to evacuate into the Soyuz capsule. The first period of no events from 2003 to 2008 is accredit to an improved conjunction assessment process: More precise determinations of the ballistic coefficient along with more accurate modeling of the atmosphere have reduced the uncertainties and, thus, false alarms [57]. The second period of DAM-free events started in late 2016. Newly implemented processes allowed the ground personal once again to predict trajectories at a higher accuracy and to react faster. Even though the required DAMs have stagnated for now, the danger of a hazardous collision of the ISS with debris is still present. Any avoidance optimizations have their physical limits in the actual size of the involved objects. After all, space debris keeps passing the ISS' orbit at a growing number.

2.3 Mitigation Measures

2.3.1 Surveillance

Rather than observing each and every object in space permanently, a trajectory of a known object is related to it when the object passes through a radar's field of view. This way, some objects, even when noticed during their passage, stay unassigned as no knowledge of their origin or trajectory is available. Moreover, a trajectory needs to be assigned to the same object at least twice to define the objects parameters. Investigations, therefore, concentrate on an improved tracklet association [117, 116], an increase of surveillance through a scheduled algorithm for a more reliable observation of specific particles [50], and the limitation of observation errors [113]. Those measures intend to increase prediction capabilities to warn operators of active satellites and give recommendations to perform avoidance maneuver. Even though observation methods differ for LEO and GEO, the applications of the developed algorithms are transferable.

2.3.2 Official Guidelines

The IADC as of today counts 12 space organizations[7] [51]. After 9 years of existence, first recommendations concerning the mitigation of space debris were published in 2002. In 2007 they were verified by the United Nations Committee on the Peaceful Uses of Outer Space (UNCOPUOS) in their main features [124]. The guidelines comprise seven main points covering space system design, launch, operation, and disposal:

Guideline 1: Limit debris released during normal operations.

Guideline 2: Minimize the potential for break-ups during operational phases.

Guideline 3: Limit the probability of accidental collision in orbit.

Guideline 4: Avoid intentional destruction and other harmful activities.

Guideline 5: Minimize potential for post-mission break-ups resulting from stored energy.

Guideline 6: Limit the long-term presence of spacecraft and launch vehicle orbital stages in the low Earth orbit region after the end of their mission.

Guideline 7: Limit the long-term interference of spacecraft and launch vehicle orbital stages in the geosynchronous region after the end of their mission.

[7] ASI, British National Space Centre (BNSC), Centre National d'Etudes Spatiales (CNES), China National Space Administration (CNSA), Deutsches Zentrum für Luft- und Raumfahrt (DLR), ESA, ISRO, JAXA, NASA, National Space Agency of Ukraine (NSAU), Russian Federal Space Agency (ROSCOSMOS) and Canadian Space Agency (CSA)

The published guidelines present recommendations and are, therefore, not mandatory to be implemented. For that reason, ESA published its own requirements in April 2008, stating management, design and operational aspects without whose compliance a launch will not be allowed to proceed. An understanding of Guideline 6 agrees on residual whereabouts of satellites in space for 25 years after their end-of-life (cf. Ref. [33] and Ref. [128]).

A common significant feature of the various space debris mitigation guidelines is the focus and emphases on the mitigation (or reduction) of the rate at which new pieces of space debris are generated during the conduct of space activities. However, the established requirements focus on the expansion rate of *new* space objects and their generation. The impact of those measures on a long-term use of outer space for humankind is limited and needs further support by the actual removal of existing pieces of debris as stated in Section 2.2. Being aware of the years it took to agree on the existing guidelines, the implementation of respective ADR guidelines will take a long time.

2.4 Active Debris Removal

2.4.1 Challenges

The challenges that come along with ADR include a detailed cost analysis, new ADR policies and guidelines, a reliable source of funding, legal and liability issues, and the development of viable removal techniques. A brief overview in the respective topics is given for integrity of the subject.

Cost Analysis Aspects that need attention within a cost analysis are the costs for long-term removal missions, the costs of lost mission time due to avoidance maneuvers and the costs of supplying the satellite with enough propellant to perform those maneuvers. All these aspects differ from spacecraft to spacecraft. Removal missions depend on the targeted object(s) and the intended achievements. Those achievements could, for example, limit the targets' orbit to meet the required end-of-life residence time in space to 25 years, or actively guide the target into Earth's atmosphere for a controlled re-entry. The costs of the time lost during a DAM must be calculated by the operator. They might even change for different periods as, for example, specific areas needing intense observation for limited time only. Regarding the propellant used for a DAM, the operator will have less reserves at the mission's end. Mission goals might be out of reach with multiple DAMs performed. After all, operators must decide on the risk they are willing to accept.

ADR Policies and Guidelines It took 9 years for the IADC to develop the existing guidelines for the limitation of creating new space debris and another 5 years for a final verification by the UNCOPUOS [124]. To further reduce the growth rate of debris particles, including ADR as an additional chapter or develop new guidelines is necessary. The discussion about the dual use of ADR technologies will be most difficult. These technologies are likely to be militarized in acts of spying, interference, or other non-agreed interactions. Especially with on-going ASAT tests by Russia, China and the United States [133], transparency is requested when it comes to the actual removal of space debris. As only the launching state is officially allowed to interact with its satellite, one idea is to first demonstrate ADR capabilities on one's own satellite [35]. In a later step, this capability could be offered as service to other launching states. Another idea is the foundation of a leading organization that coordinates such missions [65]. By sharing information about developments, may that be prior notification of missions and/or increasing the public awareness through media presence, trust will be built, and suspicion avoided.

Funding The active removal of debris must be performed for multiple decades when considering the removal of a few high-potential objects per year. Cost estimations vary for the size and number of objects removed, as well as for the technique in use. They start at $10 M per object per year, considering large-sized objects [78]. Depending on the final set-up of the responsible party - e.g., performed by the government or by a joint venture - multiple funding sources come into play: (1) The space agencies themselves fund a project, which gives their partner states the opportunity to have their debris removed. (2) Insurance companies may be interested as they could provide a safer access to space. (3) International taxes could be raised, reminding the people that keeping space acceptable is a global challenge, which must be solved as a community with everyone taking its part. (4) Donations may help as support, as people would be able to give on their own terms, rather than be forced by government. A combination of those funding sources will most likely provide a solid basis for a business plan that grants funding for the required time.

Legal and Liability The Outer Space Treaty (OST) from 1967 [125] frames legal and liability properties of satellites and objects in space. It states the liability and retention of jurisdiction of the launching state for its space objects while in outer space. As a result, no third party is allowed to remove an object without former consultation with the launching state. As long as no framework has been set to provide legal security, interested parties will have to concentrate on the removal of their own objects. However, with the United States passing the U.S. Commercial Space Launch Competitiveness Act on November 25th, 2015 [77], allowing their citizens to privately mine asteroids and,

thus, bypassing the OST: While the OST states that no celestial object can be claimed ownership upon a nation, the act addresses the mined parts of the body. It might be possible to find similar regularization for space debris. A transformation of such bypassing procedure could include a consensus on the legal definition of space debris. The debris could then be officially allowed to be removed by a third party.

Technical Challenges Existing ideas on how to remove uncontrolled objects from space are investigated, with the most promising ones described in Section 3.4. None of these techniques have been tested in space. With ADR required for a stable environment, this thesis supports the technical approach of the problem. First, criteria for a qualified selection of the mission design must be set. As stated before, 5 to 15 large objects must be removed per year. To limit costs and, thus, be most efficient, multiple targets should be de-orbited during one mission. When de-orbiting large objects, high probabilities exist that some parts survive the re-entry. Therefore, the de-orbit needs to be performed onto a safe area with humans unscathed. In Section 3.1.2 multiple approaches are analyzed accordingly. To react to possible failures and allow for an abort, the spacecraft design needs to provide enough resources for multiple berthing maneuvers per target. The challenge of close vicinity must be addressed as well as limitations for reaction time in case of unexpected events. This said, the target is unguided and most probably in a tumbling state. The removal technology, thus, must address the stabilization for the controlled re-entry. Additionally, chaser and target are required to remain unscathed during the docking as the generation of new debris is the least favorable situation when aiming to limit its amount. The mentioned challenges shall guide the mission design for the presented removal mission, its spacecraft design, and failure management.

2.4.2 ADR Concept Studies

With the threat of space debris increasing, various studies, technologies, and derived concepts for on-orbit servicing or debris removal are under development. A representative selection is listed in Table 2.4 with Technology Readiness Level (TRL), Integration Readiness Level (IRL) and System Readiness Level (SRL) following official ratings.

The concepts presented differ according to the targeted object size, the way of changing the targets' orbit or status, and their TRL. For most of them, an IRL or SRL is not yet assigned; however, the general concept can be derived. Advantages and disadvantages exist for each of them. A benefit, which is addressed by 4 out of 9 concepts, is, for example, the formerly stated desired removal of multiple targets. A drawback of 8 of them is the limited reusability of the implemented system as this makes an abort and retry nearly impossible. The adaptivity of most of the concepts to the targets' type and,

Table 2.4: Concepts for active debris removal. The applied Technology Readiness Level (TRL), Integration Readiness Level (IRL), and System Readiness Level (SRL) follow official ratings.

	Clamp Study [129]	Adhesives [94]	Agora [66]	Harpoon [9]	ADRAS-1 [5]	Biomimetic [16]	PacMan [46]	Autonomous Docking [122]	Net [39]
TRL 2016	3	6	2	3	-	2	5	2	6
IRL 2016	-	7	-	-	-	-	-	-	-
SRL 2016	-	2	-	-	-	-	-	-	-
Reusability	No	Yes	Partly	No	Partly	Partly	No	No	No
Multiple Removal	No	Yes	Yes	No	Yes	Yes	No	No	No
Target type	All	All	All	All	All	All	Small S/Cs	R/Bs	All
Complexity of Design	High	High	High	Normal	High	High	Normal	Very high	Normal

thus, its size allows for a wide range of application and is favorable. However, a high complexity of design levels this benefit.

After working through the listed literature concerning space debris and its active removal, including the existing concepts, it is decided to develop an additional concept standing on its own. This way, considerations can be made from scratch, allowing formulation of an over-all concept that is tailored to the technical challenges mentioned. By understanding the nature of the mission, and designing the corresponding spacecraft, the challenges of the close approach and safety requirements can be addressed with a solid basis for discussion.

3 Mission Design

With the need for ADR emphasized and technical challenges stated, a mission design is created. General consideration on the actual size of possible targets and their re-entry are leading to an identification of suitable objects. Missions that performed comparable operations are introduced to provide their lessons learned. Available technologies for capture are discussed thereafter with the final concept concluding this chapter.

3.1 General Considerations

3.1.1 Long-term vs. Short-term Protection

Large objects provide the prime source for a cascade-effect and, thus, influence the population growth on a long-term perspective. Medium sized fragments, however, are identified as the main threat to operational spacecraft in general. They should be targeted when aiming for a short-term protection of the space environment. Theoretically, both, long- and short-term protection, are required to stabilize the environment. As stated earlier, small sized objects of 5 mm to 1 cm make up most of the population - 79.5% of all objects. The medium sized objects from 1 to 10 cm account for about 20% of them, large objects combine 0.5%. Figure 3.1 shows the cumulative size distribution of the LEO-crossing objects. Marked are the threats for Spacecraft (S/C) today and drivers for the future. The prospective environment is highly influenced by large objects, as they have the capability to create more particles occupying an even larger area and feeding the number of small and medium sized debris.

Realizing space around Earth is a limited resource just like Earth itself, long-term protection and availability needs to be ensured by the current population. Moreover, avoiding a threat should always be the priority before reacting to it. For this thesis, large human-made objects in the most critical areas around Earth are, thus, targeted. To stop, or at least slow down, the near-term development of debris in space, the focus is put on their short-term removal.

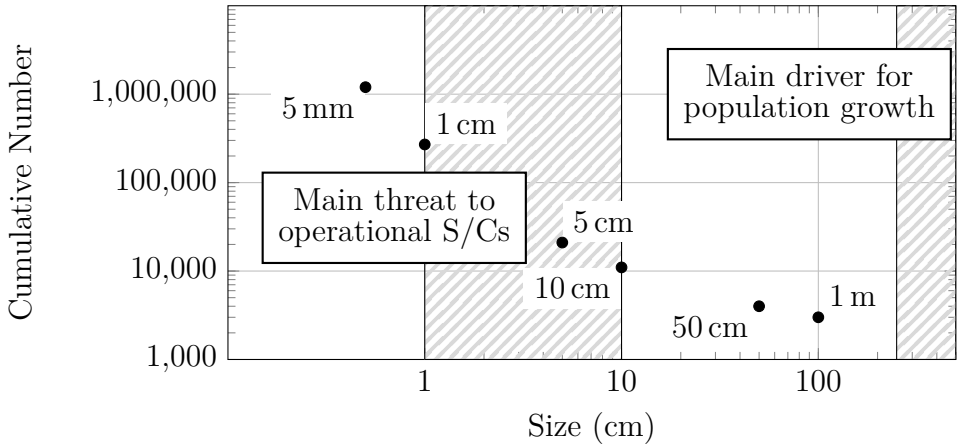

Figure 3.1: Cumulative size distribution of the LEO-crossing objects in 2011 after Ref. [69].

3.1.2 Active vs. Passive Removal

The preferred maximal residual time in space of 25 years after completion of mission is an add-on to the guidelines mentioned. In altitudes above 550 km, this lifetime is exceeded if no further activity takes place[1]. Any removal should, thus, guide an object to an altitude below 550 km to comply with these guidelines. An alternative is the re-orbit into a less endangered orbit. Aiming for long-term protection of space, this alternative will not be considered, as it forwards the problem rather than solving it.

In 2015, 461 objects (out of 17 385) have disappeared from the Space Surveillance Catalog [110] and are considered to have descended. 327 of them are labeled to be small with an RCS smaller than 0.1 m^2, 63 of them are larger than 1.0 m^2 in RCS and 45 are in between. The remaining 26 are of unknown size. Figure 3.2 displays the last recorded position of the 63 large objects (average mass: 1.4 t). None of the decays was reported to have harmed any property. Especially with a slow descent and a small size, the vaporization of the descending object in the atmosphere is most likely. Depending on the re-entry trajectory and the material the object is made of, some parts, however, can survive the re-entry. The probability for survival increases for objects exceeding an initial mass of 1 t [48]. Since the beginning of spaceflight, more than 30 reentries into inhabited areas have been officially reported.

The probability of reentering objects falling on land or water was calculated by Matney in 2012 [76]. Considered were the cases of a single impact point and a breakup scenario. The latter spread over a length of 800 km with no width and followed the direction of the satellite's trajectory. Depending on the object's inclination, the probability to land

[1] cf. Ref. [135] - for objects with a drag coefficient of 2.7, a mass of 1 t and a cross sectional area of 2 m^2

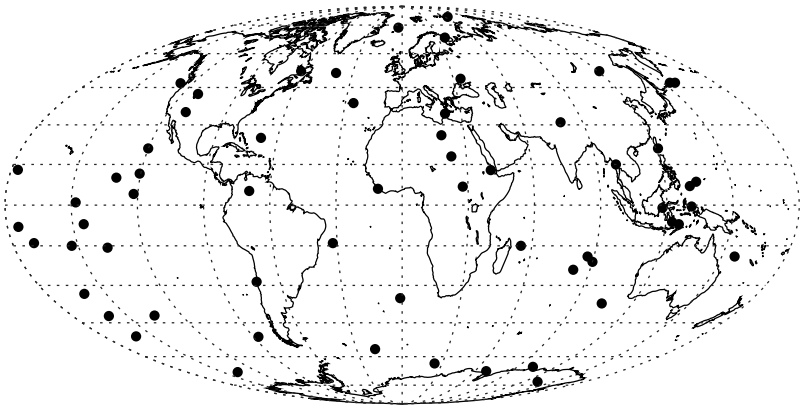

Figure 3.2: Last recorded position of the 63 large objects in 2015 (cf. Ref. [110]). Each black dot represents a decayed object larger than 1.0 m^2 in RCS. 36 of them are rocket bodies.

completely in water varies, accordingly, from 70% to 79% for the single impact point and 59% to 65% for the breakup scenario. In both predictions, Antarctica was counted as water surface. At 83° inclination, for example, the probability to impact on land is about 24% for a single impact point and about 37% for a break-up scenario of this size. With about 4% of Earth's landscape inhabited, the probability to hit humans or property is of 1.48%. When aiming to remove a maximum of 15 large, non-vaporizing objects per year, casualties can be expected to occur at least every 4.5 years if no further precaution is taken. Official considerations performed for a reentering object allow for a probability of 0.5 per mil, not exceeding the officially accepted probability of 1/1 000 [24]. Taking the recorded non-vaporized objects into account, the probability of harming life and property on Earth due to uncontrolled impacts by human-made space objects cannot be neglected. It is, therefore, recommended and pursued within this thesis, to follow an active and controlled removal. As a footprint-area of at least 800 km by 30 km width can be assumed [114], the Pacific Ocean, presenting the largest uninhabited area available for an inclination of 83°, is chosen as preferred landing site for the mission.

3.2 Target Identification

Objects qualifying as major drivers for the generation of new fragments should be removed first. They are found at inclinations from 70 to 100 deg and altitudes from 800 to 1000 km (cf. Figure 2.3). With no official 'high-collision-probability'-ranking for those drivers available, the approach proposed by Klinkrad [61] is followed with slight adaptions. The formulae and data are transformed into a filter for these high-risk objects by Weigel [134] and are adapted for the purpose of this thesis. In the following, the filter and the extensions made are described. The last part presents the resulting targets.

3.2.1 Filter Process for High-Risk Objects

The script to filter high-risk objects describes a sphere representing the LEO environment. Its orbits around Earth are set from 550 km to 2 000 km. Both values differ from the ones proposed by Klinkrad [61]: Objects in lower orbits are likely to de-orbit within 25 years due to atmospheric drag, a significant accumulation in higher orbits is not recorded.
The calculations focus on the impact flux in inertial control volumes within the LEO-sphere and the obtained kinetic flux. The impact flux F is derived from

$$F = v \cdot D, \tag{3.1}$$

with v presenting the objects velocity and D the spatial density in the given control volume. The initial control volume is displayed in Figure 3.3 and determined by:

$$V_{r,k} = \frac{2}{3}\left(3r_r^2 + \frac{1}{4}(\Delta r)^2\right)\cos\delta_k \sin\left(\frac{\Delta\delta}{2}\right)\Delta\alpha\Delta r, \tag{3.2}$$

with r, and k presenting the indices in radial direction r_r and declination δ_k, $\Delta\alpha$ forming a full circle of 2π. The radial direction range Δr is set to 10 km, the declination range $\Delta\delta$ to 2 deg. To give the objects an order, the object's resident probability within the control volume, derived from its Keplerian elements, is multiplied by its flux. This probability reflects the time between two cell passage events relative to the orbit period. For more details on the calculation see Klinkrad [61].

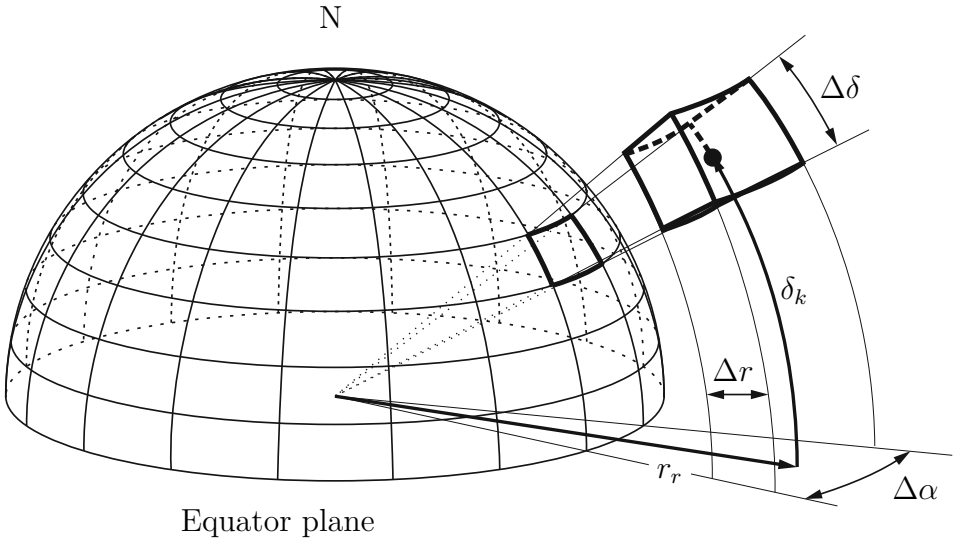

Figure 3.3: Control volume cell in respect to Earth's center.

High-risk objects in the context of this thesis are defined as objects with a large impact on the debris population in space when colliding. As the creation of debris depends on the hazardousness of the collision, the results of the object's initial flux are multiplied with its kinetic energy, resulting in the kinetic energy flux as extension of the filter for the objects. This way mass, relative velocity, and distribution are considered and with such not the collision itself, but the impact on the environment. As a result, the objects kinetic energy flux is chosen as indicator for the risk of an object and a ranking is derived accordingly.

The information concerning the included objects are extracted from three different catalogs: The TLE data is provided by `www.space-track.org`, containing information about the objects Keplerian elements, name, designated number, object type and RCS. Information on the size (length, height, depth) and mass of an object is extracted from the Database and Information System Characterising Objects in Space (DISCOS)-database and the Union of Concerned Scientists (UCS) satellite database. For unknown or unavailable data within the catalogs, further research is performed to assign officially provided parameters to the respective objects. The original filter code by Weigel [134] is extended by the object's actual mass rather than assuming an averaged density. In about 30% of the cases, an actual size could be added. In cases of unavailable data, a density[2] of 128 kg/m^3, default values of 0.3^2 m^2 for the cross-section area, and 0.3^3 m^3 for the default volume are assigned. Active satellites are removed from the list as they are not considered as debris (yet). A detailed list with parameters such as mass, inclination and altitude or the name of the 'Top 200' is given in Table B.1. With the following section, the list is re-interpreted with specific targets chosen for further investigation.

3.2.2 Multiple Target Solution

The intended removal of 5 to 15 large objects has been stated. The high-risk object list is therefore analyzed according to the objects distance to each other. The analyses concerning the required Δv - and with such required propellant for orbit changes - are performed for in-plane and out-of-plane maneuvers. The Δv requirements are displayed in Figure 3.4 and refer to a circular orbit of 83 deg inclination, a Right Ascension of the Ascending Node (RAAN) of 200 deg and an altitude of 980 km. Accordingly, the change of 0.4 deg with an out-of-plane maneuver and a 100 km change in altitude, both, require a Δv of about 50 m/s. The boundaries for a multiple target solution are, thus, set to ± 0.2 deg and ± 50 km, to search for suitable targets.

[2]The average of 1 000 known spacecraft.

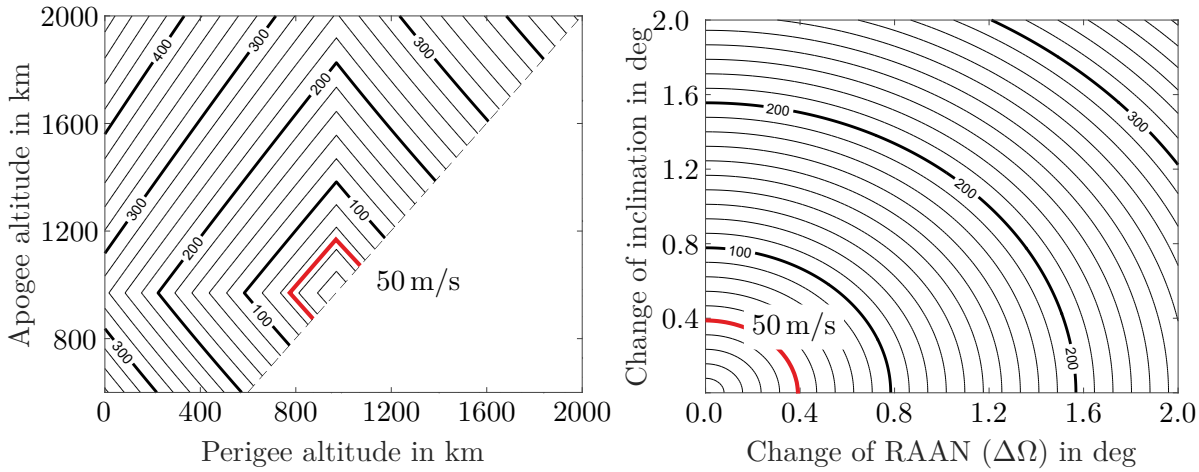

Figure 3.4: Δv requirements in m/s for in-plane (**left**) and out-of-plane (**right**) maneuvers. For the maneuvers from the circular reference orbit to different (elliptical) orbits Hohmann transfers are applied. The red lines mark a 50 m/s-boundary.

With the chosen boundaries, the 'Top 200' list is re-interpreted. While mainly SL-16 R/Bs and non-functioning satellites lead the original 'Top 200' list, SL-8 R/Bs result as most promising candidates when it comes to multiple target removal. The advantage of a similar geometry of the targets has furthermore a positive impact on the design of the capturing part of the mission. Focus can be put on one type of object, which again eases the construction and testing.

The SL-8 R/Bs accumulate in specific orbits, making them quite eligible for a multiple target removal mission. Figure 3.5 displays their distribution. The $\Delta\Omega$s of SL-8 R/Bs listed in the 'Top 200', however, sum up to at least 6.4 deg. To minimize this range, all known SL-8 R/Bs are investigated according to their position in orbit relative to each other. This way, at least ten cluster á five targets are identified with a maximum $\Delta\Omega$ of 4.9 deg. To specify a reference mission, the targets of the cluster with the lowest $\Delta\Omega$ are chosen for further investigation. They are marked in Figure 3.5 by a red circle, their data is given in Table 3.1. The resulting scenario focuses, thus, on a circular orbit with an inclination of 82.9 deg, an altitude of 980 km, and a RAAN of 162 deg.

As a $\Delta\Omega$ of nearly 2 deg exceeds the aimed range of ± 0.2 deg, other measures will have to be found to shuttle from one target to the other in a propellant-efficient way. One solution is using the J_2-drift, or $\dot{\Omega}$, calculated by

$$\dot{\Omega} = -\frac{3 \cdot \sqrt{\mu} \cdot r_e^2 \cdot J_2}{2\sqrt{a^7} \cdot (1-e^2)^2} \cdot \cos i. \tag{3.3}$$

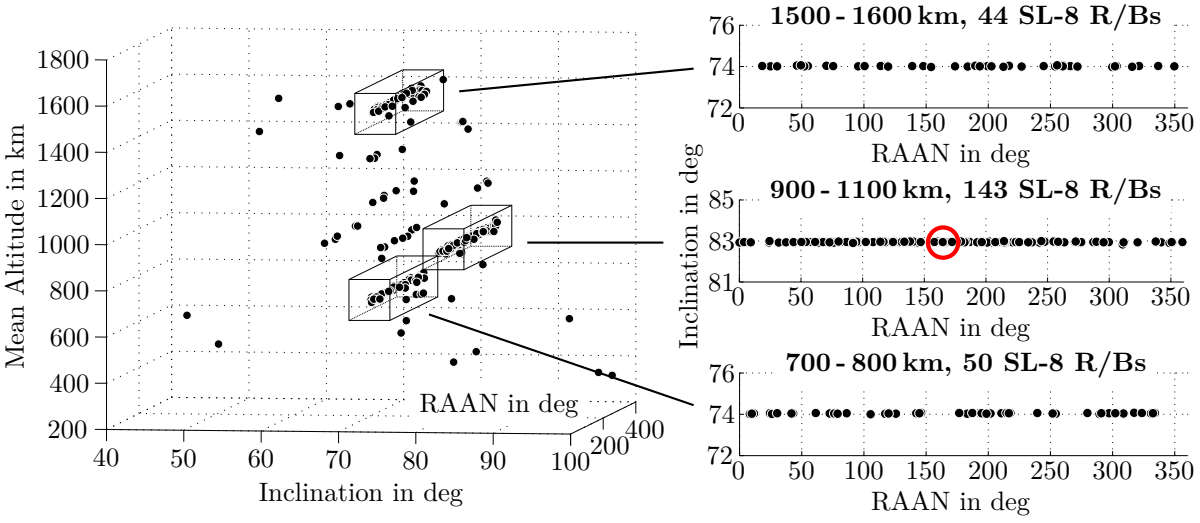

Figure 3.5: Target identification process: All known 292 SL-8 R/Bs in low Earth orbit as of June 2014 (**left**) and SL-8 R/B distribution according to the designated boxes (**right**). The (red) circle frames the five R/Bs of the reference mission. [100]

r_e of Equation 3.3 presents the Earth's radius, J_2 the Earth's second dynamic form factor, and μ its gravitational parameter. a is the semi-major axis, e the eccentricity of an orbit, and i the inclination. The drift is created by the non-uniform gravitational field of the rotating Earth and given in Table 3.1 for further considerations.

Table 3.1: Orbital data of the targeted SL-8 R/Bs. The displayed values are taken from the TLE-data set, dating January 13, 2013, and postulated to January 15, 2013 to equalize different recording times.

Norad-ID	Altitude in km	Incl. in deg	Ecc. e	RAAN in deg	Launch date	$\dot{\Omega}$ in deg/s
11668	984.557	82.947	0.002	160.727	14.01.1980	-8.568E-06
22591	978.758	82.931	0.002	162.040	01.04.1993	-8.611E-06
13128	979.646	82.926	0.003	162.500	08.04.1982	-8.613E-06
17240	991.828	82.933	0.003	162.795	17.12.1986	-8.556E-06
7350	962.313	82.939	0.002	163.412	27.06.1974	-8.669E-06

3.2.3 Target Properties

SL-8 R/B is the United States Department of Defense (US-DoD) designation for Kosmos launcher, with the Sheldon designation C-1 [108]. The Soviet Union rocket bodies were launched between 1964 and 2010. They are also known as *Kosmos 3M Upper Stage* or *S3M Upper Stage*. Their engine is the Khim-Mash 11D49, an engine allowing the stage to steer under the assistance of four Vernier thrusters. Figure 3.6 and Table 3.2 give an overview on the upper stage's details. The dry mass of the R/B is about 1430 kg. Residual propellants can range from 0 to 15% of the initial propellant load, for example, due to the configuration of the pipes in use or the mixture ratio [12]. The SL-8 R/B has a quite simple geometry and an optimal propellant exploitation[3]. The lower case of that range is, thus, adapted: 170 kg residual propellant are assumed, presenting slightly less than 1% of the initial propellant loading. The SL-8 R/B's mass for further calculations is, therefore, estimated to 1600 kg.

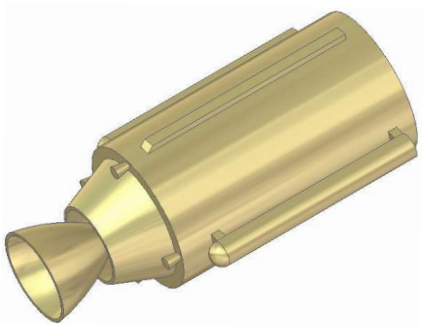

Figure 3.6: Computer-Aided Design (CAD)-model of the SL-8 R/B.

	SL-8 R/B
Length h	6.585 m
Diameter d	2.44 m
Lift-Off Weight $m_{\mathrm{Lift-Off}}$	21.20 t
Propellant Weight m_{Fuel}	18.41 t + 1.36 t*
Engines	1x 11D49
Propellant	UDMH / AK-27I
Total Thrust (vac) F	157.5 kN + 6.4 kN*
Specific Impulse (vac) I_{SP}	2972 s
Burn Time t	347.5 s
Area Ratio ϵ	103.4

Table 3.2: SL-8 R/B specifications [13]. *incl. Vernier-Engine

3.2.4 Tumbling Rate

Uncontrolled objects in space are most likely to start tumbling at some point. Considering the active removal of such object, this motion needs to be compensated for by the serving spacecraft if Rendezvous & Docking (R & D) shall take place. To plan and develop proximity and docking operations, knowing the tumbling rates at an early stage is required. Available determination types must be combined to receive the best results.

[3]The SL-8 R/B performed 424 successful missions, hardware updates resulted in the optimal exploitation of propellant.

Determination On-Ground Determination of a rocket body's tumbling from ground applies telescope data. The provided light curves depend on a target's orientation and rotation state and are, thus, constantly changing for a tumbling object. Cowardin [17] had the idea to determine the tumbling rate of SL-8 R/Bs in an orbit of about 450 km and 980 km, by comparing scaled on-ground measurements of a mockup with actual telescope data. Three potential rotational movements, which are spin-stabilized rotation along the longest axis, end-over-end rotation, and a 10 deg 'wobble' out of the Center of Mass (CoM), were analyzed to find consensuses with the actual data. As a result, no spin-stabilized objects where found and a separation between the 'wobble' and the end-over-end rotation could not be defined. Another study, performed by Praly [103], investigated Ariane upper stages in orbits around 700 km. For kinematic observation precession in the range of 0.1 deg/sec tracking and imaging radar was applied. The conclusion suggests "that one can expect debris to have only low angular rates after a few years in space." No actual numbers are given, and none were found in further literature. Before the actual launch of an ADR-mission, more investigation is, therefore, required to ensure the targets movements do not exceed the capabilities of the spacecraft. For this thesis, a tumbling rate with a maximum of 3 deg/sec in the according x-, y-, and z- axes is assumed. The rate follows investigations performed for the Environmental Satellite (Envisat), which was observed to spin at a rate of 2.67 deg/sec in 2013 [115].

Determination in Space Determination of a rocket body's tumbling performed by the rendezvousing object has the advantage of small distances. Smaller distances allow for higher resolutions and a higher precision of the observation. Challenges can derive, for example, from changing illumination or weird tumbling motions. Details on the target's movement shall be observed from space for this thesis to calculate the approach trajectory accordingly.

3.3 Mission Concept

The concept of operations describes the characteristics of the mission proposed. Already conducted missions with comparable maneuvers are presented to provide lessons learned. The mission's architecture and the resulting removal scenario are presented thereafter.

3.3.1 Review on Conducted Rendezvous and Docking Missions

The mission as of now aims for the controlled removal of SL-8 R/Bs. A controlled removal, again, requires rendezvous with and capturing of the target. Missions that have already performed a rendezvous and/or docking (or capturing) procedure in space attempted to improve on-board autonomous systems - in addition to demonstrate the capability of R & D. On-board systems are believed to increase the spacecrafts capabilities, resulting in more mission time available and more complex tasks possible to process. Figure 3.7 compares investigated missions according to their level of autonomy and type of target approached. Type of target, in this case, refers to targets either *cooperative*, *partly cooperative*, or *not cooperative*. R & D was (mainly) successfully performed with *cooperative* targets. The attempt to autonomously dock with a *partly cooperative* object failed at least once (cf. the Demonstration of Autonomous Rendezvous Technology (DART) [83]). The two additional missions, that performed R & D with a *partly cooperative* target were military missions. The reports are very brief but give the impression of full success. Efforts to berth with a fully *uncooperative* target are not reported. Attempts for R & D have started as early as 1967; however, only a few missions are reported. Apparently, the need for such operations was low and the challenges too high. With space debris gaining more and more attention and ADR pushed forward, it is, however, important to include their lessons learned in the design process. Main points derived are the ability to intervene in case the autonomy fails for any reason and the desire for extensive testing on-ground.

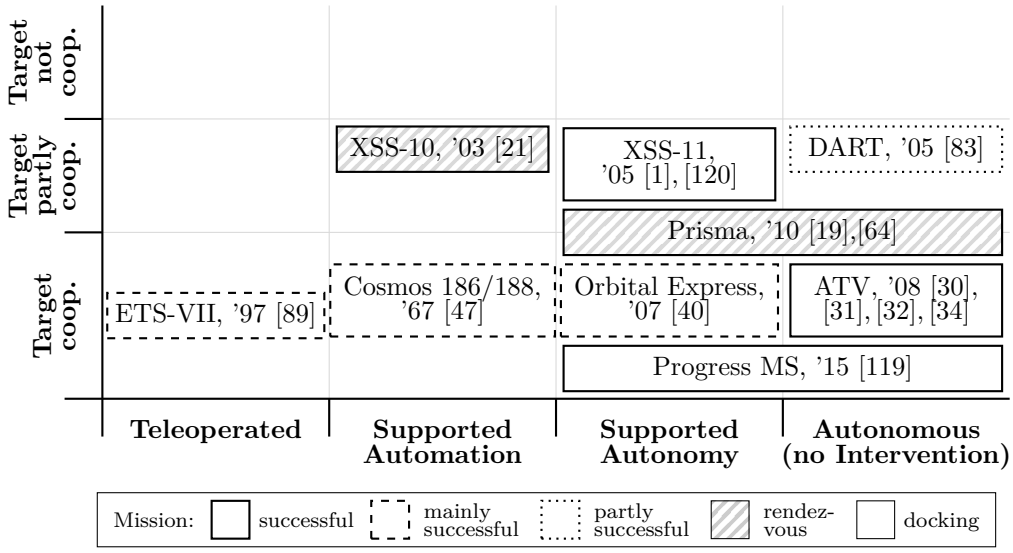

Figure 3.7: Missions that performed robotic rendezvous and/or docking maneuver, distributed according to their different level of system autonomy.

3.3.2 Summary of Requirements for Mission Design

The tasks derived from former argumentation are, so far, a controlled re-entry into the Pacific Ocean, the removal of multiple SL-8 R/Bs, and a safe capturing maneuver. The latter shall allow for aborts in case of failures and the ability to react to unexpected events. Additionally, the mission must be standardized due to the yearly removal of 5 to 15 targets. The idea of on-board decision-making processes of previous R & D missions promises to add to the cost-effective challenge and safety considerations: Allowing the spacecraft to act by itself enlarges its capabilities. More complex tasks can be performed and the work load for ground personal can be limited. The presented mission design will, therefore, include relevant components. Further considerations on the operational concept and the derived satellite design follow. The name for the set-up resulting from the tasks mentioned will be Active Debris Removal Satellite - #A (ADReS-A), whereas 'A' addresses the first of its kind.

3.3.3 Mission Architecture

Division of Tasks

Different options concerning the requirements stated for the multiple target removal are considered. They are described below in detail and plotted in Figure 3.8. The acting spacecraft within is referred to as *Chaser* and/or *ADReS-A*. The options show different division of tasks for the respective combination of spacecraft. Table 3.3 provides a rating accordingly. The considered criteria are also applied for the removal technologies with further explanation on their influence given in Section 3.4.2.

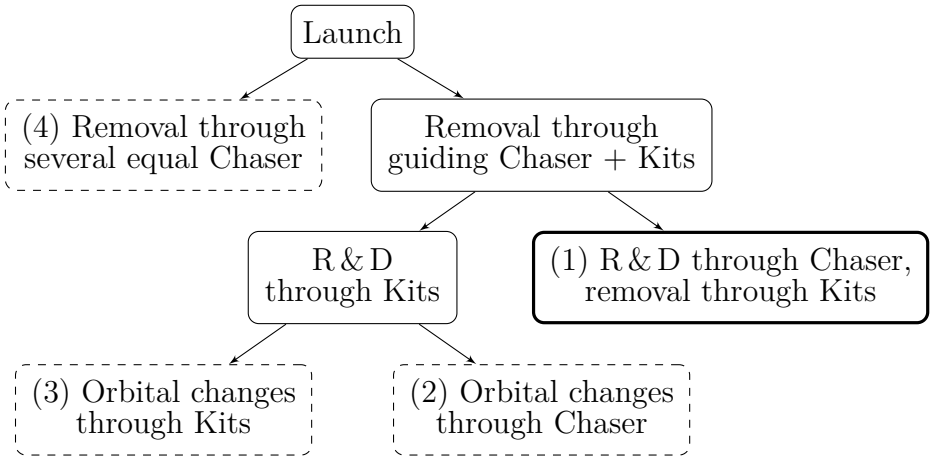

Figure 3.8: Various options for multiple active space debris removal.

(1) R & D by Chaser, removal by Kits Attaching the Kits to a R/B requires ADReS-A to have handling and R & D capabilities. While the Kits concentrate on the de-orbit of the target, ADReS-A shuttles between the orbits and objects. An impulsive maneuver enables a controlled active removal to a designated area. The benefits of one launch per mission and the removal of multiple targets are ensured. The Kits can be designed relatively simple if the chaser performs all R & D and shuttle maneuvers. In case the chaser fails, however, a second chaser may have to carry on the mission.

(2) Orbital changes by Chaser By assigning the shuttle-part to the chaser and leaving the R & D maneuver with the De-orbit Kits, a more complex Kit-design is required than for Option (1). The De-orbit Kits perform the de-tumbling of the target and de-orbit with it to ensure a controlled removal. A drawback is, thus, the loss of a highly complex spacecraft during re-entry. A benefit is the robustness against failures as the Kits can replace each other in case of a malfunction.

(3) Orbital changes by Kits / (4) Removal by several equal Chaser Carrying De-orbit Kits in a transfer orbit by a chaser or launching several equal chaser in a specific orbit would result in a similar mission. The options differ in the necessary orbital plane changes, as a chaser could transfer Kits in a more precise orbit relative to the targets than a launcher. The complexity of the spacecraft and the execution of the mission are similar for both options. Keeping in mind, that a controlled re-entry ends with the loss of the removing spacecraft, the high complexity for R & D maneuver and orbital changes of each spacecraft will require more resources than for the other options.

Table 3.3: Options for multiple ADR, weighted. *0* stands for the least admirable one, *2* represents the most preferred option for the according criteria, and *1* is anything in between. The weighing factors follow Table B.3.

	Resources requ.	Heritage/TRL	Reusability	Compl. of Design	Costs	Compl. of Capture	Mass/Volume	Versatility	Reliability	Testing on-ground	Efficiency	Distance to target	Tumbling rate	Type of Contact	Type of Connect.	Hazardousness	Total	Weighted
(1) R&D by Ch., removal by Kits	2	1	1	2	2	1	2	1	0	1	2	1	1	1	1	1	20	**1.26**
(2) Orbital changes by Ch.	1	1	1	1	1	1	1	1	1	1	1	1	1	1	1	1	16	1.00
(3)/(4) Orbital changes by Kits	0	1	1	0	0	1	0	1	2	1	0	1	1	2	2	2	15	0.89
Weighing Factor	6.1	6.9	8.4	6.5	6.9	7.3	6.1	4.6	8.0	8.0	8.8	2.7	5.0	2.3	3.4	9.2	(%)	

Resulting Scenario Table 3.3 compares the given options. Option (1) states the separation of the tasks - enabling a controlled re-entry as well as the saving of resources. Most of the complexity is concentrated within the chaser and, therefore, in orbit. A loss of the simpler configured De-orbit Kits during re-entry is more bearable than de-orbiting a highly complex apparatus with each removal. Accordingly, this thesis focuses on a complex chaser, leaving the Kits' design to be as basic as possible.

Transportation of the De-orbit Kits

An additional consideration that follows the now fixed satellite combination, is the transportation of the De-orbit Kits. One option (Option (a)) is having ADReS-A transport all Kits at once, shuttling from target to target, and leaving one Kit after another with the designated R/B. Another option (Option (b)) is keeping the De-orbit Kits in a Parking Orbit (PO), with ADReS-A handling one Kit at a time and shuttling between the PO and the targets' orbit back and forth. A third option (Option (c)) is anything in between e.g., ADReS-A transports a limited amount of De-orbit Kits and picks up more once these are attached to their designated R/B. Table 3.4 gives a rating of these options with similar criteria applied as for Table 3.3. Due to the close vicinity, not all the criteria are suitable. Others, such as being most flexible and agile to react to possible changes of the environment - may that be external or internal changes - are added. Following Table 3.4, Option (b) is selected for further investigations.

Table 3.4: Transport options for ADR, weighted. *0* stands for the least admirable one, *2* represents the most preferred option for the according criteria, and *1* is anything in between. The weighing factors follow Table B.4.

	Propellant	Compl. of Design	Costs	Compl. of Capture	Mass/Volume	Robustness	Testing on-ground	Efficiency	Agility	Hazardousness	Total	Weighted
(a) Chaser transports all Kits at once	2	0	1	0	0	1	0	1	0	1	6	0.62
(b) Kits parked in PO	0	2	1	2	2	1	1	1	2	2	14	**1.48**
(c) Kits parked in PO & Kits transported together	1	1	1	1	1	1	0	1	1	1	9	0.94
Weighing Factor	5	5	12	7	8	10	6	14	16	16	(%)	

Tasks and CONOPS for the De-orbit Kits

Dividing the complexity and functions between chaser and Kits leaves ADReS-A with tasks such as shuttling between the orbits, approaching the respective object, capturing and stabilizing the target, and managing unexpected events and failures. The De-orbit Kits, once attached to the target, are responsible for the actual removal. During their time in the parking orbit, they need to survive on their own. The Kits' design must ensure that sensors support ADReS-A during pickup by communicating their orbit and attitude status. After ADReS-A has transported and attached one De-orbit Kit to the target, the Kit will need to hold on to the rocket body and ignite the thruster for de-orbit. A spin-up of the two objects before the ignition will support the stabilization during re-entry, the command for the de-orbit will be given by ground control. This way it is ensured that ADReS-A is far enough away, and the controlled re-entry takes place over the Pacific Ocean.

The Concept of Operations (CONOPS) for a De-orbit Kit in space results in operational modes which can be separated into a *spin mode*, a *waiting mode*, and a *de-orbit mode*. The *spin mode* follows the disconnection of the launcher and generates attitude stabilization of a Kit. All the Kits that are not attached to ADReS-A to be transported, will go into spin stabilization and by such be transferred into the *waiting mode*. During the *waiting mode*, the thruster is deactivated. The main task of this mode is to keep the De-orbit Kits from getting to close to each other. Just before ADReS-A arrives to pick up a new Kit, the chosen one will have to de-spin. The mode of the designated Kit turns back in *spin mode*. During the shuttle process, the *waiting mode* is active again. The *de-orbit mode* is active once the Kit is attached to the rocket body. Its main thruster is activated to de-orbit the target and itself while ADReS-A is on its way back to the parking orbit.

3.4 Technologies for ADR

3.4.1 Capture and Orbit Change Mechanisms

With the mission architecture derived, a suitable technology for capture is now in focus. As space debris varies in size, different technologies have been developed by multiple parties with a pending level of maturity. The most popular removal technologies are presented in Figure 3.9 and classified below. In addition to the addressed target size categorized in the figure, the type of contact between is assigned to the respective technology. While *Multiple Contact* refers to a mechanism interacting with the target

through multiple mechanical contact points, *Point Contact* concentrates on one single physical contact. *No Contact* refers to an interacting spacecraft establishing no physical contact with the target. The graphic also reveals if the technology is suitable for active removal and how the connection between target and spacecraft is established. Active removal technologies can also remove targets in a passive way as the passive removal forms the basis for all given technologies. Concerning the connection, either a *rigid*, *tethered* or *open connection* is available. The latter establishes no bonding connection to the target. *Tethering*, and with such a connection through a robe or cable, enables for pulling. A *rigid* connection forms a stable link, allowing a chaser to push and/or pull the target in the desired direction. In case no chaser is involved in the orbit change, as for the sail, balloon, or tether option, a passive change of orbit is assumed.

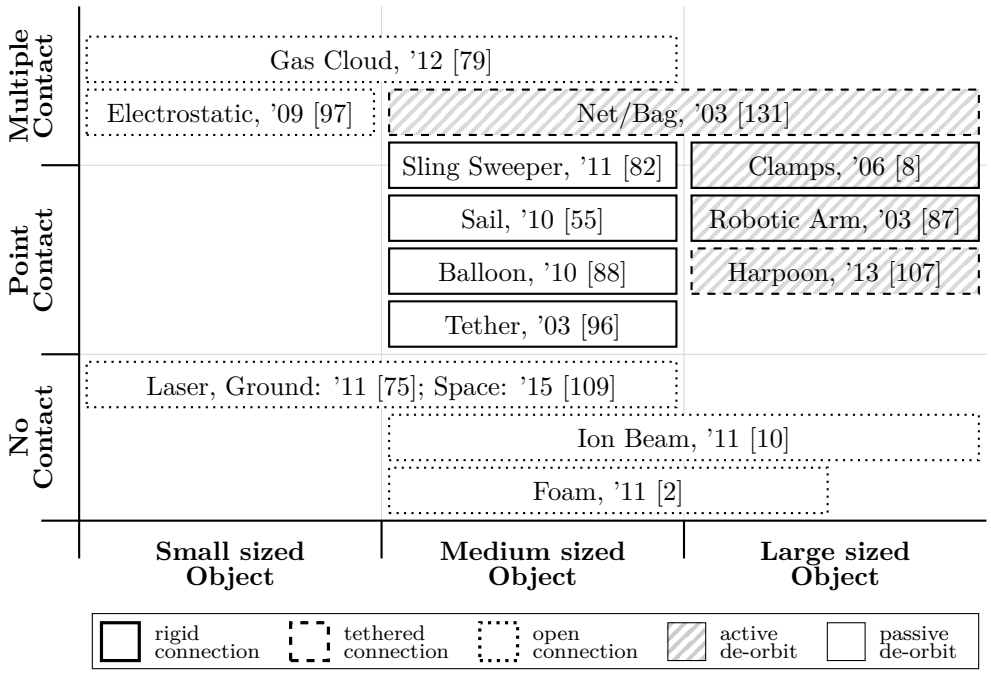

Figure 3.9: Most popular debris removal technologies, classified according to the target's size, the possible contact-type, the way a connection between the chaser and the target is performed, and the kind of de-orbit. Multiple publications are found for some technologies, the year and reference of the earliest study is given.

Figure 3.9 reveals the preference of developers for a rigid or open connection in combination with a passive de-orbit for medium sized objects: eleven out of the thirteen presented technologies form a rigid (six) or open (five) connection, nine are designed for passive de-orbit only. The distribution on object size is spread with concentration on medium sized and large objects with the foam technology limited to objects up to 1 t. Most of the technologies for large sized objects agree on active removal.

Gas Cloud An unconventional idea to decelerate objects in space is the increase of the atmospheric drag right in front of them. A cloud of 100 to 500 m in diameter is proposed to be launched into the orbit of the respective object. Due to the friction resistance the passing objects will decrease their orbit [79]. With the small particles spread, a high pollution is the result. This will affect the targeted object but also all other objects in the same orbit.

Electrostatic Due to electrostatic charges, reusable electro-adhesion can be used to attach a chaser to a target. Preferably close to the CoM and with pressure from the far side to avoid delamination, momentum comprehensions and de-orbit can be started. So far, electro-adhesion clamps have been successfully demonstrated in thermal vacuum, with Ultraviolet (UV)-exposure and with an electron source. Tests have been performed with substrate materials commonly found on spacecraft (e.g., anodized or bare aluminum, capton or polyimide). Electro-adhesion can attach to any surface. The interaction with already charged debris, however, needs further investigation. [97]

Net/Bag The idea is to fire a net towards the target, leaving 20 to 300 m between target and chaser. Connected via rope or wire, the net would wrap around the target and tighten its ends by either weights or cube satellites in formation flight. The ratio of net mass to debris mass is proposed to be in the range of 1 to 8 [137]. Other study foci are the material of the net, its shape, and the knot-technique. The net-wrap-technique has been space-proven [58], however, the dynamics of the net, rope and an uncooperative debris are not trivial. A drawback is the one-time use of a net, not allowing for a second try in case of a missed shoot. Existing examples are *D-CoNe* [7], *ROGER* [131], or *REDCROC* [137].

Sling Sweeper This conceptual technique proposes a satellite with two variable arms on opposite sides with collectors on each end. The collectors are designed as cups with shutters to catch and redirect objects. The redirection happens due to the change of the arm length as well as the sweeper turning around his own axis, releasing the target with lower energy. The impulse transferred to the chaser shall be used to power the sweeper and guide it through different orbits to various objects. This concept requires extremely precise path planning and limited possibilities for corrections of such. [82]

Sail Increasing the surface of an object by adding a sail requires the process of docking a sail-extension device to the target - either before launch or by a chaser. Sails are quite light and require little volume as well as an extension mechanism. At least two ideas for sails exists: for one, a solar sail with a few micrometer thick foil - promising a de-orbit of the same medium sized object from a height of 750 km in 190 days rather than in 160.5 years [67]; for another, an electric solar wind sail, consisting of conducting

tethers, which are kept either positively or negatively biased to repel the respective particles (e.g., positively biased for solar wind ions). The set-up promises to increase the effective physical area by multiple times. [55]

Balloon A balloon increases the surface area of an object when inflated. Like the sail, the system needs to be attached to the target and should be considered as a PMD-technology. The example of *GOLD* can control the inflation which allows a control of the target's time in orbit. For a satellite of about 700 kg at 780 km altitude and calculated 97 years before decay, a *GOLD*-system of 47 kg promises the decay within 143 days [88].

Conductive Tether Due to the magnetic field of the Earth, a cable attached to an object would create a reverse magnetic field and consequently decelerate the object. Lorentz force in opposite direction of the motion is generated via interaction between the current in the tether and the geomagnetic field of the Earth. The system is very low in power consumption and would hardly increase the surface area of the target. It needs, however, to be actively attached to the target. The *EDDE* [96] is one concept following this idea.

Clamps Clamps, or tentacles, can either be installed as an extension of a robotic arm or as part of the satellite that splays out its clamps and closes them around the target with terminal force applied at multiple points. Required is a minimum of two clamps that fix the target in between. Clamps have been investigated within the e.deorbit study of ESA by OHB, Thales Alenia, and Airbus Defence and Space [8]. They are considered a feasible solution for the removal of large objects with masses of more than 8 t. A standardized attachment point is not required.

Robotic Arm So far, robotic arms are the only technology already used for docking maneuver in space. With multiple degrees of freedom, the manipulator system can grab a non-cooperative, tumbling target. The arm itself would be pneumatic or mechanically operated, requires electrical energy, and keeps the distance between the involved bodies. Respective projects like *DEOS* [85, 4, 105], *SDMR* [86, 87], or *FREND* [23, 59] have been initiated. Their development level regarding uncooperative objects varies between conceptional study, 1-g proven technology, or Phase B.

Harpoon With a harpoon, a penetrator on a loose rope impales the debris and extends a fixing mechanism to avoid detachment. While the penetration seems relatively simple, concerns exist about the small attachment point where load concentration increases. A possible creation of centimeter-sized debris and the fact that it is not reusable are additional drawbacks. Airbus Defence and Space developed a prototype, able to fire

from a distance of 10 m with an accuracy of about 5 cm on a target not heavier than 9 t [107].

Laser Lasers for slow deceleration of objects can either be ground-based [75] or space-based [109]. Both use high-power lasers to ablate material off an object. The ablated material serves as a small rocket-like thrust. The uncontrolled de-orbit by a ground-based laser would require 5 to 10 kW power and is said to be suitable for objects orbiting at 600 to 1100 km altitude. A space-based laser would need to follow the target for a significant time and release additional material into the opposite direction to compensate the recoil.

Ion Beam Proposed is the use of space electric propulsion [10]. The quasi-neutral plasma is accelerated by an ion thruster, or a similar plasma propulsion device, and directed against the surface of the targeted object. The exerted force is applied in a distance of a few times the size of the target. To de-orbit 5 t debris within 5 months, *IBS* requires 300 kg total mass. The de-orbit of multiple targets is possible. Drawbacks include e.g., a two-propulsion system for counteraction, like a laser, or formation flying requirements during the entire process.

Expanding Foam Ejecting foam to a target's surface and, thus, enlarging its surface, requires formation flying during the process but no docking procedure. Investigations performed concluded, that an area-to-mass ration of 0.07 is required at an altitude of 900 km to passively de-orbit an object within 25 years [2]. As all surface extending technologies, the possibility to collide with another object during the de-orbiting process must be considered. A maximum radius of 10 m is therefore proposed, which leads to a maximum mass of 1 t for a removal object.

3.4.2 Selection Process

Selection criteria of importance for the derived mission are compiled and listed in Table 3.5, the single criteria are described thereafter. As some criteria will influence the mission more than others, they are also weighted among each other. Technologies, that do not fulfill the requirement of active removal of large objects are excluded, as they cannot be used for the purpose of this thesis. For an overall comparison, points from 1 to 5 on how well the respective technology matches the criteria compared to the other ones are assigned. The more points are assigned to a technology, the better it matches the criterion. A detailed breakdown on the underlying parameter and weighting can be found in the Appendix in Table B.2 and Table B.3, respectively.

Table 3.5: Popular debris removal technologies. The higher the assigned points, the better the parameter is met by the technology. The weighing factors follow Table B.2.

	Net/ Bag	Clamps	Robotic Arm	Harpoon	Weighing Factor (%)
Resources required	3	2	2	3	6.1
Heritage/TRL	3	2	5	2	6.9
Re-usability	1	5	5	1	8.4
Complexity of Design	3	2	2	3	6.5
Costs	3	2	2	3	6.9
Complexity of Capture	3	2	2	3	7.3
Mass/Volume Ratio	4	2	3	4	6.1
Versatility	4	2	2	2	4.6
Reliability	4	4	4	4	8.0
Testing on-ground	4	4	4	3	8.0
Efficiency	2	5	5	2	8.8
Distance to target	3	2	2	4	2.7
Tumbling rate	3	2	3	4	5.0
Type of Contact	2	3	2	1	2.3
Type of Connection	2	5	5	2	3.4
Hazardousness	4	3	3	2	9.2
Total	48	47	51	43	
Weighted	3.0	3.1	**3.3**	2.7	

Table 3.5 reveals the technology of a robotic arm as most suitable for the planned mission. It will, therefore, be implemented in the system design and applied for further considerations of the mission.

Selection Criteria

Resources Required Power and required Δv - and with such propellant necessary to perform the removal - are considered valuable resources in space. The more resources required, the fewer points assigned.

Heritage/TRL Heritage, or an assigned TRL, reflects the level of development of a technology. Included are the application in space, a tested or untested prototype on-ground, computer supported constructions or simulations, as well as conceptual ideas. The higher a TRL, the more points are assigned.

Re-usability The systems capability to repeat a task multiple times and adapt to changed circumstances is a key task to perform in an unknown environment. Full points are assigned, when the criterion is fulfilled, one point is given for single-use.

Complexity of Design Higher complexity increases the chance for failures, high points are, therefore, assigned to low complexity. The design should be simple and easily integrated into the satellite itself with low impact on the chaser during performance. This criterion can also be referred as system complexity of the mechanism.

Cost Costs for the removal should be kept as low as possible. The long-term project does not allow for short-term results. Investments are, thus, more difficult to justify. Costs include recurring (in future missions) and non-recurring costs. Low costs are reflected by high points.

Complexity of Capture Capture precision requirements and stress concentration must be considered. The more complex the capture is, the more failures are likely to happen. High complexity results, therefore, in low point assignment. This criterion can also be referred as system complexity of operation.

Mass/Volume Ratio Mass and Volume depend on and influence the required maneuver, the resulting propulsion requirements, and the size of all other systems. The lower the ratio between the mass and/or volume of the removing satellite and the mass and/or volume of the target, the more effective is the concept considered to be and the more points are assigned.

Versatility Versatility describes the expected successful application of a technology to multiple types of targets. The more flexible the application of a technology is, the less it must be modified in case of a change in target. This includes the mass and size of the target as well as its shape. High versatility is reflected by high points.

Reliability The number of failures or malfunctions need to be limited as it is close to impossible to repair a system once it is in space. High points go to high reliability.

Testing on-ground Technologies in space experience vacuum and microgravity. While vacuum can be tested on-ground, microgravity is more difficult to test for, as e.g., drop towers offer limited 'weightlessness'. The less adequate or more expensive test possibilities are, the fewer points are assigned.

Efficiency Removing a considerable number of large objects from space within a given time frame reflects high efficiency of a technology. Its re-use can be one indicator. High efficiency is reflected by high points.

Distance to target As close approach to an uncooperative target has not been tested and is considered most challenging, larger distances between the involved objects are considered safer than smaller ones. The wider a distance is kept during the capture the more points are assigned.

Tumbling rate Due to their natural movement and environmental influence, targets will have a tumbling or spinning rate, which will have to be compensated by the capturing satellite. The higher a tumbling rate that can be compensated by the technology, the more points are given.

Type of Contact For the removal of large objects, either multiple or point contact is available. As multiple contacts spread over a larger area and limit stress on the target as well as on the chaser, higher points go to this contact type.

Type of Connection As type of connection to large objects either *tethered* or *rigid* is available. A more stable connection allows for a better target handling, rigid connections get, thus, higher points than tethered ones.

Hazardousness Hazardousness describes the capability of a technology to create more debris than it was supposed to remove. High points are assigned to low debris creation capability.

3.4.3 Deceleration Mechanisms

After the capture of the target, the de-orbit must be initiated. For the active and controlled removal to an assigned area, technologies that use the drag of the atmosphere or the sun must be excluded. Constant thrust by electrical or ionized thruster do not allow for a controlled re-entry to a specific area either. Chemical thruster that change the orbit energy of the target within a short time frame, are, therefore, proposed for this mission. Those thrusters work with mono- or bi-propellant systems and are evaluated during the system design.

3.5 Final Concept

In summary, ADReS-A has two main components: the chaser, which takes care of transport, approach, grabbing, and departure; and the De-orbit Kit, which can be described as propulsion extension for the rocket bodies. The chaser shall carry the name of the mission - ADReS-A.

Figure 3.10 displays the concept: One launcher will transport ADReS-A and multiple Kits into the PO. According to implementation procedures, the first part includes the pre-launch phase, launch to the PO and early operations, the commissioning phase, and the de-orbit of the launcher. ADReS-A will then transport one Kit at a time to an allocated SL-8 R/B while the others stay in the PO until picked up for transport to their designated R/B. Ones shuttled to its destination, each Kit will be attached to the target and de-orbit with it.

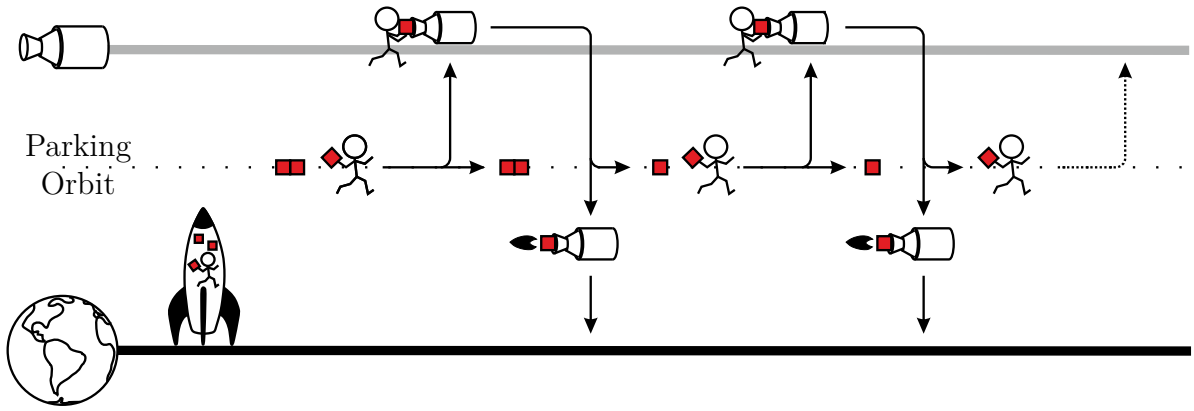

Figure 3.10: Bar chart displaying the resulting mission architecture. One Kit at a time is taken from the parking orbit to the designated target. After the target is de-tumbled by ADReS-A, the Kit is attached. Kit and target de-orbit while ADReS-A shuttles back to the next Kit to transport it to the next target. [100]

3.5.1 Rendezvous and Docking

With the robotic arm chosen as capture technology, the mission architecture is extended by the actual procedure for rendezvous and docking. On that account, the actual tumbling rate and attitude of the rocket body must be known. The work of Gomez [45], which implemented findings of this thesis, focuses on the investigation of Visual Light Cameras (VLCs) in combination with Time of Flight Cameras (ToFCs). The VLC tracks the target in distances from 8 m to up to a few kilometers. By comparing the stored data about the actual form of the target to the pixels recorded, it measures the distance to the object. Once a distance of 20 m is reached, the ToFC supersedes the VLC. A 3D-model is calculated. Working on infrared light, the camera measures the time the light needs to reach and be reflected by the target. The tumbling mode and axis of rotation of the target are determined and potential docking point movements predicted. The distance between the camera and the spin rate axis needs to be about 13 m for an accuracy of $\pm 10^{-4}$ deg/sec, and to about 20 m for an accuracy of $\pm 10^{-2}$ deg/sec [45]. For further considerations, those distances shall serve as envelope data.

The two cameras presented need decent illumination to generate the required data. As an orbit around Earth provides an illumination and an eclipse phase, the actual capture planning needs to concentrate on the former. Additional unfavorable for successful data generation is glare. The direct sun in the Field of View (FoV) of the cameras, or the direct reflection of the sun by the target, thus, need to be avoided. As the FoV of the instruments is between 20 and 30 deg [45], the illumination phase must be limited by 60 deg to derive the actual time available for the approach. The different phases and time per orbit are illustrated in Figure 3.11, calculations are given in Appendix A.3.1.

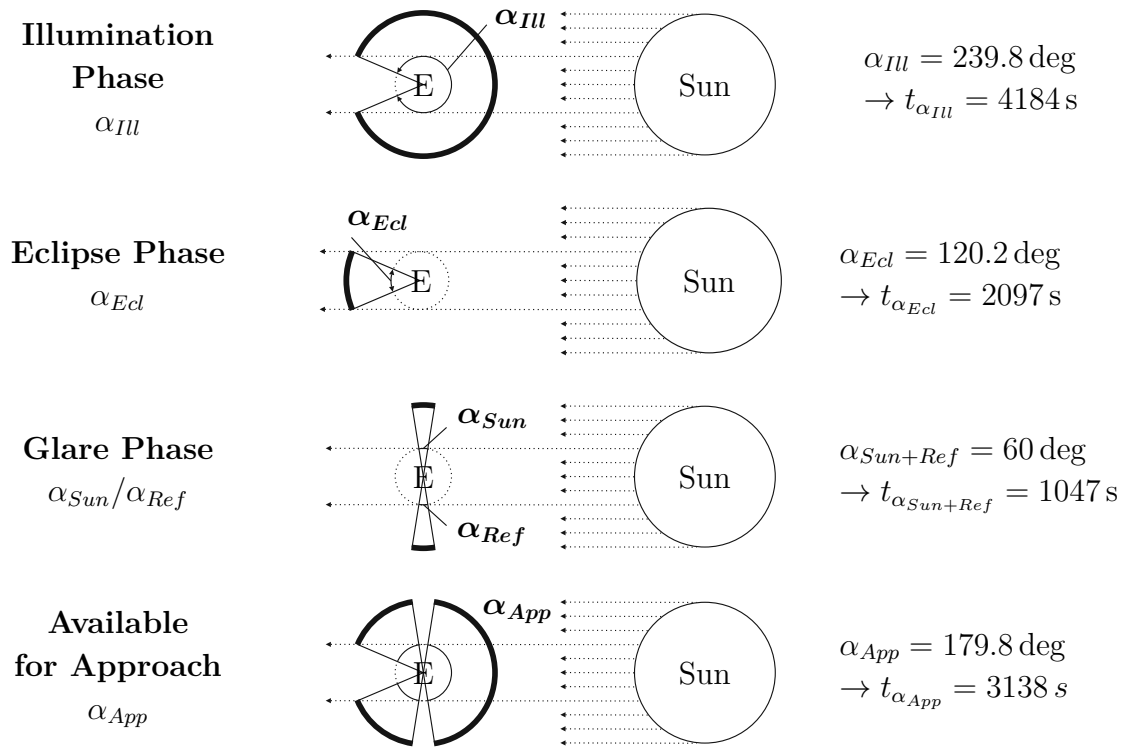

Figure 3.11: Different phases and respective lighting conditions for the determination of the tumbling mode of the target. The phases are calculated for the reference orbit at 980 km with a period of 6281.32 s. Updated from Ref. [101]

The objects will drift during the docking process. Targeting a fixed single point would result in constant position regulation of the chaser. As this is unfavorable for the grabbing process, a berthing box next to the docking point shall be aimed for. Its volume is defined by the dimensions (the length) and the flexibility of the arm. The resulting berthing box enables the grabbing without permanent position regulation by thrust application. In case the tolerances are exceeded, the grabbing will stop, and thruster will reposition ADReS-A for further procedure.

3.5.2 Delta-v Budget

Mission times and respective Δvs are good indicators for the efficiency of an approach. The impulsive velocity change Δv_{ch} is a combination of in-orbit and out-of orbit value adaptions, resulting in

$$\Delta v_{ch} = \sqrt{v_i^2 + v_f^2 - 2 v_i v_f \cos \Delta A} \tag{3.4}$$

with

$$\Delta A = \cos i_i \cos i_f + \sin i_i \sin i_f \cos \Delta\Omega$$

and

$$v_{i/f} = \sqrt{\mu \left(\frac{2}{r_{i/f}} - \frac{1}{a} \right)}, \qquad a = \frac{r_1 + r_2}{2}. \tag{3.5}$$

r_i presents the initial orbit radius and r_f the targeted (final) orbit. The indexes for the inclinations i and the velocities v work likewise.

The five main targets listed in Table 3.1 show a maximum deviation in inclination of 0.02 deg. To stay within the self-set range for a multiple target solution of 50 m/s, the $\Delta\Omega$ shall not exceed 0.39 deg. Maximum deviation, however, is at 2.69 deg. One solution is the adaption of the $\Delta\Omega$ through the J_2-drift, given in Equation 3.3 in Section 3.2.2. As the Kits in the PO have a different drift then the targets in the Target Orbit (TO), the $\Delta\Omega$ can be compensated by adapting the time ADReS-A stays in the various orbits. To enable multiple of such maneuver, an additional orbit, the Catch Orbit (CO) must be defined, in which ADReS-A compensates the piled $\Delta\Omega$ of the Kits.

As the 50 m/s is a self-set range, mission time and Δv_{ch} *with* and *w/o drift* in use are compared. The plot of an exemplary mission analysis, given in Figure 3.12, additionally shows the different processes required for each approach. Afterwards, the optimal PO - TO distance *w/o drift* is investigated. The same investigation is then performed for the PO - TO distance *with drift* applied.

For Figure 3.12, the PO is set to 30 km below the TO, the CO 10 km below the PO. The plotted processes for a mission with impulsive thrust implementation (*w/o drift*) follow the mission architecture given in Figure 3.10. Additional processes required for a mission applying the J_2-drift are dashed underlined. One week is assumed for the R & D of each target and each De-orbit Kit, respectively. The initial commissioning follows time recommendations of Ref. [135]. For the plot, the actual data of the targets, provided by Table 3.1, is inherited. Table 3.6 lists the initial position of the Kits, which are assumed as single point mass for the calculations. Averaged are the targets' data with their altitude lowered by the stated 30 km. The De-orbit Kits' RAAN mirrors the

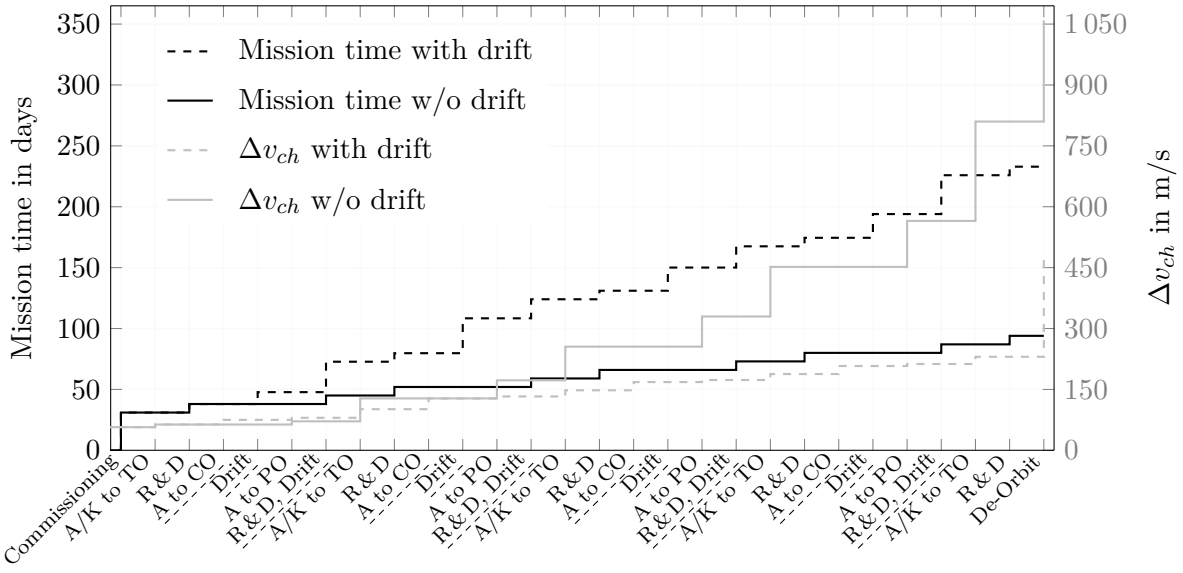

Figure 3.12: Displayed are the mission time and the Δv_{ch} required for the concept - with and without (w/o) J_2-drift implemented. One week is applied for each R & D process. The dashed processes are added for the cases J_2-drift is applied for compensation of the $\Delta\Omega$. W/o J_2-drift applied, shuttling concentrates between TO and the PO, with drift, the CO is additionally required.

largest RAAN available among the group of targets. For mission *w/o drift* Figure 3.12 reveals a mission time of 94 days and a Δv_{ch} of 1059 m/s. For a mission *with drift*, the mission time increases to 233 days, Δv_{ch} is reduced to 480 m/s.

Table 3.6: Orbital data of the Kits and the Catch Orbit (CO) based on the mission architecture of Figure 3.10 and the target data of Table 3.1.

	Altitude in km	**Incl. in deg**	**Ecc. *e***	**RAAN in deg**	**Launch date**	**$\dot{\Omega}$ in deg/s**
Position Kits	949.420	82.935	0.002	163.412	-	-8.727E-06
Catch Orbit (CO)	939.420	82.935	0.002	-	-	-8.769E-06
Average targets	979.420	82.935	0.002	162.195	26.05.1983	-8.603E-06

Figure 3.13 displays the mission time and the Δv_{ch} for different distance between PO and the TO when compensating the $\Delta\Omega$ through impulsive thrust maneuver. Time-wise, one month for spacecraft test purposes and commissioning after placing ADReS-A into orbit and one week for every R & D maneuver is assumed (cf. Ref. [135]). The calculations are based on the processes for maneuver *w/o drift* given in Figure 3.12. Accordingly, the minimum Δv_{ch} of 767 m/s is reached at a PO of 80 km below the TO.

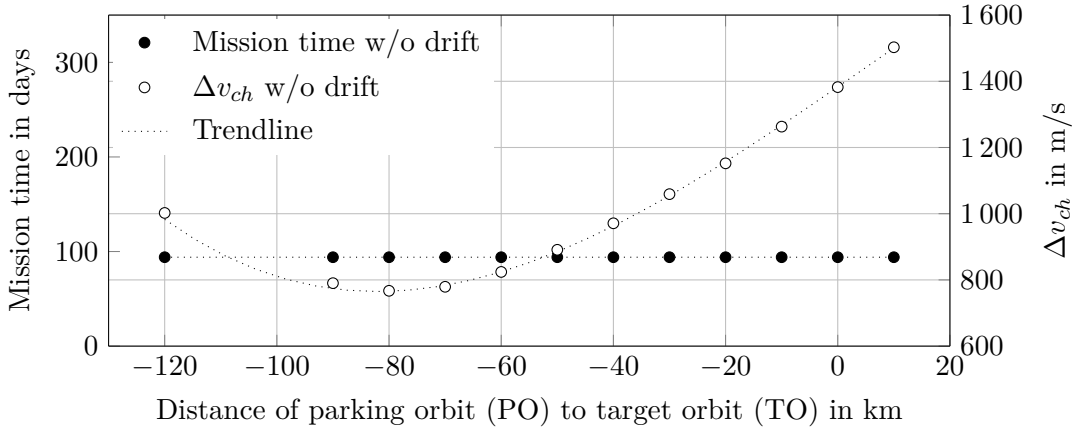

Figure 3.13: Distance of different POs to the TO with resulting Δv_{ch} requirements. The $\Delta\Omega$ is compensated by impulsive thrust application.

The investigations concerning the PO - TO distance are repeated with a $\Delta\Omega$ compensation through the implementation of J_2-drift and a CO of 10 km. Figure 3.14 shows the results. Due to the varying time necessary for drifting to adopt to the investigated orbits, the involved targets and Kits have passed the range for which a compensation by drift is still possible for some investigated POs. Displayed are, therefore, fewer results of investigated orbits than in Figure 3.13. The outer boundaries of the successful cases result in a Δv_{ch} of 434 m/s with a respective mission time of 301 days for a PO of 20 km, and a Δv_{ch} of 493 m/s with a respective a mission time of 219 days for a PO of 33 km.

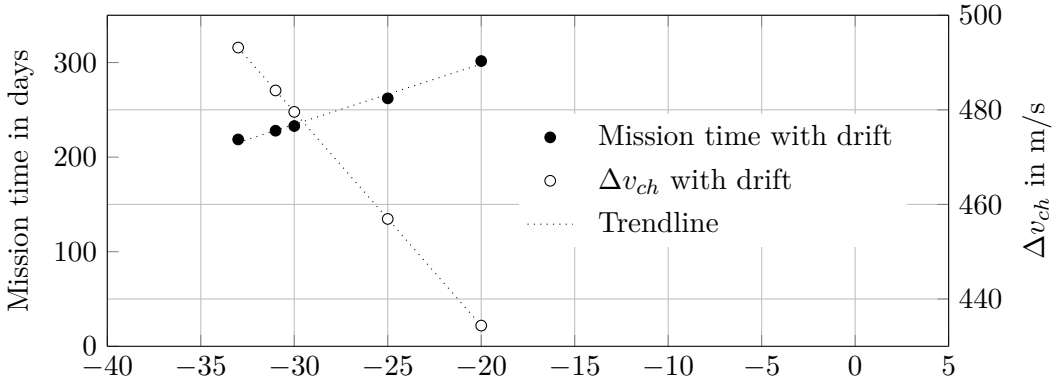

Figure 3.14: Distance of different parking orbits with resulting Δv_{ch} requirements. The RAAN is compensated by drift and, thus, time.

Once the last Kit has been attached to its designated R/B, ADReS-A is required to de-orbit itself - preferably together with a target. An orbit of 80 km altitude is aimed for, as the re-entry of similar objects have shown this altitude as break-up altitude [93]. Accordingly, Δv adds up to 244 m/s when starting from an altitude of 980 km (cf. Appendix A.2). Additionally, each Kit has to de-orbit together with its R/B from slightly

different orbits. The respective Δv range from 239 m/s to 247 m/s. The Δv-requirements for the synchronization with and grabbing of the target will be in very low m/s-range and are, therefore, not listed as an additional mission part.

Comparing the results for the different approaches, an optimized mission *w/o drift* will lead to a Δv of 767 m/s and with such to a propellant mass of 428 kg hydrazine. The mission time will be about 94 days. An optimized mission *with drift* will lead to a Δv of 434 m/s and, thus, a propellant mass of 243 kg hydrazine with a mission time of about 301 days. With an available mission time of up to one year, the approach *with drift* shall be preferred for the removal mission.

To keep close to the lowest Δv_{ch} and to allow some back-up time for the whole mission, the final PO is set to -30 km. The CO is kept at 10 km below the PO as this distance allows to keep the mission time within range and compensation through drift applicable. The further considered Δv_{ch} for transfer and de-orbit results to 480 m/s.

True Anomaly

Additional adjustments must be performed for the true anomaly Θ and with such the position of the target in its orbit. This parameter is highly dependent on the period and changes constantly within one period between 0 and 360 deg. Equation 3.6 together with Equation 3.7 give an idea of the complexity for calculations. Numerical methods are required to solve them. E is the eccentric anomaly and $(t - t_0)$ is defined as time elapsed since passage of the perigee (t_0).

$$\cos\Theta = \frac{\cos E - e}{1 - e\cos E} \tag{3.6}$$

with

$$E - e\sin E = \sqrt{\frac{\mu}{a^3}}(t - t_0) \tag{3.7}$$

At this point of the mission design, the adjustment of the true anomaly by ADReS-A will not be investigated. This decision is based on its non-closed-form solution as well as on further disturbances not considered for exact positioning and forecasting of trajectories. With the mission planned for one year, some of the drift time for RAAN-adjustment will have to be spent for the adjustment of the true anomaly, an optimization between propellant consumption and time availability will be the result.

3.5.3 Additional Remarks

For a complete mission design, additional segments such as launcher or the communication strategy must be considered. As they are out of the scope of the analyses for this thesis, they are mentioned in sparse detail in the following paragraphs.

Original Launch Site The carrier rocket for the targets has been the Kosmos 3M with its stages RS-14 as lower stage and S-3M as upper stage, the second one representing the target for this mission. The launch site has been Plessezk, 800 km north-east of Moscow with an inclination range of 66 - 98.5 deg. To reach the targets at 83 deg, using the original launch site would be one option. As an inclination larger than the one at the launching pad can be approached without much effort, alternatives are considerable.

Available Launcher The requirements for the launcher state the need to launch at least 3.4 t of payload (cf. Chapter 4 for calculations). Technologies available are manifold and include, but are not limited to, the Antares 121 by Orbital ATK or the Falcon 9 by SpaceX. According to the respective costs per launch and due to liability reasons, out of those two the latter is advisable.

Ground Station Nominal situations for ADReS-A shall apply guidance and support from ground. The close approach that asks for self-awareness shall be supervised with a possibility for intervention. The ESA Tracking Station (ESTRACK) offer a network of stations around the world. Fehse [37] analyzed the network for an orbit of 766 km, showing that an uninterrupted coverage of up to 25 min two or three times a day is possible. Data exchange shall be applied to the respective communication windows.

Space Segment While ADReS-A shall be designed to communicate with Earth and act autonomously in the critical situation of the R & D, the Kits are mainly designed to de-orbit the target. Each Kit will have a receiver for commands for a controlled de-orbit into the Pacific Ocean, avoiding any traffic routes (ship or airplane). Housekeeping data will be exchanged with ground station to ensure its functionality and to pursue its trajectory, easing its capture by ADReS-A.

Radiation and Electrostatic Charges The mission is analyzed according to the radiation and electrical charges in the targeted orbit [74]. No unusual exposure is found. Especially with the mission's time line set for one year, no extraordinary precaution must be initiated at this point.

4 System Architecture

With the reference scenario defined and the associated mission architecture for the intended removal described, ADReS-A and the De-orbit Kit are designed in more detail. This part of the thesis approaches ADReS-A and the Kit separately and covers details down to subsystem level. The results provide more realistic data for the self- & failure-management and the simulation. The architecture of the Kit is discussed first, as its design is more dependent on the identified target than on the design of ADReS-A.

4.1 De-orbit Kit

4.1.1 Design Tasks

A Kits' main task is the de-orbit of an SL-8 R/B. With the rocket body's nozzle providing the physically most stable point, the Kit is designed to be attached there. This enables the final set-up to keep a stable position and direct the applied thrust through the CoM along the R/B's z-axis, minimizing its torque. Additionally, the Kit must survive up to one year in the PO and support its capture by the chaser. Table 4.1 provides an overview of the subsystems related to the respective requirements and derives associated design tasks. As the subsystems of a S/C highly influence each other, Table 4.1 focuses on first level requirements derived from the former chapters and lists directly involved subsystems.

4.1.2 Design Specifications

The resulting design tasks of Table 4.1 are individually addressed by different design options considered. A trade table is given in Table 4.2. The specific criteria applied are significant for the decision-making process. The more points an option gets, the more it suits the criteria in a positive way. The options with the highest points are boxed and selected for the final design.

Table 4.1: Design tasks for the De-orbit Kit.

Requirement	Addressed subsystem	Resulting Design Tasks
Controlled de-orbit of SL-8 R/B	Structure	· Top part fits into R/B-nozzle · Attachment mechanism · Compact structure
	Propulsion	· Chemical propulsion · High thrust level
	Communication	· Signal for de-orbit command · Enable supervision of system
	AOCS	· Enable orientation · Enable positioning
Ease capture for ADReS-A	AOCS	· Provide reflectors for capture
	Structure	· Provide capture structure
Survival during one year in space	Structure	· Solar arrays for recharge
	Power	· Provide recharge capability
	Propulsion	· Enable stabilization
	AOCS	· Enable stabilization

In the following, each decision is further explained:

- Fitting the upper part of the De-orbit Kit into the R/B-nozzle can result in a cylindrical, an orthogonal, or a square shape of the Kit's top. While the former requires a full-surface connection to fit, the latter offers only a few connection points. The orthogonal shape promises a satisfying compromise. Additionally, with flat surfaces, the areas are easier to manufacture compared to the cylindrical option.
- By pushing an attachment mechanism against the inside of the R/B-nozzle, a more stable connection is achieved than by grabbing the nozzle's rim. A magnetic connection may cause unfavorable results for the electronics involved.
- Using the Kit's nozzle for capture is like using the R/B-nozzle - a capability ADReS-A will have included.
- A compact structure is more likely to be achieved with solar panels body mounted.
- Concerning the de-orbit, a combination of 400 N apogee-thruster with LOX/LCH4 propellant is aimed for. The cryogenic bi-propellant may replace the ending supply of the mono-propellant hydrazine, the 400 N thruster enables an optimization between a fast de-orbit and a thruster's mass, size, and volume.
- For the attitude stabilization, low-thrust thrusters will be required. Cold gas thrusters with nitrogen are commonly used and, thus, well tested.

Table 4.2: Trade table of the design specifications for the De-orbit Kits.

	Task / Design Option	Complexity	Mass	Power requ.	Flexibility (for handling)	Flexibility (to changes)	Performance	Costs	Reliability	Size/Vol.	Precision	Hazard	Range	Sum
Structure	'Top part fits into R/B-nozzle' ⇒ Shape of nozzle integration													
	cylindrical	1	1	-	0	0	1	1	1	1	1	-	-	**7**
	orthogonal	2	1	-	2	2	2	1	1	1	1	-	-	**13**
	square	0	1	-	2	2	1	1	1	1	0	-	-	**9**
	Attachment mechanism													
	magnetic	1	1	0	2	2	1	1	1	2	2	-	-	**13**
	grab nozzle rim	0	2	1	1	1	0	1	1	1	1	-	-	**9**
	push against nozzle inside	2	2	1	2	2	2	1	1	1	2	-	-	**16**
	Compact structure / Solar arrays for recharge													
	panels	1	1	1	0	2	1	1	1	1	1	-	-	**10**
	body mounted	2	1	1	2	1	1	1	1	2	1	-	-	**13**
	Provide capture structure													
	use Kit's nozzle	1	2	-	1	0	1	2	1	2	1	-	-	**11**
	provide handle	0	1	-	2	0	1	1	2	1	1	-	-	**9**
Propulsion	Chemical propulsion - De-orbit													
	mono-propellant (hydrazine)	2	0	1	1	1	1	2	2	1	1	0	-	**12**
	bi-propellant (LOX/LCH4)	0	2	1	1	1	2	1	1	1	1	2	-	**13**
	'High thrust level' ⇒ De-orbit thruster													
	500 N	1	1	1	0	0	2	1	1	0	0	-	-	**7**
	400 N	1	2	1	1	0	2	1	1	1	1	-	-	**11**
	multiple 22 N	0	0	1	1	1	1	1	1	1	2	-	-	**9**
	multiple 10 N	0	0	1	1	1	0	1	1	1	2	-	-	**8**
	'Enable stabilization' ⇒ Attitude stabilization													
	multiple 10 N	1	0	1	0	0	1	1	1	0	0	-	-	**5**
	multiple 5 N	1	1	2	1	1	1	1	1	1	1	-	-	**11**
	multiple 1 N	1	2	2	2	2	1	1	1	2	2	-	-	**16**
	'Enable stabilization' ⇒ Low thrust propulsion													
	cold gas	2	0	1	2	1	0	2	2	1	1	-	-	**12**
	bi-propellant	0	2	0	0	1	1	1	1	2	1	-	-	**9**
Communic.	Signal for de-orbit command													
	on-board	0	1	1	1	1	1	2	1	1	0	-	-	**9**
	from ground	1	1	1	2	2	2	1	2	1	1	-	-	**14**
	Enable supervision of system													
	parabolic antenna	1	1	1	1	2	2	0	1	0	2	-	1	**12**
	omnidirectional antenna	2	2	2	2	1	1	1	1	2	1	-	2	**17**
AOCS	'Enable orientation' ⇒ Provide sensors for orientation													
	FSS	1	1	1	1	1	-	2	1	2	2	-	0	**12**
	MSS	1	0	1	1	1	-	1	1	1	1	-	1	**9**
	CSS	2	2	2	1	2	-	0	1	1	1	-	2	**14**
	ST	1	0	0	0	2	-	2	1	0	2	-	1	**9**
	ES	1	0	0	1	2	-	2	1	0	2	-	2	**11**
	IMU	0	1	1	1	2	-	2	1	1	2	-	1	**12**
	'Enable positioning' ⇒ Provide sensors for positioning													
	from ground	1	2	2	1	1	0	1	1	2	0	-	-	**11**
	GPS	2	1	1	2	2	2	1	2	1	2	-	-	**16**
	Provide reflectors for capture													
	active	0	1	0	2	2	1	1	1	1	1	-	-	**10**
	passive	2	2	2	1	1	1	2	1	2	1	-	-	**15**
	'Enable stabilization' ⇒ Spin stabilization with actuators													
	thruster	1	1	1	2	2	2	0	1	1	-	-	-	**11**
	gyros	0	1	1	1	1	1	0	1	2	-	-	-	**8**
	reaction wheels	1	1	1	1	1	0	1	1	2	-	-	-	**9**
Power	Provide recharge capability													
	one string Li-Ion batteries	1	1	1	0	0	1	1	1	1	1	-	-	**8**
	multiple strings Li-Ion batteries	0	1	1	2	1	1	1	1	2	2	-	-	**12**

- Communication wise, the final signal for de-orbit shall be sent from ground. This feature enables higher time-accuracy and flexibility to condition on ground.
- The signal will be transmitted through omnidirectional antennas. Their advantage is the wide coverage angle and, thus, possible permanent contact, while providing a sufficient link budget.
- For orientation and positioning, the implementation of multiple different sensors is preferred - mainly for redundancy reasons. For the former, a combination of Coarse Sun Sensor (CSS), Earth Sensor (ES), and Inertial Measurement Unit (IMU) is chosen. As ADReS-A ensures the capture and handling of the R/B and the Kit, it can perform finer adjustments. The data of the given sensors will support the determination of the Kit's attitude and with such ease the capture for ADReS-A.
- To localize a Kit for pick-up, Global Positioning System (GPS) for the positioning of a satellite is well-proven and more accurate than trackers from the ground. Accordingly, GPS sensors are implemented in the Kit's design.
- Passive reflectors for capture are preferred, following the desire of a simple Kit-design.
- For the stabilization of the Kit during its *waiting mode*, and for the de-orbit, spin shall provide stabilization. The spin will be initiated and ceased by thrusters, the same ones as used for the attitude control.
- While body mounted solar arrays are used to collect energy, the storing of it shall be provided by two different strings of Li-Ion batteries with different capacity. This way, more flexibility for the different parts of the mission is provided.
- The tasks that derive from the requirement to survive at least one year in space are covered by the over-all configurations and are not listed separately.

4.1.3 Interaction Software Tool

As the subsystems highly influence each other, some specifications of the Kit's design need to be derived by a supporting tool. The specifications are determined in a follow-on process by a *Matlab/Simulink* tool, developed to reflect the interactions among the subsystems of the Kit and ADReS-A. Figure 4.1 gives a visual model of the tool: Specific input parameters derived from prior chapters and additional considerations, for example concerning the safety parameters, are included through an external link. The large dashed box demonstrates the multiple integration cycles between the main subsystems of a spacecraft and power and mass requirements. While the required specifications for each subsystem are derived from calculations following the Space Mission Analysis and Design (SMAD) [135], the input parameters can be changed and adapted during the design process. This way, for example, the number and size of the solar arrays are configured.

A choice of calculations different to the SMAD originals are found in Appendix A.3. The output the tool records are the resulting mass and power requirements. Internal validation tests ensure that limits are kept within the allowed range. A warning is given if a parameter exceeds the limits and is, thus, no longer compatible with the whole system. It than has to be adapted. The tool is used (with slight differences) for the configurations of ADReS-A and the Kit.

The derived data for the respective mass and power of each subsystem have been verified by the SMAD-tool [135][1]. The slightly divergent numbers are ascribed to the different geometry of the spacecraft and an inhomogeneous distribution of the systems within, resulting, e.g., in the change of inertia torque and dependent data.

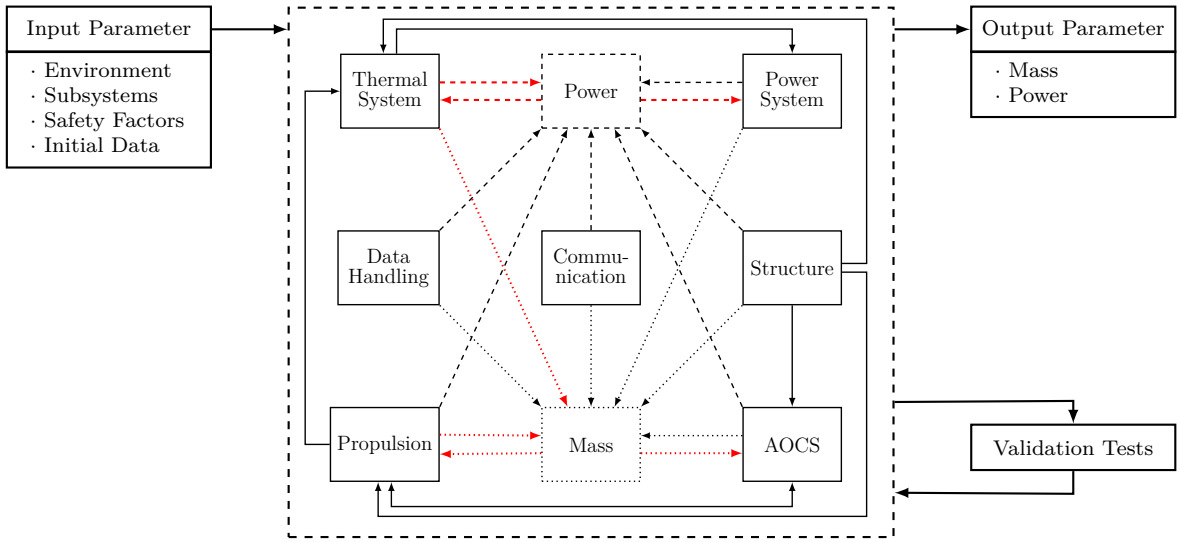

Figure 4.1: The designed tool processes the input parameter and gives the resulting output parameter. Power and mass are virtual boxes to provide a better understanding of the exchanged data. Solid lines in the middle part present any data other than mass or power, dashed lines reflect the power exchange and dotted lines show the influence of changing mass. An arrow is red, if the data was first assumed and later rewritten by the multiple intervals of the code.

4.1.4 Resulting Design Configurations

The designed tool helps to test and set different configurations of components. The input, however, needs to include some specifications. Only uncommon design configurations that extend the formerly stated ones will be mentioned in the following, e.g., sensors for health monitoring will be implemented, but not listed.

[1] Comparison of the respective results is found in Appendix B.3 in Table B.7

Structure By using cryogenic fuel for the Kit, the propulsion system, for example, needs specific insulation. This again influences the structure and is addressed by a physical separation of the propulsion system from the electronic components. By dividing the De-orbit Kit into an upper and a lower part, the propellant can be stored close to the thrusters in the lower part. The attachment mechanism and electronics are configured for the upper part. As the former shall attach the Kit into the R/B's nozzle by pushing against the inside (cf. Table 4.2), paraffin actuators will force cushioning against the nozzles surface. The Kit's size is defined by the size of the R/B's nozzle.

Power System The operational modes concluded from the CONOPS are the *spin mode*, the *waiting mode*, and the *de-orbit mode*. Each mode has its own power requirements, listed in Table 4.3. The chosen configuration of multiple Li-Ion strings must be designed and triggered accordingly. While the *spin mode* requires the low-thrust thruster, most systems are put into stand-by mode during the *waiting mode*. After pick-up and transportation to the target and before the spin for the *de-orbit mode* is initialized, the paraffin actuators need to ensure the stable connection to the target. For the actual de-orbit, the apogee-thruster takes over from the spin-thrusters. Two different types of Li-Ion batteries are derived from the tool presented. While the VES 16 cover the low energy mode, VL 48E are switched on in addition for the de-orbit. The batteries are charged by the solar arrays.

Table 4.3: Power budget of the different operational modes of a De-orbit Kit's life.

		Spin	***Waiting***	***De-Orbit***	
	required time		up to 1 year	600 s	1200 s
Structure	Actuators	-	-	120 W	120 W
Data Handling		20 W	20 W	20 W	20 W
Communication		32 W	32 W	32 W	32 W
Propulsion	CGT	80 W	-	80 W	-
	400 N thruster	-	-	-	35 W
AOCS	Sensors	32.5 W	32.5 W	32.5 W	32.5 W
Margin		15%	15%	15%	15%
Required Power		**189.18 W**	**97.18 W**	**327.18 W**	**275.18 W**

Thermal System The cryogenic propulsion for the De-orbit Kit results in the requirement for additional insulation of the tanks. As the Kit may be exposed to insolation in an unintended way during attachment or shuttling, louver are implemented to protect the radiators at the top part of the satellite.

Propulsion For CGTs, Nitrogen is most commonly used as it offers low storage density, good performance, and a lack of contamination concerns [3]. The gas will also be applied for the re-pressurization of the membrane tanks of the LOX/LCH4.

Functional Architecture Summarizing the recently given configurations, the functional architecture displayed in Figure 4.2 gives an overview between the interaction of the mentioned components.

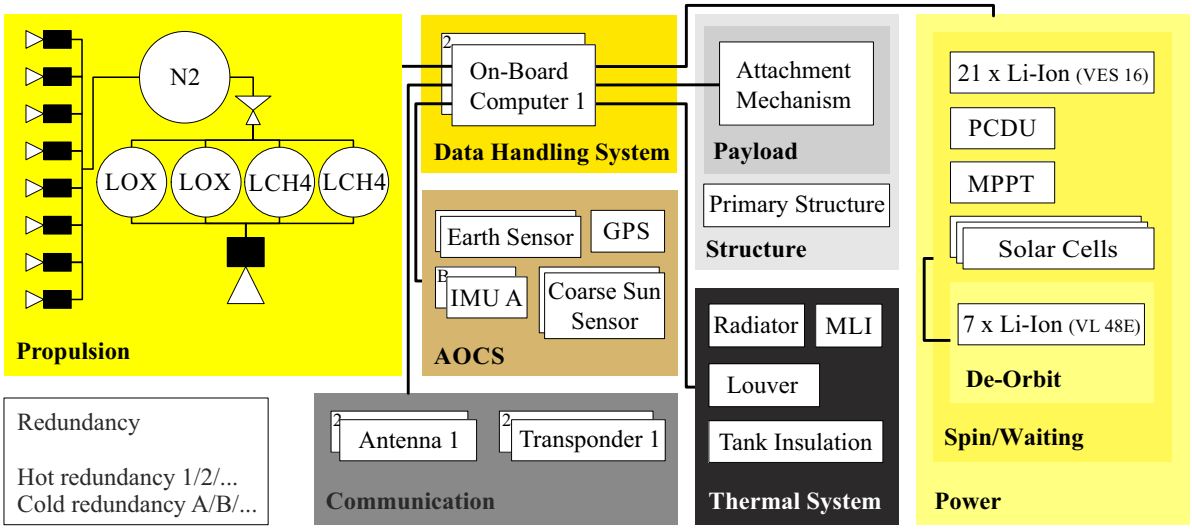

Figure 4.2: Functional architecture for the De-orbit Kit. Updated from Ref. [102]

CAD-Design The CAD-design of Figure 4.3 follows the various requirements and specifications stated.

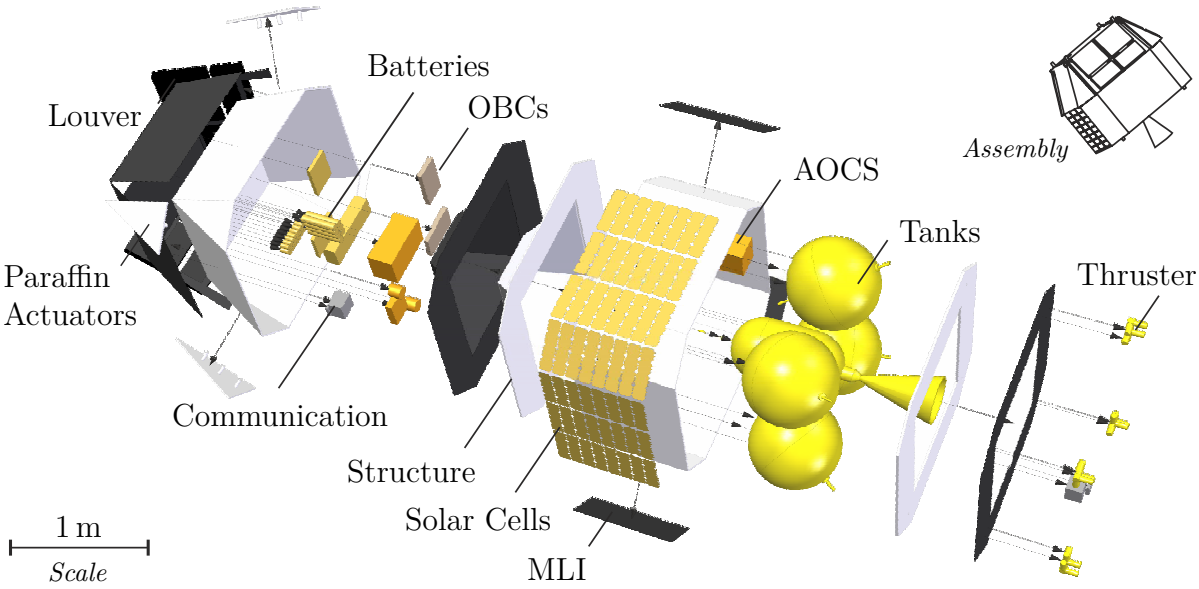

Figure 4.3: Exploded view and assembly of the De-orbit Kit.

4.2 ADReS-A

4.2.1 Design Tasks

ADReS-A takes on multiple tasks, the main ones covering a safe capture of the SL-8 R/B, the shuttling between the Kits' and the target's orbit, and the transport of a Kit. This results, e.g., in its need to be agile and flexible to perform a safe R & D-maneuver and react fast to unexpected events. Table 4.4 lists considered design tasks, focusing on the directly involved subsystem. Respective design options are given in the following.

Table 4.4: Design tasks for ADReS-A.

Requirement	Addressed subsystem	Resulting Design Tasks
Agile and flexible	Structure	· Low moments of inertia · Compact structure
	Propulsion	· Chemical propulsion · Precise low thrust
Safe R & D	AOCS	· Precise sensors · Stay within berthing box
	Structure	· Grabbing mechanism · Sensors for determination
	Data Handling	· Process sensor data fast
React to unexpected events	Data Handling	· Enable self-management · Enable failure-management
Stabilize tumbling target	Data Handling	· Black box
Transportation of Kit	Structure	· Provide adapter for Kit
	Propulsion	· Chemical propulsion · Medium thrust level
	AOCS	· Enable orientation · Enable positioning
	Communication	· Enable supervision
Survival during one year in space	Structure	· Solar arrays for recharge
	Power	· Provide recharge capability
	Propulsion	· Enable stabilization
	AOCS	· Enable stabilization

4.2.2 Design Specifications

Similar to the derived design specifications for the Kit, a trade table is developed to investigate different design options to cover the tasks specified in Table 4.4. Table 4.5 addresses the first-level subsystems of Table 4.4, further configurations result from additional considerations concerning the design. These are included in the adapted *interaction software tool* presented.

- One design constraint on the chaser is a compact structure with low moments of inertia. ADReS-A is, thus, designed to incorporate the Kit during transport.
- Body mounted solar arrays enable the recharge of batteries during the mission time.
- During transport and while ADReS-A captures the target, two linear arms pull the Kit inside ADReS-A. Once the target is securely captured, they will push it into the R/B's nozzle, where the Kit attaches itself. For the pick-up of the Kit, the robotic arm will use the Kit's nozzle. As the paraffin actuators for attachment to the target's nozzle are placed on the other side of the De-orbit Kit, the linear arm will be extendable. This way, the robotic arm can position the Kit in the correct direction into ADReS-A.
- Different to the Kit, mono-propellant is chosen for propulsion, as the chaser must be more reliable than one single Kit due to its diverse tasks.
- For transportation and movement, a combination of 1 N and 22 N is envisaged. The 1 N promises precise movements, the 22 N thruster enables the shuttling process.
- The Attitude and Orbital Control System (AOCS) is similar to the one of the Kit but extended by reaction wheels. They allow for fine-pointing and promise a more precise maneuvering, which is required for the safe R & D process.
- A berthing box supports the safety of the maneuver, the 1 N low-thrust thrusters will support the reaction wheels in case the berthing box' dimensions are exceeded before the maneuver is finished.
- The safe R & D process, again, is addressed by the implementation of self-management with the capability of managing significant failures. Those features are made possible by on-board processing on separate computers. This spacial division of the involved computers shall inhibit interruptions between the internal operations of the spacecraft and the actual capture.
- The capture is addressed through a black box, as the design of the robotic arm is not part of this work. The internal operations include the self- and failure-management.
- Supervision of the system and the possibility to interact is one of the lessons learned. Reasons for using the resulting antenna as well as the implementation of multiple battery strings mirror the reasons given for the design of the Kit.

Table 4.5: Trade of the design specifications for ADReS-A.

	Task / Design Option	Complexity	Mass	Power requ.	Flexibility (for handling)	Flexibility (to changes)	Perform.	Costs	Reliability	Size/Vol.	Precision	Hazard	Heritage	Sum
Structure	Low moments of inertia													
	embody Kit	1	1	1	2	1	-	1	1	2	2	-	-	**12**
	attach Kit external	1	1	1	1	2	-	1	1	1	1	-	-	**10**
	Compact structure / Solar arrays for recharge													
	solar arrays body mounted	2	1	1	2	1	1	1	1	2	1	-	-	**13**
	solar array panels	1	1	1	0	2	1	1	1	1	1	-	-	**10**
	Grabbing mechanism													
	robotic arm	defined in Section 3.4.2												
	Sensors for determination													
	VLC and ToFC	defined in Section 3.5.1												
	Provide adapter for Kit													
	linear arm(s)	2	2	2	0	0	1	2	2	2	1	-	-	**14**
	second robotic arm	0	1	1	2	2	1	1	1	1	2	-	-	**12**
Propulsion	Chemical propulsion - Agile and flexible													
	mono-propellant (hydrazine)	2	0	1	1	1	1	2	2	1	1	0	2	**14**
	bi-propellant (LOX/LCH4)	0	2	1	1	1	2	1	1	1	1	2	0	**13**
	Precise low thrust / Enable stabilization													
	multiple 10 N	1	0	1	0	0	0	1	1	0	0	-	-	**4**
	multiple 5 N	1	1	2	1	1	1	1	1	1	1	-	-	**11**
	multiple 1 N	1	2	2	2	2	1	1	1	2	2	-	-	**16**
	Chemical propulsion - Transportation of Kit													
	cold gas	2	0	0	1	1	0	2	1	0	0	-	-	**7**
	hydrazine	1	2	1	1	1	1	1	1	1	1	-	-	**11**
	Medium thrust level / Enable stabilization													
	multiple 22 N	2	1	1	1	1	2	1	1	2	1	-	-	**13**
	multiple 10 N	1	1	1	1	1	1	1	1	1	2	-	-	**11**
AOCS	'Precise sensors' / 'Enable orientation' ⇒ Provide precise sensors for orientation													
	FSS	1	1	1	1	1	-	2	1	2	2	-	-	**12**
	MSS	1	0	1	1	1	-	1	1	1	1	-	-	**8**
	CSS	2	2	2	1	2	-	0	1	1	1	-	-	**12**
	ST	1	0	0	0	2	-	2	1	0	2	-	-	**8**
	ES	1	0	0	1	2	-	2	1	0	2	-	-	**9**
	IMU	0	1	1	1	2	-	2	1	1	2	-	-	**11**
	'Stay within berthing box' / 'Enable stabilization' ⇒ Provide actuators													
	thruster	1	1	1	2	2	2	0	1	1	0	-	-	**11**
	gyros	0	1	1	1	1	1	0	1	2	1	-	-	**9**
	reaction wheels	1	1	1	1	1	0	1	1	2	2	-	-	**11**
	'Enable positioning' ⇒ Provide sensors for positioning													
	from ground	1	2	2	1	1	0	1	1	2	0	-	-	**11**
	GPS	2	1	1	2	2	2	1	2	1	2	-	-	**16**
Data Handling	Process sensor data fast													
	on-board	0	1	1	2	1	2	2	1	1	1	-	0	**12**
	on ground	1	2	1	1	0	0	1	1	1	1	-	1	**10**
	Enable self- & failure management													
	all-in-one computer	1	1	1	1	1	1	1	1	1	1	-	1	**11**
	separate (additional) computer	2	1	1	2	2	1	1	1	1	1	-	0	**13**
Comm.	Enable supervision													
	parabolic antenna	1	1	1	1	2	2	0	1	0	2	-	-	**11**
	omnidirectional antenna	2	2	2	2	1	1	1	1	2	1	-	-	**15**
Power	Provide recharge capability													
	one string Li-Ion batteries	1	1	1	0	0	1	1	1	1	1	-	-	**8**
	multiple strings Li-Ion batteries	0	1	1	2	1	1	1	1	2	2	-	-	**12**

4.2.3 Resulting Design Configurations

The *interaction software tool* supports the configuration of the subsystems and areas not covered with the design tasks. Like the design configuration of the Kit, further considerations concerning, e.g., safety, are included for the actual design on subsystem level. Described in the following are ADReS-A specified configurations, standard spacecraft instrumentation or already addressed design specifications are not mentioned.

Structure Similar to the Kit's design, an orthogonal structure promises a compact structure and less complex design than, for example, a cylindrical surface. This way, solar arrays and other surface covering materials can be attached on plain areas. As the design of the robotic arm is not part of this thesis, the properties of *DEOS*-arm [85] are applied. In terms of mass, power, and size, *DEOS* has the most developed arm with a similar application. Role models for linear arms can be found in Earth based applications [53].

Power System With solar arrays in use, illumination is important for the recharge of the batteries. For the approach, a period is divided into *Illumination* and *Eclipse* with an *Approach Phase* resulting (cf. Figure 3.11). As ADReS-A also covers the transport, *Shuttling* is added. The respective energy budget is given in Table 4.6. During the *Illumination*, the cameras sensors are in use to detect the target while the other systems operate on a standard mode. Batteries can be recharged. The *Eclipse* is used for a possible desaturation of the reaction wheels, with a heater compensating the low

Table 4.6: Power budget of the different phases for ADReS-A.

		Illumination	***Eclipse***	***Approach***	***Shuttling***
time per period (6269 s)		4172 s	2097 s	900 s	-
Structure	Arms	-	-	350 W	-
	Sensors	50 W	25 W	50 W	-
Thermal System		-	260 W	-	260 W
Data Handling		100 W	100 W	100 W	100 W
Communication		32 W	32 W	32 W	32 W
Propulsion	Thruster	18 W	165 W	165 W	140 W
AOCS	Reaction Wheels	60 W	60 W	60 W	60 W
	Sensors	32.5 W	32.5 W	32.5 W	32.5 W
Margin		15%	15%	15%	15%
Required Power		**337 W**	**775 W**	**908 W**	**719 W**

temperatures of the space environment. The *Approach*, which takes part during the *Illumination*, requires all systems to operate. For the *Shuttling* between the orbits, the thermal system compensates for temperature variations. The low-thrust thruster will not be in use during this phase. For the determination of the target and the actual approach about 3126 s are theoretically available. The *Approach* itself with all instruments in use shall take a maximum duration of 900 s. Like the Kit's power system set-up, the additional power requirements of the *Approach* are covered by extra batteries.

Data Handling The close approach of an uncooperative target requires fast data processing and safety concerns for ADR missions are relatively high. The mentioned self-awareness in combination with significant failure-management capabilities shall address this challenge. Both are further specified and investigated in Chapter 5. Basically, the self-awareness shall enable the system to react to failures or unexpected events. The hazardousness of failures is varying - depending on the failure itself. The self-awareness and the feedback of the system about its momentarily capability with respect to the failure shall be situation based. Decisions are made between whether a successful maneuver is still possible, adapting the approach, or aborting the R & D maneuver.

Functional Architecture The functional architecture of the ADReS-A, as displayed in Figure 4.4, summarizes the described configurations. The subsystems follow the color scheme used for the De-orbit Kit.

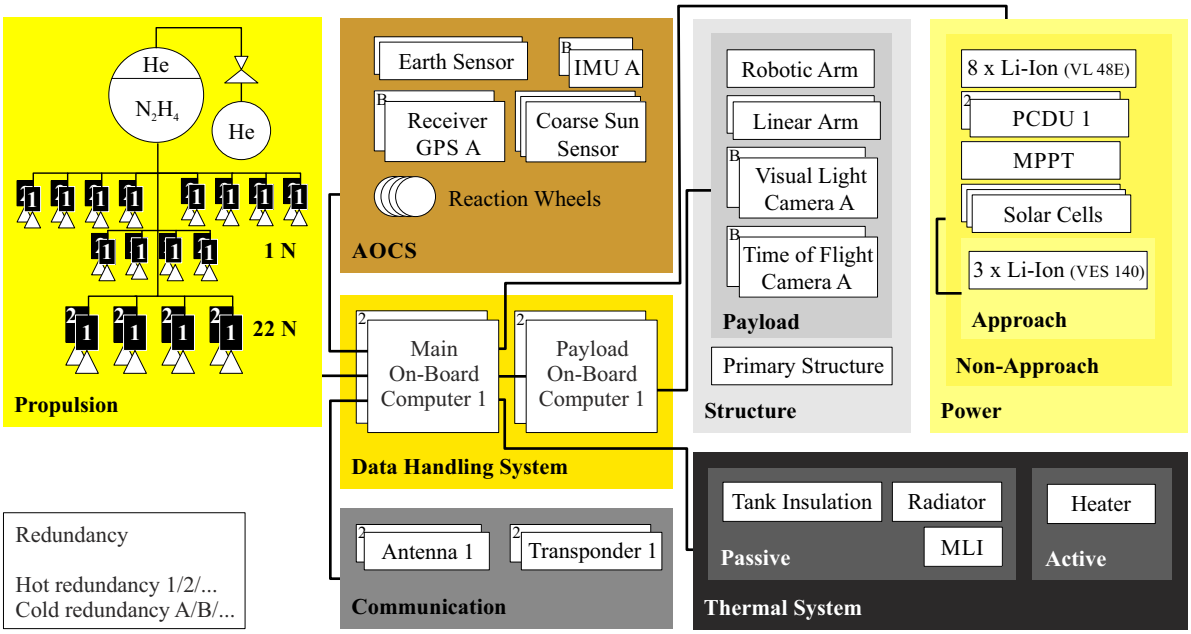

Figure 4.4: Functional Architecture of ADReS-A. Updated from Ref. [102]

CAD-Design The configurations, the mission set-up, and all named requirements lead to the design of ADReS-A presented in Figure 4.5.

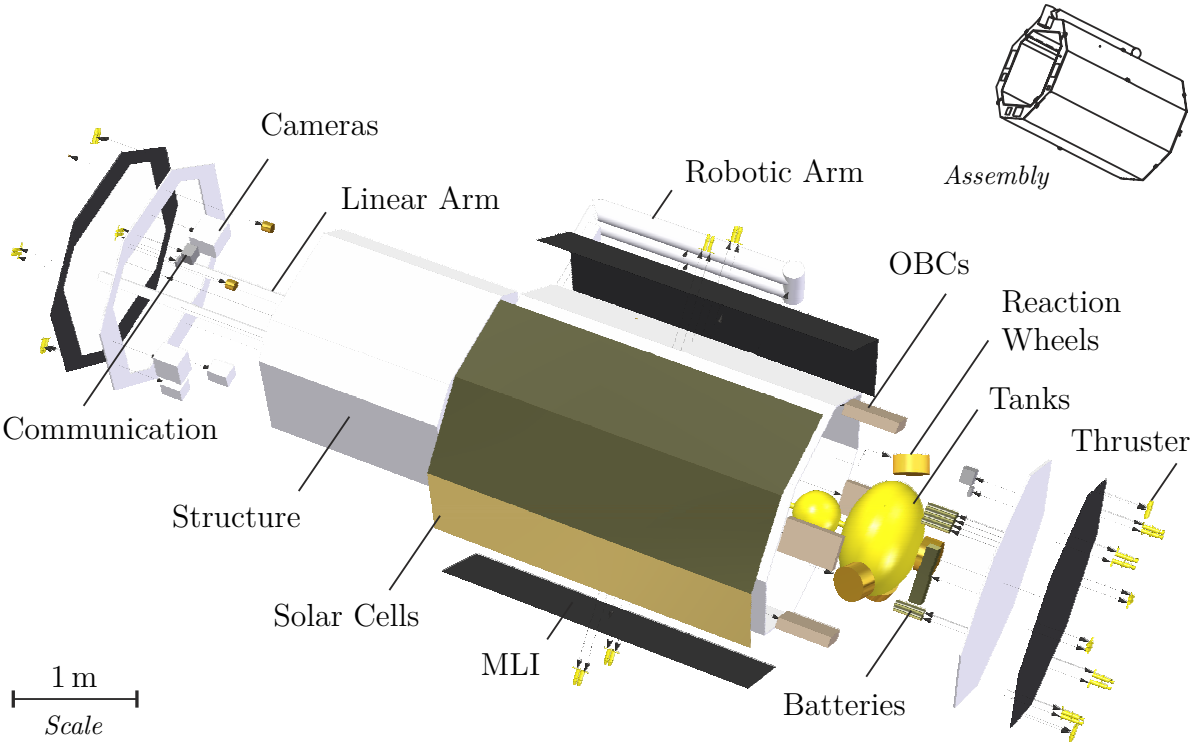

Figure 4.5: Exploded view and assembly of ADReS-A.

4.3 Mass Budget

To summarize this chapter, Table 4.7 lists the mass budget of the involved subsystems. The structure's total mass has a 15% margin included within the software tool. Appendix B.3 provides details on the listed specifications according to mass and power budget of ADReS-A and one Kit. The Δv requirements and resulting propellant mass is derived from Figure 3.12 with

$$m_T = m_{end}\left(e^{\frac{\Delta v}{I_{sp}\cdot g_0}} - 1\right). \tag{4.1}$$

m_T is the mass of propellant, m_{end} the dry mass of ADReS-A. For the respective phases the dry mass additionally includes either the embodied Kit or the target to be de-orbited. The specific impulse I_{sp} is of hydrazine (320 s). g_0 presents the gravitational acceleration. The stated Δv of 480 m/s for transfer and de-orbit is multiplied by 130 %. This factor includes the pre-design margin of at least 20 % and an extra 10 % to address

the case in which too much time is required for the compensation of the true anomaly. In this case, the RAAN differences must be covered by impulsive maneuvers, which can be quite propellant intense. For the Kit's de-orbit together with the target, the Δv for de-orbit of 244 m/s provides the basic data that is multiplied by 130 %. As the target with a mass of about 1600 kg must be removed, the resulting propellant adds up to 198 kg.

Table 4.7: Mass budget for the different subsystems for ADReS-A and one De-orbit Kit.

	ADReS-A	**De-orbit Kit**
Structure	439 kg	72 kg
Power System	50 kg	28 kg
Thermal System	11 kg	7 kg
Data Handling	42 kg	11 kg
Communication	4 kg	4 kg
Propulsion	65 kg	96 kg
AOCS	41 kg	10 kg
Margin	15 %	15 %
Total, dry	**750 kg**	**262 kg**
130% Δv	642 m/s	317 m/s
Resulting propellant mass	354 kg	198 kg
Total, wet	**1104 kg**	**460 kg**

5 Self- & Failure-Management

A solid self- & failure-management capability is required for a standardized removal of large debris from space. The challenge of the close proximity of two objects in space is one of the main reasons for such need. Handling an uncooperative object, never designed to be removed and as such without any helpful sensors to provide knowledge about its motion, without any aid for an adapt mechanism, and most probably tumbling in some way, drives the need for new approaches. Additional to the geometrical challenge, the chance for an unforeseen time critical event is most serious. A constant connection to ground may be theoretically possible if the observation capabilities are enlarged. It is, however, highly unlikely to become a standardized procedure for removing 5 to 15 objects per year over a long period. More realistically, a constant observation and connection to ground cannot be guaranteed. The available bandwidth is another open challenge. The chance to transmit all relevant information to ground in the available time frame is small. Here, the operator still needs to process the received data and develop a strategy to bypass the event, which brings the challenge back to the time issue.

Giving the satellite the possibility to process the unforeseen event or failure in a self-managed way, allows for reaction time to be reduced. The worst situation for a removal satellite is to become debris itself by, e.g., colliding with the target. By allowing the spacecraft's on-board system to make decisions on the activities to be performed when unplanned events are detected, safety will be increased.

This chapter concentrates on the conceptualization of the self- and failure-management for the ADReS-A-mission. The actual programming needs to be done by experts, once the spacecraft is designed in more detail. The considerations given cover the chaser as described in Chapter 4, with exemplary failures taken into account. The developed strategy is framed by definitions, theoretical background, technical requirements, and reported failures from existing satellites.

Definition

In General Self-management of a system, also referred to as autonomy, is very close to automation, as it derives from it. Concerning technologies, both terms refer to processes that may be executed independently from start to finish without any human intervention. Automated processes replace hereby routine manual processes with soft- and/or hardware ones. They follow a step-by-step sequence that may still include human participation. Autonomous processes have the goal of emulating human processes rather than replacing them [123]. Instead of following patterns, autonomy has self-managed responses to scenarios that are not pre-defined in every detail and, thus, require the awareness of the system in its entirety.

ECSS In 2008 the European Cooperation for Space Standardization (ECSS) has defined mission execution levels for spacecraft applications [26], given in Table 5.1. According to Olive [90], modern spacecraft had reached Level E2 by 2012, some deep space spacecraft use decision making capabilities implemented after launch, using On-Board Control Procedures (OBCP), and can be considered to reach Level E3 [132]. Before sending ADReS-A into space, Level E4 should be successfully tested.

Table 5.1: Mission execution autonomy levels following [26].

Autonomy level	Description	Functions
E1	· Mission execution under ground control · Limited on-orbit capability for safety issues	· Real-time control from ground for nominal operations · Execution of time-tagged commands for safety issues
E2	· Execution of preplanned, ground-defined, mission operations on-board	· Capability to store time-based commands in an on-board scheduler
E3	· Execution of adaptive mission operations on-board	· Event-based autonomous operations · Execution of on-board operations control procedures
E4	· Execution of goal-oriented mission operations on-board	· Goal-oriented mission re-planning

Processor Capacity

The increase of the processor capacity over the years is favorable for the actual implementation of self-management in a spacecraft. With a high enough processor capacity, decision-making processes are likely to be transferred from ground to spacecraft. As benefit, the human operator would be released from observing an increasing volume of data. This way, the supervision of the data could be concentrated on the crucial rather than the trivial ones. As of today, the rough number of 15 years delay in processor capacity transport from ground to space applications are observed, as Figure 5.1 reveals. In the plot, the processor capacity of several space missions is compared with the processor capacity available in ground applications in the same year. As the processor capacity on ground is still increasing, higher self-management capabilities implemented in satellites become more probable soon - even with the 15 years delay.

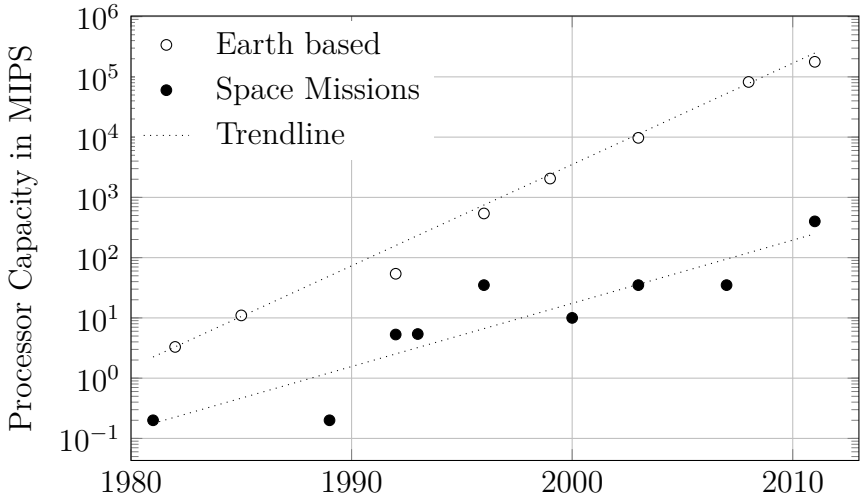

Figure 5.1: The processor capacity improvement of Earth-based and space-mission computers over the years. For performance measurement, Million Instructions Per Second (MIPS) are chosen. The data is collected from Ref. [6], [18], and [29].

5.1 Self-management Requirements for ADReS-A

Before conceptualizing the self-management for the mission, the theoretical background on the respective properties needs to be developed in more detail. The properties are based on Ref. [130] and are adapted for ADReS-A to meet mission execution Level E4. Critical aspects need to be specified to generate rules and priorities for the system to react accordingly. Requirements of the mission with an impact on the self-management are given.

5.1.1 Self-managing Properties

Knowledge The knowledge of the system refers to component values and margins, theories, problem-solving strategies, functional modes, rules of the reasoning process, data contents, and data structure. The knowledge specifies internal system and environment structure and behavior. The component's and system's capabilities of interaction and integration with other systems on the various level is additionally included. Further categorization can either be done into internal knowledge about the system itself and external knowledge about the system environment - or into a-priori knowledge and situational knowledge. The former is given to the system by the developer, the latter is gained from analysis of the performance during the process. This categorization depends on the self-management concept in use. The knowledge enables a system to adapt to changing situations by providing the mathematical background as it handles dynamic and situation dependent values.

Monitoring For ADReS-A, monitoring is performed by using sensors. This *input* obtains knowledge about the component's health as well as the environmental status. Monitoring is, therefore, essential to develop awareness to detect changes.

Awareness The system needs to understand the implications of changes, which implies self-awareness and context-awareness. The former covers the state of each component, the entities, capacities, capabilities, and physical connection. The latter contains the negotiation, communication, interaction with the environment, and anticipation of the environmental states, situations and changes. In case the expected margins are exceeded, awareness recognizes such. Awareness, thus, delivers the knowledge to the monitored status. For the approach of ADReS-A, the distance to the target, its docking point position, its component status, and the chaser's attitude are constantly changing.

Adaptability Responding to a recognized unexpected change is one of the key capabilities of a self-managed system. The general ability to decide on-the-fly about an adaption to an observed behavior is crucial for the final approach to an uncooperative target. Decision making processes and concepts are, thus, further investigated.

Dynamicity While adaptability refers to the conceptual change concerning behaviors, dynamicity addresses the technical ability to act at run-time. For the ADReS-A mission, data processing and reaction in time is a huge challenge. As such, the concept as well as the technical ability depend on each other. The mentioned processor capacity increase is indispensable for this self-management property.

Resilience Resilience is the ability of technical systems not to fail completely in the event of a partial failure. It also enables the system to distinguish between temporary disruptions and actual failures. For ADReS-A, the failure-management is responsible for this property.

Summary Additional requirements, such as robustness or mobility, find their application within the system without being addressed separately - specifically given are the main aspects for ADReS-A. Concluding the self-management properties, monitoring of the system together with the awareness allows for a recognition of a change. The knowledge then puts that change into context. If the residuals exceed the allowed limits and cannot be explained through other sources, adaptivity and dynamicity decide about the possibilities of the failure-management, which again is provided by the resilience.

5.1.2 Critical Aspects

Unexpected events The active removal of an object never designed for such will naturally lead more often to unexpected events, failures, or misleading sensor-data than established spacecraft missions. When implying automated processes, the switch into *safe-mode* is the normal process in such cases. *Safe-mode* refers to a mode, where serious anomalies prevent the system from proceeding in the intended manner. During this mode, the satellite can continue its operation with reduced functionality. This procedure ensures the satellite's vital functions while the failure is being analyzed on ground. An unexpected event can either be internal - for example a component failure - or external - for example an obstacle in the desired flight path.
With the satellite unable to move after changing into *safe-mode*, the close vicinity to the target in combination with drift can become critical for ADReS-A. The switch into *safe-mode* must, thus, not be activated during the final approach.

Collision The worst case for the mission is to collide with the target. The possibility to become debris itself or create ejecta - and with such even more debris - must be avoided in any case. Before switching into *safe-mode* and allowing for a possible investigation by ground command, a safe position without harming drift needs to be obtained. The self-management is required to give the satellite the capability to react based on the situation and bring that respective situation into a context.
Once the decision for an abort is made, the satellite will direct itself to a safe distance. Here, the switch into *safe-mode* can help to safe the mission. Safe in this context refers to a distance and position, where drift and residual relative velocity hardly affects the relative distance to the target.

Failure The category *fault or failure* implies an unauthorized deviation of a technical system. The sources of failures vary and cover the whole spectra of design failures to environment-anticipation failures. Some failures are difficult to categorize as they straddle several categories. An affiliation is then given to the category they are primarily correlated with. An overview of investigated ones is given in Section 5.2.1.
While different approaches on failure detection and isolation are investigated in other research, for example by Wander [132], ADReS-A concentrates on the recovery part and with such on the interpretation of symptoms. Different failures can have similar symptoms and vice versa. For the success of the mission it is therefore important to interpret those symptoms and react according to this interpretation - at least during the close proximity operations to avoid the risk of collision at any time.

Illumination For the actual final approach, illumination is vital but assumed to be sufficient for the scope of this thesis. It is mentioned within the critical aspects, as the external timing for the approach needs to ensure to avoid the critical phases in which the cameras in use are unable to process the data adequately. Illumination could be one interest of further investigation of the topic and is, therefore, listed within the recommendations in Section 7.2.

5.1.3 Capacity and Quality Requirements

Further steps to develop the strategy for ADReS-A's self-management are the determination of the system's requirements. Categories the requirements are divided into are *capacity* and *quality requirements*. The former specifies the system's range of capacity, the latter gives priority to the qualities and constrains of the system's work environment.

Capacity Requirements

The system observes its status and acts when limits are exceeded. It considers on-board resources, their constraints, the capability to execute an activity, and the ability to cope with unexpected events such as faulty devices or contingencies.

For the considered mission, the external range of capacity is expressed by the relative distance limits the spacecraft has, as well as its relative velocity. The distance of the CoMs, e.g., is limited in its minimum value by the body's dimensions. The maximum distance between the two object is limited by the camera properties. The relative velocity, again, is limited by the thrusters in use. Within the resulting available time

frame, the actual values change with each step, beginning with the start of the approach and finishing the moment the docking points meet.

The internal environment is limited to the components of ADReS-A. The CSS, for example, shows a 120° FoV and provides the spacecrafts attitude in respect to the Sun with an accuracy of ±5 deg. The components value constraints relevant for failure handling during the approach are given in Table 5.2. Even though software failures also provide failure sources, concentration is put on the hardware. As the internal parameters undergo constant changes, just as the external ones, each step for the approach will need a specifically assigned value. The maximum and minimum values stated frame their scope. They present hereby an example and will differ in case another component type is chosen.

Table 5.2: Internal component value constraints for the self- and failure management. Given are the maximal and minimal values for the respective components according to the presented mission. When available, accuracy and/or bias are provided.

Component	Max. value	Min. value	Accuracy/Bias
CSS	Vector Sun		±5 deg
ES	Vector Earth		Ang.: 0.06°, 3 σ
GPS	absolute orbital data		10 m; 0.15 m/s
IMU	relative attitude data		Ang.: 1°, 1 σ; Vel.: 1 σ
ToFC	40°×40°FOV		200×200 pixel á 45×45 µm
1 N Thruster	1 N	0 N	0.027 N sec min. imp. bit
Tank (Hydrazine)	461.2 l	69.18 l	-
Valve	1	0	-
Reaction Wheels	angular momentum: 45 Nms;		
	motor torque: 75×10^{-3} Nm		±6000 rpm
OBC	data processing		-
Battery VES140	3×39 Ah, 140 Wh		-
Battery VL 48E	8×48 Ah, 170 Wh		-
Antenna/Transponder	S-Band link		-
Surface Heat sensors	373.15 K	143.15 K	-
Internal Heat sensors	303.15 K	283.15 K	-

Quality Requirements

The quality requirements for the mission are expressed in percentage for this work. The respective value reflects a component's required data available for determination, and the margins included in the satellite design. In case of cold or hot redundancy, the redundant component is not included in the percentage value and is left as a recovery option. The spacecraft includes, for example, six CSS - one on each long side, with the Solar Arrays counted as complementary sensors. With at least two of them on opposite sides working properly, or three of them on connected surfaces, the required vector can be calculated. At least 30 to 50% of the sensors need to work at full capacity to meet the constrains of the system. Similar considerations are taken into account for the other components, resulting in Table 5.3.

Table 5.3: Internal component success rate constraints for self- and failure-management. The given success rate must be reached for a full functioning system. Safety factors are not included in the constraining percentage.

Component	# of Components	Redundancy hot/cold	Success Rate
CSS (+SA)	3 (+3)	-	30 to 50%
ES	2	-	80%
GPS	2	cold	80%
IMU	2	cold	95%[a]
ToFC	2	cold	30%[b]
1 N Thruster	24	hot	95%[a]
Tank (Hydrazine)	1	-	69.4% [44% buffer]
Valve	2	cold	95%[a]
Reaction Wheels	4	-	75%
Main OBC	2	hot	98%[a]
PL OBC	2	hot	98%[a]
Battery VES140	3	-	41.4% [141.5% buffer]
Battery VL 48E	8	-	78.25% [27.8% buffer]
Antenna/Transponder	2/2	hot	50%
Surface Heat Sensors	pending	-	95%
Internal Heat Sensors	pending	-	95%

[a] 100% are preferred, but cannot be guaranteed
[b] Highly depends on time available for calculations

5.2 Failure-Management

Especially for deep-space missions, the development of autonomous and automatic procedures has been pushed forward. In this context, the term Fault Detection, Isolation, and Recovery (FDIR) was developed. *Detection* refers to the monitoring and awareness properties stated earlier, sensors for internal and external monitoring are in use. *Isolation* identifies the faulty part by working its way through different layers. Those layers are defined by the designer. They usually start by identifying the wider area of an unacceptable deviation and end by to pin-pointing the actual fault. Generally, many sensors are involved and not all of them can be analyzed at the same time. Supervision needs, therefore, to be carried out through those layers. System knowledge about causal dependencies between the data are used. *Recovery* reconfigures and implements newly activated logic behavior. The logic behavior of the system is included by the designer. The updated version considers the new configuration and, thus, the faulty part. Concerning the self-management properties, failure-management can be connected to resilience. Adaptivity and dynamicity are included into the recovery solution. The simplest recovery is the use of a redundant component. For the AOCS system, for instance, a combination of the various sensors is implemented as they generate overlapping data.

Nearly every satellite is designed as a prototype, failures have always occurred and will always occur. Intensive testing on-ground can limit but not eradicate them. To get an idea of the possible failures satellites face, once they are in space, a failure overview and their probability & distribution is described int the following. The approaches for their identification, detection, and recovery follow. The overview is based on Harland [49], the failure probability & distribution additionally apply the more recent and more detailed work of Taferzoli [121] and Castet [14]. Their application to the mission concludes this section.

5.2.1 Sources

Overview

Design Failures Design failures describe failures that occur even though the environment remains within expectations and each subsystem functions correctly. Unexpected interactions between the subsystems are believed to be the cause, a more careful design, simulations and testing can help to prevent such flaws.

Propulsion System Failures Failures of the propulsion system are difficult to find as tests are difficult to perform. The number of valves and filters the flow goes through generates different temperatures, which again influences the other systems. The dynamic effect due to low gravity is also challenging to test on ground. Learning from previous missions and developing adequate simulations is the momentarily approach to limit the uncertainties.

Attitude Control System Failures Sensors for AOCS have the advantage to complement each other. They have been reported to fail quite often, but do not necessarily lead to a lost mission. The capability of other sensors to take over is most probably the reason. The implementation of redundant components helps to further decrease a mission loss.

Electrical Failures One main contribution to electrical failures is the space environment, as degradation affects the components much faster than on Earth. Chemical reaction, electromagnetic interference, and/or frequency variations support the early breakdown.

Environment-anticipation Failures Environmental failures occur when the actual environment does not meet the expected one. The understanding of the environment in space has greatly improved over the years. Challenges like dust, strong ultraviolet light, nuclear radiation, or heat are countered by improved shielding. Still, shielding for radiation, for example, is usually specified to one of the known sources: on board the spacecraft, high energy particles from astrophysical sources (galactic cosmic rays), solar wind particles, or charged particles circulating the magnetosphere.

Structural Failures A structure provides a fixed position for most of the transported components. The most challenging part here are the strong vibrations during the launch. Mechanisms - also counting as structure - have the additional challenge of lubrication and temperature changes. Especially due to degradation, temperature ranges differ from the original ones with time. As the mission time for ADReS-A is set to one year, such temperature changes pose small influence on the satellite.

Operator and Software Errors An operator error happens due to erroneous commands sent to the spacecraft or a misleading interpretation of the data collected. This human error is pretty much unavoidable. Training, however, increases the chance for success. Software failures can generate anomalies due to large number of data points in unknown states - a failure that is not testable. Sending a smaller amount of commands at any given time is one successful approach.

Failures on the Ground Failures during the construction or during ground tests are considered as avoidable when enough care is taken. Ground tests shall find design flaws, inaccurate testing however can cause damage. Other failures on the ground are due to forgotten lessons learned. Reasons are slipping schedules, trimmed back testing campaigns, or fast approaching deadlines that rush the production - a process very likely to generate avoidable failures. As the thesis concentrates on the approach, this type of failure is not further considered.

Failure Probabilities & Distribution

The studies performed on failure probability and distribution by Castet [14], Harland [49], and Tafazoli [121] follow different levels of detail. To match their conclusion, a common denominator had to be set. Figure 5.2 focuses on the generalized failure sources, Figure 5.3 concentrates on the affected subsystems. The failure sources mainly follow the ones introduced in the failure source overview. The propulsion system failures, attitude control system failures, electrical failures and structural failures are summarized in the hardware bar. The subsystems of Figure 5.2 mirror the ones introduced in Chapter 4.

Additional to the different categorizations, the three studies analyzed different periods: while Harland investigated about 2500 incidents occurring between 1962 and 1988, Tafazoli had 156 failures from 1980 to 2005 to observe. Castet, again, set his time frame from 1990 to 2008 with 1584 satellites reviewed.

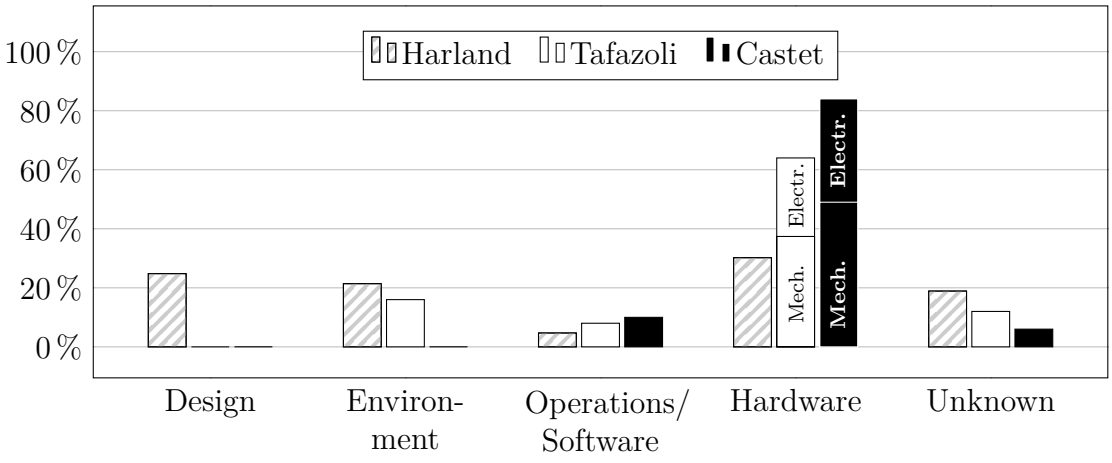

Figure 5.2: The results of Harland [49], Tafazoli [121], and Castet [14] regarding the failure sources, are displayed. The types are combined as the references use different breakdowns. *Mech.* refers to mechanical and thermal failures, *Electr.* to electrical and electronics.

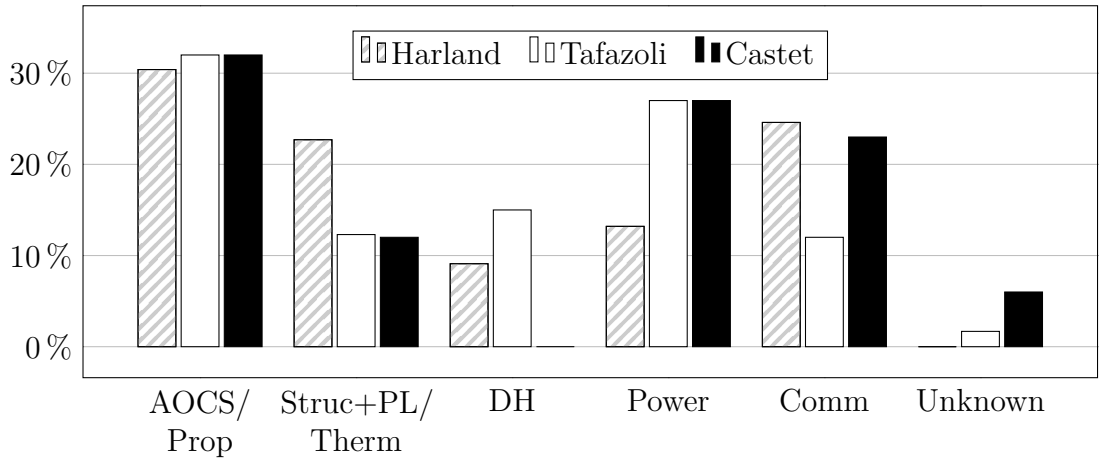

Figure 5.3: Failure distribution according to the affected subsystems by Harland [49], Tafazoli [121], and Castet [14].

The comparison of the studies reveals electrical and mechanical failures as the main contributors. The AOCS subsystem is affected most often and very susceptible for failures. 40% of the failures result in a loss of mission, in 65% a mission degradation had to be accepted. The sources concur that most of the failures occur within the first year of operation.

Failures for ADReS-A

To generate a more detailed failure-management for ADReS-A at component level, the work of Castet and Tafazoli is further investigated. The available data is consolidated to have a common denominator and presented for each author separately in Figure 5.4 and Figure 5.5. Failures relevant for the approach of ADReS-A are extracted. The publications address infant mortality as well as wear-out failures. As the approach starts after ADReS-A is commissioned, infant mortality can be excluded. The failure-management will, therefore, focus on the wear-out failures.

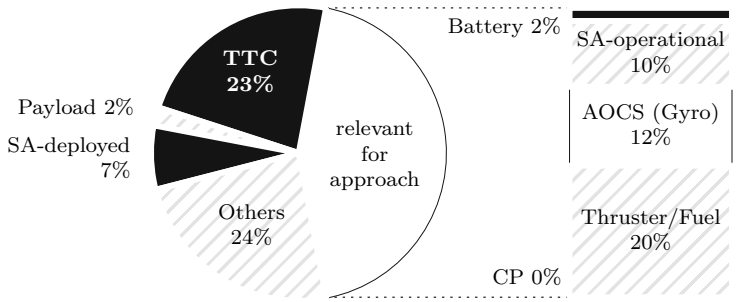

Figure 5.4: Component failures according to Castet. The **left** pie chart displays all investigated failures, the **right** chart the ones relevant for the final approach of a target.

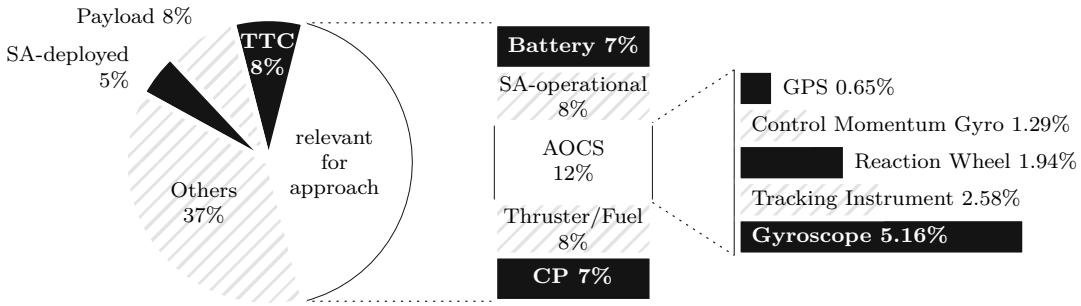

Figure 5.5: Component failures according to Tafazoli. The **left** pie chart displays all investigated failures and the **middle** chart the ones relevant for the final approach of a target. More detailed information is given in the **right** chart, allowing for further investigations of the AOCS.

For ADReS-A, about 44% (cf. Figure 5.4) and 42% (cf. Figure 5.5) of the displayed failures, respectively, are relevant to the final approach. All relevant failures, except a failure in the operating Solar Arrays (SA-operational), can become hazardous. This results in both investigated cases to about 34%. Possible failures of the Solar Arrays are important for the mission outside the close approach. Such failures will be used as an example for an uninterrupted approach.

5.2.2 Identification/Detection

For the analysis of failures, so called Fault Tree Analyses (FTAs) and Failure Mode, Effects, and Criticality Analyses (FMECAs) are performed within the space sector. The FTA represents a top-down analysis that starts with the undesired symptom and implements Boolean logic to merge a series of lower-level events. A FMECA works the other way around - it refers to a bottom-up analysis that concentrates more on the avoidance of failures rather than on failure detection. It involves investigating as many components and subsystems as possible to identify failure modes, their causes, effects, and criticalities. A specific FMECA worksheet is recorded for each identified component, with the regarding failure modes and resulting effects on the rest of the system. For ADReS-A, symptoms and their interpretation are most important. The approach through the FTA is, thus, chosen. The result is displayed in Figure 5.6. Both, software and hardware failures, are considered. If an *or* connection is given, one or the other cause will lead to the higher-level event, an *and* connection needs all included lines to fail at the same instance. Redundant input is given by overlaying circles. Figure 5.6 reveals a final probability for failure to 12.55%.

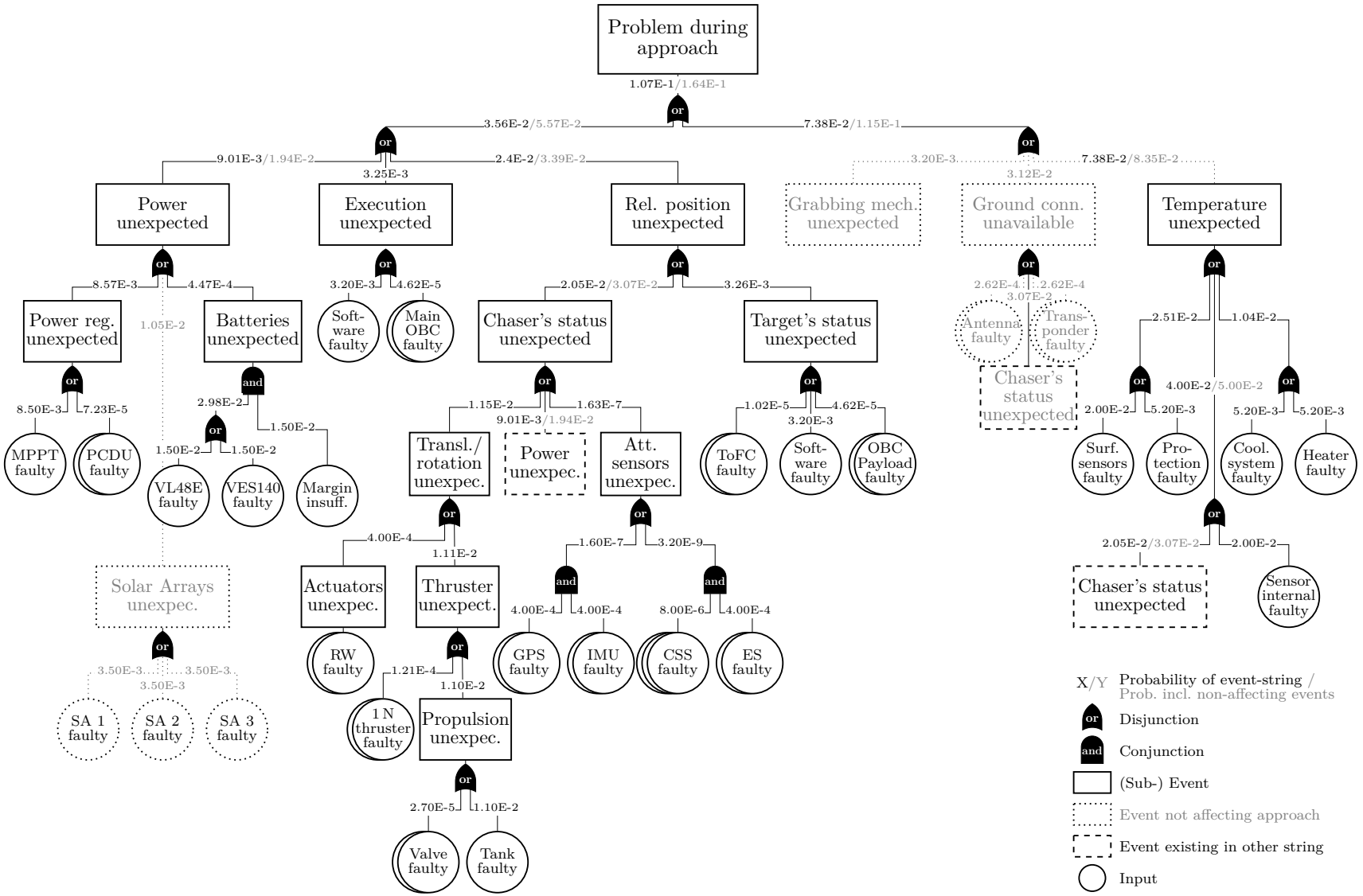

Figure 5.6: Fault tree analysis of possible failures for ADReS-A. The given and resulting probabilities - with *1* representing *100%* and *0* representing *0%* - are taken from Castet [14]. The gray numbers include the probability of non-affecting events.

5.2.3 Recovery

By addressing a symptom rather than the failure source, the depth of analysis can be kept lower, which again requires less processor capacity and time for calculations. The reaction to a deviation between the actual orientation and the intended one, for example, could either be caused by perturbations, a faulty sensor, or a broken component. The reaction in all cases is first to check if the other sensors confirm the deviation. If so, backup-margins are screened. In case they are sufficient, the system is put back on track. If not, an abort is commanded.

5.2.4 FDIR for ADReS-A

The self-management concept for ADReS-A is developed for the final approach. Accordingly, the system's capabilities will be managed, the initiated reaction follows. The described properties of the self-management take a relevant role in design, development, and verification. The recovery decides about the mission's way of proceeding.

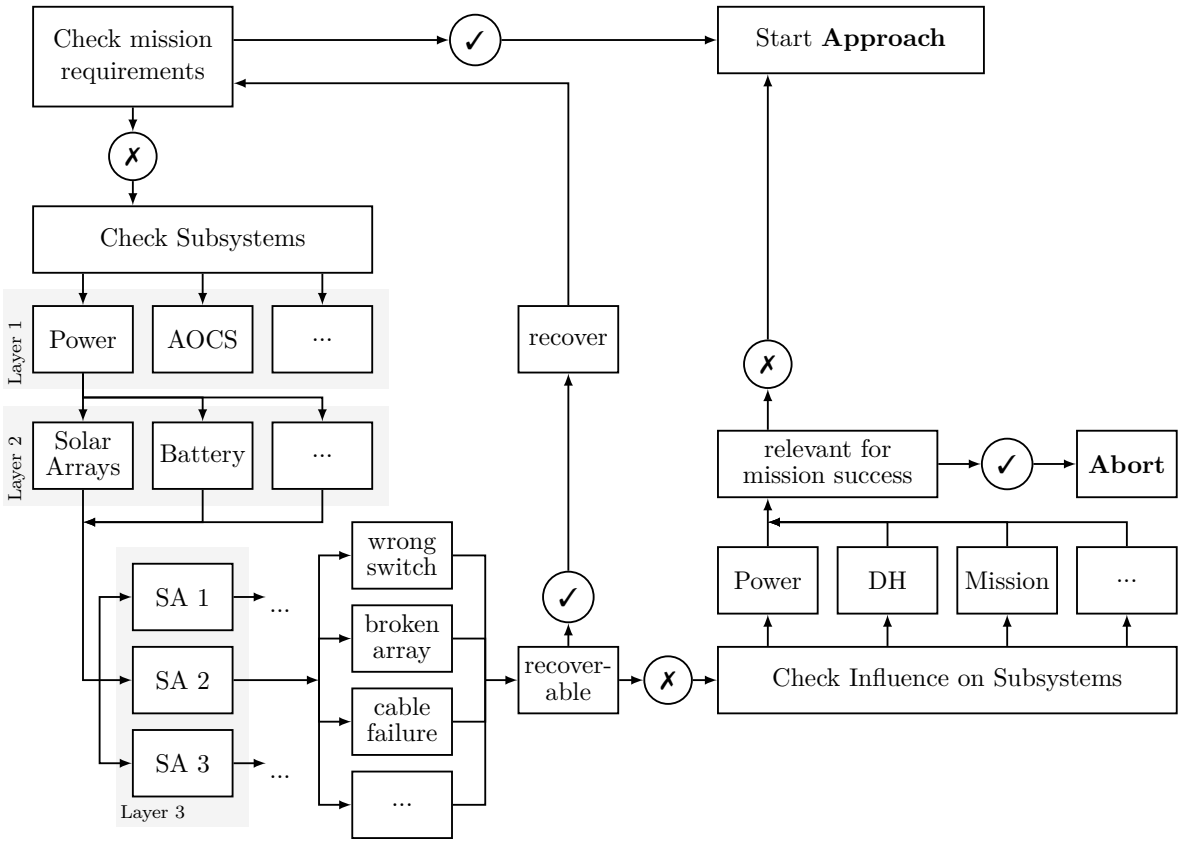

Figure 5.7: First level of failure scenario approach to detect the faulty part within the Solar Arrays (SAs) in Layer 3 and react accordingly.

A failure of a redundant component will lead to a switch from the faulty to the redundant one. In case no redundant part exists, a back-up solution is developed. Figure 5.7 gives the example of under-performing power data. Displayed is the decision-making path through different layers. The path starts by assigning the faulty subsystem (Layer 1), analyzing the behavior of the combination of components (Layer 2), and identifying the relevant one (Layer 3). Pin-pointing the type of failure follows. Options for recovery and their influence on all subsystems are tested with a final decision for an abort or an (adapted) approach taken.

For the displayed case of the loss of power a longer exposure of the other arrays to the sun is one option. This, however, will change the mission's timeline as the other arrays would have to extend their time of illumination to generate the same amount of power. Additionally, the involved batteries would take longer to recharge. If the analysis and adaption methods ensure the availability of enough power and the success of the mission is further confirmed, the approach is initiated with the respective changes necessary.

In general, the influence on all subsystems must be investigated to adapt their processes to the new situation. Table 5.4 gives an overview of possible impacts caused by the failed SA (cf. Figure 5.7). A validation of adaptability verifies if the values of the intended solution comply with specific requirements of the involved subsystems and components.

Table 5.4: Influences on the subsystems after a failed Solar Array, complementing Figure 5.7.

Subsystem	Involved component	Possible impact
Power	Solar Array	· Margins cover shortage
		· Other arrays need to cover shortage
	Battery	· Increased recharge time
Data Handling	OBC	· Recalculation to protect other sensors
Mission	Time	· May take longer
	Approach	· Extra recharge time
	Attitude alignment	· Provide longer exposure to sunlight for other Solar Arrays

Mission Continuation / Further Approach An approach in case of a failure can still be performed, if the approach itself is not affected or if other components can cover the loss. SA-operation, for example, is one of the leading failures according to the stated failure distribution. This failure is unfortunate for the whole mission but will most probably not harm the actual approach. The failure-management will decide to proceed and check for work-arounds after the Kit is successfully attached to the target.

Mission Abort Safety states one of the main goals for ADReS-A. If the system is unable to proceed with the approach, an abort is required. Many failures lead only in combination with specific circumstances to an abort - such as the dysfunction of a battery when the others cannot cover the shortage. Others will lead there right away, such as a failure of two reaction wheels at once. Some parameters only influence themselves, like a frozen arm joint, others influence the whole system. An abort is not always the best choice as such will cost propellant - one of the limiting factors of the mission. Switching, for example, to a redundant part, may be the better solution - if available. Decision making processes are, therefore, investigated in the following.

5.3 Decision-making Concepts

Performing failure-management includes the handling of inexact knowledge. The literature reveals different types: *uncertainty* about the truth, *incomplete knowledge*, *defaults or beliefs*, which are assumptions of the truth, *contradictory knowledge*, and *vague knowledge* [118]. In the case of ADReS-A, the last type is the most applicable. The sensors in use give a range of values, and with such a graded truth. It is neither exactly true nor false and depends on the combination of the values. *Vague knowledge* about the subsystems status is, thus, the further investigated type of inexact knowledge.

With the self-management requirements set and failure cases identified, available concepts for data uncertainty need to be investigated for application to ADReS-A. The concepts given in the following have been tested for the application of FDIR in space - either theoretical, in simulations, in on-ground hardware tests, or in-flight.

Bayesian Networks Bayesian networks interpret probabilities, generated as a degree of belief. They describe conditional probabilities and consist of two parts: a mostly graphical structure that forms a *direct analytical graph*, and an underlying mathematical interpretation of the signs. Every node of the graphical structure presents a probabilistic variable, either continuous or discrete. The edges model dependencies of the variables. Every probabilistic node is associated with a *conditional probability table* in which for every combination of its parental nodes a conditional probability is listed[1]. The application of Bayesian networks has been implemented, e.g., for landing site selections [112], or the Sojourner (Mars rover) system level for FDIR [27]. ESA additionally conducted a study on Advanced FDIR (A-FDIR) with probabilistic reasoning through Bayesian networks in combination with causal networks [20].

[1] A low-level example of the graphical interface and mathematical approach is given in Appendix A.4.

Dempster-Shafer Evidence Theory The Dempster-Shafer (D-S) Evidence Theory extends the Bayesian Theory by assuming a second degree of belief. Rather than assigning a truth or falsehood, it combines the source's accuracy of its degree of belief with a plausibility of the outcome and a probability range with an upper and lower boundary, respectively. A sensor with a reliability of 0.8, thus, does not result in a failure range of 0.2, but in an accuracy range of 0.8 to 1.0 as the user simply doesn't know, what happens in 20% of the cases [118]. The D-S evidence theory was investigated when comparing the Bayesian probability theory, the fuzzy set theory, and the D-S belief theory for a landing algorithm for other planets [112] .

Fuzzy Logic Fuzzy Logic was analyzed, e.g., in the SMART-FDIR study [20] or for subsystems on spacecraft in general [92]. It presents the mathematical interpretation of fuzzy knowledge by allowing each rule to be true (or not true) to a certain degree as more than two true states exist (e.g., black, white, and gray). Also, linguistic expressions can be mathematically processed. The degree of affiliation with one of the states is expressed by a Membership Function (MF). The MF states at which degree of belief a figure X is part of a set and can take any desired form. The form usually depends on the content-related question, e.g., if the transition between the sets is linear or rather exponential. Fuzzy logic is interpreted in three steps: After the input parameters are defined, the fuzzification determines the degree of belief of the parameter to the sets. In the second step, linguistic rules can be applied, so called fuzzy-inferences. The last step is the generation of one result (de-fuzzification). As the characteristics of the system cannot be changed except to process the data again, the pre-processing of data is very important for this method, and pre-validation of algorithm is required to ensure correct output.

Neural Networks Artificial neural networks are inspired by biological neural networks. They are capable of progressively improving their performance to accomplish tasks without being told to do so. Neural networks in aerospace applications have been investigated for use in robotic spacecraft [54]. While implemented at a low-level sophistication, it showed good failure tolerance, but precision and speed were challenging.

Analytic Model Based FDI The model-based approach to Fault Detection and Isolation (FDI) exceeds the hardware redundancy approach by mathematical models. They process a residual analysis based on observation of data and parity equations. The residuals are a product of faults, disturbances, modeling errors, and/or noise. While the system needs to be sensitive to faults, it needs to be insensitive to the other sources [22]. The approach was researched for on-board data handling [36], actuators [95], or space robots [41].

Cognitive Automation The approach of cognitive automation separates knowledge from knowledge processing, interpreting Rasmussen's model of human performance incorporation [106]. Figure 5.8 gives its interpretation by Onken and Schulte [91], who transferred it into the cognitive process. The a-priori-knowledge is modeled by the developer representing the domain expert's knowledge about the system. This knowledge is generated during the design process. The situational knowledge is created during run time, representing the actual situation. The cognitive sub-functions are represented by the outside arrows, using the situational knowledge to run the process. Enabling full access to the whole body of knowledge allows for self-awareness, even though the sub-functions have a preferred area to process information. To implement the theory into a framework, the Cognitive System Architecture (COSA) has been developed [104]. The system was successfully tested on drones [80] and is further developed for space application by Wander [132].

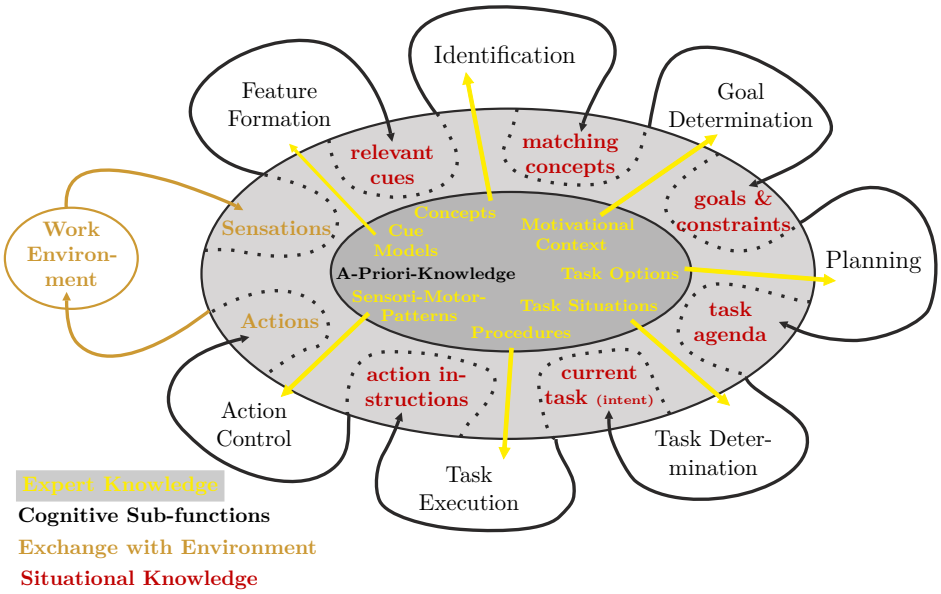

Figure 5.8: The cognitive process after Onken [91], displayed in the form of an amoeba.

Summary Table 5.5 gives an overview of the benefits and drawbacks of the respective concepts. After all, a solution may be built from multiple algorithms and based on different concepts. Focusing on one and applying such, however, is aimed for in a simple configuration such as the presented one. In case the concept is further developed, a modular set-up within the testing environment will enable a replacement (cf. Section 6.1).

For now, a relatively easy-to-understand and relatively easy-to-implement concept shall be chosen. While the approach of *COSA* is, for example, promising in terms of adaptivity to a changing environment during the approach, no further actions in its improvement

Table 5.5: Failure-management concept analysis: Benefits and drawbacks.

Concept	Benefit	Drawback
Bayesian Networks	✓ Immediate recognition of dependencies ✓ Graphical structure ✓ Training period medium	✗ Poor adaptivity to changing environment ✗ Few libraries
Dempster-Shafer Evidence Theory	✓ Combine information from different sources ✓ Extending truth or falsehood by probability range	✗ Range of trust of a source not quantified ✗ Few libraries ✗ No graphical structure
Fuzzy Logic	✓ Training period very low ✓ Covering of many cases by few rules ✓ Graphical interface ✓ Fast adaption of MFs	✗ Random MFs ✗ Loss of information by inept choice of MF
Neural Networks	✓ Good failure tolerance ✓ Learning capability	✗ Slow and complex
Model Based FDI	✓ Parity equations exceed sensor redundancy ✓ Decoupling of faults from other sources for residuals	✗ Dynamic system very complex ✗ Faults predefined
Cognitive Automation	✓ Interpretation of human behavior ✓ Self-awareness capabilities include large system	✗ Training period difficult ✗ Documentation leaks heavily

have been followed by the developers. Additionally, the documentation leaves great space for interpretation. All concepts presented can surely be adapted with sufficient results to the ADReS-A-mission. Out of the presented ones, however, *fuzzy logic* offers the fastest training period and a user-friendly graphical interface. Moreover, its interface and mathematical background is available by tools such as *Matlab*. The implementation of identified failures according to Table 5.3 can be performed with only a few rules defined. The rules are adaptable for specific desires of the developer and comprehensible by a foreign user. The other concepts are more complex. *Fuzzy logic* shall, therefore, serve as failure-management concept to develop the basic principles accordingly.

5.4 Application

With *fuzzy logic* chosen for decision-making concept, an algorithm that combines the identified failures and interprets them in accordance with Table 5.3 is created. Figure 5.9 shows the symptoms derived from the FTA of Figure 5.6 and forms the basis of the developed algorithm. Accordingly, a combination of different symptoms leads to different suggestions for reactions. Once a symptom - or a combination of symptoms - is identified, a reaction is derived. As the input is often neither fully true nor fully false, fuzzy logic interprets the data according to its settings.

At first, Symptoms 1 to 5 of Figure 5.9 are assigned to a specific subsystem, and with such to specific sensors. Symptom 2, for example, is assigned to *AOCS external*, which combines the sensors, that give information on the spacecraft's attitude. Namely, those are the ToFC and the GPS for this thesis.

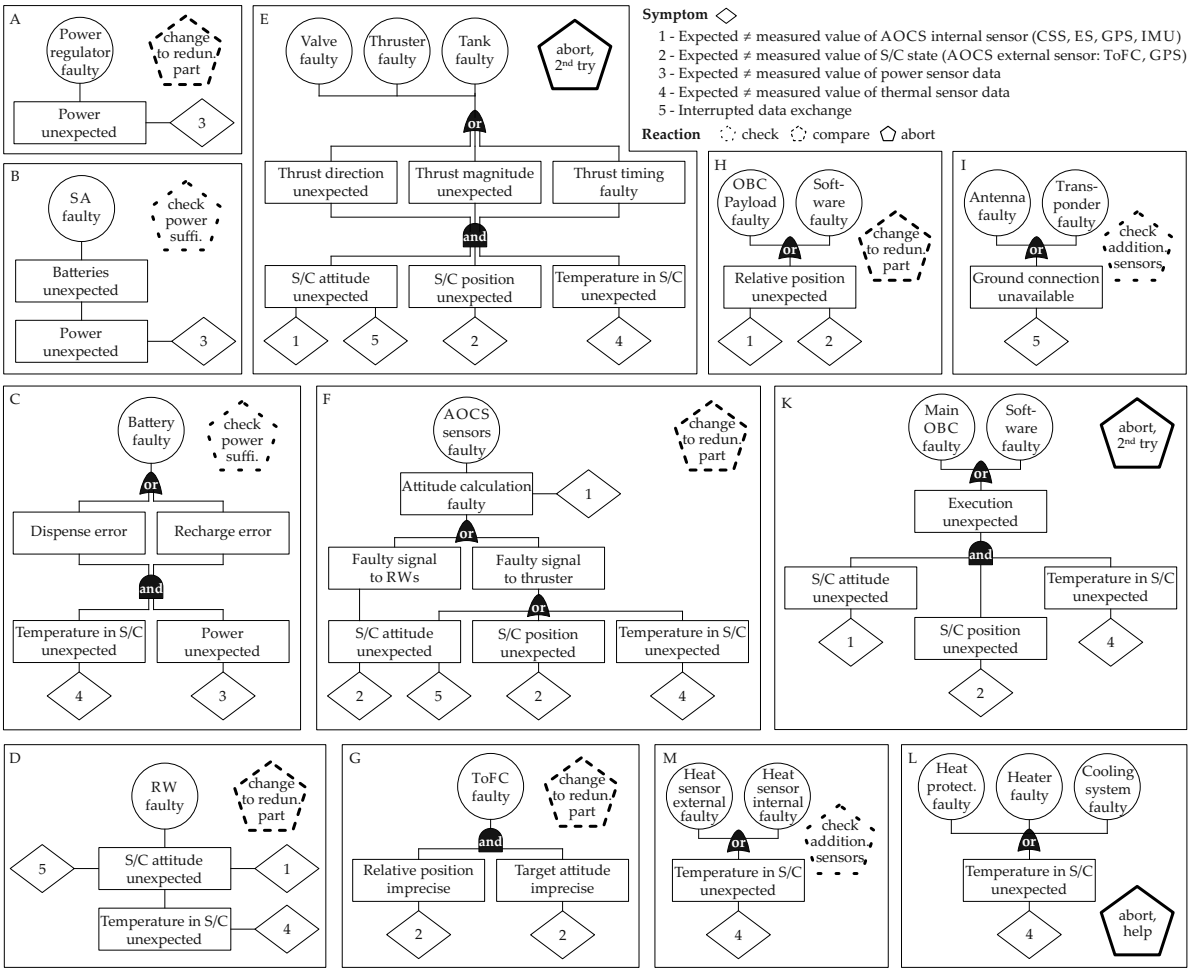

Figure 5.9: Symptoms of spacecraft failures derived from the FTA (cf. Figure 5.6).

Secondly, rules are assigned under which conditions the subsystem is still operational. Table 5.6 shows the ones for *AOCS external* and with such, if and how the ToFC and the GPS influence each other.

Table 5.6: Fuzzy rules for Symptom 2 - $\text{AOCS}_{external}$.

ToFC	&	GPS	→	$\text{AOCS}_{external}$
good	&	good	→	good
low	&	low	→	low

Additionally, MFs need to be defined. As the dependencies of *good* and *low* of the presented case are considered linear, the trapeze-member-functions are in use. The criteria of each sensor are taken from Table 5.3 - for the ToFC, 30% data knowledge is required for success, for the GPS, 80% is listed. Figure 5.10 visualizes the respective MFs with an exemplary ToFC of 25% and an assumed GPS of 80%. The resulting 72.8% of the $AOCS_{external}$ is not fully *good*, as the gray area shows.

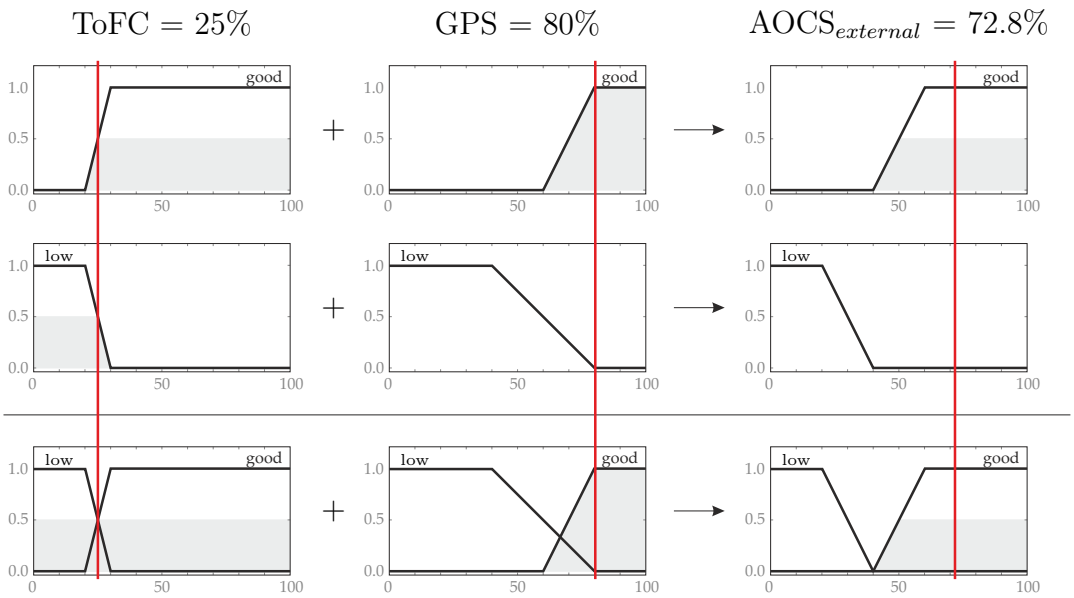

Figure 5.10: Graphical interface of the fuzzy logic for the example of $\text{AOCS}_{external}$. The upper rows present the two rules with the MFs applied, the lower row gives their summary.

To interpret the derived value, de-fuzzification is required. The presented mission, however, first combines the different results from the symptoms. In total, 32 rules are assigned to the combination of symptoms derived from Figure 5.9[2]. Figure 5.11 shows the information flow and assigned MFs from the sensors to the symptoms to the output.

[2]The list follows the example given in Table 5.6. It is attached in Table B.8.

The one assigned for the output is a triangular-shaped membership function. This MF allows for specific conclusions. In the displayed case, the change to a redundant part *(a) Check margins* is the reaction. For cases not defined, the abort with a followed-on support from the ground station is suggested. For cases that result in two different reactions - such as the ones given in Box M and Box L - the worst case *(d) Abort, help* is chosen. To identify the involved subsystem in which the redundant part shall be replaced, the developed algorithms points back to the sensor(s) causing the reaction and provides suggestions.

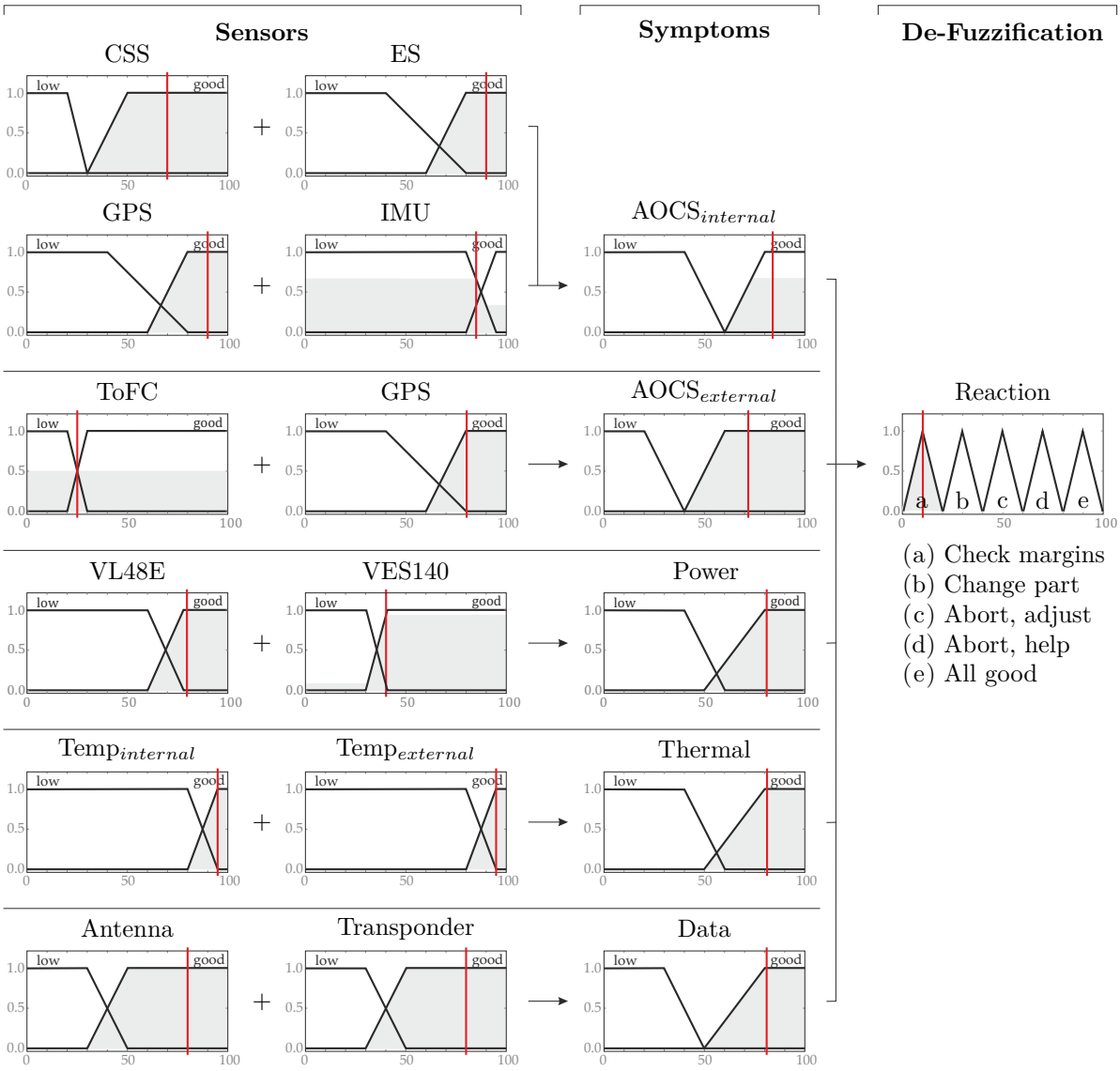

Figure 5.11: Graphical interface of the fuzzy logic for the ADRe-A-mission. The two left columns show the MFs of the sensors, the third column their input on the symptoms' MFs. The right column combines all input and gives a de-fuzzification (reaction) of such.

6 Analysis

This chapter combines the results of Chapter 3 to 5: The mission design forms the frame in terms of the environment, the orbit, the target, and the overall removal concept. The system architecture provides data on the targets and the designed spacecraft. The self- & failure-management allows for an on-board decision-making feature, which can be implemented in future research.

The chapter starts with a presentation of the developed simulation. Considered simplifications and the modular architecture are introduced. The second part of the chapter details the various modules of the simulation tool. The third part analyses specific parameter of the tool. Focus is put on the required maneuver time, resulting maximum thrust and torque, and the calculated propellant consumption when assuming hydrazine.

6.1 Simulation

The motivation for creating a simulation for the docking process derives from the need of extensive testing before realizing such mission. The presented simulation is introduced through its architecture and followed by a more detailed description of the implemented modules.

6.1.1 Considered Simplifications

The simulation itself must cover the close approach of ADReS-A. It requires in its basics the operational specifications, the dynamics of the objects involved, and an output for analysis of the trajectory. As a simulation will never reflect the actual reality in all its detail, considered simplifications are discussed before generating the simulation's architecture.

Orbital Disturbances

Orbiting in LEO leaves a satellite with five main environmental disturbances: the solar radiation pressure, the satellite's aerodynamic drag, the gravity-gradient, the flattening of Earth's poles (J_2-term), and the magnetic field. The first two highly depend on a space object's cross-section. The gravity gradient and the J_2-term affect a satellite's orbit in attitude and position. The magnetic field perturbation depends on an objects dipole moment and is usually in the order of $1/4^{th}$ of the gravitational perturbation. With both, target and chaser (including the Kit), being in the same orbit during the capture - and showing similar size and mass - the listed disturbances are considered to affect the objects almost equally.

The General Mission Analysis Tool (GMAT) will be used for the verification and validation of the simulation and is, therefore, also applied to validate the neglect of the mentioned disturbances. Compared within GMAT is a scenario with the same orbit as the ADReS-A mission and both non-tumbling objects 17 m apart along the direction of the orbital velocity vector. The pre-determined time for the approach is set to 900 sec. The first case covers the scenario without a gravity model, nor drag or solar radiation pressure, and models Earth as point mass. The second case applies the JGM-2 model for gravity, the JacchiaRoberts atmospheric model, a spherical solar radiation pressure model, and the Moon and Sun as point masses (for details see GMAT documentation [44]). Any other data of the approach calculation is retained.
The comparison of the two cases, given in Table 6.1, reveals that during an approach of 900 sec, deviations do not exceed the micrometer-per-second range for the relative velocities with a maximum of 9.3 µm/s, nor the micrometer range for the relative position with a maximum of 12.6 µm, nor the milligram range for the required hydrazine with a deviation of 14.47 mg. As these values are small compared to the absolute numbers, perturbations are further neglected within the simulation.

Table 6.1: Comparison of an approach of 900 sec, based on the ADReS-A mission, with and without (w/o) environmental disturbances.

	Rel. pos. in m			**Rel. vel. in mm/s**			**Hydrazine**
	ξ	η	ζ	$\dot{\xi}$	$\dot{\eta}$	$\dot{\zeta}$	**in mg**
With disturb.	-5.282	1.081	-0.001	19.85	26.75	0.00	24621.2
W/o disturb.	-5.282	1.081	-0.001	19.86	26.74	0.00	24635.6
Deviation	12.6 µm	6.8 µm	3.0 µm	9.2 µm/s	9.3 µm/s	3.5 µm/s	14.4 mg

Geometry & Docking Points

The involved objects are modeled as CAD-model, the derived Moments of Inertia (MoI) as well as mass and size are slightly adapted for the simulation. As the distribution of the presented components is preliminary, the MoIs in the simulation are derived from homogeneous mass distributions with the bodies simplified to homogeneous cylinders. This form is closest to the designed body and allows for an analytical mathematical approach when calculating the angular velocities and trajectories to follow. Additionally, the docking points must be pre-assigned. Figure 6.1 illustrates the docking point positions outside a theoretical sphere enveloping the bodies for the simulation. The simulation ends once the docking points match in position and velocity.

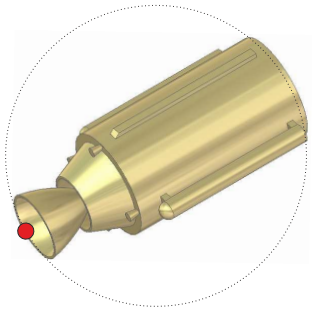

(1) Target CAD model

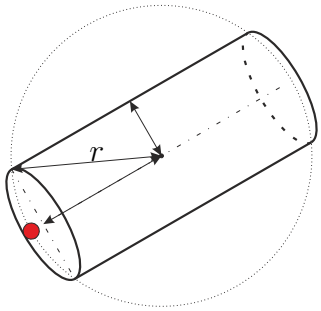

(2) Target cylindrical model

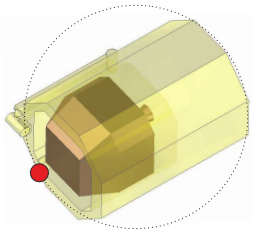

(3) ADReS-A & Kit (chaser) CAD model

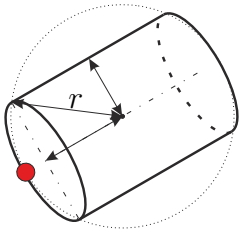

(4) ADReS-A & Kit cylindrical model

Figure 6.1: Geometric simplification of the target and the chaser. **(1)** and **(3)** show the CAD-model of the target and ADReS-A with an embodied Kit as presented in former chapters. **(2)** and **(4)** display their cylindrical shape as geometric simplification. Additionally, the respective positions of the docking points, marked as red dots, are displayed. The dotted circles reflect the spheres enveloping the bodies.

6.1.2 Modular Architecture

The simulation's architecture with the various modules and their interaction is given in Figure 6.2. The setup allows for configuration, adding, and/or the exchange of individual modules. Situation specific constraints can be added, changed, and deleted if required.

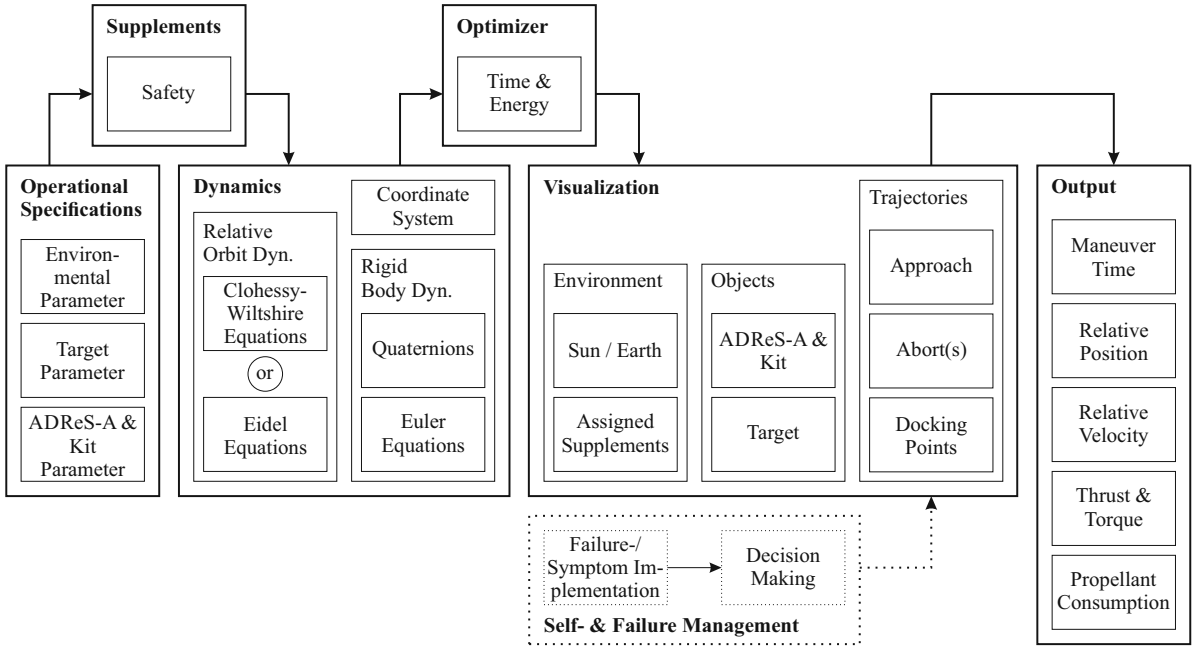

Figure 6.2: Modular architecture of the simulation. The solid modules form the present setup, the dotted module is an example for further development and possible extension of the simulation. Updated from Ref. [98].

The *Operational Specifications* comprise information about the space environment concerning altitude and inclination. Information about the target and ADReS-A with the incorporated kit are mainly derived from system architecture. *Supplements* extend the input data and can be amplified if desired. The physical behavior of the objects in space are implemented by the *Dynamics*. For a propellant saving trajectory, an *Optimizer* is altered and improved. The respective tool [81] is modified for the presented mission with abort trajectories added. The calculations are then *Visualized*, displaying the objects, trajectories, and the environments generated. The *output* gives information on the required maneuver time, on relative velocity and distance of the docking points, on applied thrust and torque, and on the resulting propellant consumption. The *Self- & Failure-Management* can be added in a further development of the simulation. As the approach and abort trajectories are calculated before the capture process is initiated, this feature shall decide which path to pursue, based on the non-nominal symptoms recognized during the approach.

6.2 Module Analysis

6.2.1 Operational Specifications

Environmental Parameter In accordance with Chapter 3, an inclination of 82.9 deg at an altitude of 980 km frames the simulation. Orbital disturbances are excluded as the influence on the trajectories are marginal.

Target Parameter The data of the targeted rocket bodies concerning their mass and size is given in Section 3.2.3, their MoIs are derived from the CAD-model. The considered residual propellant is assumed to distribute homogeneously, despite the chance for sloshing within the body[1].

ADReS-A & Kit Parameter Similar to the target, the CAD-model of ADReS-A and the Kit provide information about mass and size. The MoIs are derived from the cylindrical model with the homogenous distribution of the spacecrafts mass. ADReS-A and Kit are considered as one object as they form a rigid body during the approach. They are further considered as *chaser*.

Initial Distance The initial distance of the two bodies for the starting maneuver derives from the cameras in use. Depending on the required accuracy for spin rate determination, the investigations for the ToFC have been performed for distances between 11 and 20 m between the camera and the cylinder axis. The distance(s) and respective dimensions of the two objects are displayed in Figure 6.3.

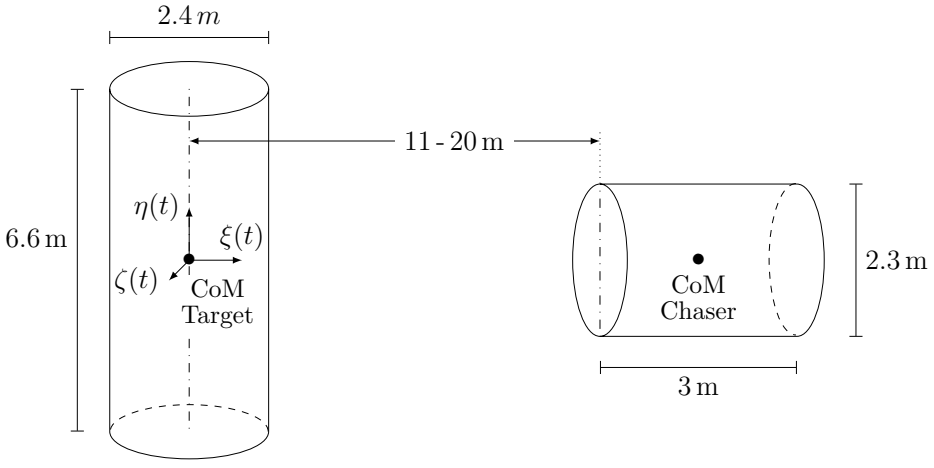

Figure 6.3: Dimensions of and initial distance between target and chaser.

[1]Remaining propellant will most probably lead to sloshing - a feature addressed in Eidel's work at the Universität der Bundeswehr München. As the mathematical approach is quite complex, this approach may find application in ground testing first - depending on the development of space proven processors.

The according spin rate accuracy for distances shorter than 13 m is determined to $\pm 10^{-4}$ deg/sec, for further distances to $\pm 10^{-2}$ deg/sec [45]. The final distance depends on an optimization between tumbling mode and safety as well as agility capabilities. An initial distance smaller than 11 m is not recommended for safety reasons.

Following the analysis of orbital dynamics (cf. Section 6.2.3), the drift along the ξ-axis affects the bodies the least. The starting point for the approach shall, thus, be at:

$$\begin{bmatrix} \xi_0 \\ \eta_0 \\ \zeta_0 \end{bmatrix} = \begin{bmatrix} 12.5...21.5 \\ 0 \\ 0 \end{bmatrix}. \tag{6.1}$$

Resulting Input Data (Constants) The operational specifications result in applied constants given in Table 6.2. The sphere radius required for the rendezvous calculations is derived from the objects' sizes, calculated by

$$r^{C/T} = \sqrt{\left(\max\left(l_f^{C/T}, l_b^{C/T}\right)\right)^2 + \left(r_{Cyl}^{C/T}\right)^2}. \tag{6.2}$$

Table 6.2: Constants for the simulation and values for the ADReS-A-mission.

Constant	Value	Description
d_i^C $i = x, y, z$	$[2\ 0\ 0]^\top$	Chaser's docking point within its body-fixed coordinate axes [m]
d_i^T $i = x, y, z$	$[3.6\ 0\ 0]^\top$	Target's docking point within its body-fixed coordinate axes [m]
J_{ii}^C $i = x, y, z$	$[831\ 1515\ 1491]^\top$	Chaser's moment of inertia [kg/m^2]
J_{ii}^T $i = x, y, z$	$[1258\ 3187\ 3336]^\top$	Target's moment of inertia [kg/m^2]
m^C, m^T	[1600 1600]	Chaser's/Target's mass [kg]
l_i^C $i = f, b$	$[1.5\ 1.5]^\top$	Length CoM-front/back chaser [m]
r_{Cyl}^C	1.15	Radius cylinder chaser [m]
l_i^T $i = f, b$	$[3.3\ 3.3]^\top$	Length CoM-front/back target [m]
r_{Cyl}^T	1.2	Radius cylinder target [m]
u_{max}	1	Maximum thrust (Chaser) [N]
M_{max}	1	Maximum torque (Chaser) [Nm]
r^C, r^T	$[3.51\ 1.89]^\top$	Minimal sphere radius around chaser/target [m]
a	7 353 000	Orbit semi-major axis [m]
μ	$3.986 \cdot 10^{14}$	Earth's standard gravitational parameter [m^3/s^2]

6.2.2 Supplements

Safety Safety is addressed by an area which must not be penetrated at any time. Both objects rotate around their CoM. The envelope forms a sphere, illustrated by dotted circles in Figure 6.1. This sphere is extended with the support of a safety parameter C_{Err}. The resulting safety radius $s_{t,Err}$ adapts according to the distance of the approach trajectory already passed, following

$$s_{t,Err} = \max(C_{Err} \cdot |\vec{r}_{Err}|, r^C + r^T). \tag{6.3}$$

C_{Err} can be set between 0 and 1, with *0* adding no extra distance for security enhancement, *1* maximizing it. $\vec{r}_{Err}$ is the position vector of the chaser at the time an anomaly or failure is detected. The decreasing sphere (when getting closer) allows for sufficient security requirements during the approach and enables the objects to get close enough to eventually match their docking points.

Safety Parameter C_{err} The safety parameter and the resulting safety area has a strong influence on the abort paths, as the area must not be penetrated at any time. The closer the chaser gets to the target, the less area is available between the two objects. Figure 6.4 displays the propellant consumption of an abort path in respect to the safety parameter. For visibility reasons, the plot is limited to a few exemplary paths: Abort Path 2 reflects the first three paths (Path 1 - 3), that head back to the first safety point. For the investigated discretization, the safety parameter does not influence those paths in respect to the propellant consumption. Abort Path 9 (and the not displayed Abort Path 10) are likewise hardly affected by different C_{err}. The path most influenced is Abort Path 4, the required propulsion ascends parabolic with the safety parameter.

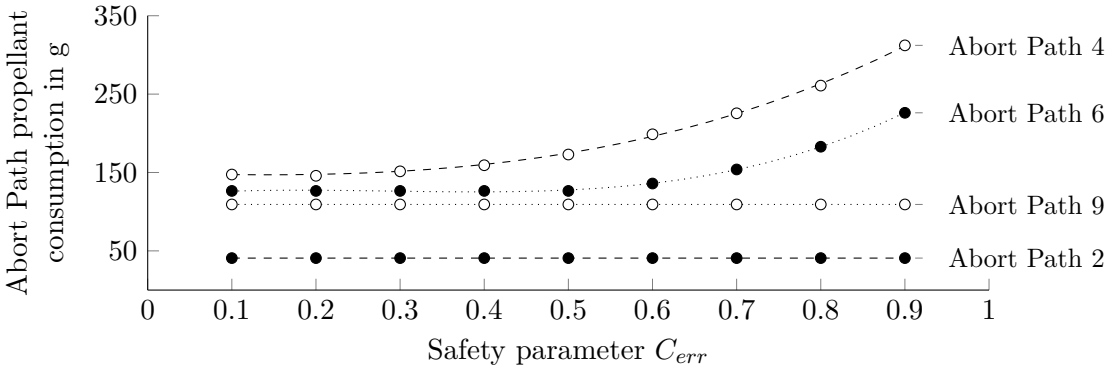

Figure 6.4: The influence of the desired safety parameter C_{err} on the propellant consumption. Displayed is the consumption of an abort with a maximal maneuver time of 600 s, the initial distance of the approach is set to 17 m.

Accordingly, a larger safety parameter results in a wider avoidance maneuverability in case of a failure, which again leads to a higher propellant consumption. Moreover, aborts cannot be repeated too often due to the high propellant-burn. It will depend on the final safety requirements, which safety parameter is favorable and how much propellant consumption can be approved. As the safety parameters can be adjusted during the mission, their value may be adapted to the residual propellant available at that time.

6.2.3 Dynamics

Coordinate Systems The Local Vertical, Local Horizontal (LVLH)-system shall be the reference system for the relative orbit dynamics. The point of origin is placed in the CoM of the target. As displayed in Figure 6.5, its ζ-axis points towards the center of gravity of Earth, its ξ-axis is in the direction of the orbital velocity vector. Its η-axis is perpendicular to the orbital plane, opposite to the angular momentum vector, and complementing the system. Additionally, Body Fixed Coordinate (BFC)-systems are defined for both objects. The BFC-systems have their origin in the particular CoM, its axes are aligned with the principle axes of inertia. This way, the respective rotational dynamics are modeled. Position and orientation relative to the reference system can be described and the docking points assigned can be derived. Figure 6.5 displays the three systems relative to each other.

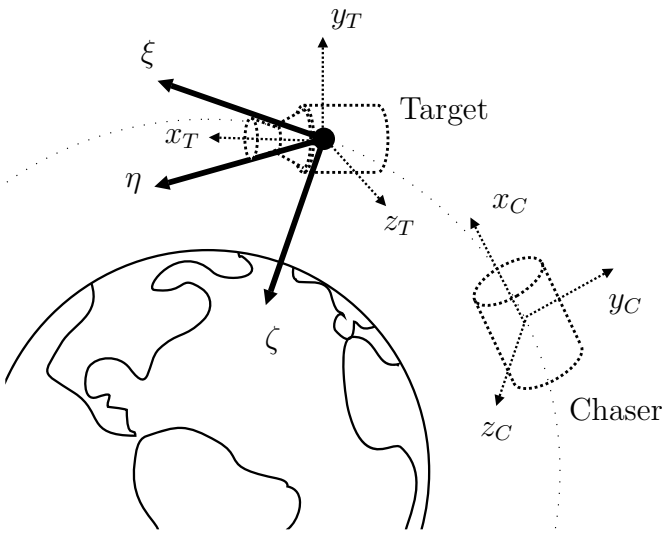

Figure 6.5: Coordinate systems of the simulation. The LVLH system is reflected by ξ, η, and ζ. The BFC-system of the target is reflected by x_T, y_T, and z_T and the BFC-system of the chaser by x_C, y_C, and z_C.

Relative Orbit Dynamics

Relative orbit dynamics are considered adequate for any distance $r_{rel} << R$, with r_{rel} presenting the relative distance and R the orbit's radius. For the discussed orbit and a r_{rel} smaller than 100 m it is, thus, legitimate to apply them. As the simulation aims to provide a tool for analysis and verification of different strategies - and dynamics are highly counter-intuitive in space - an analytical approach rather than a numerical one is chosen to calculate the relative dynamics. It supports the understanding of the influences that the changes in motions have on the system. The analytical approaches of Clohessy-Wiltshire (CW) and the one of Eidel are described and compared for suitability.

Clohessy-Wiltshire Equations Very common for relative dynamics are the Hill's equations - or CW-equations - as they provide a suitable approximation compared to the numerical approach. They are derived for near-circular orbits and consider a point mass:

$$\begin{aligned} \ddot{\xi} &= 2 \cdot \omega_{0_{CW}} \cdot \dot{\zeta} + \frac{F_x}{m} \\ \ddot{\eta} &= -\omega_{0_{CW}}^2 \cdot \eta + \frac{F_y}{m} \\ \ddot{\zeta} &= -2 \cdot \omega_{0_{CW}} \cdot \dot{\xi} + 3 \cdot \omega_{0_{CW}}^2 \cdot \zeta + \frac{F_z}{m} \end{aligned} \tag{6.4}$$

where

$$\omega_{0_{CW}} = \sqrt{\frac{\mu}{a_T^3}}. \tag{6.5}$$

m is the mass of the chaser and $[F_x, F_y, F_z]^\top$ the thrust vector applied on the satellite. The vector $[\xi, \eta, \zeta]^\top$ is the position of the chaser in relation to the LVLH coordinate system within the target.

Eidel Equations Eidel's equations [28] are derived for elliptical orbits with eccentricities smaller than 0.1. They extend the CW-equations by an additional term, indicating a higher dependency of the three directions of movement and allowing an influence by the Eccentricity e:

$$\begin{aligned} \xi_{Eid} &= \xi^{(0)} + e\xi^{(1)} \\ \eta_{Eid} &= \eta^{(0)} + e\eta^{(1)} \\ \zeta_{Eid} &= \zeta^{(0)} + e\zeta^{(1)}. \end{aligned} \tag{6.6}$$

While the first part ($\xi^{(0)},\ \eta^{(0)},\ \zeta^{(0)}$) reflects the solution of the CW-equation, the second part ($e\xi^{(1)},\ e\eta^{(1)},\ e\zeta^{(1)}$) defines the relative dynamics more precisely. The full definition of the Eidel-equations is found in Appendix A.5.

Comparison As the SL-8 R/Bs show an eccentricity of about 0.003, both presented approaches are considered suitable. Figure 6.6 provides the deviations the analytical CW- and Eidel-approaches generate - compared to the numerical approach. Displayed is a holding position of 21.5 m distance to the target ($\xi_{0_{max}}$ according to Equation 6.1) with relative velocities of 0.005 m/s in each direction. After three periods, the identifiable deviation from the numerical approach is in the range of 1700 mm for the CW-approach. During that time, the objects have moved about 300 m apart. For the Eidel-approach, the deviation for the same amount of time do not exceed the 16 mm range. The deviations through the CW-equations result to 0.54%, the ones through the Eidel-equations to 0.005%. The latter are, therefore, about 100 times more precise. Additionally, Eidel reveals a higher dependency among ξ, η, and ζ.

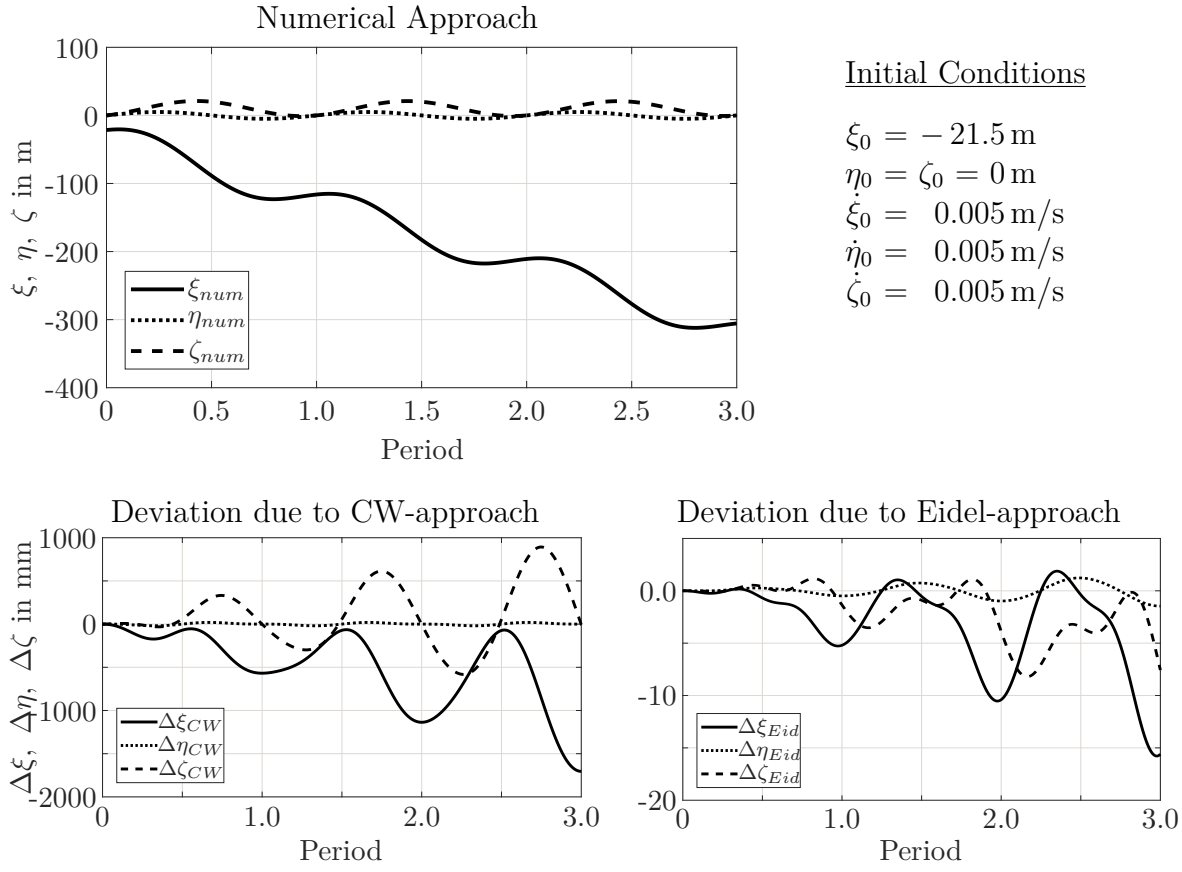

Figure 6.6: (Top) The relative position of the two objects for the time of three periods for an initial spacing of -21.5 m and an initial relative velocity of 0.005 m/s in each direction. **(Bottom)** The deviations of the CW-approach and the Eidel-approach, compared to the numerical approach.

Table 6.3 and Table 6.4 give the values for the specific deviations[2]. Accordingly, a holding-point in ξ-direction shows the highest stability. The analyses also reveal, that relative velocities increase the deviations. For the mission planning, these results need to be kept in mind. Limiting the effects by avoiding an unsuitable setup should be the first approach.

Table 6.3: The maximal distance of the two objects for each direction with no relative velocity. Given are the maximum values within three periods.

Rel. pos. in m			**Numeric in m**			**CW-dev. in m**			**Eid-dev. in mm**		
ξ_0	η_0	ζ_0	ξ_{num}	η_{num}	ζ_{num}	$\Delta\xi_{CW}$	$\Delta\eta_{CW}$	$\Delta\zeta_{CW}$	$\Delta\xi_{Eid}$	$\Delta\eta_{Eid}$	$\Delta\zeta_{Eid}$
-21.5	**0.0**	**0.0**	-21.6	0.0	0.0	0.13 (0.60%)	0.00	0.00	-3.89 (0.02%)	0.00	0.19
0.0	**-21.5**	**0.0**	0.0	±21.6	0.0	0.00	0.15 (0.69%)	0.00	-1.80	5.43 (0.03%)	0.00
0.0	**0.0**	**-21.5**	2457.2	0.0	-152.3	25.64 (1.04%)	0.00	-8.14 (5.34%)	112 (0.01%)	0.00	-467 (0.31%)

Table 6.4: Deviation of CW- and Eidel-approach from numerical approach with different initial relative velocities (rel. vel.). The initial holding-point of the chaser is set 21.5 m behind the target.

Rel. vel. in m/s			**Numeric in m**			**CW-dev. in mm**			**Eid-dev. in mm**		
$\dot{\xi}_0$	$\dot{\eta}_0$	$\dot{\zeta}_0$	ξ_{num}	η_{num}	ζ_{num}	$\Delta\xi_{CW}$	$\Delta\eta_{CW}$	$\Delta\zeta_{CW}$	$\Delta\xi_{Eid}$	$\Delta\eta_{Eid}$	$\Delta\zeta_{Eid}$
0.000	**0.000**	**0.000**	-21.6	0.0	0.0	-0.13 (0.60%)	0.0	0.0	-3.89 (0.02%)	0.00	0.19
0.005	**0.000**	**0.000**	-307.8	0.0	20.1	-1703.7 (0.55%)	0.0	863.2 (4.29%)	-14.6 (0.01%)	0.0	-7.6 (0.04%)
0.000	**0.005**	**0.000**	21.6	±5.0	0.0	-132.5 (0.61%)	±19.4 (0.39%)	0.0	-4.0 (0.02%)	-1.3 (0.03%)	0.0
0.000	**0.000**	**0.005**	-41.5	0.0	±5.0	-90.6 (0.22%)	0.0	±39.0 (0.78%)	-7.1 (0.02%)	0.0	±1.3 (0.03%)
0.005	**0.005**	**0.005**	-312.1	5.0	21.1	-1704.7 (0.54%)	19.5 (0.39%)	892.8 (4.23%)	-15.8 (0.01%)	±1.5 (0.03%)	-8.2 (0.04%)

The deviations for the CW-approach differ maximal 5.34% from the actual value. This value shall be considered detailed enough, especially with the simplifications considered. The Eidel-solutions show a maximal deviation of 0.31% and are in average 45 times more precise than the CW-solutions. They are kept available in case a more precise calculation is required. The chosen holding-point with no relative velocities shows hardly any drift, it can be considered safe.

[2]Further analysis on the influence of a residual relative velocity is provided in Appendix C.

Rigid Body Dynamics

In addition to the relative position of the objects, the modeling of their orientation in space is required. To avoid singularity issues, the spacecraft's and target's orientation in space is modeled using quaternions ($q_i^{C/T}$) rather than Euler angles.

Quaternions A quaternion presents an orientation referring to an unrotated reference coordinate system. The four elements form a unit quaternion $\mathbf{q} = [q_1\ q_2\ q_3\ q_4]^\top$.

Euler Equations As the simulation enables a rotation of the rigid bodies, Euler's rotation equations are applied. Assuming that the mass distribution is constant over time, the dynamics of the angular velocities in combination with the principle moments of inertia can be solved. For further details refer to Ref. [81].

6.2.4 Optimization Tool

Time & Energy The calculations for the trajectory are performed by the software package *OCPID-DAE1*, an optimization algorithm for satellite application [81, 43]. The optimization algorithm "applies a robust Sequential Quadratic Programming method combined with a gradient calculation using sensitivity Differential Equations (DAEs) and is suitable for optimal control problems subject to differential algebraic equations of index one" [81]. The package allows for the optimization on multiple subjects. Within the context of this thesis, the tool is altered to concentrate on minimum energy consumption within a given time frame. Minimum energy allows for cost limitations as it is directly proportional to the propellant consumption. The tool is adapted to the data listed in Table 6.2 and special settings for the initial data as starting constraints. Additionally, different geometries and the safety areas are implemented.

Sections The final state of the tool is the mating of the two docking points with minimum relative velocity. Due to the time constraints for the approach and possible abort, the calculations for the abort paths are performed a-priori as their computing time does not allow for real-time calculations. To generate the abort paths in advance, the approach trajectory is divided into multiple sections. A visualization of the approach is given in Figure 6.7. Each Approach Trajectory Section (ATS)'s end provides the start for an Abort Path (AP). In case of an abort-requiring failure within that section, the abort path following that section will be pursued. All abort paths aim for a point in safe distance to the target - the safety-point. Two of such points exist for this mission - the initial holding-point and the safety-point on the other side of the target along the orbital velocity vector.

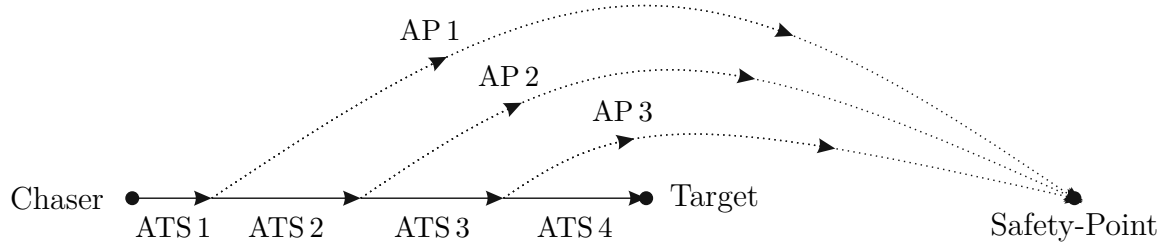

Figure 6.7: Model for the Approach Trajectory Sections (ATSs) and respective Abort Paths (APs). The arrows show the possible direction of movement for the chaser.

6.2.5 Self- and Failure-Management

The presented mission has a great capacity for unexpected failures. The failure-management concept is designed to handle possible symptoms. The chosen fuzzy logic concept, however, has the mentioned drawbacks. The decision to be made for this thesis is whether to approach or to abort - depending on the circumstances. In case of an abort, the decision on which trajectory to follow to be most fuel efficient and, thus, to allow for a maximum number of approaches, is required. While approach trajectories and abort paths are designed within the simulation, the self- and failure-management shall be included in future adaption of this work. The theoretical background is provided with options for developments and briefly mentioned here.

Failure Implementation The connection between self- and failure-management has been stated in Chapter 5. A decision must be made if the failure - may it be caused by disturbing sensor data, a malfunction of a system, or contradictory data input - allows for a continued approach or requires an abort to avoid a collision at any cost.

Decision Making By classifying the symptoms of a failure, the presented fuzzy-logic decides on the hazardousness of such and acts accordingly. The classification and the according rules follow Figure 5.9 and Table 5.6, respectively.

6.2.6 Visualization

The output generated is a rendering of the multiple trajectories: The approach trajectory follows the optimized path with no interruptions. Multiple abort trajectories allow for an abort any time during the approach in case a failure occurred. The self- and failure-management shall decide on-board for an abort or for a further approach, depending on the calculated consequences for the mission in case of an unexpected occurrence or unknown failure. As visualization supports the understanding of such system, the *Unity GameEngine* for rendering and a space model for the orbit dynamics are applied.

The visualization is performed with the *Unity GameEngine*. *Unity* is a freeware cross-platform game engine to develop, for example, 2D and 3D simulations. Using *Unity* provides the advantage of generating scenes without much knowledge about graphical calculations. Pre-defined 3D models can be implemented with the drag-and-drop function, scripting through C# regulates their behavior with the mathematical calculations performed by the GameEngine. Further information on *Unity* can be found in Ref. [126] and Ref. [127].

Environment

Sun/Earth Sun and Earth are neglected for disturbance calculations. While the Sun is included as point light with no rigid body, Earth forms a sphere which seems to rotate while the maneuver takes place. Both objects are taken from the *Unity*-GameObject library available.

Chosen Supplements Displayed for now are the spheres enveloping target and chaser. While the sphere around the chaser has a defined radius, the sphere around the target adapts to the distance of target and chaser as explained within Equation 6.3.

Objects

ADReS-A & Kit While the calculations are performed for cylinders, the visualization displays the chaser as designed in Chapter 4. This way, the position of the docking point and the chaser's attitude during the approach are easily understood and programming failures involving false assignment of them can be identified at an early stage.

Target The same object features as for the chaser are implemented for the target.

Trajectories

Docking Points The approach calculations stop once the two docking points match in velocity and position. As the objects are not allowed to collide, the distance between them is limited by their enveloping sphere (cf. Figure 6.1). While the docking point of the target follows the adjusted angular velocities of the simulation, the docking point of the chaser is oriented towards its targeted position. In the simulation, the docking points are marked with tripods in the coordinate systems of chaser and target. The yellow lines that eventually meet as shown in Figure 6.8 display their position over time.

Approach Trajectory The approach describes the most propellant-saving trajectory considering the given values. Any considerations about the stabilization of a potentially tumbling target are not part of the simulation and, therefore, not part of the discussion. Figure 6.8 displays one exemplary approach. As stated, the center of the LVLH-system lies within the CoM of the target. The light blue line shows the direct approach, the ξ, η, and ζ-axes are presented by the red, blue, and green straight lines.

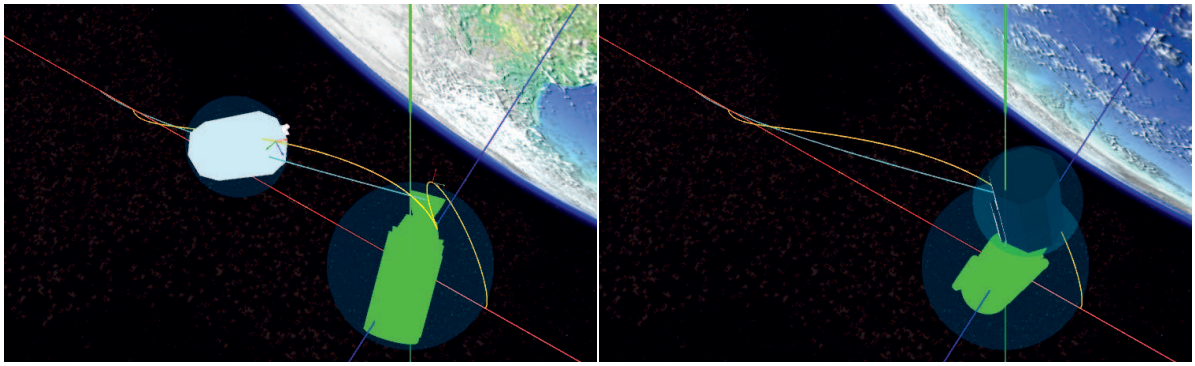

Figure 6.8: The approach of the chaser towards the target with angular velocities ω_x set to $1°/s$ and ω_y set to $0.5°/s$. Updated from Ref. [102].

Abort Path As a collision of the two bodies involved would most probably result in a mission failure - if not the destruction of target and chaser - the possibility for an abort is given. As stated, once the whole approach has been initiated and a failure occurs during the maneuver, the chaser will choose from its memory the abort path next to come. Just as the approach, the abort shall be propellant efficient and is, thus, based on the same optimization algorithm. The number of sections must be assigned by the user, as well as the safety parameter. For Figure 6.9, which shows the same approach as Figure 6.8, ten potential abort paths with a safety parameter C_{Err} of 0.9 are added through magenta paths. Due to pre-calculation of the abort paths, the actual discretization can be as precise as desired.

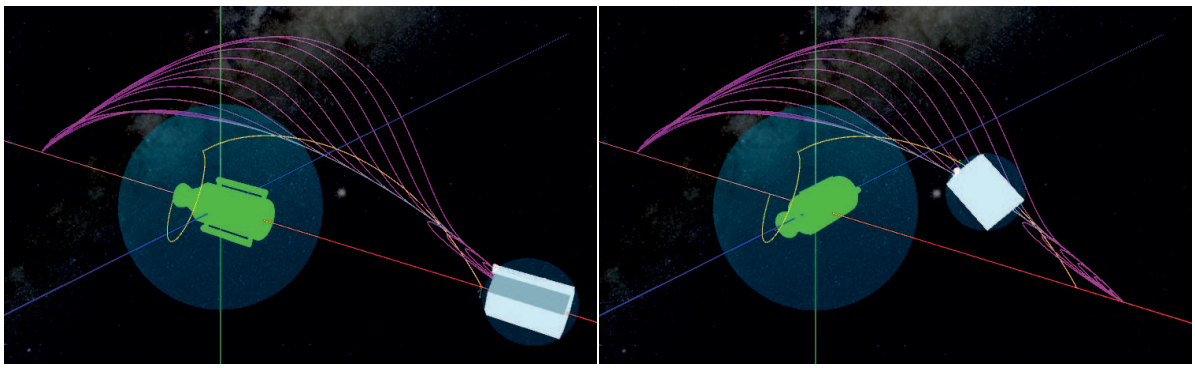

Figure 6.9: Approach trajectory and possible abort paths calculated with a C_{Err} of 0.9. The discretization is set to 10 steps, resulting in 10 abort paths. Updated from Ref. [102].

While an early intervention of the approach leads to an abort of the chaser to its starting-point, later failures lead to an abort to the second safety-point in front of the target's orbit direction. Those two points are placed along the ξ-axisOnce at those positions, the malfunction can be communicated to the ground station. Plans for further approaches shall then be identified.

6.2.7 Output on the Example of a Reference Scenario

Before generating an output, input concerning a defined scenario is assigned. The data for the reference scenario is taken from the mission's constants from Table 6.2, the initial values for the variables are given in Table 6.5. The output file (*OCODE01*) delivers the variable's changing value for each increment calculated for the whole maneuver.

Variables for the Simulation Input

The variables for the simulations are based on the stated dynamics. They involve relative position and velocity of the chaser in the LVLH system of the target, both object's angular velocities and the quaternions to describe the dynamics. ξ, η, and ζ are replaced for the simulation by $x(t)$, $y(t)$, and $z(t)$, respectively. The vector components undergo

Table 6.5: Key for the simulation's output file.

Column	Key	Init. Value	Note
[**1**]	$[\ t_{norm}\ ]$	-	Normalized time (0-1)
[**2 3 4**]	$[\ x(t)\ y(t)\ z(t)\ ]$	$[17\ 0\ 0]^\top$	Rel. position chaser
[**5 6 7**]	$[\ v_x(t)\ v_y(t)\ v_z(t)\ ]$	$[0\ 0\ 0]^\top$	Rel. velocity chaser
[**8 9 10**]	$[\ \omega_x^C(t)\ \omega_y^C(t)\ \omega_z^C(t)\ ]$	$[0\ 0\ 0]^\top$	Angular velocity chaser
[**11 12 13**]	$[\ \omega_x^T(t)\ \omega_y^T(t)\ \omega_z^T(t)\ ]$	$[1\ 0.5\ 0]^\top$	Angular velocity target
[**14 15 16 22**]	$[\ q_1^C(t)\ q_2^C(t)\ q_3^C(t)\ q_4^C(t)\ ]$	$[0\ 0\ 0\ 1]^\top$	Quaternion chaser
[**17 18 19 23**]	$[\ q_1^T(t)\ q_2^T(t)\ q_3^T(t)\ q_4^T(t)\ ]$	$[-0.5\ 0\ 0\ 0.866]^\top$	Quaternion target
[**20**]	-	[0]	Costs thrust
[**21**]	-	[0]	Costs momentum
[**24 25 26**]	$[\ u_x(t)\ u_y(t)\ u_z(t)\ ]$	(max. 1 N)	Thrust control
[**27 28 29**]	$[\ M_x(t)\ M_y(t)\ M_z(t)\ ]$	(max. 1 Nm)	Momentum control
[**30**]	$[\ t_{ges}\ ]$	-	Maneuver time
[**31**]	-	-	Squared distance C-T

a constant change, their initial data as well as targeted final values for relative position and velocity have to be assigned for calculations. The distance for the reference scenario is set to 17 m, as this is the medium distance between $\xi_{0_{min}}$ and $\xi_{0_{max}}$ from Equation 6.1. The respective parameters for the reference scenario are listed in Table 6.5.

Maneuver Time

The time each maneuver requires depends on the angular velocities of the target and the initial distance of the objects. For the reference scenario, 410.44 s are calculated.

Relative Position

The output file provides the chaser's CoM relative position within the target's LVLH-system. To localize the position of the docking points, their movements within their coordinate system must be calculated, based on the respective quaternions. Figure 6.10 gives both information graphically over the time of the approach. The CoMs in the upper graph are apart by the size of the objects' dimensions.

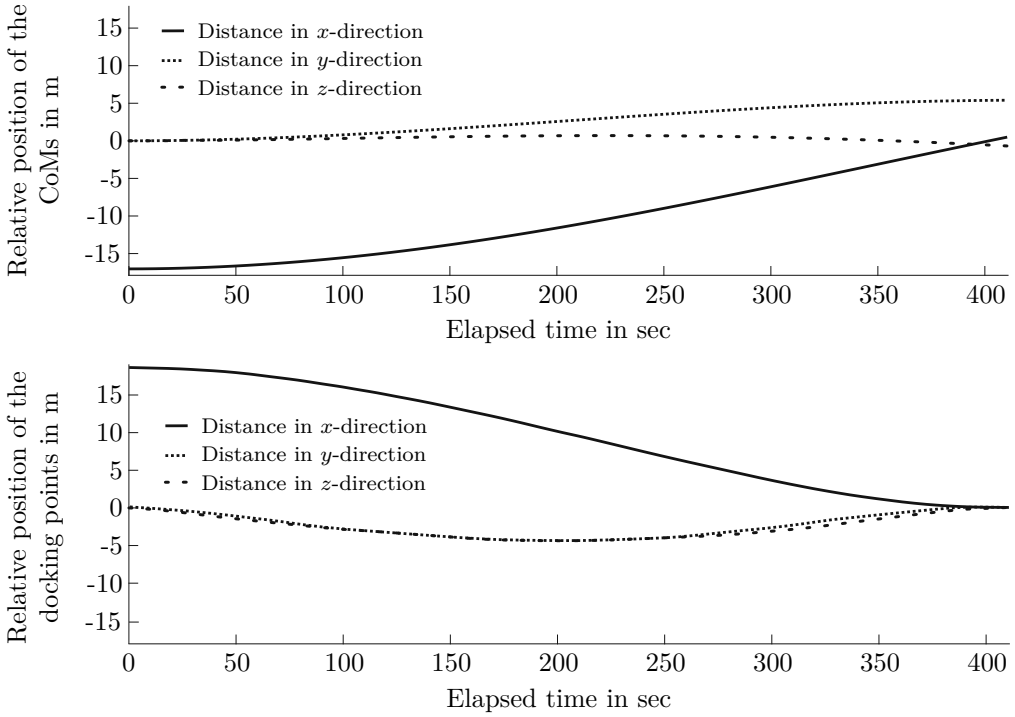

Figure 6.10: Relative position of the CoMs **(Top)** and the docking points **(Bottom)** of the two objects during the approach. The point of origin is the target's CoM.

Relative Velocity

The velocities of the chaser in respect to the target are displayed in the upper graph of Figure 6.11. In its lower graph, the docking points' relative velocity is calculated using Equation 6.7:

$$v_i = \frac{\Delta s_i}{\Delta t},\ i = x, y, z. \tag{6.7}$$

The distance Δs_i is based on the relative position. Δt is the time interval.
The simulation stops once the docking points meet. The relative velocity of the CoMs and the docking points is predicted for the future if no liaison occurs. As no forces are applied, a constant behavior is anticipated.

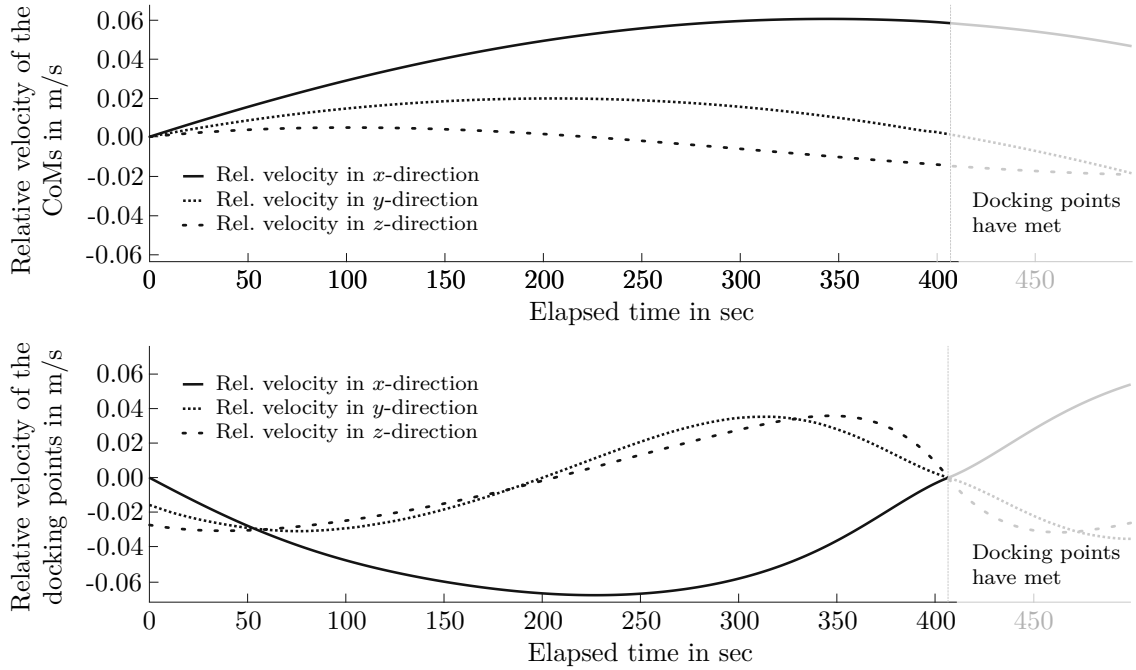

Figure 6.11: Relative velocity of the CoMs **(Top)** and the docking points **(Bottom)** of the two objects during the approach. The point of origin is the target's CoM. The predicted movement without a liaison is given in gray.

Thrust and Torque

The applied thrust for the successful approach is displayed in Figure 6.12. The sequences mirror the 68 intervals calculated as the thrust is applied by multiple impulses. The impulse can accelerate, leading to positive values, and decelerate, leading to negative values. The torque is initiated by the reaction wheels and does not require propellant at this stage.

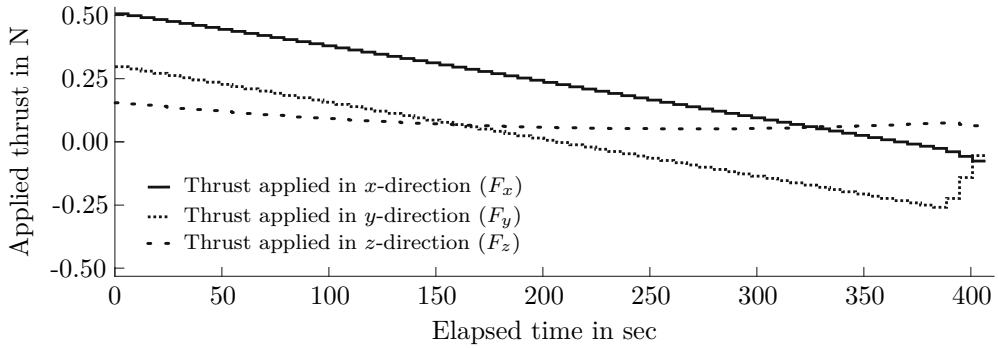

Figure 6.12: Chronological sequence of the thrust applied during the approach. Updated from Ref. [98].

Propellant Consumption

The required propellant can be derived from the thrust applied in each direction for each increment using Equation 6.8:

$$m_{ges} = \sum \frac{|\Delta F| \cdot \Delta t}{I_{sp} \cdot g_0}. \tag{6.8}$$

Figure 6.13 plots the propellant consumption predicted for the successful approach incremental (black, dotted) and accumulated (red, solid). While for the first part of the approach the propellant consumption decreases with each interval, the second part shows at first a constant consumption. Eventually, the final positioning demands a slight increase. About 84 g hydrazine is required for the whole process.

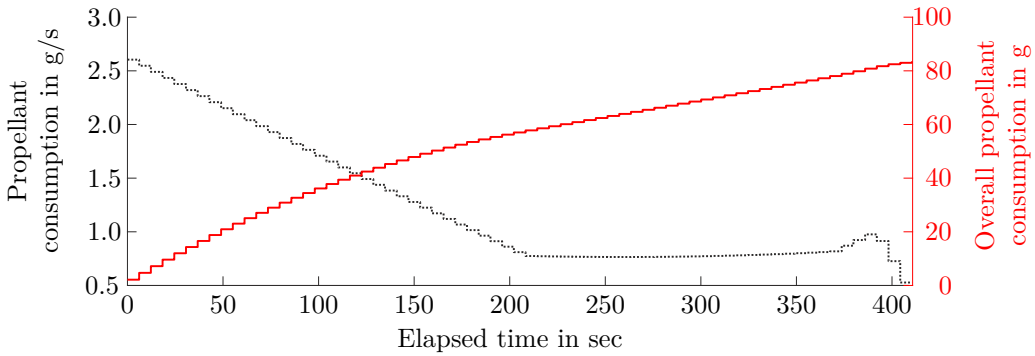

Figure 6.13: Incremental and overall propellant consumption of the successful approach, considering hydrazine as propellant. Updated from Ref. [101].

Figure 6.14 gives the overall propellant consumption required for the respective abort paths. The solid (red) line reflects the successful approach, the dotted ones are calculated with two exemplary safety parameters. The bullets reflect the moment in which the respective abort is initiated. The initiation starts along the approach trajectory as

modeled in Figure 6.7. Path 1 to 3 of Figure 6.14 - the abort paths aim for the original starting-point as safety-point - reveal that those maneuvers are hardly affected by different C_{err}. The abort paths aiming for the second safety-point, however, are influenced: The largest avoidance maneuver for the presented discretization of 10 intervals is calculated for Abort Path 4 after 143.6 sec. Here, the safety area has its maximum size for both C_{err}. The chaser takes a wide detour to avoid the safety area and to reach the second safety-point. As the safety area decreases with smaller distances between chaser and target, further detours for any following abort paths require less propellant. Figure 6.14 also reveals that smaller C_{err} - and with such smaller safety areas around the objects - lead to fewer propellant consumption[3].

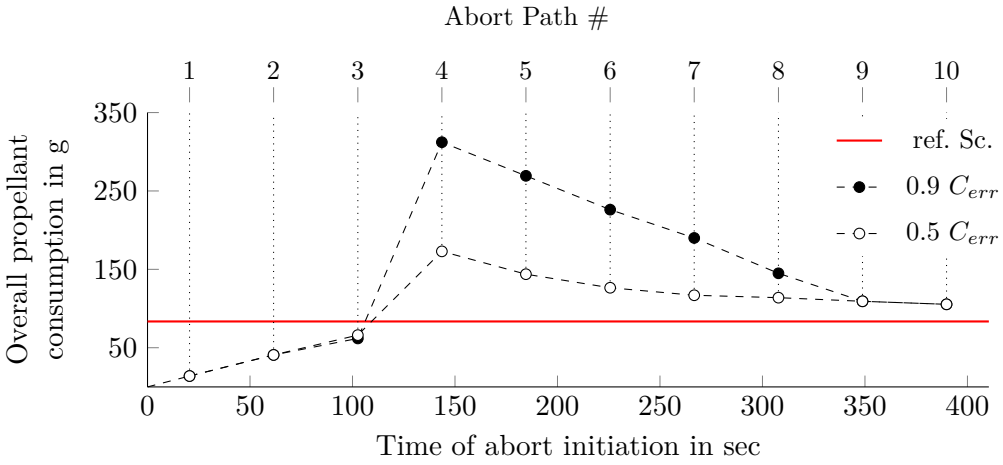

Figure 6.14: Propellant consumption of the respective abort paths for a safety parameter C_{err} of 0.9 and 0.5. The solid horizontal line reflects the propellant requirement of the successful approach. The abort can last max. 450 sec.

Berthing Box

The docking maneuver will be performed while ADReS-A stays within a berthing box. The box' dimensions shall not exceed the robotic arm's length. A hemisphere of 2 m in radius around the target's docking point is, therefore, formed. As long as the satellite stays within this area, the robotic arm can perform the grabbing maneuver and the final attachment. With the object's CoMs being at least the dimensions of the two objects apart, drift will affect them. Limited time is, thus, available for the actual attachment.

The analysis of the respective berthing box uses the CW-approach and investigates residual relative velocities. The final position and velocity conditions of the reference

[3]Further analysis on the subject was provided in Section 6.2.2.

scenario are taken as initial conditions for the berthing box. The residual distance mirrors the distance of the CoMs. Due to the tumbling included in the reference scenario in *Unity*, the values are distributed among all three axes. Figure 6.15 displays the absolute distances of the CoMs of the chaser and the target, moving apart. The red dotted-dashed line is the distance of the Docking Points (DPs). The available hemisphere around the target's DP is displayed by the gray area. Accordingly, the time available for grabbing for this scenario is limited to about 75 sec. A limitation of the residual velocities to 5 mm/s would increase the attachment time to about 800 sec. Figure 6.16 displays, hence, that residual velocities need to be further limited to allow for a safe docking process. Using the implemented thruster to lower the effects of the drift is not an option as this will interfere with the grabbing process and may harm the robotic arm.

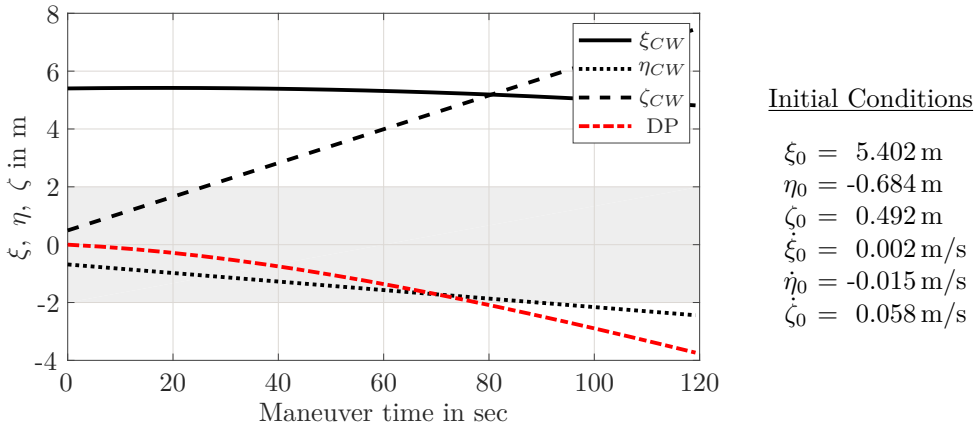

Figure 6.15: Drift in berthing box with residual conditions of reference scenario. The black lines reflect the CoMs, the red line the DP's distance.

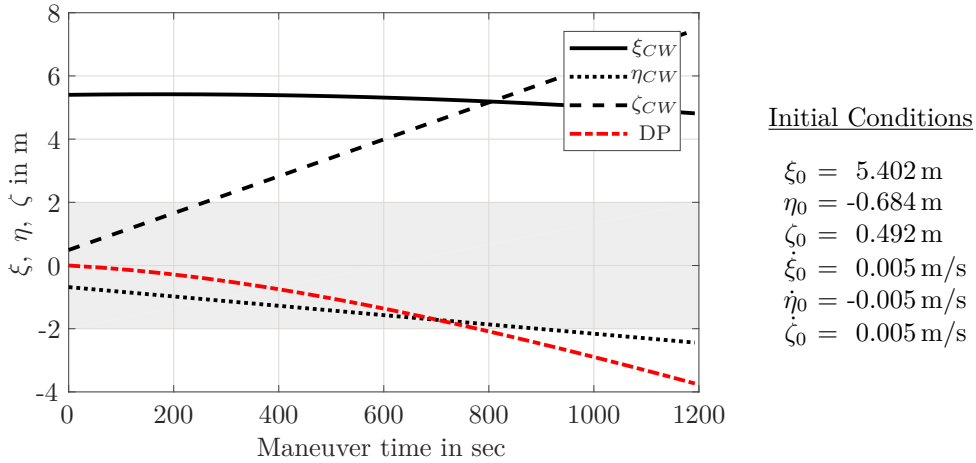

Figure 6.16: Drift in berthing box with adapted conditions. The black lines reflect the CoMs, the red line the DP's distance.

6.3 Tool Variables

The successful approach of the reference scenario requires about 410 sec until the two docking points meet. For the abort maneuver, maximal available time to reach the safety-point must be assigned in advance. As the tool focuses on minimal propellant consumption, the available time is generally maxed out. In the following, the initial values of available maneuver time, initial distance, quaternions of the target, semi-major axis, and moments of inertial of the target are varied and plotted for the respective overall propellant, maneuver time, maximal applied thrust, and maximal applied torque for the case of a successful approach.

6.3.1 Available Maneuver Time for Abort

In Figure 6.17, the influence of different maximal maneuver time for the abort available is displayed. The vertical axis gives the hydrazine consumption of the approach. The bullets show the moments the respective abort is initiated. The plot reveals that the more time is available, the less propellant is consumed. Additional time allows for an optimized implementation of the environmental circumstances such as drift. Less time requires a more direct path towards the safety-point. In correlation with earlier analysis, the approach trajectory is divided into 10 sections, Abort Path 4 requires the most propellant. In summary, the distance to the target when initiating the abort path affects the propellant consumption from the moment the second safety-point is targeted. From then on, the its influence is decreasing.

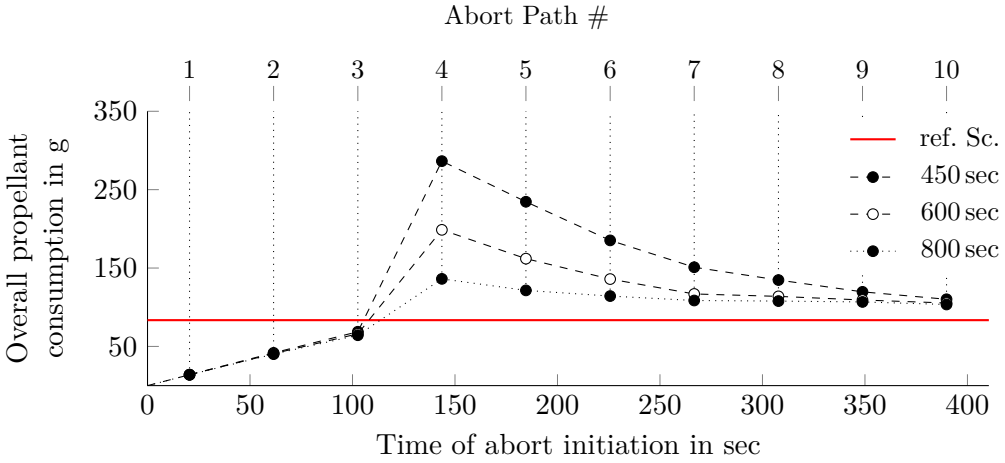

Figure 6.17: The influence of the available maximum maneuver time for an abort path on the overall propellant consumption. Displayed is the consumption of an approach with a C_{err} of 0.6.

6.3.2 Initial Distance

The cameras in use allow for initial distances of the object's CoMs between 12.5 and 21.5 m. Figure 6.18 illustrates the influence of the initial distance on the required propellant and the required time for the successful approach. Unsurprisingly, the further the objects are initially apart, the longer the approach takes. At the same time, more overall propellant is required. While the influence on the propellant is linear, the influence on the required maneuver time is slightly hyperbolic curved.

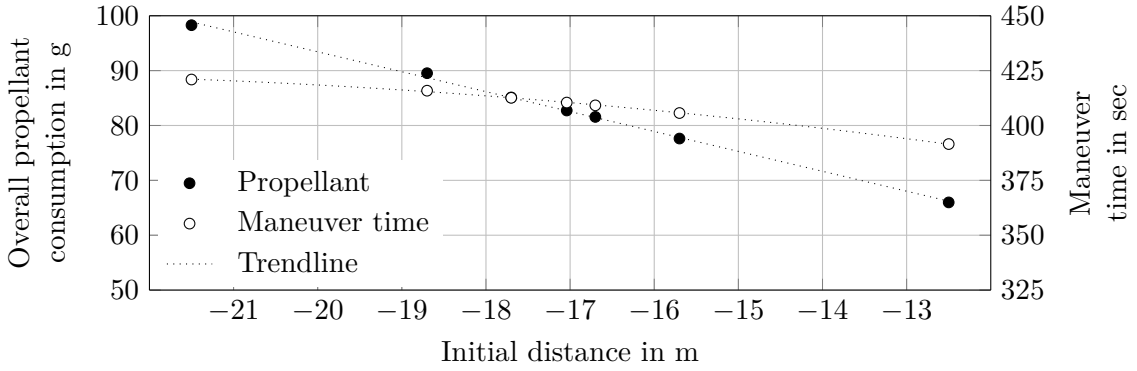

Figure 6.18: Propellant and time requirements for the reference scenario, altering the initial distance between the chaser and the target.

The maximum thrust and torque applied also increase with the initial distance of the approach. As Figure 6.19 displays, the thrust behaves slightly hyperbolic curved, the torque acts virtually linear. With the angular velocity kept at 1.0 deg for ω_x^T and 0.5 deg for ω_y^T, the targeted docking point moves constantly. Therefore, in addition to the increased initial distance, the position of the docking point changes with the additional time required to overcome the gap. Both influences add up to the resulting graphs.

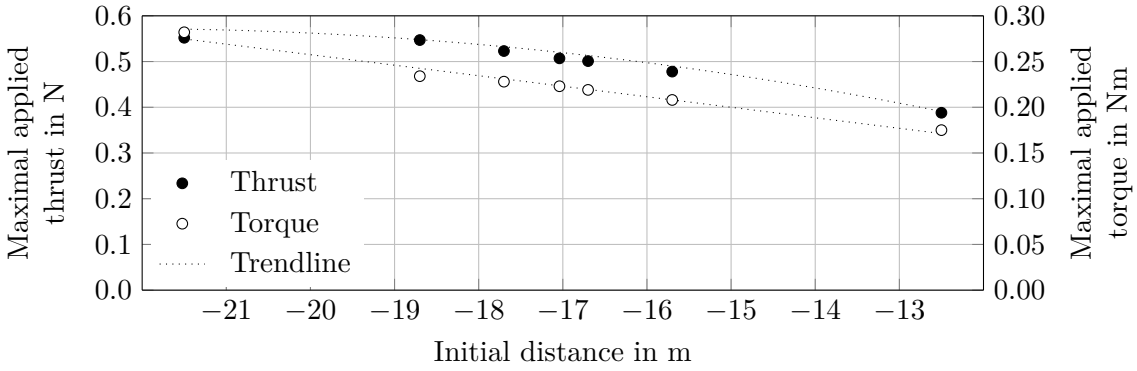

Figure 6.19: Maximum torque and thrust requirements for the reference scenario, altering the initial distance between the chaser and the target.

6.3.3 Quaternions of the Target

Quaternions describe the target's attitude. Changing them results in a different orientation of the target and with such in a different docking process. The information is interesting for different tumbling modes of the target. For Figure 6.20 and Figure 6.21, different q_1^Ts - the Quaternion 1 of the target - are analyzed[4]. The initial distance is set to -12.5 m. The trendline for the maneuver time shows a parabolic curve, the resulting propellant plot has a wave-like behavior.

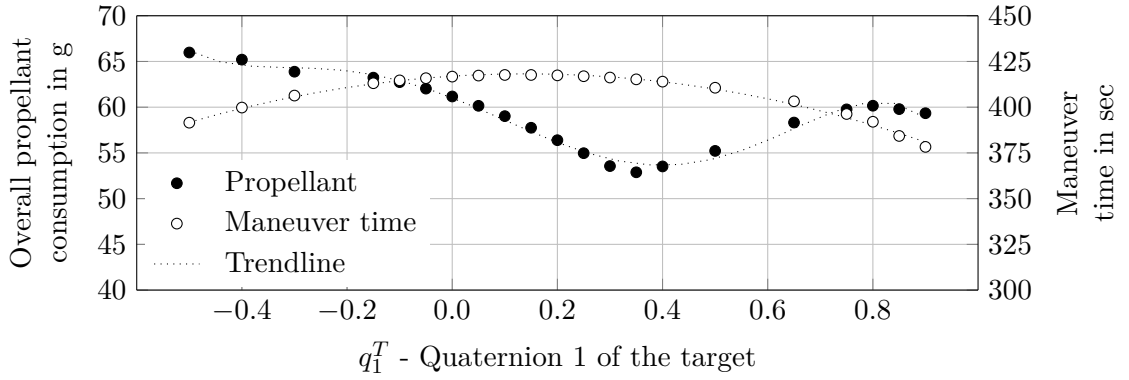

Figure 6.20: Propellant and time requirements for the reference scenario, altering Quaternion 1 of the target (q_1^T).

The graph of the maximal applied thrust can also be described as wave-like. The maximal applied torque shows a parabolic behavior, with the last two dots plotted sticking out. At this point, the optimized approach trajectory requires another movement of the chaser, which explains the change.

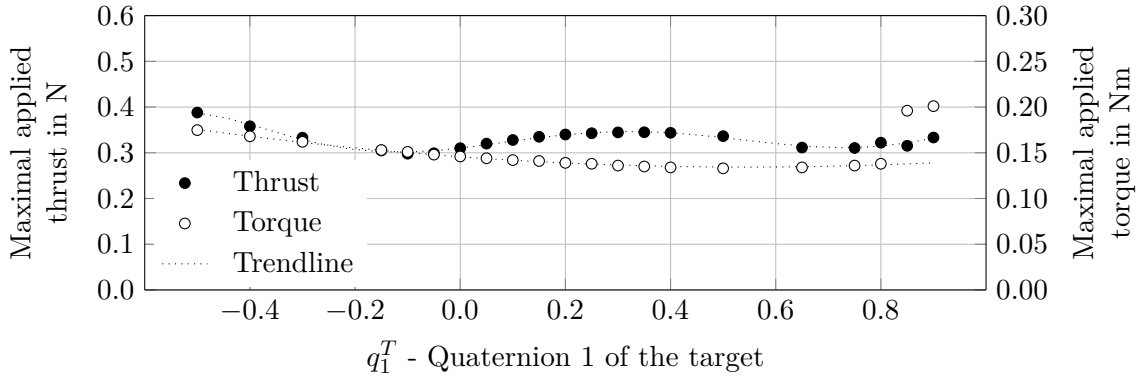

Figure 6.21: Maximum torque and thrust requirements for the reference scenario, altering Quaternion 1 of the target (q_1^T).

[4]By changing q_1^T, also q_4^T undergoes a change. Investigations, however, concentrate on q_1^T.

6.3.4 Semi-Major Axis

The Semi-Major Axis (SMA) of the orbit, and with such the SMA of the target, is varied by about 1000 km for this analysis. The SMA mainly influences the period of an orbit and the environmental perturbations. The latter excluded from the calculations which leaves the focus on the resulting period and its influence on the investigated parameter. Figure 6.22 and Figure 6.23 reveal the quite small impact the SMA's variation actually have on the considered parameter. The propellant consumption and the maneuver time slightly decrease for higher altitudes.

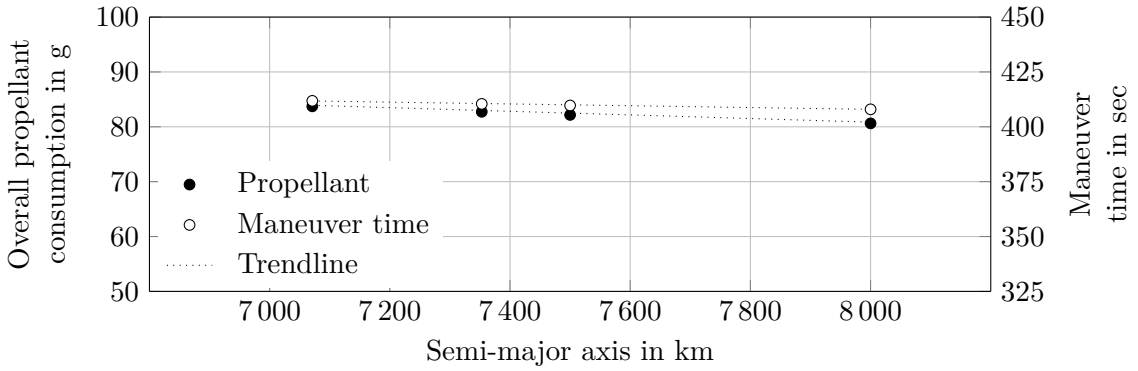

Figure 6.22: Propellant and time requirements for the reference scenario, altering the semi-major axis of the maneuver.

Maximum thrust and torque increase marginally with higher SMA. It is, however, quite difficult to investigate the SMA with the software in use. As stated earlier, only 10% of the investigated combinations run successfully. For the investigation of the SMA, only the displayed values could be extracted. With the given values, however, it can be stated, that a change in the SMA hardly effects the output values.

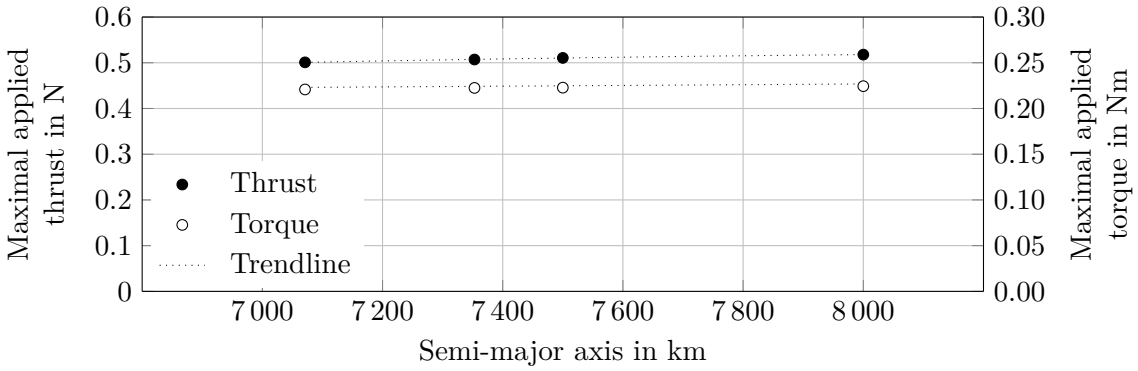

Figure 6.23: Maximal torque and thrust requirements for the reference scenario, altering the semi-major axis of the maneuver.

6.3.5 Moments of Inertia of the Target

For the presented calculations, a homogeneous distribution of the target's mass was assumed. The following graphs investigate different MoIs - and with such different mass distribution - and their influence on the presented output parameter. For the investigation, J_{xx}^T is kept at 1258 kg/m^2 while J_{yy}^T and J_{zz}^T change. With the cylindrical form of the target, both parameters are varied by the same value as the dimensions in y- and z-axis are identical. The trendlines given in Figure 6.24 for the required propellant and the maneuver time both show a hyperbolic behavior - with the difference, that with rising MoIs, the required propellant decreases while the maneuver time increases.

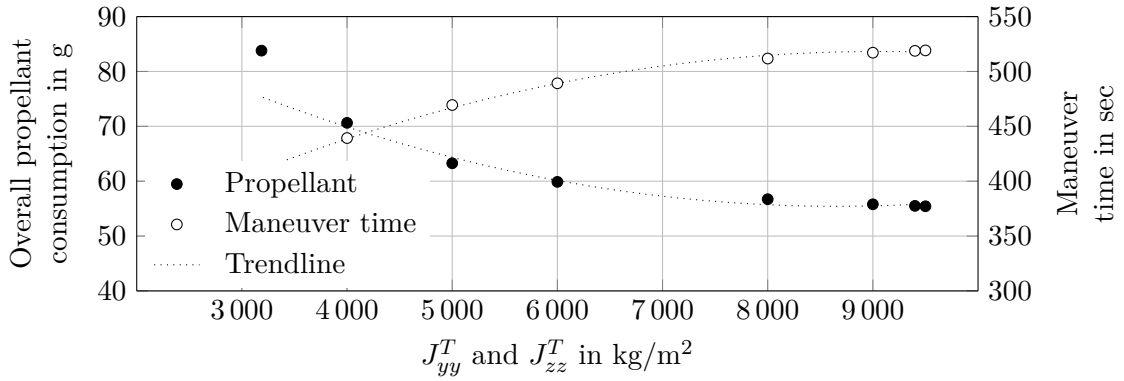

Figure 6.24: Propellant and time requirements for the reference scenario, altering J_{yy}^T and J_{zz}^T of the target.

For the maximal applied thrust and torque, the hyperbolic curved trendlines given in Figure 6.25 show a similar behavior as the one for the required propellant: with increasing MoIs, both parameters decrease.

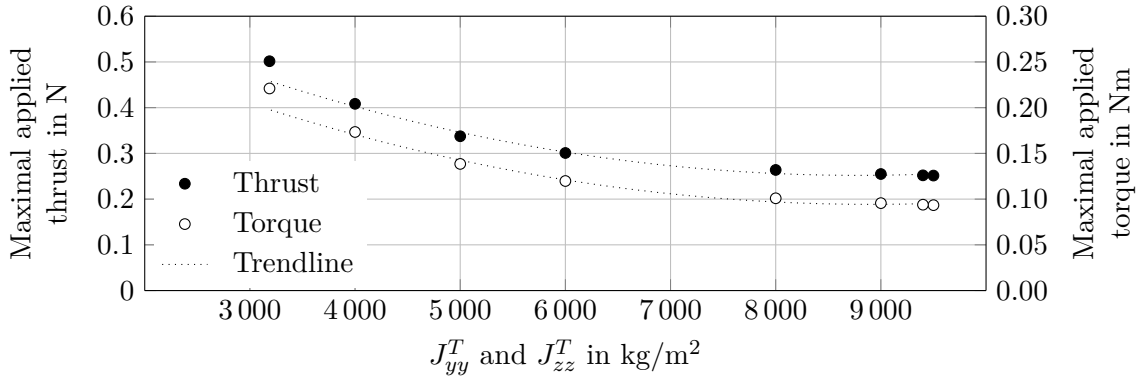

Figure 6.25: Maximal torque and thrust requirements for the reference scenario, altering J_{yy}^T and J_{zz}^T of the target.

The results of the MoI-investigation show the influence of the target's possible movement on the trajectory. This parameter cannot be changed by the chaser. It's investigation, however, gives an idea on the order of magnitude and the according frames for the investigated parameters of the approach.

6.3.6 Further Investigations

About 90% of the investigated parameter combinations could not be calculated with the tool. Investigations concerning different angular velocities are included. As one of the requirements for on-orbit decision making is a stable forecast, especially for unknown parameter such as the actual angular velocity of the target, the presented tool will need an update and improvement on its success rate.

Further investigations concerning altered thrust level were considered. The maximally required thrust in the given graphs, however, never exceeded 0.55 N. It is, thus, concluded, that there is no need for a higher thrust than 1 N.

6.3.7 Influence on the Mission Planning

According to the investigated initial data, strongest influence concerning propellant is revealed for available maneuver time, followed by the initial distance and the MoI of the target. While the first two can be adapted by the mission planning, the latter has to be considered when setting margins for actual propellant consumption. The SMA shows hardly any influence. The targets can, thus, be chosen based on other selection criteria than propellant consumption during the approach. The influence of the quaternions of the target are like its MoI - it is not possible to change them, but predictions concerning consumption of propellant can be derived. Applied thrust and torque stay within low variations for all investigated parameters. They do, thus, not required much further adaption for the presented mission.

7 Conclusion

7.1 Summary

In this thesis, a mission concept for the removal of space debris is developed. Focus is set on an effective and save approach to address the rising issue of uncontrolled objects in space. The concept includes the mission architecture, the satellite design and the failure-management. A simulation visualizes the developed mission. An analysis investigates the influence of different parameter in the required time, overall propellant, maximum thrust, and maximum torque for the final approach.

An introductory presentation of the issue of space debris creates a profound basis for discussion. Stated is the development of historic debris in space, with an average of 300 objects added per year since 1957 to the official catalog. As of today, more than 26 000 objects are counted. Additionally, their predicted increase in number for the cases of implemented and non-implemented ADR is provided. Accordingly, a stable status is kept if a removal of 5 to 15 large objects starts immediately. Otherwise, an uncontrollable increase is highly probable for the future. Considerations of the acting agencies are listed, resulting in the need for active removal of large debris from space - a task this thesis addresses.

The mission design reveals the accumulation of multiple large objects in specific orbits. SL-8 R/B are concluded as targeted objects. An architecture describing how to remove multiple rocket bodies with one launcher is presented. A division of tasks between a complex chaser and multiple De-orbit Kits emerges. The chaser is designed to transport the Kits from a parking orbit to their designated target, the Kits actively remove the objects and vaporize attached to them during re-entry. The presented calculations show the limits and capabilities of the presented concept. Limits are reflected by the available time and propellant for shuttling and orbit compensation. The capabilities show, that at least 5 targets can be removed within one year.

The design of the two spacecraft is derived from the stated requirements, the investigated detail of design is down to subsystem level. The spacecraft's mass and power

requirements are determined, concentrating on effectiveness. The developed calculation tool is presented with the subsystem's dependencies visualized. In addition to the calculations, a CAD model is provided for reasons of clarity and comprehensibility.

Further addressed is a strategy for self-managing properties. This includes the failure-management, which is presented in more detail. Fuzzy logic is chosen as decision-making concept for a developed algorithm. The established program interprets - and with such decides about - the symptoms detected. The result is either an abort - in case the symptom(s) affect the approach in an interruptive way - or a continuation of the removal - in case the symptom(s) do(es) not affect the approach at this point. Different reactions for abort and approach are provided.

A simulation for visualization of the successful approach or a necessary abort is furthermore provided. The stated architecture of the simulation allows for modification and extension of the implemented modules. Additionally to the operational parameter and the relative dynamics for trajectory calculation, safety adaptions and an optimizer for a fuel and time efficient approach are included. The simulation's output provided allows for further investigation of different approach strategies. A reference scenario - based on all parameters concluded from former chapters - provides an exemplary set-up. The results of the analysis show dependencies of the investigated parameters. No single parameter is identified as most influencing or challenging. It is more a complex overlapping of them that influences the actual approach.

7.2 Recommendation

7.2.1 Choice of Targets

Medium Sized Objects The thesis reasons why large objects should be removed first. Still, any debris can cause a hazardous collision. Extending the mission architecture to middle-sized objects will increase the number of debris reachable and removable within one mission and as a result within one year. To be similarly effective, more objects will must be removed within that timeframe. As the smaller objects are very likely to vaporize during re-entry, the satellite design may be adapted, allowing for passive removal of the debris. The developed strategy for the close approach can be retained when docking is required.

SL-8 R/B + X The thesis recommends the removal of SL-8 R/B for various reasons. To increase the number of reachable objects within one mission, the selection can be extended to other objects. ADReS-A will need adapted knowledge of the new targets and the kits will have to be customized. Even though this contradicts a standardized removal as aimed for, the extension may proof valid in terms of propellant saving ambitions.

7.2.2 Simulation Improvement

Perturbations The simulation gives many opportunities for specialization as the existing modules are configured to be improved and extended. The simplified version includes, for example, no perturbations. With some effort, such as the implementation of the Earth-Centered Inertial (ECI)-coordinate frame, an implementation is conceivable.

Geometry The object's bodies are modeled as cylinders with an enveloping sphere as safety area. Adjusting the bodies to the more realistic form and adapting the safety area will increase approach options. Moreover, the spacecrafts are assumed as homogenous bodies. An adaption will derive more complex, but more realistic, scenarios.

Relative Dynamics Another feature presented are the Eidel-equations. They can improve the analytical approach of the CW-equations if more precision for relative dynamics on that level is required. The optimization tool in use could additionally be optimized for different parameters such as the thrust, torque, time, or any combination possible.
Recommended as well is the implementation of different optimization approaches as the presented one revealed large gaps for many tested cases. The question on how the tumbling rate of the target influences the propellant consumption and time requirements remain unanswered and may be solved with another optimizer.

Failure Implementation Integrating the failure implementation into the *Unity* visualization will improve the understanding of the user immensely and allow for different test scenarios that concentrate on approach and abort strategies. Symptoms will also be more conceivable when supported by the visualization.

7.2.3 Failure-Management Implementation

A-FDIR The top-down analysis of the failure-management presented focuses on the symptoms and reacts according to the component failure(s) assumed. Failures, however,

do not necessarily derive from a faulty part. Sensor data could also be the source. The approach of Seidel [111] proposes the creation of a network dependency between the elements and sensors. With multiple sensors monitoring the health, a faulty sensor can be detected through majority rating. Moreover, with the dependency using mathematical and physical formulas, a faulty component can be detected with a higher probability.

Symptom Analysis The presented failure-management concentrates on symptoms extracted for the specific spacecraft design. As the close vicinity will provide unexpected events, the failure-management will need improvement. More symptoms and their combination have to be derived to cover such events. For now, an unknown symptom combination leads to an abort trajectory. By improving the analysis according to symptoms, unnecessary aborts can be avoided and fuel, thus, be saved.

Decision-making Concepts The approach of fuzzy logic is chosen to handle the failure-management for this thesis. Other concepts for decision-making processes are presented. The more complex the spacecraft (simulation) becomes, the more suitable another concept may be. The listed ones should be extended by concepts addressing an outside-the-box-thinking such as the cognitive automation. The goal is to transfer the process to an autonomous one with the satellite able to implement the strategy presented, based on the self-properties. To realize such concept, a variety of codes will have to be written that concentrate on the developed spacecraft. A strategy such as the presented one can be used as guideline.

Illumination The cameras in use for the presented chaser require specific lightning conditions to determine the target's tumbling mode. Within this thesis, an illumination, eclipse, and glare phase are considered. The time available to provide suitable conditions could be extended by a flashlight attached to the chaser. Additionally, the location of the chaser in respect to the target can be varied to allow for an optimization of the circumstances.

7.2.4 Self-Management Implementation

The self-management needs to embody the failure-management. By knowing its own status, the satellite will be able to adapt its goals, prioritize, and decide on the reaction. Once the approach is standardized, an adaption for the actual stabilization of the target and the attachment of the Kit should be targeted. This way, ground control can concentrate on other tasks and supervise the mission rather than being required to react to standard situations.

Bibliography

[1] Air Force Research Laboratory. XSS-11. *http://www.kirtland.af.mil/shared/media/document/AFD-070404-108.pdf* (Accessed: 2012-10-23).

[2] Andrenucci, M., Pergola, P., Ruggiero, A., Olympio, J., and Summerer, L. Active Removal of Space Debris: Expanding foam application for active debris removal. *Final Report, ESA, Contract No. 4000101449/10/NL/CBi* (2011).

[3] Anis, A. Cold Gas Propulsion System - An Ideal Choice for Remote Sensing Small Satellites. In *Remote Sensing - Advanced Techniques and Platforms* (2012), pp. 447–462.

[4] Astrium. Astrium wins DEOS contract to demonstrate in-orbit servicing - Press Release Astrium. *http://www.astrium.eads.net/en/press-centre/kx9.html* (Accessed: 2013-07-08).

[5] Astroscale. ADRAS 1 - Spacecraft EOL Solutions and Active Removal. *4th International Workshop on Space Debris Modelling and Remediation* (2016).

[6] Bassing, S., Handrich, M., Federer, C., et al. Liste der Mikroprozessoren von Intel. *https://de.wikipedia.org/wiki/Liste_der_Mikroprozessoren_von_Intel* (Accessed: 2014-09-01).

[7] Benvenuto, R., and Lavagna, M. R. Flexible Capture Devices for Medium to Large Debris Active Removal: Simulations Results to Drive Experiments. *ASTRA 2013* (2013).

[8] Biesbroek, R., Hüsing, J., and Wolahan, A. The e.Deorbit study in the Concurrent Design Facility: System and Concurrent Engineering for the e.Deorbit Mission Assessment Studies. *http://congrexprojects.com/docs/default-source/14c08_docs/system-and-concurrent-engineering-for-the-e-deorbit-mission-assessment-studies.pdf?sfvrsn=0* (Accessed: 2016-05-15).

[9] Biesbroek, R., Innocenti, L., Estable, S., Oswald, M., Haarmann, R., Hausmann, G., Billot, C., and Ferraris, S. The e.Deorbit Mission: Results of ESA's Phase A Studies for an Active Debris Removal Mission. *66th International Astronautical Congress*, IAC-15 A6.6.5 (2015).

[10] Bombardelli, C., Merino-Martínez, M., Galilea, E. A., Peláez, J., Urrutxua, H., Herrera-Montojo, J., and Iturri-Torrea, A. Active removal of space debris: Ion beam shepherd for contactless debris removal. *Final Report, ESA, Advanced Concepts Team, Ariadna (10-4611c)* (2011).

[11] Bonnal, C., Ed. *4th International Workshop on Space Debris Modelling and Remediation* (June 2016), CNES.

[12] Bonnal, C. Expert Memo on Potential Residual Propellants on board Upper Stages of SL8, (2018). private conversations.

[13] Brügge, N. Kosmos-3. *http://www.b14643.de/Spacerockets-1/East-Europe-3/Kosmos-3/Description/Frame.htm* (Accessed: 2016-05-19).

[14] Castet, J.-F., and Saleh, J. H. Satellite and satellite subsystems reliability: Statistical data analysis and modeling. *Reliability Engineering and System Safety 94* (2009), 1718–1728.

[15] Chen, S. The Space Debris Problem. *Asian Perspective 35*, 4 (2011), 537–558.

[16] Chen, X., Zhu, M., Li, Z., and Gong, Z. A biometric Approach for Active Debris Removal . *66th International Astronautical Congress*, IAC-15 A6.5.2 (2015).

[17] Cowardin, H., Ojakangas, G., Mulrooney, M., Lederer, S., and Liou, J.-C. Optical Signature Analysis of Tumbling Rocket Bodies via Laboratory Measurements. In *AMOS Technical Conference Proceedings* (2012).

[18] Culver, J. The CPUs of Spacecraft Computers in Space. *http://www.cpushack.com/space-craft-cpu.html* (Accessed: 2014-09-01).

[19] D'Amico, S., Ardaens, J.-S., and Florio, S. d. Autonomous formation flying based on GPS - PRISMA flight results. *Acta Astronautica* (2012).

[20] David, P. TEC-SWE: Fault Detection Isolation Recovery. *http://bssc.esa.int/fdir.htm* (Accessed: 2013-04-02).

[21] Davis, T. M., and Melanson, D. XSS-10 Mission Results and Lessons Learned. *http://smartech.gatech.edu/bitstream/handle/1853/8036/SSEC_SD3_doc.pdf?sequence=2* (Accessed: 2012-10-23). Paper No. GT-SSEC.D.3.

[22] de la Fuente, M. J. Model-Based FDI using Analytical Redundancy. *http://www.isa.cie.uva.es/maria/model-basedFDI_parametros.pdf* (Accessed: 2016-10-23).

[23] Debus, T. J., and Dougherty, S. P. Overview and Performance of the Front-End Robotics Enabling Near-Term Demonstration (FREND) Robotic Arm. In *Proc. AIAA Infotech Aerospace Conference* (2009), 2009-1870, pp. 1–12.

[24] DLR. ROSAT. *http://www.dlr.de/dlr/desktopdefault.aspx/tabid-10424/* (Accessed: 2016-05-14).

[25] Dunbar, B. NASA - Frequently Asked Questions: Orbital Debris. *http://www.nasa.gov/news/debris_faq.html* (Accessed: 2012-09-27).

[26] ECSS Secretariat. Space engineering: Space Segment Operability. *ECSS-E-ST-70-11C: Requirements & Standards Division* (2008).

[27] Eickhoff, J. *Onboard Computers, Onboard Software and Satellite Operations: An Introduction*. Springer Science & Business Media, (2012).

[28] Eidel, W. Bahnanalyse für Ellipsenbahnen mit e«1. Universität der Bundeswehr München, (2015). internal document.

[29] Ellery, A. *An Introduction to Space Robotics*. Springer Verlag, (2000).

[30] ESA. ATV Overview. *http://esamultimedia.esa.int/docs/ATV/infokit/english/01_ATVOverview.pdf* (Accessed: 2012-10-09).

[31] ESA. ATV Rendezvous and Docking Technology. *http://esamultimedia.esa.int/docs/ATV/infokit/english/04_ATVRendDockTech.pdf* (Accessed: 2012-10-09).

[32] ESA. Automated Transfer Vehicle (ATV). *http://esamultimedia.esa.int/docs/ATV/FS003_12_ATV_updated_launch_2008.pdf* (Accessed: 2012-10-09).

[33] ESA. Requirements on Space Debris Mitigation for ESA Projects. *http://www.cnsa.gov.cn/n615708/n676979/n676983/n893604/appendix/200852915833.pdf* (Accessed: 2012-10-22).

[34] ESA. ATV Integrated Cargo Carrier. *http://www.esa.int/SPECIALS/ATV/SEM3ZYOR4CF_0.html* (Accessed: 2012-10-29).

[35] ESA. Clean Space - e.Deorbit. *http://www.esa.int/Our_Activities/Space-Engineering-Technology/Clean-Space/e.Deorbit* (Accessed: 2016-05-14).

[36] Falcoz, A., Henry, D., and Zolghadri, A. Robust fault diagnosis for atmospheric reentry vehicles: A case study. *IEEE Transactions on Systems, Man, and Cybernetics-Part A: Systems and Humans 40*, 5 (2010), 886–899.

[37] Fehse, W. Rendezvous with and Capture/Removal of non-cooperative Bodies in Orbit. *Journal of Space Safety Engineering 1*, 1 (2012), 17–27.

[38] Flegel, S. Maintenance of the ESA MASTER Model. *Final Report, ESA, Contract 21705/08/D/HK* (2011). Technische Universität Braunschweig, Institut of Aerospace Systems.

[39] Forshaw, J., Aglietti, G., Navarathinam, N., Kadhem, H., Salmon, T., Joffre, E., Chabot, T., Retat, I., Axthelm, R., Barraclough, S., et al. An in-orbit Active Debris Removal Mission - RemoveDEBRIS: Pre-Launch update. *66th International Astronautical Congress*, IAC-15 A6.6.3 (2015).

[40] Friend, R. B. Orbital Express Programm Summary And Mission Overview. In *Defense and Security 2008: Special Sessions on Food Safety, Visual Analytics, Resource Restricted Embedded and Sensor Networks, and 3D Imaging and Display* (2008), vol. 6958, pp. 1–11.

[41] Fusco, F., Gallerini, R., and SpA, T. European robotic arm: The problem of preventing collisions. In *6th ESA Workshop on Advanced Space Technologies for Robotics and Automation* (2000).

[42] Garcia, M. Space Debris and Human Space Flight. *https://www.nasa.gov/mission_pages/station/news/orbital_debris.html* (Accessed: 2016-12-20).

[43] Gerdts, M. Optimal Control and Parameter identification with Differential-Algebraic Equations of Index 1. *http://www.unibw.de/lrt1/gerdts/software/ocpiddae1.pdf* (Accessed: 2014-07-24).

[44] GMAT. General Mission Analysis Tool (GMAT) - User Guide. *http://gmat.sourceforge.net/doc/nightly/html/index.html* (Accessed: 2018-01-24).

[45] Gomez Martinez, H. C., and Eissfeller, B. Autonomous Determination of Spin Rate and Rotation Axis of Rocket Bodies based on Point Clouds. In *AIAA Guidance, Navigation, and Control Conference* (2016), 2016-0886.

[46] Gorret, B., Métrailler, L., Moreau-Getien, L., Voilat, R., Frei, T., Lauria, M., Mäusli, P.-A., Guignard, A., and Richard-Noca, M. Status of the development of the CleanSpace One capture system. *4th international workshop on Space Debris Modelling and Remediation* (2016).

[47] Grahn, S. Radio observations of Kosmos 186/188. *http://www.svengrahn.pp.se/trackind/K186188/K186188.html* (Accessed: 2016-05-19).

[48] Grihn, C. Konzeptionelle Abschätzungen für die De-Orbit-Konzepte zur aktiven Rückführung von Weltraumrückständen. Master's thesis, Universität der Bundeswehr München, (2013).

[49] Harland, D. M., and Lorenz, R. *Space Systems Failures: Disasters and Rescues of Satellites, Rockets and Space Probes.* Springer Science & Business Media, (2007).

[50] Hinze, A., Fiedler, H., and Schildknecht, T. Optimal Scheduling for Geosynchronous Space Object Follow-Up Observations Using a Genetic Algorithm. In *AMOS Technical Conference Proceedings* (2016), pp. 1036–1045.

[51] IADC. Homepage. *https://www.iadc-home.org/* (Accessed: 2012-10-22).

[52] IADC. Stability of Future LEO Environment. *https://www.iadc-home.org/documents_public/file_down/id/4134* (Accessed: 2013-08-09).

[53] IAI GmbH. Intelligent Actuator IF. *http://www.eu.intelligentactuator.de* (Accessed: 2014-05-19). Prospect for IF series.

[54] Jaekel, S., and Scholz, B. Utilizing Artificial Intelligence to achieve a robust architecture for future robotic spacecraft. In *Aerospace Conference, 2015 IEEE* (2015), IEEE, pp. 1–14.

[55] Janhunen, P., Toivanen, P. K., Polkko, J., Merikallio, S., Salminen, P., Haeggström, E., Seppänen, H., Kurppa, R., Ukkonen, J., Kiprich, S., et al. Invited Article: Electric solar wind sail: Toward test missions. *Review of Scientific Instruments 81*, 11 (2010), 111301–1–11301–11.

[56] Johnson, N., and Klinkrad, H. The International Space Station and the Space Debris Environment: 10 years on. *5th European Conference on Space Debris* (2009).

[57] Johnson, N. L. Current characteristics and trends of the tracked satellite population in the human space flight regime. *Acta Astronautica 61* (2007), 257–264.

[58] Kaya, N., Iwashita, M., Tanaka, K., Nakasuka, S., and Summerer, L. Rocket experiment on microwave power transmission with Furoshiki deployment. *Acta Astronautica 65*, 1-2 (2009), 202–205.

[59] Kelm, B., Angielski, J., Butcher, S., Creamer, N., Harris, K., Henshaw, C., Lennon, J., Purdy, W., Tasker, F., Vincent, W., and Whalen, B. FREND: Pushing the Envelope of Space Robotic. Tech. rep., Naval Research Lab Washington DC, (2008).

[60] Kessler, D. J., and Cour-Palais, B. G. Collision frequency of artificial satellites: The creation of a debris belt. *Journal of Geophysical Research: Space Physics 83*, A6 (1978), 2637–2646.

[61] Klinkrad, H. *Space debris: Models and Risk Analysis*. Springer u.a, Berlin, (2006).

[62] Klinkrad, H. Keynote: Space Debris - a Key Aspect of Space Situational Awareness. *10th AIRTEC 2015 International Congress Proceedings* (2015).

[63] Krapke, P.-W. *Leopard 2: Sein werden und seine Leistung*. Books on Demand GmbH, Norderstedt, (2004).

[64] Krebs, G. D. PRISMA. *http://space.skyrocket.de/doc_sdat/prisma.htm* (Accessed: 2012-10-04).

[65] Krolikowski, A., and David, E. Commercial on-orbit satellite servicing: national and international policy considerations raised by industry proposals. *New Space 1*, 1 (2013), 29–41.

[66] Kumar, K., Gómez, N. O., Jankovic, M., Martin, J. M. R., Topputo, F., Walker, S., Kirchner, F., and Vasile, M. AGORA: Mission to demonstrate Technologies to actively remove ARIANE Rocket Bodies. *66th International Astronautical Congress*, IAC-15 A6.6.1 (2015).

[67] Lappas, V., Fernandez, J., Visagie, L., Stohlman, O., Viquerat, A., Prassinos, G., Theodorou, T., and Schenk, M. *Advances in Solar Sailing*. Springer Berlin Heidelberg, (2014), pp. 153–167.

[68] Liou, J.-C. An active debris removal parametric study for LEO environment remediation. *Advances in Space Research 47*, 11 (2011), 1865–1876.

[69] Liou, J.-C. Engineering and technology challenges for active debris removal. *EUCASS Proceedings Series 4* (2011), 735–748.

[70] Liou, J.-C. Orbital Debris Quarterly News. *http://www.orbitaldebris.jsc.nasa.gov/newsletter/newsletter.html* (Accessed: 2012 through 2019).

[71] Liou, J.-C., Johnson, N., and Hill, N. Controlling the growth of future LEO debris populations with active debris removal. *Acta Astronautica 66*, 5-6 (2010), 648–653.

[72] Liou, J.-C., and Shoots, D. Avoiding Satellite Collisions in 2009. *Orbital Debris Quarterly News 14*, 1 (January 2010), 2.

[73] Liou, J.-C., and Shoots, D. Increase in ISS Debris Avoidance Maneuvers. *Orbital Debris Quarterly News 19*, 4 (October 2015), 1–2.

[74] Mai, W. Space Debris Removal - Strahlungsanalyse. Universität der Bundeswehr München, (2013). internal document.

[75] Mason, J., Stupl, J., Marshall, W., and Levit, C. Orbital debris-debris collision avoidance. *Advances in Space Research 48*, 10 (2011), 1643–1655.

[76] Matney, M. On the Probability of Random Debris Reentry Occuring on Land or Water, Part II. *Orbital Debris Quarterly News 16*, 2 (April 2012), 6.

[77] McCarthy, K. US Commercial Space Launch Competitiveness Act. *Public Law* (2015), 114–90.

[78] McKnight, D. Pay Me Now or Pay Me More Later: Start the Development of Active Orbital Debris Removal Now. In *AMOS Technical Conference Proceedings* (2010).

[79] McKnight, D., Di Pentino, F., Kaczmarek, A., and Dingman, P. System Engineering Analysis of Derelict Collision Prevention Options. *63rd International Astronautical Congress*, IAC-12-A6.5.2 (2012).

[80] Meitinger, C. *Kognitive Automation zur kooperativen UAV-Flugführung*. PhD thesis, Universität der Bundeswehr München, (2008).

[81] Michael, J., Chudej, K., Gerdts, M., and Pannek, J. Optimal rendezvous path planning to an uncontrolled tumbling target. *IFAC Proceedings Volumes 46*, 19 (2013), 347–352.

[82] Missel, J., and Mortari, D. Sling Satellite for Debris Removal with Aggie Sweeper. *21st Space Flight Mechanics Meeting*, AAS 11-256 (2011).

[83] NASA. Overview of the DART Mishap Investigation. *http://www.nasa.gov/pdf/148072main_DART_mishap_overview.pdf* (Accessed: 2012-10-24). Results for public release.

[84] NASA. Orbital Debris Evolve Model. *http://orbitaldebris.jsc.nasa.gov/model/evolmodel.htm#LEGEND* (Accessed: 2013-11-28).

[85] Naumann, W. Deutsche Orbitale Servicing Mission (DEOS). *http://www.spacetech-i.com/deutsche-orbitale-servicing-mission.html* (Accessed: 2012-10-30).

[86] Nishida, S.-I., Kawamoto, S., Okawa, Y., Terui, F., and Kitamura, S. Space debris removal system using a small satellite. *Acta Astronautica 65*, 1-2 (2009), 95–102.

[87] Nishida, S.-I., and Yoshikawa, T. Space debris capture by a joint compliance controlled robot. *IEEE/ASME International Conference in Advanced Intelligent Mechatronics (AIM)* (2003), 496–502.

[88] Nock, K., Gates, K., Aaron, K., and McRonald, A. Gossamer Orbit Lowering Device (GOLD) for Safe and Efficient De-Orbit. *AIAA/AAS Astrodynamics Specialist Conference, Guidance, Navigation, and Control and Co-located Conferences* (2010).

[89] Oda, M. ETS-VII: Achievements, Troubles and Future. In *Proceeding of the 6th i-SAIRAS 2001* (2001).

[90] Olive, X. FDI(R) for satellites: How to deal with high availability and robustness in the space domain? *International Journal of Applied Mathematics and Computer Science 22*, 1 (2012), 99–107.

[91] Onken, R., and Schulte, A. *System-ergonomic design of cognitive automation: Dual-mode cognitive design of vehicle guidance and control work systems*, vol. 235. Springer-Verlag, Berlin and Heidelberg, (2010).

[92] Ortega, G., and Giron-Sierra, J. Fuzzy logic techniques for intelligent spacecraft control systems. In *IEEE International Conference on Systems, Man and Cybernetics* (1995), vol. 3, pp. 2460–2465.

[93] Pardini, C., and Anselmo, L. Reentry predictions of three massive uncontrolled spacecraft. In *23rd International Symposium on Space Flight Dynamics* (2012), Deutsches Zentrum für Luft-und Raumfahrt e.V. Cologne.

[94] Parness, A. Orbital Debris Removal with Gecko-Like Adhesives: Technology Development and Mission Design. *66th International Astronautical Congress*, IAC-15 A6.5.1 (2015).

[95] Patton, R. J., Uppal, F. J., Simani, S., and Polle, B. Robust FDI applied to thruster faults of a satellite system. *Control Engineering Practice 18*, 9 (2010), 1093–1109.

[96] Pearson, J., Carroll, J., Levin, E., and Oldson, J. Overview of the Electrodynamic Delivery Express EDDE. *AIAA 2003*, 4790 (2003).

[97] Pelrin, R. Microrobot Inspectors: Electroadhesive wall Climbing Robots and more. *In-Space Non-Destructive Inspection Technology Workshop* (2012). Johnson Space Center.

[98] Peters, S., Eidel, W., Förstner, R., and Fiedler, H. Architecture and First Achievements of a Simulation for the Approach to an Uncooperative Target. *Journal of the British Interplanetary Society 70* (2017), 134–142.

[99] Peters, S., Förstner, R., and Fiedler, H. Autonomy for Active Space Debris Removal: Research Issues and Approaches. In *Deutscher Luft-und Raumfahrtkongress* (2013), p. 7 ff.

[100] Peters, S., Förstner, R., and Fiedler, H. Mission Architecture for active Space Debris Removal using the Example of SL-8 Rocket Bodies. In *Space Safety is No Accident*. Springer, (2015), pp. 23–28.

[101] Peters, S., Förstner, R., and Fiedler, H. Mission Design and Simulation Considerations for ADReS-A. In *AMOS Technical Conference Proceedings* (2016).

[102] Peters, S., Pirzkall, C., Fiedler, H., and Förstner, R. Mission Concept and Autonomy Considerations for Active Debris Removal. *Acta Astronautica 129* (2016), 410–418.

[103] Praly, N., Hillion, M., Bonnal, C., Laurent-Varin, J., and Petit, N. Study on the eddy current damping of the spin dynamics of space debris from the Ariane launcher upper stages. *Acta Astronautica 76* (2012), 145–153.

[104] Putzer, H. J. *Ein uniformer Architekturansatz für kognitive Systeme und seine Umsetzung in ein operatives framework*. PhD thesis, Universität der Bundeswehr München, (2004).

[105] Rank, P., Mühlbauer, Q., Naumann, W., and Landzettel, K. The DEOS Automation and Robotics Payload. In *Symp. on Advanced Space Technologies in Robotics and Automation, ASTRA* (2011).

[106] Rasmussen, J. Skills, rules, and knowledge; signals, signs, and symbols, and other distinctions in human performance models. *IEEE Transactions on Systems, Man and Cybernetics 13*, 3 (1983), 257–266.

[107] Reed, J., and Barraclough, S. Development of Harpoon System for Capturing Space Debris. *6th European Conference on Space Debris*, ESA SP-723 (2013).

[108] Russian Space Web. Cosmos-1 and Cosmos-3 launch vehicle development history. *http://www.russianspaceweb.com/cosmos3.html* (Accessed: 2013-12-10).

[109] Schmitz, M., Fasoulas, S., and Utzmann, J. Performance model for space-based laser debris sweepers. *Acta Astronautica 115* (2015), 376 – 383.

[110] Scitor. Space Situational Awareness Service. *https://www.space-track.org/* (Accessed: 2015-11-20).

[111] Seidel, R., Herpel, H.-J., and F"orstner, R. Innovative Fault Detection, Isolation and Recovery - Project Description. In *19th IFAC Symposium on Automatic Control in Aerospace* (2013), pp. 96–100.

[112] Seraji, H., and Serano, N. A Multidecision Fusion System for terrain Safety Assessment. *IEEE Transactions in Robotics 25*, 1 (2009), 99–108.

[113] Setty, S. J., Cefola, P. J., Fiedler, H., and Diaz, J. Optimal Scheduling for Geosynchronous Space Object Follow-Up Observations Using a Genetic Algorithm. In *AMOS Technical Conference Proceedings* (2016), pp. 1380–1396.

[114] Sgobba, T. Space Debris Re-entries and Aviation Safety. In *International Association for the Advancement of Space Safety's 2013 Conference* (2013).

[115] Sharf, I., Woo, P., Nguyen-Huynh, T.-C., and Misra, A. System Rigidization and control for post-capture maneuvering of large space debris. In *Aerospace Conference, 2016 IEEE* (2016), pp. 1–12.

[116] Siminski, J. A. *Object correlation and orbit determination for geostationary satellites using optical measurements*. PhD thesis, Universität der Bundeswehr München, (2016).

[117] Siminski, J. A., Weigel, M., and Fiedler, H. Catalog Build-Up for Geostationary Orbit Using Simulated Short-Arc Tracklets. In *AMOS Technical Conference Proceedings* (2014).

[118] Singh, N. Inexact reasoning. *https://www.slideshare.net/nirdesh75/inexact-reasoning* (Accessed: 2017-06-12).

[119] spaceflight101.com. Progress MS - Spacecraft & Satellites. *http://spaceflight101.com/spacecraft/progress-ms/* (Accessed: 2016-05-19).

[120] SpaceRef.com. Cutting edge microsatellite achieves milestones. *http://www.spaceref.com/news/viewpr.html?pid=18152* (Accessed: 2012-10-24).

[121] Tafazoli, M. A study of on-orbit spacecraft failures. *Acta Astronautica 64* (2009), 195–205.

[122] Trushlyakov, V., and Yudintsev, V. Autonomous Module docking with noncooperative spent orbital stage using probe-cone mechanism. *4th international workshop on Space Debris Modelling and Remediation* (2016).

[123] Truszkowski, W., Hallock, H., Rouff, C., Karlin, J., Rash, J., Hinchey, M., and Sterritt, R. *Autonomous and autonomic systems: With applications to NASA intelligent spacecraft operations and exploration systems.* Springer Science & Business Media, (2009).

[124] UNCOPUOS. Space Debris Mitigation Guidelines of the Committee on the Peaceful Uses of Outer Space. *http://www.iadc-online.org/References/Docu/SpacenDebrisnMitigationnGuidelines_COPUOS.pdf* (Accessed: 2012-10-22).

[125] United Nations Office for Outer Space Affairs. Outer Space Treaty: Treaty on Principles Governing the Activities of States in the Exploration and Use of Outer Space, including the Moon and Other Celestial Bodies, (1967).

[126] Unity Technologies. Unity - Manual. *http://docs.unity3d.com/Manual/index.html* (Accessed: 2017-11-06).

[127] Unity Technologies. Unity - Scripting API. *http://docs.unity3d.com/ScriptReference/index.html* (Accessed: 2017-11-06).

[128] U.S. Government. Orbital Debris Mitigation Standard Practices. *https://www.iadc-online.org/References/Docu/USG_OD_Standard_Practices.pdf* (Accessed: 2012-10-23).

[129] Vasconcelas, J. GNC design and validation for rendezvous, detumbling, and de-orbiting of ENVISAT using a clamping mechanism (CLGADR study). *4th international workshop on Space Debris Modelling and Remediation* (2016).

[130] Vassev, E., and Hinchey, M. *Autonomy Requirements Engineering for Space Missions*. Springer Science & Business Media, (2014).

[131] Visentin, B., Bischof, B., Starke, H., Guenther, H., Foth W.-P., Kerstein, L., Oesterlin, Ebert, Macaire, K., Wegener, S., Krag, H., Oswald, G., Lampariello, R., and Nimelman, I. RObotic GEostationary orbit REstorer (ROGER): Phase A. *Final Report, EADS Space Transportation, ROG-SIBRE-EXS* (2003).

[132] Wander, A., and Förstner, R. Innovative fault detection, isolation and recovery on-board spacecraft: Study and implementation using cognitive automation. In *Conference on Control and Fault-Tolerant Systems* (2013), IEEE, pp. 336–341.

[133] Weeden, B. Through a Glass, Darkly: Chinese, American, and Russian Anti-satellite Testing in Space. *http://swfound.org/media/167224/Through_a_Glass_Darkly_March2014.pdf* (Accessed: 2016-01-12).

[134] Weigel, M. Interviews and Provision of Matlab code as basis for calculations, (2013). private conversations.

[135] Wertz, J. R., and Larson, W. J. *Space Mission Analysis and Design (SMAD) - 3rd Ed.* Springer u.a, Berlin, (1999).

[136] Wright, D. Colliding Satellites: Consequences and Implications. *http://www.ucsusa.org/assets/documents/nwgs/SatelliteCollision-2-12-09.pdf* (Accessed: 2012-09-27).

[137] Zinner, N., Williamson, A., Brenner, K., Curran, J. B., Isaak, A., Knoch, M., Leppek, A., and Lestishen, J. Junk Hunter: Autonomous Rendezvous, Capture, and De-Orbit of Orbital Debris. In *Proceedings of AIAA SPACE 2011 Conference & Exposition* (2011), 2011-7292.

A Mathematical Background

A.1 Kinetic Energy of Space Debris

The kinetic energy of an aluminum bullet, representing a piece of debris in space, is calculated as followed. The kinetic energy of the debris ($E_{kin,Deb}$), the mass of the debris particle (m_{Deb}), the velocity of the particle (v_{Deb}), the density of aluminum (ρ_{Alu}), the bullets volume (V_{Deb}), and the debris' diameter (d_{Deb}) result in a proportional dependence between the kinetic energy of the debris and its cubed diameter in combination with its squared velocity. Figure 2.5 visualizes the relation.

$$
\begin{aligned}
E_{kin,Deb} \quad &= \quad \frac{m_{Deb}}{2} \cdot v_{Deb}^2, \\
\text{with} \quad & \quad m_{Deb} = \rho_{Alu} \cdot V_{Deb} \\
\text{and} \quad & \quad V_{Deb} = \frac{1}{6} \cdot \pi \cdot d_{Deb}^3 \\
E_{kin,Deb} \quad &= \quad \frac{\rho_{Alu} \cdot \pi \cdot d_{Deb}^3}{12} \cdot v_{Deb}^2
\end{aligned}
$$

A.2 Hohmann

A controlled de-orbit from LEO is most effectively performed by a Hohmann-transfer in terms of propellant consumption. The following equations provide the example of a de-orbit from an altitude of 980 km[1] to an altitude of 80 km[2]. Δv represents the required velocity, v_K the velocity on a circular orbit, r_A the radius in the apogee (A) of the elliptical orbit, r_P the the radius in the perigee (P) of the elliptical orbit, $v_{Ell,A}$ the velocity in the apogee of an ellipse crossing A and P, r_K the radius of the circular orbit, and R_E Earth's radius.

$$\Delta v = |v_K - v_{Ell,A}|,$$

$$\text{Circular orbit:} \quad v_K = \sqrt{\frac{\mu}{r_K}},$$

$$\text{with} \quad r_K = R_E + 980\,\text{km}.$$

$$\text{Elliptical orbit:} \quad v_{Ell,A} = \sqrt{\mu \cdot \left(\frac{2}{r_A} - \frac{1}{a}\right)},$$

$$\text{with} \quad r_A = r_K,$$

$$a = \frac{r_A + r_P}{2},$$

$$\text{and} \quad r_P = R_E + 80\,\text{km}.$$

$$\text{results to} \quad v_K = 7360.19\,\text{m/s},$$

$$\text{and} \quad v_{Ell,A} = 7116.42\,\text{m/s}.$$

$$\Delta v = \underline{\underline{243.77}}\,\text{m/s}.$$

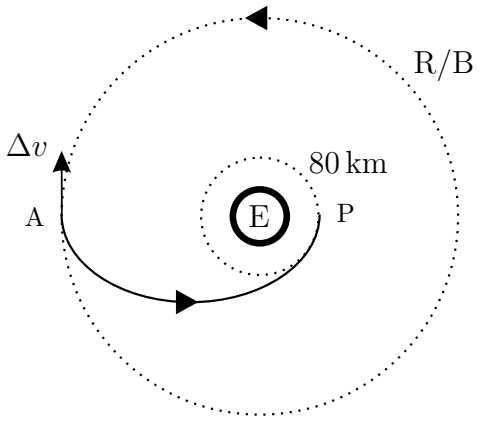

Figure A.1: Hohmann transfer.

[1] Target's orbit according to Section 3.2.2

[2] Observed from other know de-orbiting satellites as break-up altitude.

A.3 Calculations for Subsystems

A.3.1 Power System

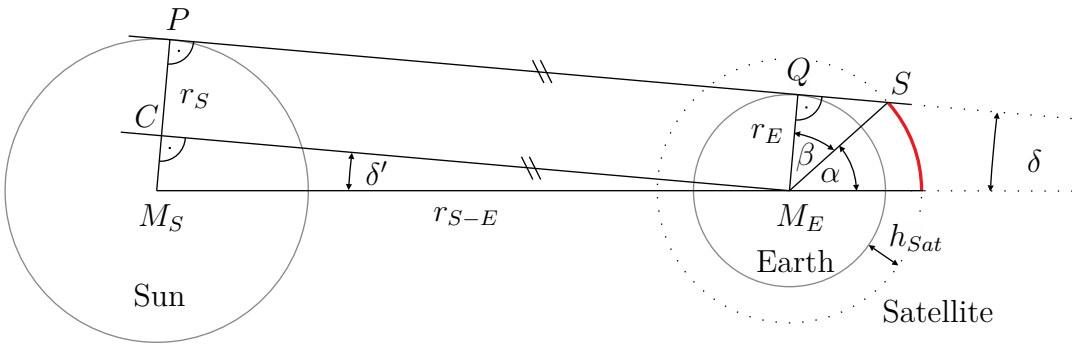

Figure A.2: Geometrical deviation of eclipse phase with non-parallel sunlight.

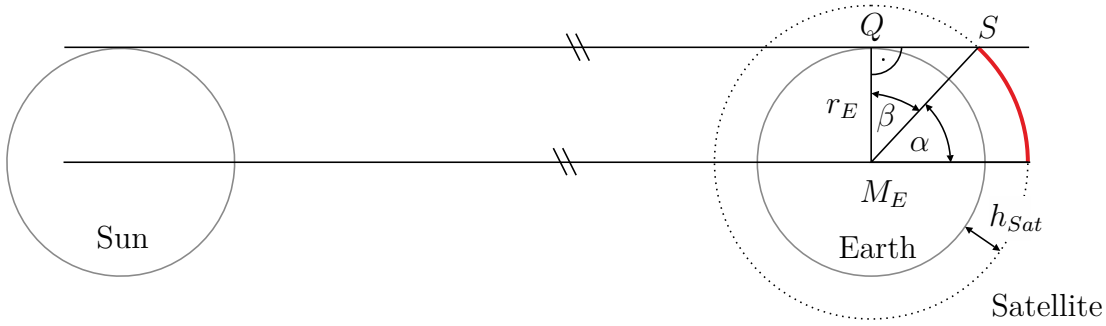

Figure A.3: Geometrical deviation of eclipse phase with parallel sunlight.

To know how long a satellite of a specific height is in full eclipse, the following considerations, based on Figure A.2, are taken: Earth orbits the Sun at a distance of r_{S-E} with $1AU$. The line segments $\overline{M_S P}$ and $\overline{M_E Q}$ show the respective radii, line segment $\overline{PQ}$ is the tangent of the two circles, displaying the Sun and Earth in 2D. When a satellite orbits Earth, it passes the eclipse for a fraction of its whole period, displayed by the angle α. The considerations concentrate on one half of the geometry, as the figures can be mirrored with the fraction of α staying the same for half a circle or the full circle.

Following Thales' theorem, line segment $\overline{PQ}$ is parallel to line segment $\overline{CM_E}$, which again allows δ' to have the same value as δ.

$$\overline{PQ} \parallel \overline{CM_E}$$
$$\delta = \delta'$$

The internal angles of a triangle combined sum up to 180°, trigonometrical functions help calculating α:

$$\begin{aligned}
\beta + \alpha + \delta &= 90^\circ \\
\sin\delta &= \frac{r_S - r_E}{r_{S-E}} \\
\cos\beta &= \frac{r_E}{r_E + h_{Sat}} \\
\rightarrow \alpha &= 90^\circ - \arccos\frac{r_E}{r_E + h_{Sat}} - \arcsin\frac{r_S - r_E}{r_{S-E}} \\
\alpha(h_{Sat} = 980\,\mathrm{km}) &= 59.826^\circ \\
&\equiv \mathbf{0.3324} \quad \text{of one period.}
\end{aligned}$$

For simpler calculation, the sunlight shines in parallel lines on Earth (cf. Figure A.3, resulting in an infinite δ. α changes to:

$$\begin{aligned}
\beta + \alpha &= 90^\circ \\
\cos\beta &= \frac{r_E}{r_E + h_{Sat}} \\
\rightarrow \alpha &= 90^\circ - \arccos\frac{r_E}{r_E + h_{Sat}} \\
\alpha(h_{Sat} = 980\,\mathrm{km}) &= 60.090^\circ \\
&\equiv \mathbf{0.3338} \quad \text{of one period.}
\end{aligned}$$

With a full period $P(h_{Sat} = 980\,\mathrm{km})$ of 6281.32 s, the difference between parallel or non-parallel illumination results in 9.21 s ($\sim 1/680$ or 0.15%). Due to the early stage of the mission planning, parallel illumination will be used for further calculations and considerations.

A.3.2 Thermal System

The thermal system of a satellite is influenced by the radiative heat transfer of the Sun $\dot{Q}_{Sol}$, of the Earth (infrared: $\dot{Q}_{IR}$ and Albedo $\dot{Q}_{Al}$), of the dissipating instruments of the satellite $\dot{Q}_{diss}$, of the Multi Layer Insulation (MLI) $\dot{Q}_{MLI}$, of the radiators $\dot{Q}_R$ and of the solar arrays $\dot{Q}_{Sol,out}$. The resulting heat flow for ADReS-A is displayed in Figure A.4 The arrows point towards the satellite for absorption and away from the satellite for emissivity.

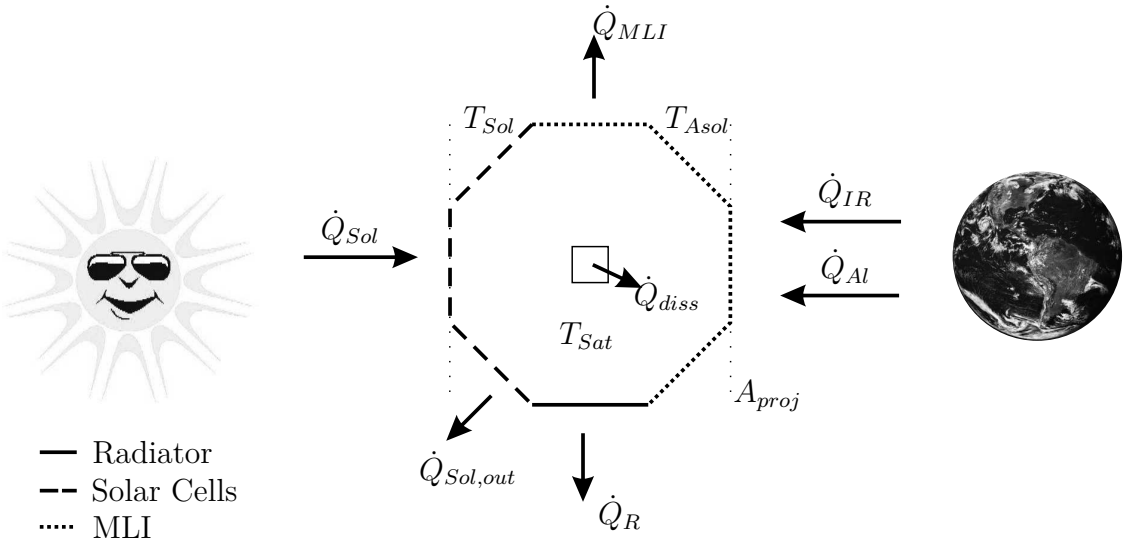

Figure A.4: ADReS-A - interior, including dissipating instruments.

Figure A.5 and Figure A.6 give the thermal models of ADReS-A for the hot and the cold case, respectively. The different outer layers of the satellite - solar arrays (SC), MLIs and radiators (Rad) - result in different absorption and emissivity in different regions of ADReS-A. Different conductivity k_X and emissivity ϵ_{eff} within the satellite enable the heat flow.

During the hot case (HC), the satellite is between Sun and Earth. Here, ADReS-A is exposed to higher temperatures than in the cold case (CC), where the satellite is in Earth's shadow. For both cases, the internal temperature T_X^Y of the satellite needs to stay within the allowed limits. Respective calculations are performed within the tool presented in Section 4.1.3 and result in the heating system suggested.

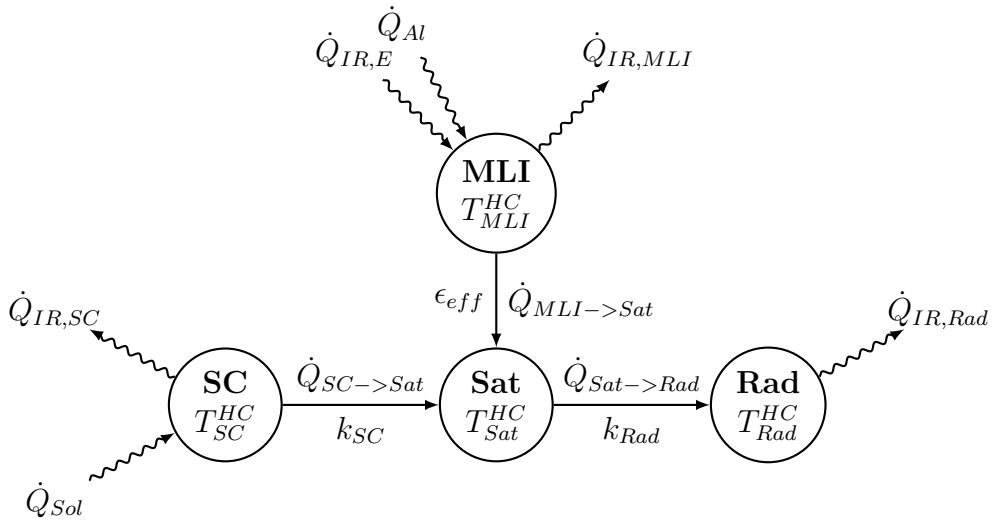

Figure A.5: Thermal model of ADReS-A in Hot Case.

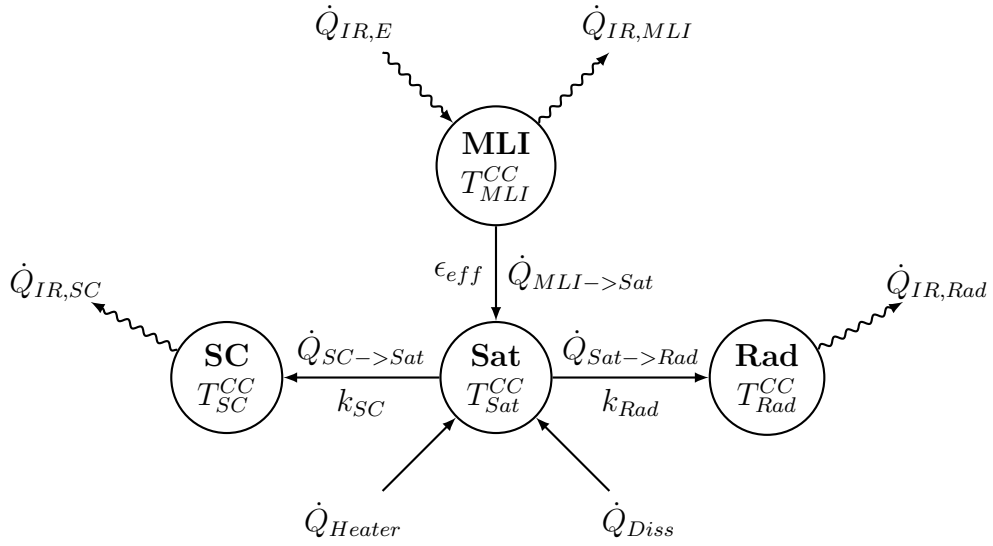

Figure A.6: Thermal model of ADReS-A in Cold Case.

A.4 Bayesian Network Example

Bayesian networks combine probabilities of different events to an overall-probability. The following example derives the probability for a faulty solar array (SA), given, the mission fails within the first year. The following statements are derived from Castet [14]:

- 3% missions fail in the first year.
- 27% of the failures are power related.
- Solar arrays have a reliability of 0.997.

Figure A.7 is created with values assigned either a case is true (T) or false (F).

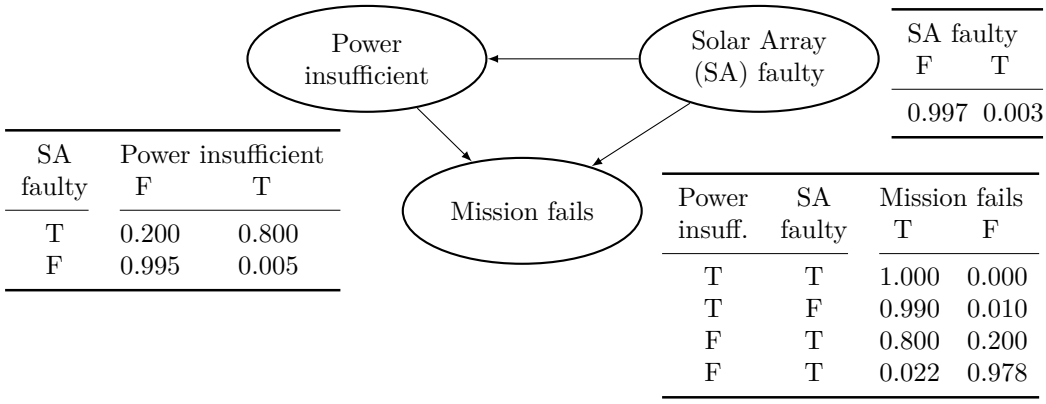

SA faulty	Power insufficient F	Power insufficient T
T	0.200	0.800
F	0.995	0.005

SA faulty F	SA faulty T
0.997	0.003

Power insuff.	SA faulty	Mission fails T	Mission fails F
T	T	1.000	0.000
T	F	0.990	0.010
F	T	0.800	0.200
F	T	0.022	0.978

Figure A.7: Graphical structure with probabilities for a Bayesian network. The two possible values for the variables are T (for true) and F (for false). The probabilities are derived from Castet [14] and own considerations.

The joint probability function is:

$$\Pr(M, P, SA) = \Pr(M|P, SA)\Pr(P|SA)\Pr(SA),$$

where the names of the variables have been abbreviated to M = Mission failed (T/F), P = Power insufficient (T/F), and SA = Solar Array faulty (T/F). The question can be described by:

$$\Pr(SA = T|M = T) = \frac{\Pr(M = T, SA = T)}{\Pr(M = T)} = \frac{\sum_{P\in\{T,F\}}\Pr(M = T, P, SA = T)}{\sum_{P,SA\in\{T,F\}}\Pr(M = T, P, SA)}.$$

From the Conditional Probability Tables (CPTs), each term can be derived, such as:

$$\begin{aligned}\Pr(M = T, &P = T, SA = T) \\ &= \Pr(M = T|P = T, SA = T)\Pr(P = T|SA = T)\Pr(SA = T) \\ &= 1.000 \times 0.800 \times 0.003 \\ &= 0.0024.\end{aligned}$$

With the numerical results (subscribed by the associated variable values) resulting to

$\Pr_{TTT} = 1.000 \times 0.800 \times 0.003 = 0.0024;$

$\Pr_{TFT} = 0.800 \times 0.200 \times 0.003 = 0.00048;$

$\Pr_{TTF} = 0.990 \times 0.005 \times 0.997 = 0.004935;$

$\Pr_{TFF} = 0.022 \times 0.995 \times 0.997 = 0.021725;$

$$\begin{aligned}\Pr(SA = T|M = T) &= \frac{0.0024_{TTT} + 0.00048_{TFT}}{0.0024_{TTT} + 0.004935_{TTF} + 0.00048_{TFT} + 0.021725_{TFF}} \\ &= \frac{288}{2954} \approx 9.75\%.\end{aligned}$$

The result correlates with the number given by Castet [14], assigning a 10% contribution of solar array (operation) failure to a failed mission if failed within the first year.

A.5 Eidel Equations

The complete system of equations according to Eidel [28] lists

$$\begin{aligned}\xi_{Eid} &= \xi^{(0)} + e\xi^{(1)}\\ \eta_{Eid} &= \eta^{(0)} + e\eta^{(1)}\\ \zeta_{Eid} &= \zeta^{(0)} + e\zeta^{(1)}.\end{aligned}$$

The first part of the Eidel equations, reflecting a solution of the CW-equations, is descried as:

$$\begin{aligned}\xi^{(0)} &= 2\zeta_0' \cos\tau + (6\zeta_0 + 4\xi_0')\sin\tau - 3(\xi_0' + 2\zeta_0)\tau + \xi_0 - 2\zeta_0'\\ \eta^{(0)} &= \eta_0 \cos\tau + \eta_0' \sin\tau\\ \zeta^{(0)} &= -(3\zeta_0 + 2\xi_0')\cos\tau + \zeta_0' \sin\tau + 2(2\zeta_0 + \xi_0')\end{aligned}$$

where τ is the nominated time variable $\omega_{0_{CW}} \cdot t$.

The second part of the Eidel-Equations follows

$$\begin{aligned}\xi^{(1)} &= 4[(5\zeta_0 + \xi_0')\cos\theta_0 - (\xi_0 - 2\zeta_0')\sin\theta_0]\sin\tau - 2[2\zeta_0'\cos\theta_0 + \xi_0'\sin\theta_0]\cos\tau +\\ &+ \frac{3}{2}(3\zeta_0 + 2\xi_0')\sin(2\tau + \theta_0) + \frac{3}{2}\zeta_0'\cos(2\tau + \theta_0) +\\ &- 3(2\zeta_0 + \xi_0')[\sin(\tau + \theta_0) - \tau\cos(\tau + \theta_0)] - 7(2\zeta_0 + \xi_0')\sin(\tau + \theta_0) -\\ &+ (\xi_0 - 2\zeta_0')\cos(\tau + \theta_0) - 3[(5\zeta_0 + \xi_0')\cos\theta_0 - (\xi_0 - \zeta_0')\sin\theta_0]\tau +\\ &+ (3\xi_0' + \frac{7}{2}\zeta_0)\sin\theta_0 + (\xi_0 + \frac{1}{2}\zeta_0')\cos\theta_0,\\ \eta^{(1)} &= (\eta_0\cos\theta_0 - 2\eta_0'\sin\theta_0)\cos\tau + (\eta_0\sin\theta_0 - \eta_0'\cos\theta_0)\sin\tau +\\ &+ \frac{1}{2}\eta_0[\cos(2\tau + \theta_0) - 3\cos\theta_0] + \frac{1}{2}\eta_0'[\sin(2\tau + \theta_0) + 3\sin\theta_0],\\ \zeta^{(1)} &= -2[(5\zeta_0 + \xi_0')\cos\theta_0 - (\xi_0 - 2\zeta_0')\sin\theta_0]\cos\tau - [2\zeta_0'\cos\theta_0 + \xi_0'\sin\theta_0]\sin\tau -\\ &- (3\zeta_0 + 2\xi_0')\cos(2\tau + \theta_0) + \zeta_0'\sin(2\tau + \theta_0) - 3(2\zeta_0 + \xi_0')\tau\sin(\tau + \theta_0) +\\ &+ (13\zeta_0 + 4\xi_0')\cos\theta_0 + (3\zeta_0' - 2\xi_0)\sin\theta_0.\end{aligned}$$

θ_0 represents the true anomaly at the beginning when t is zero. Additionally, ω_0 is redefined to

$$\omega_{0_{Eid}} = \sqrt{\frac{\mu}{(a(1-e^2))^3}}.$$

B Supporting Tables

B.1 Satellite Data of the *Top 200*

Table B.1: Top 200 objects in space according to their criticality for catastrophic collisions.

	SATNAME	NORAD ID	Mass [kg]	Altitude [km]	Incl. [deg]	Eccentr. $\times 10^{-3}$	RAAN [deg]	RCS [m^2]
1	**ARIANE 40 R/B**	20443	1764	769.0	98.75	1.15	355.12	10.576
2	**SL-16 R/B**	28353	8226	845.7	71.00	0.34	235.45	0.001
3	**ENVISAT**	27386	8111	766.5	98.45	0.11	82.15	8.620
4	**SL-16 R/B**	23088	8226	844.0	71.00	0.27	80.81	5.605
5	**SL-16 R/B**	31793	8226	845.0	70.97	0.20	189.61	9.722
6	**SL-16 R/B**	22220	8226	838.1	71.00	1.43	226.86	4.477
7	**ARIANE 40+ R/B**	23561	1764	768.9	98.61	0.73	327.81	8.480
8	**SL-16 R/B**	25407	8226	840.3	71.01	0.69	205.62	4.433
9	**SL-16 R/B**	22285	8226	842.9	71.02	0.23	9.42	7.057
10	**SL-16 R/B**	17974	8226	835.4	71.01	1.51	80.32	0.001
11	**SEASAT 1**	10967	2300	749.8	108.00	0.25	159.04	4.513
12	**SL-16 R/B**	16182	8226	838.8	71.00	0.74	174.38	9.412
13	**SL-16 R/B**	22803	8226	836.9	70.99	1.87	62.56	8.710
14	**SL-16 R/B**	23405	8226	842.2	70.98	0.49	22.45	7.909
15	**SL-16 R/B**	22566	8226	843.1	71.00	0.85	224.07	10.071
16	**SL-16 R/B**	19650	8226	840.3	71.00	1.24	179.42	0.001
17	**IDEFIX/ARIANE 42P**	27422	38067	795.7	98.37	1.18	70.51	9.515
18	**ARIANE 1 R/B**	16615	1318	788.4	98.83	1.29	49.67	4.171
19	**SL-16 R/B**	26070	8226	841.4	71.00	1.87	118.35	1.599
20	**SL-8 R/B**	12443	1421	777.6	74.05	0.43	250.21	3.031
21	**SL-16 R/B**	17590	8226	837.0	71.01	0.73	320.82	8.695
22	**SL-16 R/B**	20625	8226	844.1	71.00	1.29	307.30	0.001
23	**METOP-A**	29499	37699	820.3	98.67	0.19	72.85	4.448
24	**SL-8 R/B**	9444	1421	767.6	74.05	1.42	34.39	1.491
25	**SL-8 R/B**	16953	1421	769.3	74.01	1.38	18.80	3.670
26	**SL-16 R/B**	24298	8226	851.2	70.86	1.26	235.03	2.978
27	**SL-16 R/B**	19120	8226	828.9	71.02	2.06	146.09	0.001
28	**AURA**	28376	30015	702.5	98.22	0.08	316.32	2.986
29	**IRIDIUM 94**	27374	1750	777.7	86.39	0.33	212.45	5.722
30	**THOR AGENA D R/B**	733	694	786.4	98.98	3.41	106.06	2.968
31	**IRIDIUM 77**	25471	3398	777.7	86.40	0.16	338.50	5.387
32	**SL-8 R/B**	13992	1421	773.4	74.05	0.37	95.37	3.217
33	**SL-16 R/B**	23705	8226	842.5	71.02	1.48	186.36	2.982
34	**IRIDIUM 82**	25467	3398	777.7	86.39	0.26	338.71	0.001
35	**IRIDIUM 11**	25578	3398	777.7	86.39	0.22	212.32	4.641
36	**IRIDIUM 03**	25431	3398	777.7	86.39	0.18	212.35	3.004
37	**IRIDIUM 80**	25469	3398	777.7	86.40	0.25	338.77	4.523

Continued on next page

Table B.1 – *Continued from previous page*

SATNAME	NORAD ID	Mass [kg]	Altitude [km]	Incl. [deg]	Eccentr. $\times 10^{-3}$	RAAN [deg]	RCS [m^2]
38 IRIDIUM 84	25530	3398	777.7	86.40	0.25	306.71	5.942
39 AQUA	27424	28475	702.5	98.22	0.16	314.13	4.513
40 IRIDIUM 81	25468	3398	777.7	86.39	0.26	338.43	2.935
41 IRIDIUM 83	25531	3398	777.6	86.40	0.25	306.79	4.550
42 IRIDIUM 86	25528	3398	777.7	86.40	0.20	306.59	0.866
43 IRIDIUM 20	25577	3398	777.7	86.39	0.22	212.14	2.444
44 IRIDIUM 76	25432	3398	777.7	86.39	0.21	212.09	5.873
45 SL-16 R/B	25861	8226	638.2	97.88	1.47	333.74	0.001
46 ARGOS	25634	2490	828.6	98.83	1.05	75.72	28.372
47 SL-8 R/B	16012	1421	772.8	74.06	1.47	224.70	2.993
48 SL-16 R/B	27006	8226	996.3	99.13	1.42	197.66	1.200
49 METEOR-M	35865	26390	819.0	98.63	0.25	66.79	1.041
50 H-2A R/B	27601	4000	788.1	98.52	7.33	98.23	1.767
51 SL-16 R/B	23343	8226	643.2	98.20	0.68	0.34	0.907
52 SL-8 R/B	8924	1421	770.4	74.06	1.35	196.46	20.419
53 SL-8 R/B	22676	1421	780.4	74.04	1.98	261.59	2.089
54 SL-8 R/B	23432	1421	781.3	74.03	0.67	19.59	1.006
55 SL-8 R/B	8344	1421	763.4	74.06	2.18	227.66	1.169
56 CZ-2C R/B	31114	3800	829.3	98.30	5.92	338.24	2.639
57 ARIANE 40 R/B	22830	1764	788.9	98.75	1.05	335.42	1.199
58 SL-8 R/B	15032	1421	777.9	74.07	1.77	155.73	1.436
59 ADEOS 2	27597	3680	803.4	98.30	0.19	40.25	0.001
60 GLOBALSTAR M076	37190	9600	1413.6	52.01	0.02	283.46	0.001
61 SL-8 R/B	13149	1421	776.3	74.04	1.41	339.48	13.447
62 SL-8 R/B	16682	1421	774.4	74.03	1.57	320.22	13.847
63 OKEAN O	25860	20225	646.9	97.97	0.08	334.33	13.602
64 ARIANE 40 R/B	25261	1764	783.5	98.34	0.32	336.08	24.853
65 SL-16 R/B	25400	8226	807.9	98.28	0.98	8.82	16.420
66 COSMOS 1867	18187	1250	788.6	65.01	1.87	81.97	12.750
67 SL-8 R/B	11511	1421	771.2	74.04	1.69	50.83	17.338
68 SL-8 R/B	13028	1421	766.3	74.04	2.11	129.13	10.323
69 ARIANE 40 R/B	21610	1764	759.2	98.76	0.42	17.99	22.489
70 SL-8 R/B	21015	1421	774.0	74.05	2.16	225.14	9.334
71 CZ-4 R/B	25942	1000	776.5	98.43	10.10	317.11	20.000
72 GLOBALSTAR M081	37743	9600	1413.6	52.00	0.04	15.08	9.508
73 GLOBALSTAR M085	37742	9600	1413.6	51.99	0.04	13.11	10.451
74 METEOR 3M	27001	2500	1004.1	99.20	1.30	187.29	17.014
75 OPS 6182 (DMSP 5D-1 F2)	10820	508	778.7	98.53	1.01	192.72	12.184
76 ERS 1	21574	2141	770.8	98.24	3.48	342.01	12.338
77 SL-8 R/B	18096	1421	772.4	74.05	2.17	318.00	9.113
78 CZ-2C R/B	28480	3800	808.2	98.05	14.23	202.99	11.921
79 GLOBALSTAR M089	37744	9600	1413.6	51.99	0.02	329.17	16.696
80 SL-8 R/B	11870	1421	771.0	74.06	1.77	300.94	8.342
81 SL-8 R/B	5175	1421	767.7	74.05	3.06	308.37	15.697
82 SL-8 R/B	10121	1421	774.3	74.05	2.01	219.68	15.051
83 TERRA	25994	23800	702.5	98.21	0.11	87.95	7.658
84 SL-8 R/B	12792	1421	769.0	74.03	1.25	134.97	9.560
85 FENGYUN 3A	32958	8800	827.6	98.63	0.90	79.67	8.900
86 CZ-2C R/B	36089	3800	729.4	98.17	8.24	56.07	15.645
87 SL-8 R/B	19257	1421	769.3	74.05	2.17	311.44	8.966
88 DELTA 1 R/B	20323	24	734.8	97.06	7.44	194.23	9.607
89 SL-8 R/B	10962	1421	757.2	74.08	2.68	326.08	9.974
90 CORIOLIS	27640	6110	830.2	98.76	1.34	20.08	12.854
91 SL-8 R/B	13649	1421	770.3	74.00	2.02	115.12	10.024

Continued on next page

Table B.1 – *Continued from previous page*

SATNAME	NORAD ID	Mass [kg]	Altitude [km]	Incl. [deg]	Eccentr. $\times 10^{-3}$	RAAN [deg]	RCS [m^2]
92 SPOT 5	27421	17670	825.1	98.63	0.09	83.66	15.154
93 RADARSAT 2	32382	6240	791.8	98.58	0.10	20.46	6.911
94 ALOS	28931	3850	692.5	98.05	0.17	79.93	14.642
95 SL-8 R/B	11427	1421	769.5	74.02	2.17	127.86	9.621
96 SL-12 R/B(2)	15334	2121	843.4	71.00	0.60	202.56	9.439
97 SL-8 R/B	7434	1421	771.8	74.05	2.22	306.35	6.756
98 SL-8 R/B	21419	1421	780.7	74.04	4.21	19.70	7.989
99 GLOBALSTAR M075	37192	9600	1413.7	52.00	0.08	327.93	7.995
100 SL-8 R/B	13242	1421	774.1	74.04	2.64	81.70	14.042
101 SL-8 R/B	19039	1421	766.0	74.05	2.53	40.64	14.652
102 CZ-4B R/B	37782	1000	770.4	99.41	19.52	76.45	15.689
103 SL-8 R/B	14402	1421	774.2	74.05	2.80	342.06	14.866
104 IRIDIUM 21	25778	1750	777.7	86.39	0.26	180.73	17.463
105 CBERS 1	25940	3240	775.9	98.30	0.61	331.28	9.738
106 DELTA 1 R/B	7735	24	811.5	114.98	5.10	32.85	8.742
107 CBERS 2	28057	3240	775.0	98.16	0.16	19.29	11.848
108 CZ-2C R/B	37766	3800	678.8	98.20	4.61	142.12	8.245
109 GLOBALSTAR M091	37741	9600	1413.6	52.00	0.03	60.90	7.411
110 IRIDIUM 95	27375	1750	777.6	86.40	0.22	244.08	7.708
111 GLOBALSTAR M088	37740	9600	1413.6	51.97	0.10	102.35	10.403
112 SL-8 R/B	10677	1421	760.6	74.04	1.48	52.38	8.505
113 TRIAD 1	6173	93	734.2	89.82	5.40	259.99	12.841
114 NADEZHDA 7	27534	17850	990.3	82.94	3.48	355.35	8.043
115 SL-8 R/B	5707	1421	764.9	74.03	2.61	192.54	5.796
116 SL-8 R/B	22081	1421	782.1	74.04	3.56	155.65	10.213
117 RESOURCESAT 2	37387	6720	819.8	98.72	0.26	88.29	12.662
118 SL-8 R/B	10992	1421	972.2	82.93	1.86	41.18	9.608
119 GLOBALSTAR M073	37193	9600	1413.6	52.00	0.12	239.54	8.669
120 SL-8 R/B	6061	1421	758.8	74.06	1.90	290.83	9.564
121 GLOBALSTAR M083	37739	9600	1413.6	51.98	0.15	196.77	10.087
122 SL-8 R/B	11574	1421	758.7	74.07	1.74	326.52	8.944
123 ARIANE 40 R/B	25979	1764	607.0	98.15	0.74	132.15	12.173
124 FENGYUN 3B	37214	8800	827.7	98.78	0.15	316.80	8.074
125 SL-8 R/B	24955	1421	959.0	82.92	2.99	48.29	9.469
126 SL-8 R/B	10461	1421	975.9	82.95	3.28	135.43	19.892
127 GLOBALSTAR M079	37188	9600	1413.6	52.01	0.08	284.29	12.528
128 SL-8 R/B	7095	1421	969.6	82.95	3.66	162.76	7.570
129 SL-8 R/B	7350	1421	972.7	82.95	1.76	167.79	11.521
130 SL-8 R/B	13618	1421	976.0	82.97	3.15	258.49	10.024
131 CZ-4B R/B	25732	1000	834.3	98.83	3.78	343.82	13.489
132 CZ-4C R/B	37215	1000	740.2	98.86	8.97	356.14	10.013
133 SL-8 R/B	10020	1421	971.6	82.95	3.21	128.37	7.754
134 SL-8 R/B	22007	1421	971.8	82.93	3.10	68.61	11.899
135 SL-8 R/B	4370	1421	697.9	74.04	1.73	296.08	11.343
136 GLOBALSTAR M074	37189	9600	1413.6	52.00	0.07	284.77	7.730
137 SL-12 R/B(2)	15772	2121	822.4	71.11	3.44	151.98	10.468
138 GLOBALSTAR M077	37191	9600	1413.6	52.01	0.13	240.09	11.303
139 SL-8 R/B	9638	1421	970.8	82.94	3.23	169.86	14.326
140 SL-8 R/B	18161	1421	975.4	82.93	3.21	196.72	10.239
141 SL-8 R/B	16864	1421	759.4	74.03	3.41	207.83	12.069
142 SL-8 R/B	21153	1421	979.4	82.93	2.88	326.69	6.236
143 SL-8 R/B	20578	1421	977.3	82.95	1.35	121.69	8.455
144 SL-8 R/B	23093	1421	972.5	82.95	0.95	238.84	8.634
145 SL-8 R/B	15399	1421	978.6	82.95	3.33	126.36	6.454

Continued on next page

Table B.1 – *Continued from previous page*

SATNAME	NORAD ID	Mass [kg]	Altitude [km]	Incl. [deg]	Eccentr. $\times 10^{-3}$	RAAN [deg]	RCS [m^2]
146 SL-8 R/B	21088	1421	975.1	82.94	2.34	143.82	0.001
147 SL-8 R/B	8459	1421	771.2	74.06	1.54	202.40	7.958
148 SL-8 R/B	10600	1421	970.1	82.94	4.87	47.68	0.883
149 SL-8 R/B	9613	1421	973.6	82.95	3.12	275.11	13.288
150 SL-8 R/B	8646	1421	986.3	82.97	0.70	84.76	8.734
151 SL-8 R/B	17526	1421	975.9	82.90	4.11	170.25	4.968
152 CZ-4B R/B	32959	1000	754.9	98.92	7.18	163.07	5.075
153 SL-8 R/B	9044	1421	977.7	82.99	1.53	28.45	11.900
154 SL-8 R/B	7737	1421	963.4	82.99	1.85	218.91	9.441
155 SL-8 R/B	13354	1421	968.6	82.96	5.14	106.01	4.825
156 SL-8 R/B	7594	1421	968.7	82.95	1.58	54.44	6.712
157 SL-8 R/B	7769	1421	982.8	82.96	1.89	118.35	11.883
158 CZ-2C R/B	37731	3800	653.7	97.97	6.26	89.50	10.283
159 SL-8 R/B	9848	1421	980.2	82.95	1.79	106.69	10.796
160 SL-8 R/B	7009	1421	975.6	82.95	2.10	64.96	6.394
161 SL-8 R/B	25569	1421	985.9	82.94	2.00	86.81	7.297
162 IRS P6	28051	6720	819.9	98.77	0.33	88.70	7.379
163 SL-8 R/B	11668	1421	980.0	82.95	2.28	165.07	4.564
164 SL-8 R/B	21667	1421	981.8	82.91	2.20	135.64	9.035
165 SL-8 R/B	16369	1421	976.0	82.94	3.60	111.92	10.884
166 SL-8 R/B	13758	1421	969.1	82.91	2.74	80.27	10.482
167 SL-8 R/B	21938	1421	981.2	82.93	2.93	122.26	5.596
168 SL-8 R/B	19770	1421	764.8	74.05	0.62	152.78	7.095
169 SL-8 R/B	17067	1421	972.8	82.95	3.42	275.77	8.759
170 SL-8 R/B	25592	1421	985.6	82.93	2.63	226.80	7.040
171 SL-8 R/B	2802	1421	749.1	74.01	6.70	300.50	10.723
172 SL-8 R/B	20433	1421	773.8	74.04	4.26	87.10	9.566
173 SL-8 R/B	18130	1421	976.9	82.93	1.63	314.99	8.779
174 SL-8 R/B	17160	1421	983.6	82.93	3.85	186.45	8.133
175 SL-8 R/B	10732	1421	981.1	82.93	2.08	12.72	7.592
176 SL-8 R/B	23527	1421	987.3	82.94	2.12	148.63	19.379
177 GLOBALSTAR M071	31576	1080	1413.6	52.01	0.07	332.46	4.520
178 SL-8 R/B	11804	1421	978.2	82.94	2.19	212.58	5.895
179 SL-8 R/B	16494	1421	976.9	82.93	2.06	196.07	0.001
180 SL-8 R/B	8073	1421	979.0	82.90	2.03	95.34	9.477
181 DELTA 1 R/B	7616	24	877.9	97.73	18.65	346.79	13.352
182 SL-8 R/B	9738	1421	987.0	82.96	1.77	137.22	8.826
183 SL-8 R/B	20509	1421	980.3	82.95	4.28	83.49	8.151
184 SL-8 R/B	11681	1421	980.6	82.93	3.66	176.84	4.388
185 SL-8 R/B	15752	1421	988.9	82.95	2.29	61.25	10.001
186 SL-8 R/B	16511	1421	979.1	82.95	2.56	340.67	24.009
187 H-2 R/B	24279	2973	1083.6	98.75	30.12	136.27	10.560
188 SL-8 R/B	11321	1421	977.0	82.92	1.99	148.34	7.454
189 SL-8 R/B	10745	1421	969.8	82.93	3.40	121.71	9.582
190 SL-8 R/B	12836	1421	976.8	82.92	2.35	205.61	5.662
191 SL-8 R/B	15598	1421	976.5	82.94	2.12	230.69	6.653
192 SL-8 R/B	22308	1421	979.8	82.94	2.44	290.75	6.343
193 GLOBALSTAR M052	25773	1080	1413.6	51.99	0.11	19.54	6.060
194 NPP	37849	5040	826.9	98.74	0.14	310.66	10.357
195 SL-8 R/B	14085	1421	977.6	82.94	3.25	212.38	9.621
196 SL-8 R/B	10537	1421	981.2	82.93	1.93	239.10	8.605
197 SL-8 R/B	6708	1421	985.5	82.95	1.38	175.71	6.374
198 SL-8 R/B	8874	1421	982.5	82.96	2.54	120.18	7.714
199 SL-8 R/B	12092	1421	975.4	82.94	2.89	7.52	9.016

Continued on next page

Table B.1 – *Continued from previous page*

SATNAME	NORAD ID	Mass [kg]	Altitude [km]	Incl. [deg]	Eccentr. $\times 10^{-3}$	RAAN [deg]	RCS [m^2]
200 SL-8 R/B	24678	1421	987.1	82.94	2.56	205.27	8.165

B.2 Removal Techniques - Details and Weighing

Table B.2: Details of popular debris removal technologies according to the references given in Section 3.4.

	Gas Cloud	Net/Bag	Sling Sweeper	Clamps	Robotic Arm (RA)	Harpoon	Expanding Foam	Electrostatic	Ion Beam Shepard	Laser
Resources required	very high	middle	very low	∼RA	100 W	∼Net	very high	∼RA	very high	high
Heritage / TRL	0	6	0	3	9	3	0	3	0	0
Controlled De-Orbit	No	Possible	No	Yes	Yes	Possible	No	Yes	No	No
Re-usability	No	No	Yes	Yes	Yes	No	No	Yes	Yes	Yes
Complexity of Design	low	normal	normal	high	high	normal	normal	high	low	low
Costs	low	middle	low	high	high	middle	low	middle	low	low
Complexity of Appr./Capture	low	normal	very high	high	high	normal	normal	normal	low	low
Mass / Volume	low	1:8	200 kg	>RA	40.5 kg	∼1 kg	middle	>RA	low	low
Versatility	any	small$^+$	middle	large	large	large	middle	large	middle$^+$	mid.$^+$
Reliability	No	OK	No	OK	OK	OK	middle	middle	middle	OK
Testing on-ground	No	Yes	No	Yes	Yes	Partly	No	Partly	No	Partly
Efficiency	Rel.	mult. Nets	Yes	Yes	Yes	mult. Harp.	Rel.	Yes	Yes	Rel.
Distance to target	safe	∼7 m	0 m	<1 m	<1 m	∼20 m	<1 m	<1 m	safe	safe
Tumbling rate	any	fast	any	slow	4°/s	fast	any	middle	any	any
Type of Contact	none	mult.	point, rigid	mult.	point	point	mult.	point, rigid	none	none
Type of Connection	none	teth.	point, rigid	rigid	rigid	teth.	mult.	point, rigid	none	none
Hazardousness	very low	low	high	normal	normal	high	high	normal	low	high

While Table B.2 compares the different technologies, Table B.3 investigates the actual influence of each selection criteria. Together, they enable a profound decision for a

specific removal technique as performed in Section 3.4.2 and summarized in Table 3.5.

Table B.3: Weighing of the selection criteria for the selected removal technologies; 0 stands for less important, 1 for equal important and 2 for more important than the respective vertical criteria. The weighing factor results from the summarized points and the respective distribution among the criteria.

	Resources required	Heritage / TRL	Reusability	Complexity of Design	Costs	Complexity of Appr./ Capture	Mass / Volume	Versatility (type of target)	Reliability	Testing on-ground	Efficiency	Distance to target	Tumbling rate	Type of Contact	Hazardousness	Weighting factor (%)
Resources required	1	2	1	1	1	1	0	0	1	1	1	1	2	1	1	**6.1**
Heritage / TRL	0	1	1	1	0	1	2	1	2	0	2	1	2	2	1	**6.9**
Reusability	2	2	1	1	2	2	2	0	1	0	2	2	2	1	1	**8.4**
Complexity of Design	1	1	1	1	0	1	2	1	0	1	2	1	2	1	1	**6.5**
Costs	1	1	2	1	0	1	2	1	0	1	2	1	2	2	0	**6.9**
Complexity of Appr./ Capture	1	2	1	2	1	0	1	1	1	0	2	1	2	1	1	**7.3**
Mass / Volume	1	1	0	1	2	1	1	0	0	1	1	1	2	2	1	**6.1**
Versatility	2	0	1	0	1	1	1	0	0	1	1	2	0	2	0	**4.6**
Reliability	0	1	2	1	1	2	2	1	1	0	2	2	2	2	1	**8.0**
Testing on-ground	2	0	1	2	1	2	2	1	1	0	2	2	1	1	1	**8.0**
Efficiency	1	2	1	1	2	1	1	2	2	1	2	2	2	2	0	**8.8**
Distance to target	1	0	1	0	0	1	1	0	0	0	1	0	1	1	0	**2.7**
Tumbling rate	1	1	1	1	1	1	0	0	0	0	2	1	2	1	0	**5.0**
Type of Contact	0	0	0	0	0	0	2	0	1	0	1	0	1	1	0	**2.3**
Type of Connection	1	0	1	1	1	0	0	0	1	0	1	1	1	1	0	**3.4**
Hazardousness	1	1	2	1	1	1	2	1	1	2	2	2	2	2	1	**9.2**

Table B.4: Weighing of the selection criteria for the different transport technologies; 0 stands for less important, 1 for equal important and 2 for more important than the respective vertical criteria. The weighing factor results from the summarized points and the respective distribution among the criteria.

	Propellant required	**Complexity of Design**	**Costs**	**Complexity of Appr./ Capture**	**Mass / Volume**	**Robustness**	**Testing on-ground**	**Efficiency**	**Agility**	**Hazardousness**	**Weighting factor (%)**
Propellant required	1	1	1	0	1	0	0	1	0	0	**5**
Complexity of Design	1	1	1	0	1	0	1	0	0	0	**5**
Costs	1	1	1	2	2	1	2	1	1	0	**12**
Complexity of Appr./ Capture	2	2	0	1	1	0	1	0	0	0	**7**
Mass / Volume	1	1	0	1	1	2	1	1	0	0	**8**
Robustness	2	2	1	2	0	1	2	0	0	0	**10**
Testing on-ground	2	1	0	1	1	0	1	0	0	0	**6**
Efficiency	1	2	1	2	1	2	2	1	1	1	**14**
Agility	2	2	1	2	2	2	2	1	1	1	**16**
Hazardousness	2	2	2	2	1	2	2	1	1	1	**16**

B.3 Subsystem Details

Table B.5: Detailed list of different components of single De-orbit Kit.

	Mass[a]	Power[a]	Count	Redundancy
Structure	**72 kg**[b,c]	-		
Basic Structure (Body)	57 kg	-	1	-
Parafin Actuators	0.1 kg	10 W	12	-
Cushioning	1.1 kg	-	4	-
Power System	**28 kg**[b]			
Batteries (VL48E, VES16)	11 kg	-	7 + 21	-
Solar Array	1.2 kg	-	1	-
Basic Equipment	16 kg	-	1	-
Thermal System	**7 kg**[b]			
MLI	1.3 kg	-	1	-
Radiator/Louver	6 kg	-	1	-
Data Handling	**11 kg**[b]			
OBC	5.5 kg	10 W	2	hot
Communication	**4 kg**[b]			
Transponder	2 kg	6 W	2	hot
Antenna	0.1 kg	10 W	2	hot
Propulsion	**294 kg**[b] **(dry: 96 kg**[b]**)**			
Nitrogen	42 kg	-	1	-
LOX	75.5 kg	-	2	-
LCH4	23.5 kg	-	2	-
N2-Tank	12.7 kg	-	1	-
LOX/LCH4-Tank	6.4 kg	-	4	-
Main Engine	4.3 kg	35 W	1	-
Cold Gas Thruster	1.4 kg	20 W	2 × 4	cold
AOCS	**10 kg**[b]			
IMU	1 kg	12 W	2	cold
ES	3.5 kg	7.5 W	2	-
CSS	0.1 kg	-	2	-
GPS	1 kg	5.5 W	1	-
Margin	**15 %**			
Total	**262 kg**	**(wet: 460 kg)**		

[a] Per single unit
[b] Sum of respective subsystem, rounded
[c] Including a Safety Factor k_{Struc} of 1.15
[d] Including a Safety Factor $k_{Prop} \times k_{Trap} \times k_{load} \times k_{mix}$ of $1.15 \times 1.03 \times 1.005 \times 1.01$

Table B.6: Detailed list of different components of ADReS-A.

	Mass[a]	Power[a]	Count	Redundancy
Structure	**439 kg**[b,c]			
Robotic Arm	80 kg	230 W	1	-
Linear Arm	10 kg	50 W	2	hot
Basic Structure (Body)	256 kg	-	1	-
VLC	5 kg	25 W	2	cold
ToFC	8 kg	25 W	2	cold
Power System	**50 kg**[b]			
Batteries (VL48E, VES140)	12 kg	-	8 + 3	-
Solar Array	22 kg	-	1	-
Basic Equipment	16 kg	-	1	-
Thermal System	**11 kg**[b]			
MLI	4 kg	-	1	-
Protection Tank	6 kg	-	1	
Heater	1 kg	260 W	1	-
Data Handling	**42 kg**[b]			
OBC	10.5 kg	25 W	4	2 × hot
Communication	**4 kg**[b]			
Transponder	2 kg	6 W	2	hot
OA	0.1 kg	10 W	2	hot
Propulsion	**419 kg**[b] **(dry: 65 kg**[b]**)**			
Helium	1.5 kg	-	1	-
Hydrazine	354 kg[d]	-	1	-
He-Tank	16 kg	-	1	-
N_2H_4-Tank	35 kg	-	1	-
22 N Thruster	0.6 kg	35 W	2 × 4	cold
1 N Thruster	0.3 kg	14 W	2 × 12	cold
AOCS	**41 kg**[b]			
IMU	0.7 kg	12 W	2	cold
ES	3.5 kg	7.5 W	2	-
Reaction Wheels	7.7 kg	15 W	4	hot
CSS	0.1 kg	-	3	-
GPS	1 kg	5.5 W	2	cold
Margin	**15 %**			
Total	**750 kg**	**(wet: 1104 kg)**		

[a] Per single unit
[b] Sum of respective subsystem, rounded
[c] Including a Safety Factor k_{Struc} of 1.15
[d] Including a Safety Factor $k_{Prop} \times k_{Trap} \times k_{load} \times k_{mix}$ of $1.15 \times 1.03 \times 1.005 \times 1.01$

Table B.7: Tool and SMAD budget compared for ADReS-A. The required power for approach and shuttling of the tool are averaged to generate a comparable average power to the SMAD.

	Mass		Power	
	SMAD	**Tool**	**SMAD**	**Tool**
Structure[a]	304 kg	439 kg	0 W	0 W
Power System	110 kg	50 kg	351 W	200 W
Thermal System	24 kg	11 kg	113 W	130 W
Data Handling	29 kg	42 kg	29 W	100 W
Communication	4 kg	24 kg	31 W	32 W
Propulsion	40 kg	65 kg	21 W	153 W
AOCS	97 kg	41 kg	98 W	83 W
Margin	15 %	15 %	9 %	15 %
Total, dry	**703 kg**	**750 kg**	**1081 W**	**814 W**
Propellant mass	226 kg	354 kg		
Total, wet	**929 kg**	**1104 kg**		

[a] Includes payload (robotic and linear arms and cameras)

B.4 Fuzzy Input

Table B.8: Fuzzy rules for the simulation.

$AOCS_{int.}$	&	**$AOCS_{ext.}$**	&	**Power**	&	**Thermal**	&	**Data**		**Reaction**
low	&	low	&	low	&	low	&	low	→	(d) Abort, help
good	&	low	&	low	&	low	&	low	→	(d) Abort, help
low	&	low	&	low	&	low	&	good	→	(d) Abort, help
good	&	low	&	low	&	low	&	good	→	(d) Abort, help
low	&	low	&	low	&	good	&	low	→	(d) Abort, help
good	&	low	&	low	&	good	&	low	→	(d) Abort, help
low	&	low	&	low	&	good	&	good	→	(d) Abort, help
good	&	low	&	low	&	good	&	good	→	(d) Abort, help
low	&	low	&	good	&	low	&	low	→	(c) Abort, adjust
good	&	low	&	good	&	low	&	low	→	(b) Change part
low	&	low	&	good	&	low	&	good	→	(c) Abort, adjust
good	&	low	&	good	&	low	&	good	→	(d) Abort, help
low	&	low	&	good	&	good	&	low	→	(d) Abort, help
good	&	low	&	good	&	good	&	low	→	(d) Abort, help
low	&	low	&	good	&	good	&	good	→	(b) Change part
good	&	low	&	good	&	good	&	good	→	(b) Change part
low	&	good	&	low	&	low	&	low	→	(d) Abort, help
good	&	good	&	low	&	low	&	low	→	(d) Abort, help
low	&	good	&	low	&	low	&	good	→	(d) Abort, help
good	&	good	&	low	&	low	&	good	→	(a) Check margins
low	&	good	&	low	&	good	&	low	→	(d) Abort, help
good	&	good	&	low	&	good	&	low	→	(d) Abort, help
low	&	good	&	low	&	good	&	good	→	(d) Abort, help
good	&	good	&	low	&	good	&	good	→	(b) Change part
low	&	good	&	good	&	low	&	low	→	(b) Change part
good	&	good	&	good	&	low	&	low	→	(d) Abort, help
low	&	good	&	good	&	low	&	good	→	(d) Abort, help
good	&	good	&	good	&	low	&	good	→	(d) Abort, help
low	&	good	&	good	&	good	&	low	→	(d) Abort, help
good	&	good	&	good	&	good	&	low	→	(a) Check margins
low	&	good	&	good	&	good	&	good	→	(d) Abort, help
good	&	good	&	good	&	good	&	good	→	(e) All good

C Additional Analyses of the Relative Dynamics

C.1 Position

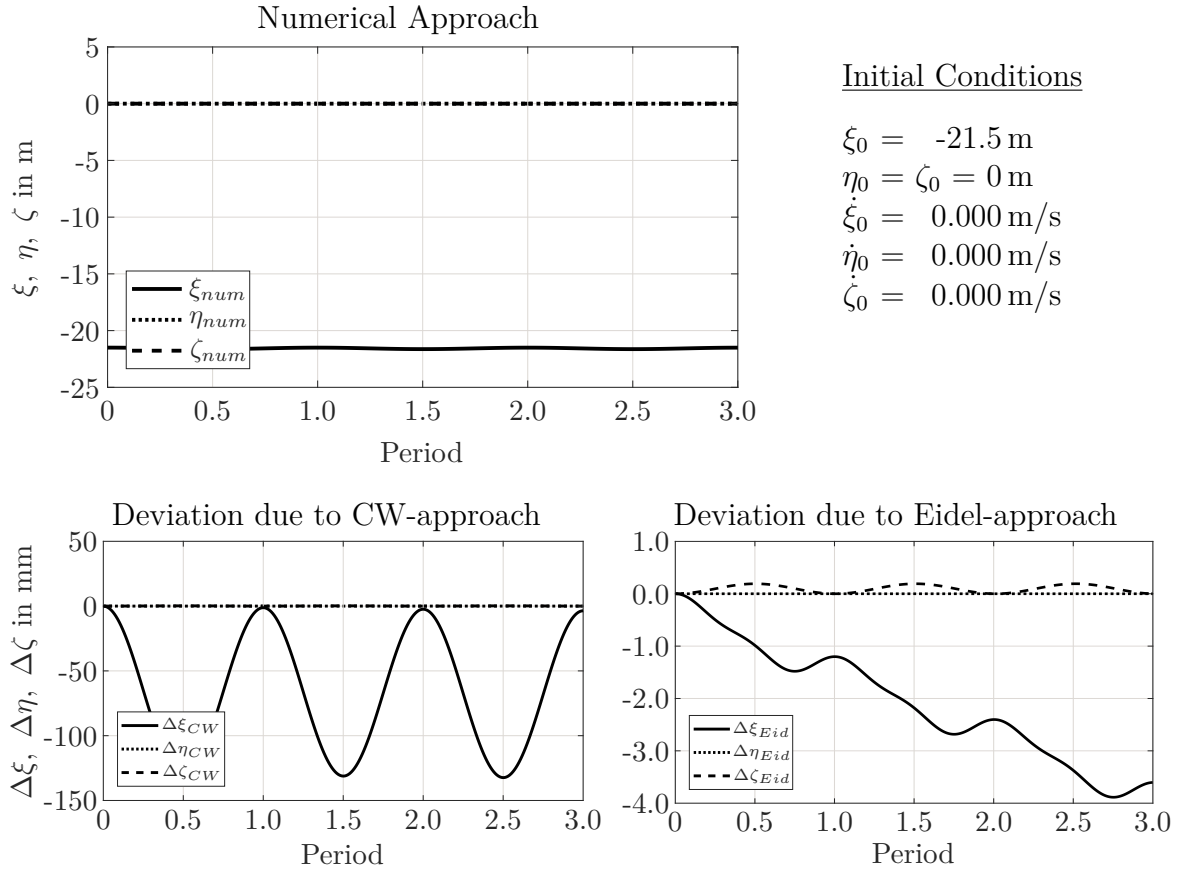

Figure C.1: (Top) The relative position of the two objects for the time of three periods for an initial spacing of -21.5 m in ξ-direction. **(Bottom)** The deviations of the CW-approach and the Eidel-approach, compared to the numerical approach.

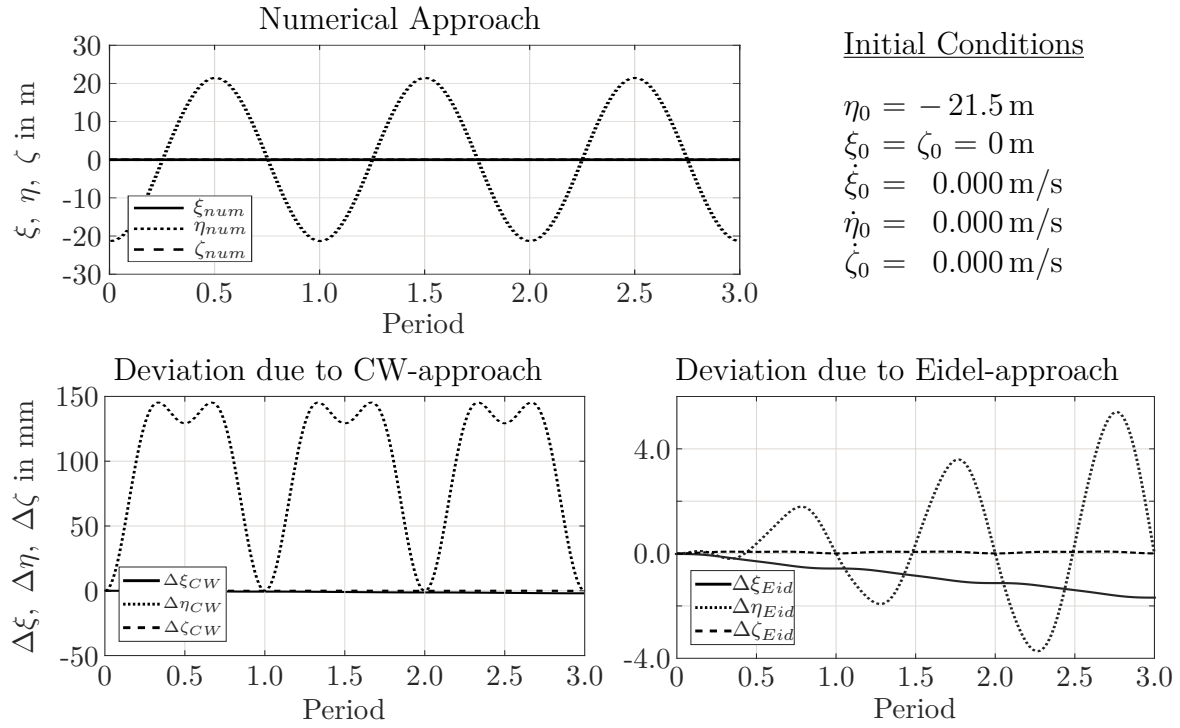

Figure C.2: The relative position of the two objects for the time of three orbital periods for an initial spacing of $-21.5\,\mathrm{m}$ in η-direction and no initial relative velocity.

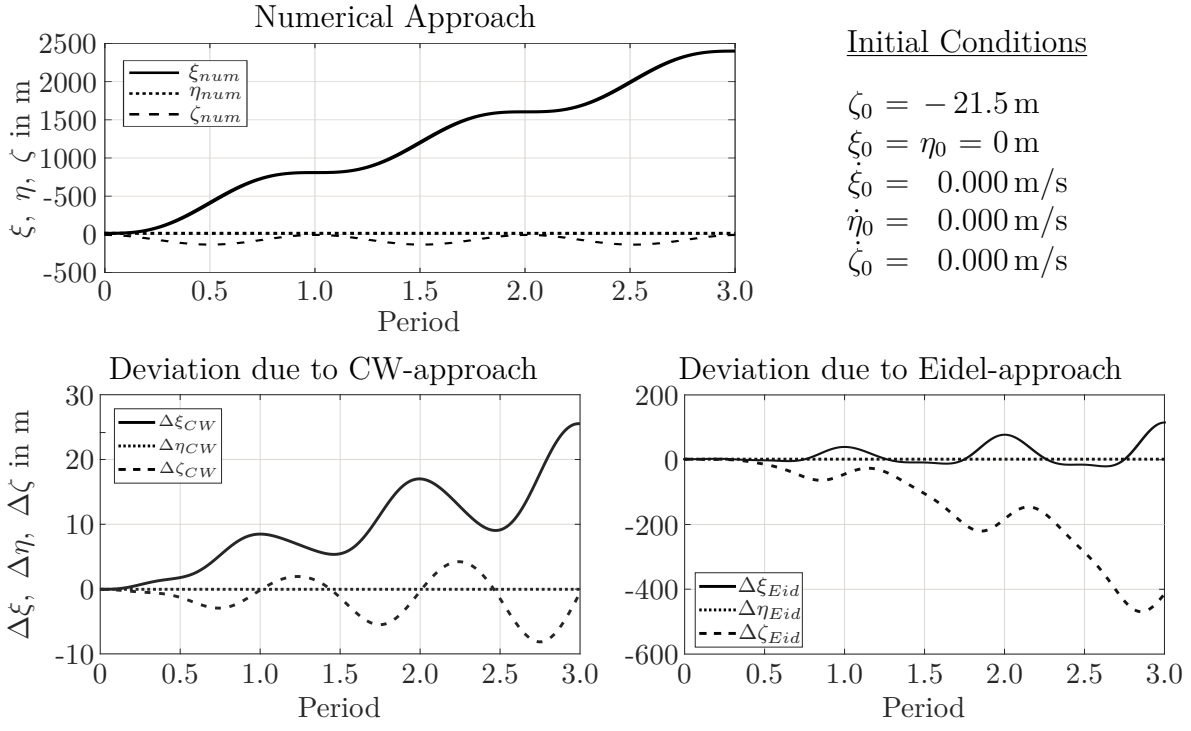

Figure C.3: The relative position of the two objects for the time of three orbital periods for an initial spacing of $-21.5\,\mathrm{m}$ in ζ-direction and no initial relative velocity.

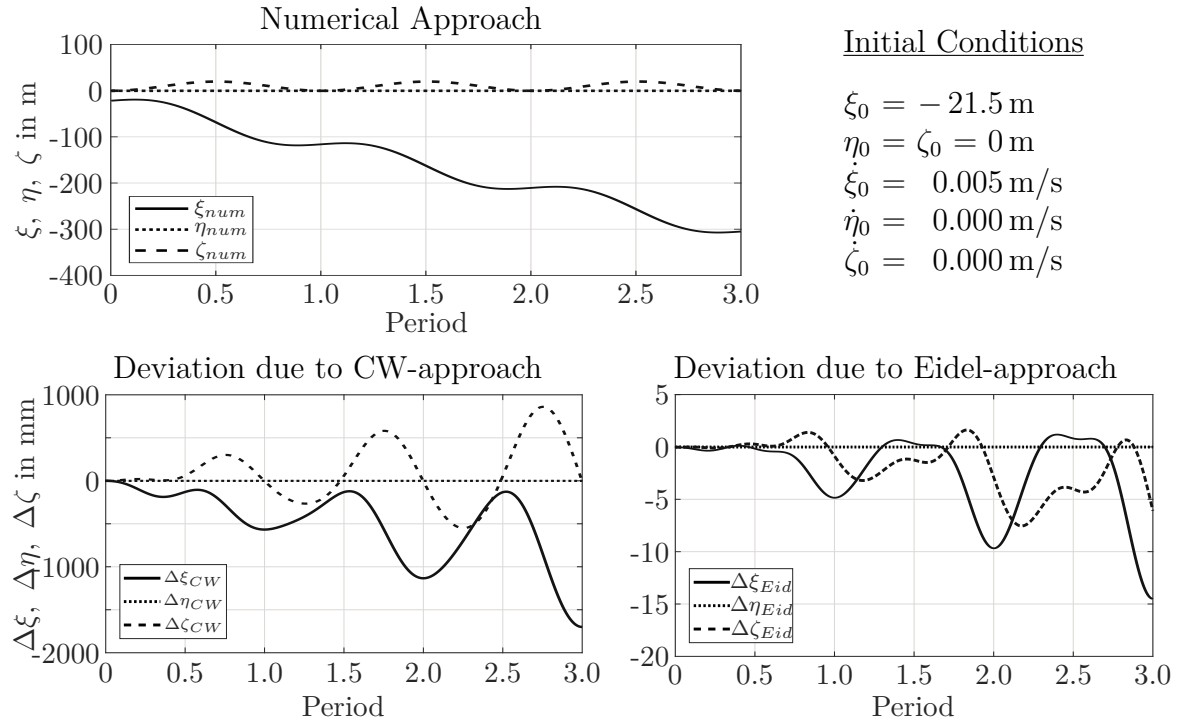

Figure C.4: The relative position of the two objects for the time of three orbital periods for an initial spacing of $-21.5\,\mathrm{m}$ and an initial relative velocity of $0.005\,\mathrm{m/s}$ in ξ-direction.

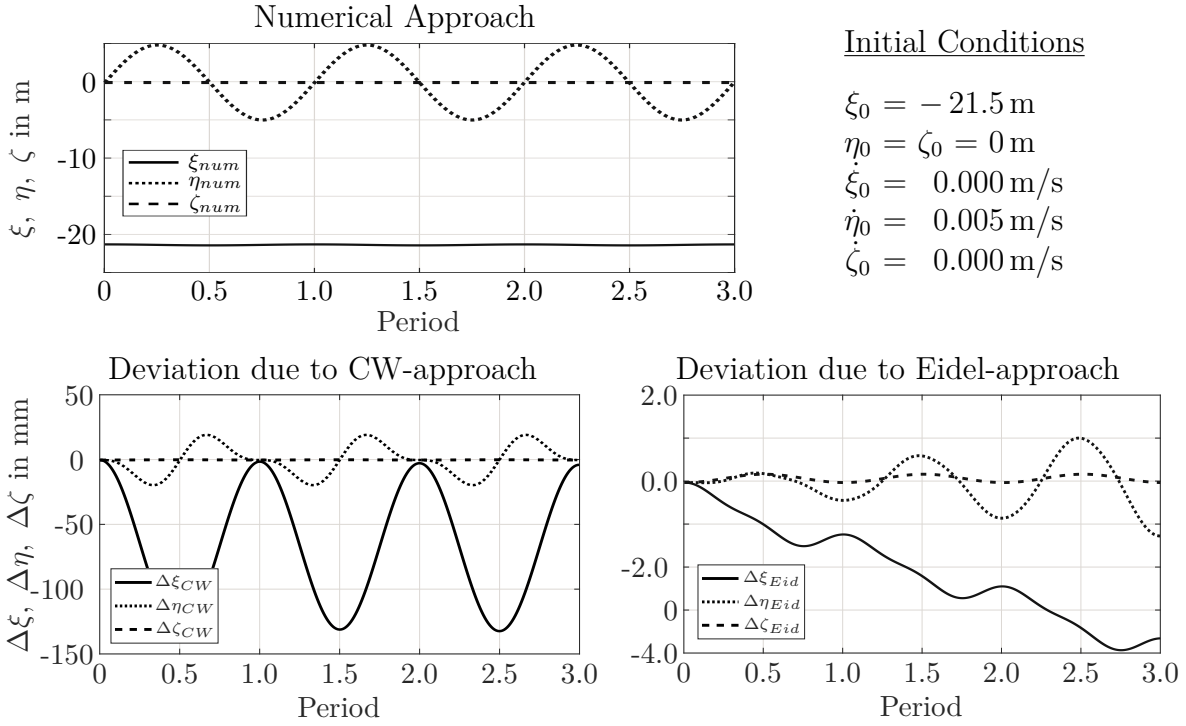

Figure C.5: The relative position of the two objects for the time of three orbital periods for an initial spacing of $-21.5\,\mathrm{m}$ and an initial relative velocity of $0.005\,\mathrm{m/s}$ in η-direction.

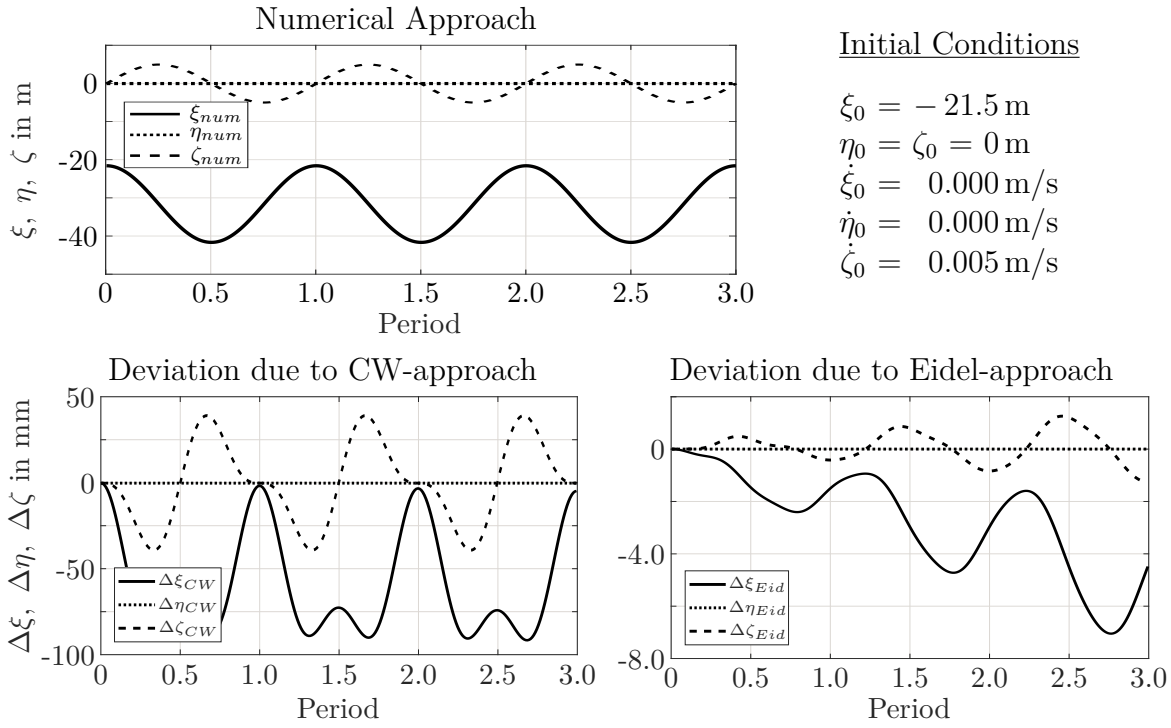

Figure C.6: The relative position of the two objects for the time of three orbital periods for an initial spacing of $-21.5\,\mathrm{m}$ and an initial relative velocity of $0.005\,\mathrm{m/s}$ in ζ-direction.

C.2 Velocity

Table C.1: The maximal relative velocity of the two objects for each direction with no relative velocity. Given are the maximum values within three periods.

Rel. pos. in m			**Num. app. in mm/s**			**CW-dev. in µm/s**			**Eid-dev. in µm/s**		
ξ_0	η_0	ζ_0	$\dot{\xi}_{num}$	$\dot{\eta}_{num}$	$\dot{\zeta}_{num}$	$\Delta\dot{\xi}_{CW}$	$\Delta\dot{\eta}_{CW}$	$\Delta\dot{\zeta}_{CW}$	$\Delta\dot{\xi}_{Eid}$	$\Delta\dot{\eta}_{Eid}$	$\Delta\dot{\zeta}_{Eid}$
-21.5	**0.0**	**0.0**	±0.06	0.00	0.00	±64.97 (100%)	0.00	±0.09 (100%)	±0.45 (0.74%)	0.00	±0.09 (100%)
0.0	**-21.5**	**0.0**	0.00	21.59	0.00	0.15 (100%)	114.02 (0.53%)	0.06 (100%)	0.15 (100%)	5.55 (0.03%)	0.06 (100%)
0.0	**0.0**	**-21.5**	259.25	0.00	±65.20	±8281 (3.19%)	0.00	±7408 (11.36%)	±98.26 (0.04%)	0.00	±108 (0.17%)

Table C.2: Deviation of the relative velocities of CW- and Eidel-approach from numerical approach with different initial relative velocities (rel. vel.). The initial holding point of the chaser is set 21.5 m behind the target.

Rel. vel. in m/s			**Num. app. in mm/s**			**CW-dev. in µm/s**			**Eid-dev. in µm/s**		
$\dot{\xi}_0$	$\dot{\eta}_0$	$\dot{\zeta}_0$	$\dot{\xi}_{num}$	$\dot{\eta}_{num}$	$\dot{\zeta}_{num}$	$\Delta\dot{\xi}_{CW}$	$\Delta\dot{\eta}_{CW}$	$\Delta\dot{\zeta}_{CW}$	$\Delta\dot{\xi}_{Eid}$	$\Delta\dot{\eta}_{Eid}$	$\Delta\dot{\zeta}_{Eid}$
0.000	**0.000**	**0.000**	±0.06	0.00	0.00	±64.97 (100%)	0.00	±0.09 (100%)	±0.45 (0.74%)	0.00	±0.09 (100%)
0.005	**0.000**	**0.000**	-34.9	0.0	±10.0	-854.7 (2.45%)	0.0	-858.2 (8.56%)	-11.2 (0.03%)	0.0	-10.4 (0.10%)
0.000	**0.005**	**0.000**	±0.1	±5.0	0.0	±65.0 (100%)	29.9 (0.60%)	±0.1 (10%)	±0.5 (0.02%)	±1.1 (0.03%)	±0.1 (10%)
0.000	**0.000**	**0.005**	±10.0	0.0	±5.0	±71.1 (0.71%)	0.0	±59.7 (1.19%)	2.6 (0.03%)	0.0	±1.3 (0.03%)
0.005	**0.005**	**0.005**	-37.2	±5.0	-11.1	±880.8 (2.37%)	±29.9 (0.60%)	±858.3 (7.70%)	±10.0 (0.03%)	±1.3 (0.03%)	±10.5 (0.09%)

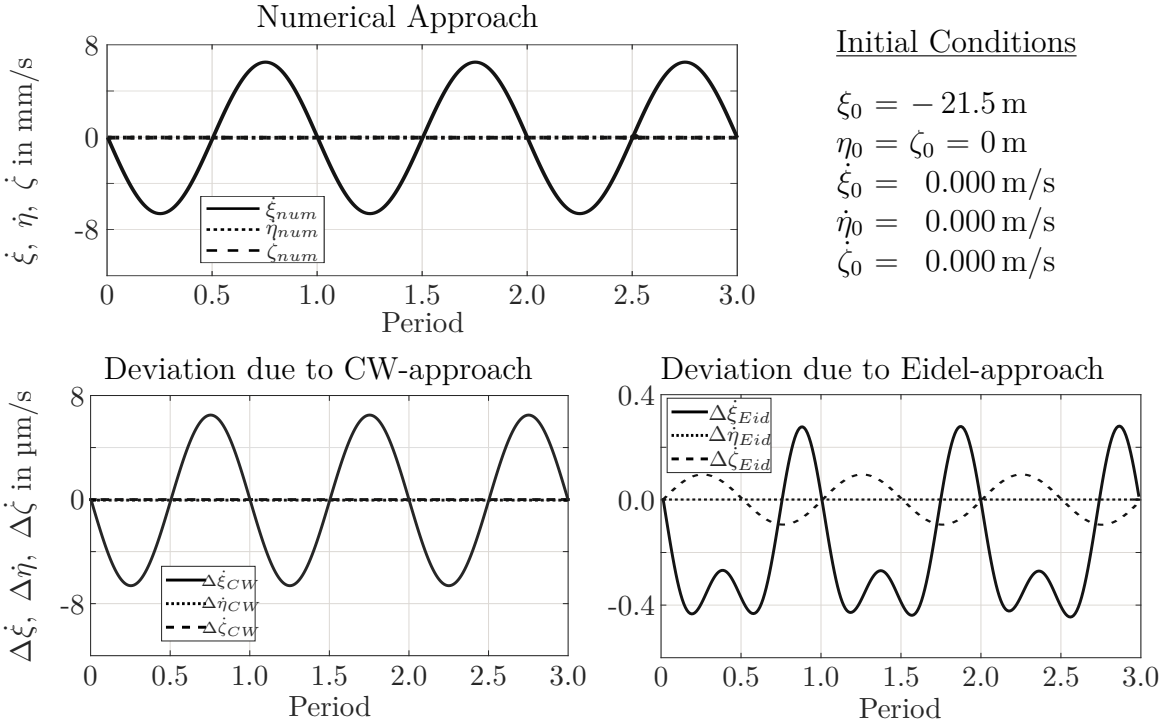

Figure C.7: The relative velocity of the two objects for the time of three orbital periods for an initial spacing of $-21.5\,\mathrm{m}$ in ξ-direction.

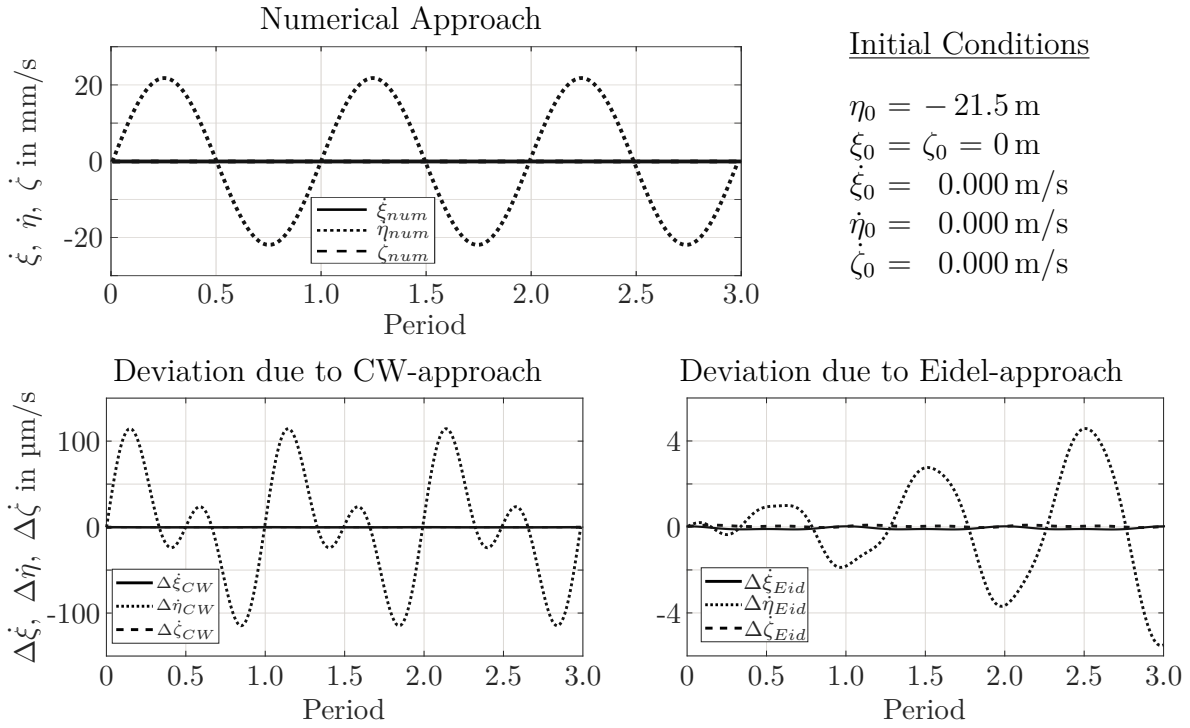

Figure C.8: The relative velocity of the two objects for the time of three orbital periods for an initial spacing of $-21.5\,\mathrm{m}$ in η-direction.

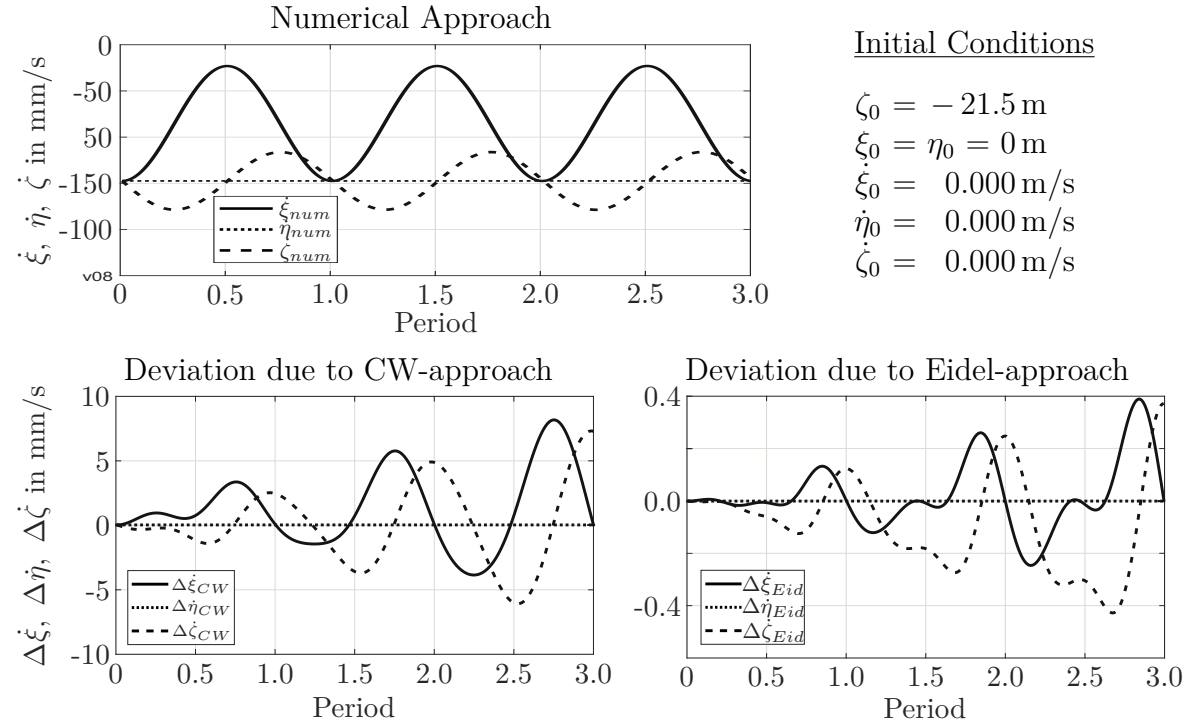

Figure C.9: The relative velocity of the two objects for the time of three orbital periods for an initial spacing of $-21.5\,\mathrm{m}$ in ζ-direction.

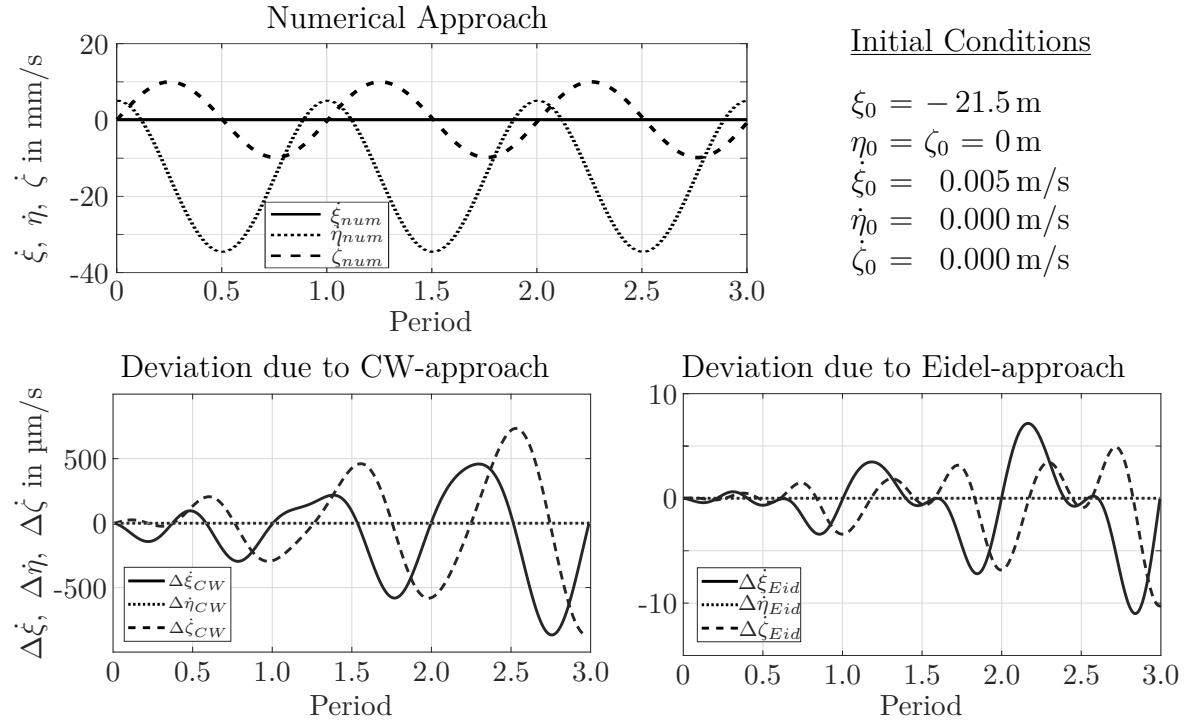

Figure C.10: The relative velocity of the two objects for the time of three orbital periods for an initial spacing of $-21.5\,\mathrm{m}$ and an initial relative velocity of $0.005\,\mathrm{m/s}$ in ξ-direction.

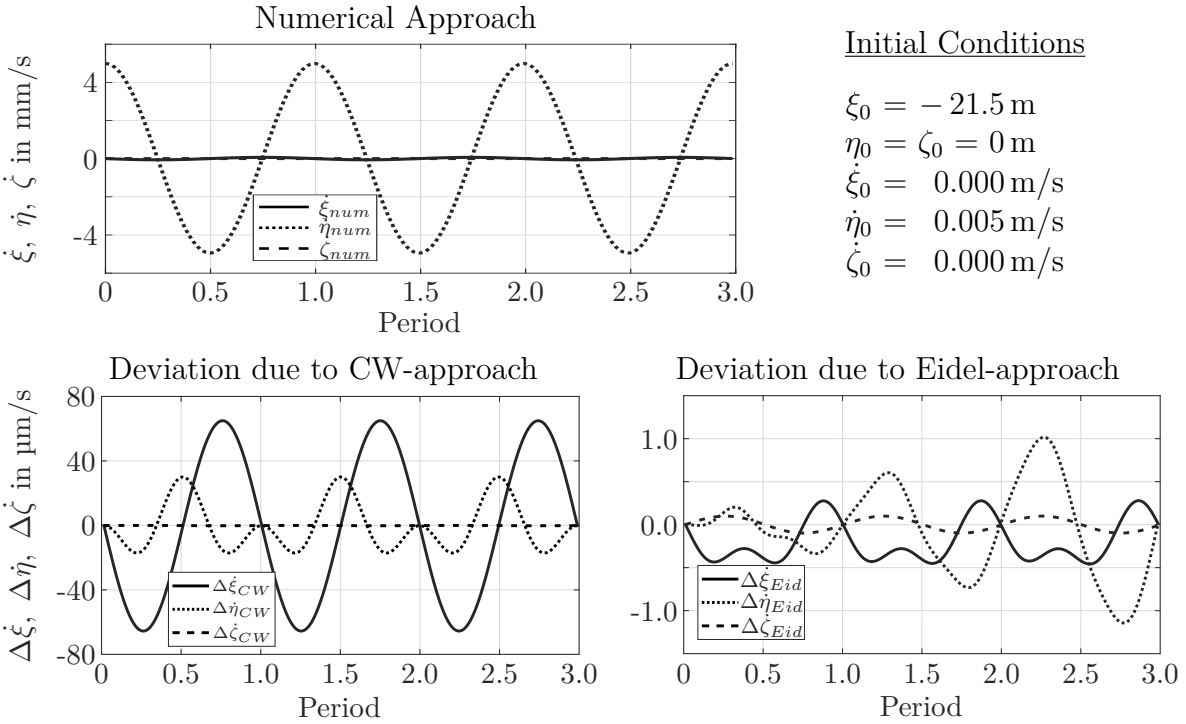

Figure C.11: The relative velocity of the two objects for the time of three orbital periods for an initial spacing of $-21.5\,\mathrm{m}$ and an initial relative velocity of $0.005\,\mathrm{m/s}$ in η-direction.

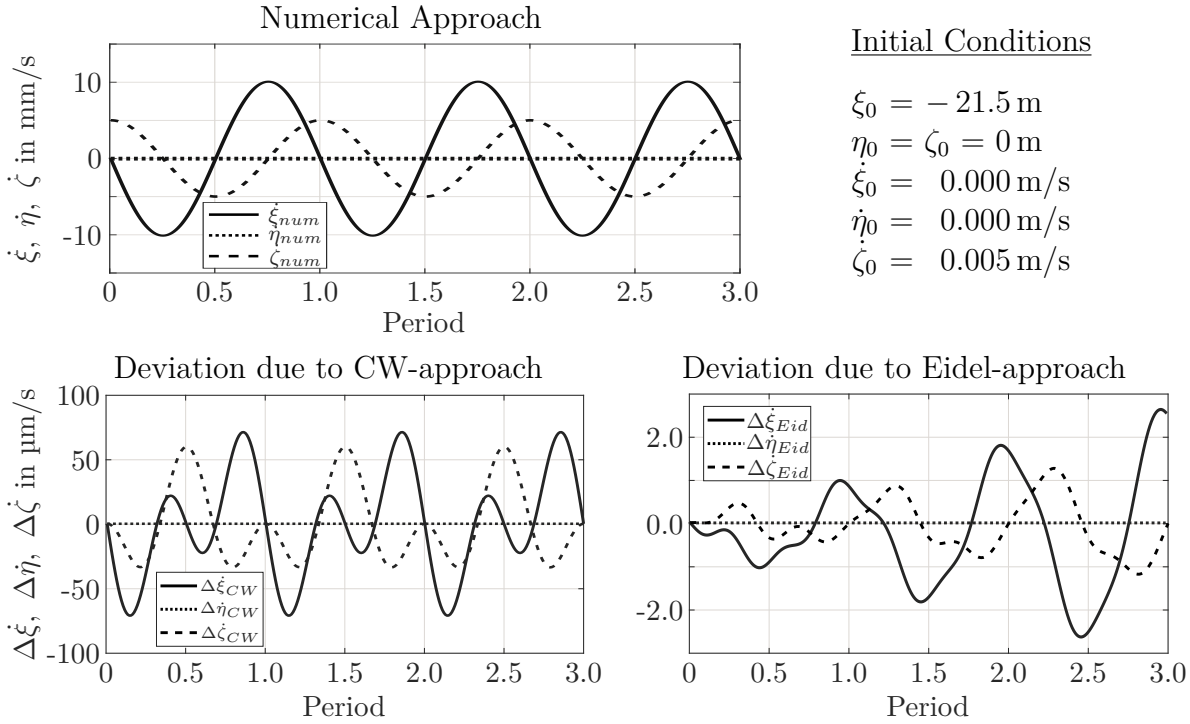

Figure C.12: The relative velocity of the two objects for the time of three orbital periods for an initial spacing of $-21.5\,\mathrm{m}$ and an initial relative velocity of $0.005\,\mathrm{m/s}$ in ζ-direction.

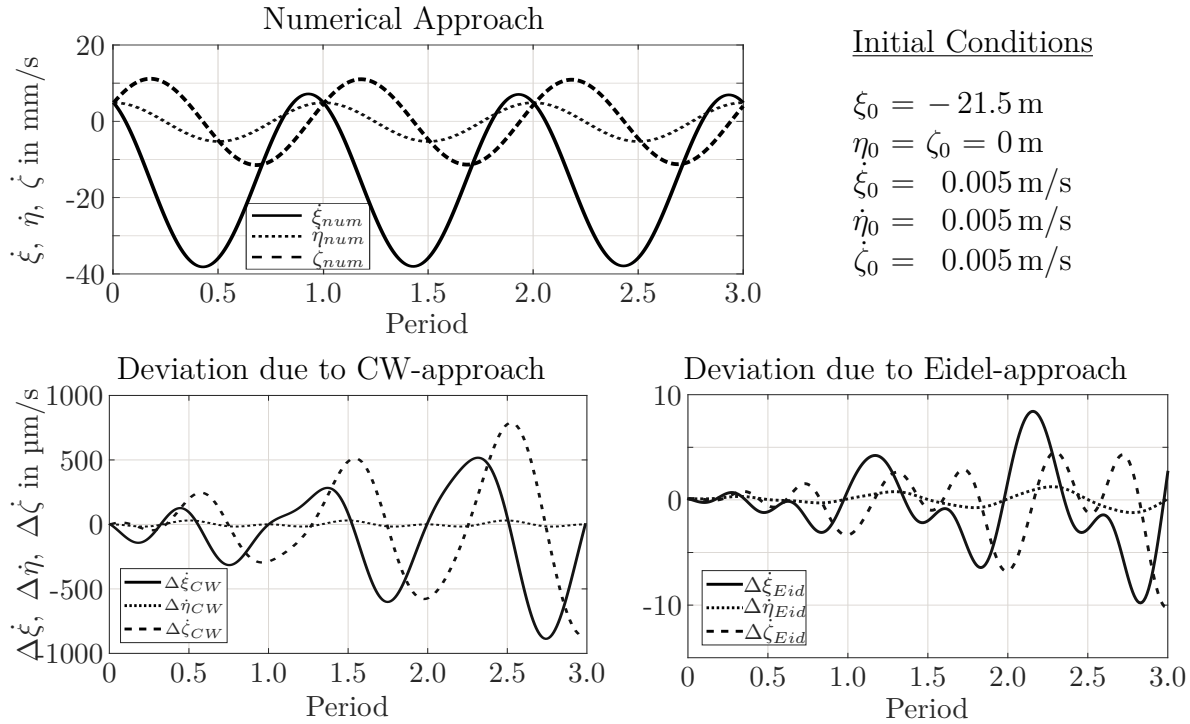

Figure C.13: The relative velocity of the two objects for the time of three orbital periods for an initial spacing of $-21.5\,\mathrm{m}$ and an initial relative velocity of $0.005\,\mathrm{m/s}$ in each direction.